

**Diamond-like carbon coatings deposited by vacuum  
arc in artificial hip joints**

**Dissertation**

**zur Erlangung eines Doktorgrades**

im

**Fachbereich D – Architektur, Bauingenieurwesen, Maschinenbau,  
Sicherheitstechnik**

der

**Bergischen Universität Wuppertal**

**- Maschinenbau -**

vorgelegt von

**Ying Ren**

aus Shanxi (23.10.1982)

Wuppertal 2013

---

## **Dedication**

*To my God.*

## **Declaration**

I declare that the work in this dissertation was carried out in accordance with the regulation of University of Wuppertal. I declare that I have written it independently and have used only the tools indicated in the dissertation. The work is original, except where indicated by special literature in the text and it has not been submitted elsewhere for examination. In addition for me no previous PhD applications have been unsuccessful.

Hiermit erkläre ich, Ying Ren, dass ich die vorliegende Arbeit selbständig ohne unerlaubte fremde Hilfe angefertigt habe und keine anderen Quellen und Hilfsmittel genutzt habe, als im Literaturverzeichnis angegeben. Alle Stellen in dieser Arbeit, die dem Wortlaut oder Sinn nach anderen Werken entnommen wurden, habe ich in jedem einzelnen Fall unter Angabe der Quelle als Entlehnung kenntlich gemacht. Die Arbeit ist noch nicht an anderer Stelle als Prüfungsleistung vorgelegt worden. Es wurde kein Promotionsverfahren ohne Erfolg beendet.

Die Dissertation kann wie folgt zitiert werden:

urn:nbn:de:hbz:468-20131023-124239-7

[<http://nbn-resolving.de/urn/resolver.pl?urn=urn%3Anbn%3Ade%3A468-20131023-124239-7>]

## **Abstract**

For biomedical application in the field of artificial hip joints diamond-like carbon (DLC) coatings have been widely studied due to their excellent mechanical, tribological and biological properties. At present the lifetime of such joints is just about 15 years and some (10%) of patients require second replacement. In consequence, it is currently an urgent need to extend the life expectancy especially for younger patients under 50 years old. As is well known, the wear particles as the main factor limiting the life expectancy of hip joints have attracted more and more interest, in particular, the amount of wear particles. However, it is rare to see the reports about wear particle size distribution.

The key contribution of this dissertation is a new approach-design of wear particle size distribution, which is an initial and important step of DLC research in artificial hip joint field. In addition, DLC coating is grown by a new deposition technique based on the vacuum arc, which allows the transition from cathodic to anodic operation mode by adjusting the anode-cathode diameter ratio. The main aim of this dissertation is to investigate the influence of deposition parameters on the wear particle size distribution, as well as the structure and tribological properties of DLC coatings. It is shown that it is possible to reduce the wear particle size by optimization of the deposition parameters.

Für biomedizinische Anwendungen im Bereich künstlicher Hüftgelenke wurden DLC- (diamond like carbon) Schichten hinsichtlich ihrer ausgezeichneten mechanischen, tribologischen und bioinerten Eigenschaften weitreichend untersucht.

Gegenwärtig beträgt die Lebensdauer dieser Implantate in etwa 15 Jahre, so dass ca. jeder zehnte Patient einen weiteren Austausch benötigt (Revisionsoperation). Folglich ist es, besonders für jüngere Patienten unter 50 Jahren von großer Wichtigkeit, die Standzeit dieser Gelenkimplantate zu erhöhen.

Da Abriebpartikeln bekanntermaßen der Faktor sind, welcher die Standzeiten dieser Hüftimplantate am meisten beschränkt, rückten diese (speziell in ihrer Quantität) in der Vergangenheit zunehmend in den Fokus der wissenschaftlichen Betrachtung.

Ungeachtet dessen gibt es nur wenige Veröffentlichungen über die Partikelgrößenverteilung.

---

Der Schlüsselbeitrag dieser Dissertation ist ein neuer Ansatz zur Beeinflussung der Partikelgrößenverteilung, welcher einen innovativen und wichtigen Schritt in der Erforschung von DLC-Schichten für künstliche Hüftgelenkimplantate darstellt.

Hierbei kommt ein neuartiges Beschichtungsverfahren, welches auf dem Vakuum-Lichtbogenverfahren basiert, zum Einsatz. Durch Variation der Elektrodendurchmesser erlaubt es dieses Verfahren, die DLC-Schichten sowohl vom kathodischen als auch vom anodischen Lichtbogen abzuscheiden.

Hauptziele dieser Dissertation sind sowohl die Erforschung des Einflusses der Beschichtungsparameter auf die Partikelgrößenverteilung sowie auch die strukturellen und tribologischen Eigenschaften der DLC-Schichten.

Es wird gezeigt, dass es möglich ist, die Größe der Abriebpartikeln durch Optimierung der Beschichtungsparameter zu reduzieren.

# Contents

<b>List of Figures .....</b>	<b>VI</b>
<b>List of Tables .....</b>	<b>X</b>
<b>1. Introduction .....</b>	<b>1</b>
1.1 The challenge .....	1
1.2 Objectives and contributions .....	2
1.3 Research discussion .....	3
1.3.1 Problem statement .....	3
1.3.2 Assumptions and their motivation .....	5
1.4 Thesis organization .....	6
References .....	7
<b>2. DLC coatings background.....</b>	<b>10</b>
2.1 Structure and properties of DLC coatings .....	10
2.1.1 Structure of DLC coatings .....	10
2.1.2 Properties of DLC coatings.....	12
References .....	13
2.2 Applications of DLC coatings .....	15
2.2.1 Biomedical applications.....	15
2.2.2 Other applications.....	17
References .....	20
2.3 Deposition techniques of DLC coatings.....	25
2.3.1 Physical vapor deposition of DLC coatings .....	25
2.3.2 CVD and other deposition techniques of DLC coatings .....	29
References .....	30
<b>3. Hip joint replacement background .....</b>	<b>34</b>
3.1 Introduction of normal hip joint and artificial hip joint .....	34
3.1.1 Composition of hip joint .....	34
3.1.2 Wear particles .....	35
3.2 Classification of artificial hip joint .....	37
3.2.1 Metal femoral heads articulating against UHMWPE cups .....	37
3.2.2 Ceramic femoral heads articulating against UHMWPE cups .....	37
3.2.3 Metal femoral heads articulating against metal cups .....	38
3.2.4 Ceramic femoral heads articulating against ceramic cups .....	39
3.2.5 DLC coated artificial hip joint .....	40
3.3 Adhesion and interface layers in biomedical materials .....	41
References .....	44
<b>4. Experimental methods for characterization of DLC coatings .....</b>	<b>49</b>

---

4.1 Morphology and structure of DLC coatings.....	49
4.1.1 Coating thickness and roughness .....	49
4.1.2 Scanning electron microscopy (SEM).....	49
4.1.3 Energy dispersive X-ray spectroscopy (EDX).....	51
4.1.4 Raman spectroscopy.....	52
4.2 Tribological evaluation of DLC coatings .....	58
4.3 Cavitation erosion test.....	59
4.4 Particle size distribution analysis.....	61
References .....	64
<b>5. Experiments for deposition of interface layer and DLC coatings.....</b>	<b>67</b>
5.1 Deposition of interface layer (Ti) by cathodic arc evaporation .....	67
5.1.1 Deposition setup (Cathodic arc evaporation).....	67
5.1.2 Deposition Process .....	68
5.2 Relationship between deposition pressure and arc voltage and current.....	70
5.3 Deposition of DLC coatings by new vacuum arc equipment.....	72
5.3.1 Deposition setup (Transition between the cathodic arc and anodic arc) .....	72
5.3.2 Deposition Process .....	73
References .....	74
<b>6. Parameters of analysis of Raman spectra and wear tests .....</b>	<b>75</b>
6.1 Analysis of Raman spectra .....	75
6.2 Parameters of tribological test .....	80
6.3 Parameters of cavitation erosion test .....	87
6.4 Parameters of particle size distribution analysis.....	91
References .....	96
<b>7. Influence of substrate bias on the particle size distribution of DLC coatings.....</b>	<b>99</b>
7.1 Anode-cathode diameter ratio of $d_a/d_c = 1/3$ .....	99
7.1.1 Density and deposition rate of DLC coatings .....	99
7.1.2 Raman spectra of DLC coatings .....	100
7.1.3 Tribological properties of DLC coatings .....	103
7.1.4 Particle size distribution of DLC coatings.....	104
7.1.5 Conclusion .....	107
7.2 Anode-cathode diameter ratio of $d_a/d_c = 1/1$ .....	108
7.2.1 Density and deposition rate of DLC coatings .....	108
7.2.2 Raman spectra of DLC coatings .....	109
7.2.3 Tribological properties of DLC coatings .....	112
7.2.4 Particle size distribution of DLC coatings.....	113
7.2.5 Conclusion .....	115
7.3 Anode-cathode diameter ratio of $d_a/d_c = 3/1$ .....	116
7.3.1 Density and deposition rate of DLC coatings .....	116
7.3.2 Raman spectra of DLC coatings .....	117
7.3.3 Tribological properties of DLC coatings .....	121

---

7.3.4 Particle size distribution of DLC coatings .....	122
7.3.5 Conclusion .....	124
References .....	125
<b>8. Influence of <math>d_a/d_c</math> on the particle size distribution of DLC coatings .....</b>	<b>127</b>
8.1 Substrate bias at $-250$ V .....	128
8.1.1 Density and deposition rate of DLC coatings .....	128
8.1.2 Raman spectra of DLC coatings .....	128
8.1.3 Particle size distribution of DLC coatings .....	130
8.1.4 Conclusion .....	131
8.2 Substrate bias at $-500$ V .....	131
8.2.1 Density and deposition rate of DLC coatings .....	131
8.2.2 Raman spectra of DLC coatings .....	132
8.2.3 Particle size distribution of DLC coatings .....	133
8.2.4 Conclusion .....	134
8.3 Substrate bias at $-750$ V .....	135
8.3.1 Density and deposition rate of DLC coatings .....	135
8.3.2 Raman spectra of DLC coatings .....	136
8.3.3 Particle size distribution of DLC coatings .....	137
8.3.4 Conclusion .....	138
8.4 Substrate bias at $-1000$ V .....	138
8.4.1 Density and deposition rate of DLC coatings .....	138
8.4.2 Raman spectra of DLC coatings .....	139
8.4.3 Particle size distribution of DLC coatings .....	140
8.4.4 Conclusion .....	140
References .....	141
<b>9. Influence of substrate bias and <math>d_a/d_c</math> on adhesion (Cavitation erosion).....</b>	<b>142</b>
9.1 Anode-cathode diameter ratio of $d_a/d_c = 1/3$ .....	142
9.2 Anode-cathode diameter ratio of $d_a/d_c = 1/1$ .....	145
9.3 Anode-cathode diameter ratio of $d_a/d_c = 3/1$ .....	148
References .....	152
<b>10. Conclusion and Future Work .....</b>	<b>153</b>
10.1 Contributions .....	153
10.2 Conclusions .....	154
10.3 Limitations .....	156
10.4 Future work.....	158
References .....	160
<b>Acknowledgments.....</b>	<b>161</b>
<b>Appendix.....</b>	<b>163</b>
<b>Lebenslauf.....</b>	<b>166</b>

---

## List of Figures

Figure 1.1 Tribological process diagram .....	5
Figure 2.1 The $sp^3$ , $sp^2$ , $sp^1$ hybridised bonding [1] .....	10
Figure 2.2 Carbon structure in (a) diamond, (b) graphite and (c) amorphous diamond-like carbon [2-4] .....	11
Figure 2.3 Ternary phase diagram for various DLC coatings with respect to $sp^3$ , $sp^2$ and hydrogen contents [7] .....	11
Figure 2.4 DLC coated products (a) Stent [1] (b) Left ventricular assist device heart pump [2] (c) artificial joint [2] (d) Ankle joint [3] (e) Hip Joint [4] .....	15
Figure 2.5 DLC coated products (a) End mill (b) Step drill (c) Engine piston (d) Gears (e) Engine tappets [58] .....	18
Figure 2.6 Hard disk architecture [59] .....	18
Figure 2.7 DLC coated IRST Dome [68] .....	19
Figure 2.8 Coaxial speaker (DLC-coated titanium centre cap) [71] .....	20
Figure 2.9 Schematic of cathodic vacuum arc [1] .....	26
Figure 2.10 Schematic diagram of a various filters: (a) 90 °filter (b) 45 °filter (c) S-filter [23].....	27
Figure 2.11 Schematic diagram of anodic vacuum arc deposition setup [32] .....	28
Figure 3.1 The normal hip joint and arthritic hip joint [1] .....	34
Figure 3.2 Schematic of a normal hip joint (left [2]), corresponding artificial hip joint (right [3]) .....	35
Figure 3.3 Metal-on-UHMWPE hip joint [25].....	37
Figure 3.4 Ceramic-on-UHMWPE hip joint [25].....	38
Figure 3.5 Metal-on-Metal hip joint [25] .....	39
Figure 3.6 Ceramic-on-Ceramic hip joint [37].....	40
Figure 4.1 Schematic diagram of scanning electron microscope (SEM) .....	50
Figure 4.2 Interaction between electron beam and surface layer of the specimen .....	50
Figure 4.3 Vibrational energy level diagram of Rayleigh scattering and Raman scattering.....	53
Figure 4.4 Characteristic Raman spectra of some carbon-based materials at 514.5 nm [19,20].....	54
Figure 4.5 Amorphization trajectory [13].....	55
Figure 4.6 Schematic diagram of influence on the Raman spectra .....	57
Figure 4.7 The tribological test setup [30] .....	58

Figure 4.8 Cavitation equipment [35] .....	60
Figure 4.9 Wear damage by cavitation erosion of DLC coatings .....	61
Figure 4.10 The equipment of particle size distribution analyzer [37].....	62
Figure 4.11 Cumulative distribution and transformed frequency distribution of sample N1 deposited with an anode-cathode diameter ratio of $d_a/d_c = 3/1$ at a DC bias of $-1000$ V .....	63
Figure 4.12 Frequency distribution $q_3(x)$ of sample N1 deposited with an anode-cathode diameter ratio of $d_a/d_c = 3/1$ at a DC bias of $-1000$ V .....	63
Figure 5.1 Schematic diagram of cathodic vacuum arc deposition system for interface layer .....	67
Figure 5.2 Interface layer of Ti deposited on P2000 .....	69
Figure 5.3 Relationship between voltage and current at the different deposition pressure .....	70
Figure 5.4 Schematic diagram of vacuum arc deposition system for DLC coatings.....	72
Figure 6.1 Raman spectra fitted with two-Gaussian fits of DLC synthesized at the DC bias of $-250$ V to $-1000$ V (the red line represents the fitted curve) .....	76
Figure 6.2 Raman spectra fitted with three-Gaussian of DLC synthesized at a DC bias of $-250$ V to $-1000$ V .....	77
Figure 6.3 Raman spectra fitted with four-Gaussian of DLC synthesized at a DC bias of $-250$ V to $-1000$ V .....	78
Figure 6.4 $I_D/I_G$ ratio of DLC synthesized at a DC bias of $-250$ V to $-1000$ V under different fitting function .....	79
Figure 6.5 SEM image of the center of worn surfaces and the corresponding EDX spectra .....	83
Figure 6.6 SEM image of the edge of worn surfaces and the corresponding EDX spectra.....	84
Figure 6.7 SEM image of the worn surfaces and the corresponding EDX spectra .....	85
Figure 6.8 SEM image of the worn surfaces and the corresponding EDX spectra .....	86
Figure 6.9 Wear damage by cavitation erosion of DLC coatings deposited with $d_a/d_c = 3/1$ at $0$ V .....	89
Figure 6.10 Wear damage by cavitation erosion of DLC coatings deposited with $d_a/d_c = 3/1$ .....	89
Figure 6.11 Wear damage by cavitation erosion of DLC coatings deposited with $d_a/d_c = 1/3$ at $0$ V .....	90
Figure 6.12 Frequency distribution of sample 4 without ultrasonic with different refractive index: $1.920$ of carbon (left) and $2.410$ of diamond (right) .....	93

---

Figure 6.13 Frequency distribution of sample 4 with 2 min-ultrasonic with different refractive index: 1.920 of carbon (left) and 2.410 of diamond (right) .....	93
Figure 6.14 Frequency distribution of sample 10 analyzed with the refractive index of carbon.....	94
Figure 7.1 Deposition rate (a) and density (b) as a function of bias voltage .....	100
Figure 7.2 Raman spectra of DLC coatings with DC bias voltage.....	101
Figure 7.3 Raman spectra fittings of DLC coatings with different DC bias voltage.....	102
Figure 7.4 Variation of D and G positions and $I_D/I_G$ ratio as a function of DC bias voltage.....	103
Figure 7.5 Friction coefficient of DLC coatings deposited at various DC bias voltages .....	104
Figure 7.6 Cumulative distribution by volume $Q_3(x)$ : comparison of substrate biases of -250 V, -500 V, -750 V and -1000 V ( $d_a/d_c = 1/3$ ).....	105
Figure 7.7 Volume density distribution $q_3(x)$ : comparison of substrate biases of -250 V to -1000 V.....	106
Figure 7.8 Particles size distribution: comparison of substrate biases of -250 V to -1000 V.....	106
Figure 7.9 Deposition rate (a) and density (b) as a function of bias voltage .....	108
Figure 7.10 Raman spectra fittings of DLC coatings with different DC bias voltage.....	110
Figure 7.11 Variation of D and G positions and $I_D/I_G$ ratio as a function of DC bias voltage .....	111
Figure 7.12 Roughness (Ra) (a), friction coefficient (b) and wear rate (c) of DLC coatings deposited at various DC bias voltages .....	112
Figure 7.13 Volume density distribution $q_3(x)$ : comparison of substrate biases of -250 V to -1000 V .....	114
Figure 7.14 Particles size distribution: comparison of substrate biases of -250 V to -1000 V.....	115
Figure 7.15 Deposition rate (a) and density (b) of DLC coatings deposited at various DC bias voltages .....	116
Figure 7.16 Raman spectrum of (a) the DLC coatings deposited at various DC bias voltage and (b) the sputtered DLC coatings deposited with different thicknesses (Varanasi et al. [18]) .....	118
Figure 7.17 Fitted Raman spectrum of the DLC coatings deposited at various DC bias voltages .....	119
Figure 7.18 Variation of D position, G position and $I_D/I_G$ ratio with DC bias voltage.....	120
Figure 7.19 Roughness (Ra) (a) and wear rate (b) of DLC coatings deposited at various DC bias voltages ...	121
Figure 7.20 SEM images of (a) original filter membrane and (b) typical particles on filter membrane .....	122
Figure 7.21 Volume density distribution $q_3(x)$ at the DC bias from -250 V to -1000 V.....	123
Figure 7.22 Variation of $q_3(x2mod)/q_3(x1mod)$ ratio with DC bias voltage .....	124
Figure 8.1 Electrodes mass flow as a function of the vacuum arc mode [1] .....	127

Figure 8.2 Density and deposition rate of DLC coatings deposited at $-250$ V with different $d_a/d_c$ .....	128
Figure 8.3 Raman spectrum of DLC coatings deposited at $-250$ V with different $d_a/d_c$ .....	129
Figure 8.4 Volume density distribution $q_3(x)$ at $-250$ V with different $d_a/d_c$ .....	130
Figure 8.5 Density and deposition rate of DLC coatings deposited at $-500$ V .....	132
Figure 8.6 Raman spectrum of DLC coatings deposited at $-500$ V with different $d_a/d_c$ .....	132
Figure 8.7 Volume density distribution $q_3(x)$ at $-500$ V with different $d_a/d_c$ .....	134
Figure 8.8 Density and deposition rate of DLC coatings deposited at $-750$ V .....	135
Figure 8.9 Raman spectrum of DLC coatings deposited at $-750$ V with different $d_a/d_c$ .....	136
Figure 8.10 Volume density distribution $q_3(x)$ at $-750$ V with different $d_a/d_c$ .....	137
Figure 8.11 Density and deposition rate of DLC coatings deposited at $-1000$ V with different $d_a/d_c$ .....	138
Figure 8.12 Raman spectrum of DLC coatings deposited at $-1000$ V with different $d_a/d_c$ .....	139
Figure 8.13 Volume density distribution $q_3(x)$ at $-1000$ V with different $d_a/d_c$ .....	140
Figure 9.1 Wear damage of cavitation erosion of DLC coating deposited with $d_a/d_c = 1/3$ at $-500$ V .....	143
Figure 9.2 Wear damage by cavitation erosion of DLC coatings .....	143
Figure 9.3 Wear damage of cavitation erosion of DLC coating deposited with $d_a/d_c = 1/1$ at $-500$ V .....	146
Figure 9.4 Light microscopy image of worn surface and corresponding analytical image by software .....	147
Figure 9.5 Deposition rate and density of DLC coating deposited with $d_a/d_c = 3/1$ as a function of bias voltage .....	149
Figure 9.6 Wear damage of cavitation erosion of DLC coating deposited with $d_a/d_c = 3/1$ at $-250$ V .....	150
Figure 9.7 Wear damage by cavitation erosion of DLC coatings deposited with $d_a/d_c = 3/1$ at different biases of $-250$ V, $-500$ V, $-750$ V and $-1000$ V .....	151

---

## List of Tables

Table 2.1 Comparison of major properties of amorphous carbons with diamond, graphite, ta-C and polyethylene [7].....	12
Table 5.1 Chemical analysis of P2000 .....	68
Table 5.2 Deposition process parameters for interface layers .....	69
Table 5.3 Comparison of effect of the bias on the arc characteristic .....	71
Table 5.4 Deposition process parameters for DLC coatings .....	73
Table 6.1 Relationship of amplitude and percentage controlled in ultrasound generator .....	87
Table 7.1 Deposition process parameters of DLC coatings of $d_a/d_c = 3/1$ .....	116
Table 8.1 Variation of G position, FWHM and the $I_D/I_G$ ratio of DLC coatings deposited at $-250$ V with different $d_a/d_c$ .....	129
Table 8.2 Variation of G position, FWHM and the $I_D/I_G$ ratio of DLC coatings deposited at $-500$ V with different $d_a/d_c$ .....	132
Table 8.3 Variation of G position, FWHM and the $I_D/I_G$ ratio of DLC coatings deposited at $-750$ V with different $d_a/d_c$ .....	136
Table 8.4 Variation of G position, FWHM and the $I_D/I_G$ ratio of DLC coatings deposited at $-1000$ V with different $d_a/d_c$ .....	139

# 1. Introduction

## 1.1 The challenge

DLC coatings play a significant role in biomedical application, especially in the field of artificial hip joints. Recently, biomaterials have made great progress in medical device industry. Every year large numbers of artificial organs are implanted into the body, for example, heart valves, cardiovascular stents and hip joints. However, the implanted materials have to be suffering from corrosion in body environment and toxic reaction. For artificial hip joints, they not only must have to resist to corrosion, but also prevent a large amount of wear debris or particles generated which result in loosening of the prosthesis. Therefore, surface modification takes on an importance in the biomedical field. DLC coatings as a new material, due to their excellent mechanical, tribological and biological properties, receive much attention in load bearing joints.

Given its importance, first many methods have been developed for the deposition of DLC coatings in biomedical applications (see Section 2.3). And some basic problems have been reported and resolved in the literature. It is widely acknowledged that a material implanted into human body has to be biocompatible. The implant has to withstand corrosive environment and not cause inflammatory or any repulsive body reaction. All studies [1-7] about biocompatibility tests of DCL-coated surface demonstrated that there are no any adverse effects on body, and DLC-surfaces also have an excellent haemocompatibility. It is known that DLC shows a very low wear and also a low friction in atmosphere against most materials.

A key challenge in the field of artificial hip joints is the limited life expectancy of implants (see Section 3.1.2). Conventional artificial joints with tribological metal-on-polyethylene pairings are subject to wear and it is well recognized that the most serious consequences come from those wear debris in the range of  $0.3 \mu\text{m} \sim 10 \mu\text{m}$  due to the formation of polyethylene debris at a rate around  $10^{10}$  particulates per year [8, 9] (see Section 3.2.1). These wear debris is identified as the main factor limiting the lifetime of the implants. Especially these particulates are phagocytosed by macrophages resulting in granulomatosis lesions, osteolysis and bone resorption, causing pain and aseptic loosening of the prosthesis [9, 10]. To address this challenge, different DLC coatings have

---

been deposited using different techniques, including vacuum arc deposition. Nevertheless the traditional vacuum arc technique has its own drawback (macro particles (so-called droplets)). Although some approaches to resolve this problem are reported [9, 11-17], there are still problems presented in industry (e.g. increase the technological complexity and hence the cost of the coated products, reduce the deposition rate as well). Here a new design for vacuum arc (see Section 5.3.1) is used to try to resolve these problems. This new design is based on the transition between cathodic arc and anodic arc (see Section 2.3.1.).

What's more, the study of wear particles has attracted growing research interest, especially about the number of particles, as reported in the literatures [18-21]. However, up to now, little is known about the effect of the distribution of particle size.

The goal of DLC coatings deposited by new vacuum arc method is to study the wear particle size distribution, thus try to modify the size distribution. The natural questions are:

1. Can the drawback of deposition technique be resolved by using new method?
2. Is it possible to deposit DLC coatings on steel substrate by using new method?
3. Can the deposition parameters influence the properties of DLC coatings and how?
4. Is it possible to adjust or reduce the wear particle size by optimizing deposition parameters?

This dissertation answers these questions affirmatively by doing a large number of experiments.

## **1.2 Objectives and contributions**

This dissertation proposes a novel approach-design of wear particle size distribution regarded as an important step in DLC research, also as one of factors which effect the lifetime of implants.

In more detail, the main objectives of this research are:

1. Develop a new deposition method-based vacuum arc technique of DLC coatings.
2. Analyze the structure of DLC coatings.
3. Obtain the wear particles using tribological test.
4. Propose a new approach-design of wear particle size distribution.
5. Study the relationship between the wear particle size distribution and DLC coatings.

To accomplish these goals, the central thesis of this dissertation is that:

*For tackling the problem of traditional plasma filtering designs, it is possible to use a vacuum arc adjustable from anodic to cathodic operation mode to deposit the DLC coatings applied in the artificial hip joints, using this it is possible to modify the wear particle size distribution by varying the process parameters.*

In this dissertation the characterization and tribological properties of DLC coatings are outlined and evaluated, additionally, the importance of wear particles in hip joint replacements is involved. In particular, the study shows that:

1. A new vacuum arc deposition method of DLC decreases the industrial cost of the coated products, and increases the deposition rate comparing with traditional plasma filtering designs.
2. A new approach-design of wear particle size distribution in DLC research of artificial hip joint is an important step and must be considered seriously.
3. The probability of controlling the wear particle size distribution can be realized by optimizing the deposition parameters.

## **1.3 Research discussion**

This section unfolds the research problems of interest and discusses the research assumptions.

### **1.3.1 Problem statement**

Presently medical metal materials used as joints, for example stainless steels, cobalt alloys and titanium alloys, lead to metal ions diffused into the surrounding tissue [20-23]. DLC can be used as a barrier coating to prevent leaching of metallic ions into the body. Here P2000, one kind of biocompatible steel, is used as the substrate. So from deposition to analysis of DLC coatings, some problems must be considered firstly.

In this research context, there are three major problems to be tackled.

1. How to deposit DLC on P2000 by vacuum arc because of bad adhesion of DLC on P2000.
2. How to get and analyze wear particles?

---

3. Whether wear particles distribution can be influenced and tuned by adjusting the deposition parameters or not?

- **Bad adhesion of DLC on P2000**

The first key issue in deposition DLC coating on P2000 steel is the adhesion. To improve adhesion of DLC on substrate, interface layer is required. According to the previous work in ref. [25], by comparing with chromium, titanium as interface layer was used. Actually although the adhesion is not the point in this thesis, a brief introduction about adhesion and interface layers in biomedical materials can be seen in Chapter 4 and the adhesion of DLC coatings to P2000 substrate is considered and evaluated. The requirement addressed here is: *How to improve the adhesion and how to be influenced by deposition parameters?*

- **Tribological test setup**

The tribological properties of DLC coating not only depend on the DLC coating itself, but also on the whole tribological surroundings, including setup and lubricant. Moreover in order to simulate like in vivo, the appropriate parameters of wear tests must be chosen, e.g. normal force and velocity, which also affect the wear particles. In this work, the size distribution of wear particles is mainly from DLC coatings, not from interface layer or substrate. In addition the concentration of wear particles is related to the tribological surroundings, which is very important for getting the particle size distribution. The traditional wear testing setup is disc-on-pin. The difficulty addressed here is: *Is it possible to get enough particles using traditional disc-on-pin setup? How to choose appropriate tribological parameters?*

- **Particle size distribution analysis**

As described in ref. [25], in particle size distribution, every possible physical principle has been used to determine these distributions and the main problem is their unknown absolute accuracy. Anyway, the characteristics of particles are related to the chosen types and measures of quantity. Here the volume distribution is chosen to characterize the size of particles. Thus the concentration of particles is required. As discussed above, it's the question whether enough particles can be generated during tribological test or not. One problem encountered is: *How to collect the particles?* Maybe there are many problems which must be faced resulting from particle size effect, e.g. particles adsorption and particles aggregation.

### 1.3.2 Assumptions and their motivation

According to three main problems maybe encountered during the experiments, there are three central assumptions.

- **Why Ti as interface layer between DLC and P2000?**

As is known, when one material is implanted into the body it must be biocompatible. The biocompatibility of Ti has been confirmed in ref. [26], furthermore, R. Hauert et al. [27] report that the adsorption of different proteins can be altered by the content of Ti. What's more, Ti can inhibit the differentiation of bone marrow cells into bone resorbing cells [28,29]. Here Ti as interface layer is deposited on P2000-steel substrate by vacuum arc (see Section 5.1 for clarification).

- **Disc-on-pin and disc-on-disc setup**

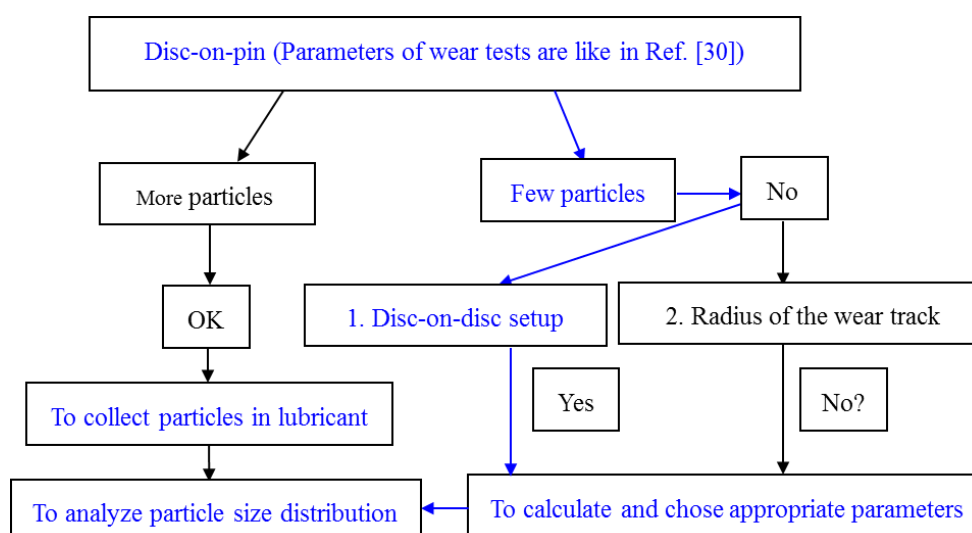


Figure 1.1 Tribological process diagram

When the traditional disc-on-pin setup is used, the parameters of wear tests are the same as described in ref. [30]. In tribological test, the flow graph shown in Fig. 1.1 depicts tribological process and solutions of problems discussed above. In this part, it is assumed that more particles can be generated using disc-on-pin setup in tribological test. If few particles are produced using disc-on-pin, it will be difficult to analyze the particle size distribution due to low concentration of particles. For this problem, there are two solutions: one is to use disc-on-disc setup, and another is to change the radius of the wear track.

---

- **Collection and analysis of wear particles**

In hip joint, the synovial fluid as a lubricant plays an important role to reduce friction between bones each other particularly. Therefore, in the tribological test lubricant must be considered. According to ref. [31], it is known that low wear seems to be not related to the protein which is present or absent in the lubricant. Thus, it is supposed that deionized water as lubricant will not influence the results of wear particle size distribution.

Moreover, in order to prevent from particles adsorption, the container made of Polytetrafluoroethylene (PTFE) called no-stick coating is used to collect the wear particles due to the lowest surface energy. If the particles float on the lubricant resulting from surface tension, not in suspension, they are not suitable for analysis of the size distribution. For reducing surface tension, the surface active agent can be used. When nano-particles are generated, they easy cluster together, appropriate ultrasonic can make them separate.

## **1.4 Thesis organization**

The dissertation is organized as follows:

Chapter 2 gives an introduction to the DLC coatings background. In the first part, the structure and properties of DLC coatings are presented. In the second part, applications of DLC in several fields are reviewed, particularly, in the biomedical applications. The third part describes the deposition techniques of DLC coatings, especially the vacuum arc deposition.

Chapter 3 gives an introduction to the hip joint replacements background, which is the main application in this dissertation. Wear particles as the main factor limiting the lifetime of artificial hip joints are presented. It also gives the background of the different kinds of artificial hip joint. Additionally it reviews the adhesion and interface layers in biomedical materials, although this part is not the main content. In this chapter failure mechanisms of DLC coatings in hip joints are also introduced.

Chapter 4 describes the characterization and tribological evaluation of DLC coatings, including the morphology and structure, as well as tribological properties. It also proposes the evaluation of adhesion by cavitation erosion test. What's more, the particle size distribution analysis is the main point in this thesis.

Chapter 5 introduces the deposition of titanium interface layer on P2000 by cathodic arc evaporation, and the deposition of DLC coatings by new vacuum arc equipment which the arc mode can be changed by adjusting the anode-cathode diameter ratio. The relationship between deposition pressure and arc voltage, as well as current is studied.

Chapter 6, 7, 8 and 9 discuss the experimental results. Chapter 6 presents how to choose the suitable parameters of analysis of Raman spectra and wear test for DLC coating deposited by new method. Chapter 7 and 8 devote to the study of how different parameter influences the particle size distribution of DLC coatings. Chapter 9 investigates the adhesion of DLC coating by cavitation erosion test, and discusses how the deposition parameters affect the adhesion.

Finally Chapter 10 draws conclusions on the accomplishments in this dissertation. The limitation in this work is also presented. In addition, several future researches are suggested.

## **References**

- [1] L.A. Thompson, F.C. Law, N. Rushton, J. Franks, Biocompatibility of diamond-like carbon coating, *Biomaterials* 12 (1) (1991) 37-40.
- [2] M. Allen, F. Law, N. Rushton, The effects of diamond-like carbon coatings on macrophages, fibroblasts and osteoblast-like cells in vitro, *Clinical Materials* 17 (1994) 1-10.
- [3] R.S. Butter, A.H. Lettington, Diamond-like carbon for biomedical applications (review), *Journal of Chemical Vapor Deposition* 3 (3) (1995) 182-192.
- [4] H.J. Steffen, J. Schmidt, A. Gonzalez-Elipe, Biocompatible surfaces by immobilization of heparin on diamond-like carbon films deposited on various substrates, *Surface and Interface Analysis* 29 (2000) 386-391.
- [5] M. Allen, B. Myer, N. Rushton, In vitro and in vivo investigations into the biocompatibility of diamond-like carbon (DLC) coatings for orthopedic applications, *Journal of Biomedical Materials Research* 58 (2001) 319-328.
- [6] M. Mohanty, T.V. Anikumar, P.V. Mohanan, C.V. Muraleedharan, G.S. Bhuvaneshwar, F. Derangere, Y. Sampaer, R. Suryanarayanan, Long term tissue response to titanium coated with diamond like carbon, *Biomolecular Engineering* 19 (2-6) (2002) 125-128.
- [7] A. Singh, G. Ehteshami, S. Massia, J. He, R.G. Storer, G. Raupp, Glial cell and fibroblast cytotoxicity study on plasma-deposited diamond-like carbon coatings, *Biomaterials* 24 (28) (2003) 5083-5089.
- [8] T.R. Green, J. Fisher, M. Stone, B.M. Wroblewski, E. Ingham, Polyethylene particles of a 'critical size' are necessary for the induction of cytokines by macrophages in vitro, *Biomaterials* 19 (1998) 2297-3202.
- [9] G. Dearnaley, J.H. Arps, Biomedical applications of diamond-like carbon (DLC) coatings: A review, *Surface and Coatings Technology* 200 (7) (2005) 2518-2524.

- 
- [10] R. Hauert, DLC films in biomedical applications, *Tribology of Diamond-Like Carbon Films* (2008) 494-509.
- [11] H.-S. Zhang, J.I. Endrino, A. Aders, Comparative surface and nano-tribological characteristics of nanocomposite diamond-like carbon thin films doped by silver, *Applied Surface Science* 255 (2008) 2551-2556.
- [12] S. Xu, B.K. Tay, H.S. Tan, L. Zhong, Y.Q. Tu, S.R.F. Silva, W.I. Milne, Properties of carbon ion deposited tetrahedral amorphous carbon films as a function of ion energy, *Journal of Applied Physics* 79 (1996) 7234-7240.
- [13] B.F. Coll, D.M. Sanders, Design of vacuum arc-based sources, *Surface and Coatings Technology* 81 (1) (1996) 42-51.
- [14] D.A. Karpov, Cathodic arc sources and macroparticle filtering, *Surface and Coatings Technology* 96 (1997) 22-33.
- [15] R.N. Tarrant, M.M.M. Bilek, T.W.H. Oates, J. Pigott, D.R. McKenzie, Influence of gas flow rate and entry point on ion charge, ion counts and ion energy distribution in a filtered cathodic arc, *Surface and Coatings Technology* 156 (2002) 110-114.
- [16] S. Anders, A. Anders, M.R. Dickinson, R.A. MacGill, I.G. Brown, S-shaped magnetic macroparticle filter for cathodic arc deposition, *IEEE Transactions on Plasma Science* 25 (1997) 670-674.
- [17] A.W. Baouchi, A.J. Perry, A study of the macroparticle distribution in cathodic arc evaporated TiN films, *Surface and Coatings Technology* 49 (1991) 253-257.
- [18] D.W. Murray, N. Rushton, Macrophages stimulate bone-resorption when they phagocytose particles, *Journal of Bone and Joint Surgery-British* 72-B (1990) 988-992.
- [19] S. Affatato, M. Frigo, A. Toni, An in vitro investigation of diamond-like carbon as a femoral head coating, *Journal of Biomedical Materials Research* 53 (3) (2000) 221-226.
- [20] A.G. Cobb, T.P. Schmalzreid, The clinical significance of metal ion release from cobalt-chromium metal-on-metal hip joint arthroplasty, *Proceedings of the IMechE Part H: Journal of Engineering in Medicine* 220 (2) (2006) 385-398.
- [21] F.A. Müller, M. Hagymási, P. Greil, G. Zeiler, A. Schuh, Transfer of metallic debris after dislocation of ceramic femoral heads in hip prostheses, *Arch Orthop Trauma Surg* 126 (2006) 174-180.
- [22] R. Lappalainen, S.S. Santavirta, Potential of coatings in total hip replacement, *Clinical Orthopaedics & Related Research* 430 (2005) 72-79.
- [23] R. Lappalainen, M. Selenius, A. Anttila, Y.T. Konttinen, S.S. Santavirta, Reduction of wear in total hip replacement prostheses by amorphous diamond coatings, *Journal of Biomedical Materials Research Part B: Applied Biomaterials* 66B (2003) 410-413.
- [24] B. Stamm, B. Kizil, O. Filipov, S. Reuter, I. Erdmann, F. Deuerler, D. Krix, K. Huba, H. Nienhaus, V. Buck, Adjustment of wear particle size distribution of DLC coatings for tribological metal-on-metal pairing in artificial hip joints, *Mat.-wiss. u. Werkstofftech* 40 (1-2) (2009) 98-100.
- [25] K. Leschonski, Representation and evaluation of particle size analysis data, *Part. Charact.* 1(1984) 89-95.
- [26] S.G. Steinemann, S.M. Perren, Titanium Alloys as Metallic Biomaterials, in *Proc. of the 5th World Conference on Titanium* 2 (1984) 1327-1334.

- [27] R. Hauert, L. Knoblauch-Meyer, G. Francz, A. Schroeder, E. Wintermantel, Tailored a-C:H coatings by nanostructuring and alloying, *Surface and Coatings Technology* 120-121 (1999) 291-296.
- [28] A. Schroeder, G. Francz, A. Bruinink, R. Hauert, J. Mayer, E. Wintermantel, Titanium containing amorphous hydrogenated carbon films (a-C: H/Ti): surface analysis and evaluation of cellular reactions using bone marrow cell cultures in vitro, *Biomaterials* 21 (2000) 449-456.
- [29] G. Francz, A. Schroeder, R. Hauert, Surface analysis and bioreactions of Ti-and V-containing a-C: H, *Surface and Interface Analysis* 28 (1999) 3-7.
- [30] S. Breuter, B. Weßkamp, R. Bischer, A. Fischer, B. Barden, F. Löffler, V. Buck, Correlation of structural properties of commercial DLC-coatings to their tribological performance in biomedical applications, *Wear* 261 (2006) 419-425.
- [31] T. Ahlroos, V. Saikko, Wear of prosthetic joint materials in various lubricants, *Wear* 211 (1997) 113-119.

---

## 2. DLC coatings background

Diamond-like carbon (DLC) is a metastable form of amorphous carbon materials that displays some of unique structure and properties of diamond and graphite.

### 2.1 Structure and properties of DLC coatings

#### 2.1.1 Structure of DLC coatings

As is well known, carbon can form many allotropes due to its valence and has three hybridizations:  $sp^3$ ,  $sp^2$  and  $sp^1$  shown in Fig. 2.1 [1].

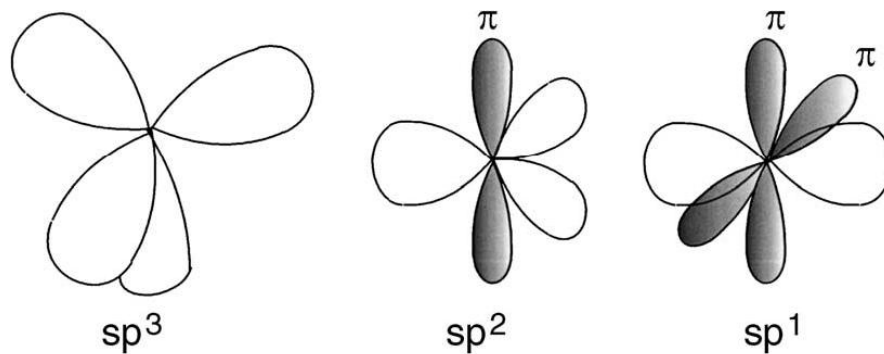


Figure 2.1 The  $sp^3$ ,  $sp^2$ ,  $sp^1$  hybridised bonding [1]

The best known are diamond, graphite and amorphous carbon which correspond to the structures as shown in Fig. 2.2 [2-4]. Diamond has a cubic crystal structure with a fourfold  $sp^3$  covalent bond structure. In the  $sp^3$  configuration, as in diamond, a carbon atom's four valence electrons will arrange themselves in three dimensional spaces to get as far apart as possible, which make a strong  $\sigma$  bond to an adjacent atom, giving diamond its great strength. Graphite has a hexagonal lattice structure with  $sp^2$ -bonded two-dimensional planes interconnected by weak forces (Fig.2.2 b). In the three-fold coordinated  $sp^2$  configuration as in graphite, three of the four valence electrons enter trigonally directed  $sp^2$  orbitals, which form  $\sigma$  bonds in a plane. The fourth electron of the  $sp^2$  atom lies in a  $p\pi$  orbital, which lies normal to the  $\sigma$  bonding plane. This  $\pi$  orbital forms a weaker  $\pi$  bond with a  $\pi$  orbital on one or more neighboring atoms. In the  $sp^1$  configuration, two of the four valence electrons enter  $\sigma$  orbitals, each forming an  $\sigma$  bond directed along the  $\pm x$ -axis, and the other two electrons enter  $p\pi$  orbital in the  $y$  and  $z$  directions. Usually, an

amorphous carbon can have any mixture of  $sp^3$ ,  $sp^2$ , and even  $sp^1$  sites, with the possible presence of up to 60 at.% hydrogen [5].

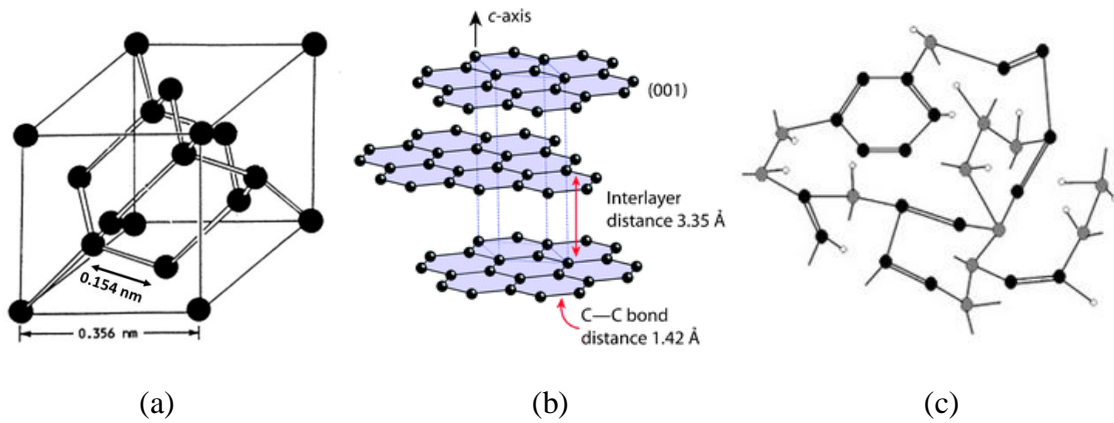


Figure 2.2 Carbon structure in (a) diamond, (b) graphite and (c) amorphous diamond-like carbon [2-4]

DLC, as one kind of amorphous carbon material, has no long range order just short and medium range order. It contains mainly  $sp^3$  and  $sp^2$  both types of bonding with  $sp^2$ -bonded graphite-like clusters embedded in an amorphous  $sp^3$ -bonded carbon matrix and clearly it is harder and more brittle if the  $sp^3/sp^2$  ratio is high [6]. In general, amorphous carbon is often abbreviated to a-C for general amorphous carbon, a-C:H for hydrogenated amorphous carbon, or to ta-C for tetrahedral amorphous carbon which has the maximum  $sp^3$  content. According to the  $sp^3/sp^2$  ratio, various forms of DLC can be shown in Fig. 2.3 [7].

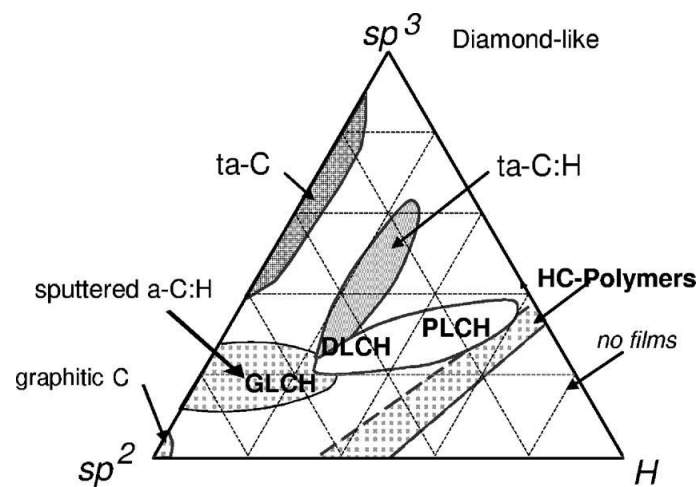


Figure 2.3 Ternary phase diagram for various DLC coatings with respect to  $sp^3$ ,  $sp^2$  and hydrogen contents [7]

It is shown that the hydrogenated forms of amorphous carbon can be classified into four types: polymer-like a-C:H (PLCH), diamond-like a-C:H (DLCH), hydrogenated tetrahedral amorphous carbon (ta-C:H), and graphite-like a-C:H (GLCH) with the H content of 40-60 at.%, 20-40 at.%, 25-30 at.% and less than 20 at.%, respectively by C. Casiraghi et al. [8] in Fig. 2.3.

The main effect of H in a-C:H is to change its C-C network by converting C=C groups into  $sp^3$  bonded CH-CH groups rather than to increase the ratio of C-C bonds compared to a-C of similar  $sp^3$  content. Therefore, most  $sp^3$  sites are hydrogen terminated which can cause the coatings with the highest  $sp^3$  content are soft and low-density, like PLCH [7, 9-10]. DLCH coatings with intermediate H content, although they have lower overall  $sp^3$  content compared to PLCH, have more C-C  $sp^3$  bonds so that the density is very high. Ta-C:H coatings in many literatures are defined as a class of DLCH. Actually ta-C:Hs are really a different category of a-C:H coatings at a fixed H content of 25-30 at.% due to the highest  $sp^3$  content (up to 70%) and higher density (up to 2.4 g/cm<sup>3</sup>) [8,11]. For GLCH coatings  $sp^2$  bonding dominates at low H content.  $Sp^2$  sites exist in a-C:H as rings as well as chains. In addition the  $sp^2$  cluster size is decreased, with increasing H content, and the band gap is increased [5].

As can be seen the structure of amorphous carbon plays an important role in the properties itself.

## 2.1.2 Properties of DLC coatings

Table 2.1 Comparison of major properties of amorphous carbons with diamond, graphite, ta-C and polyethylene [7]

	$sp^3$ (%)	H (at. %)	Density (g/cm <sup>3</sup> )	Gap (eV)	Hardness (GPa)	Refe.
Diamond	100	0	3.515	55	100	[12]
Graphite	0	0	2.267	0		[13]
ta-C	80-88	0	3.1	2.5	80	[14-16]
a-C:H hard	40	30-40	1.6-2.2	1.1-1.7	10-20	[9]
a-C:H soft	60	40-50	1.2-1.6	1.7-4	<10	[9]
ta-C:H	70	30	2.4	2.0-2.5	50	[17]
Polyethylene	100	67	0.92	6	0.01	[18]

DLC is intermediate between diamond and graphite. The properties of DLC resemble, but do not duplicate those of natural diamond. Typical properties of the various forms of DLC are compared to diamond and graphite in Table 2.1 [7].

As Table 2.1 shows, the properties of DLC coatings can vary with tailoring  $sp^3$  content according to the different demand: soft films to hard films, semimetal to insulator, and so on. DLC coating can possess some extreme properties similar to diamond, especially excellent mechanical properties such as high hardness, high elastic modulus and chemical inertness. Additionally it has low friction coefficient and low wear. Owing to its amorphous structure, DLC has no grain boundaries, which allows it to be the smoother material. Besides of these properties, there are the other excellent properties, for example, high electrical resistance and a high optical transparency. The index of refraction is dependent on the concentration of bound hydrogen and not total hydrogen content in the film [19]. As is well known, the growth temperature of diamond as a coating material is high. By contrast, DLC coating can be deposited at the room temperature and has rather low costs.

Furthermore, DLC coatings are not only chemically inert, but also biocompatible and haemocompatible [20-22]. Comparing with diamond, these advantages and outstanding properties make DLC coatings attractive for many applications and give DLC its wide range of applications noted below.

## References

- [1] J. Robertson, Amorphous carbon, *Advances in Physics* 35 (4) (1986) 317-374.
- [2] B. Bhushan, Chemical, mechanical and tribological characterization of ultrathin and hard amorphous carbon coatings as thin as 3.5 nm: recent developments, *Diamond and Related Materials* 8 (11) (1999) 1985-2015.
- [3] J.C. Tan, A.K. Cheetham, Mechanical properties of hybrid inorganic-organic framework materials: establishing fundamental structure-property relationships, *Chem. Soc. Rev.* 40 (2011) 1059-1080.
- [4] E. Staryga, G.W. Bak, Relation between physical structure and electrical properties of diamond-like carbon thin films, *Diamond and Related Materials* 14 (1) (2005) 23-34.
- [5] A.C. Ferrari, J. Robertson, Interpretation of Raman spectra of disordered and amorphous carbon, *Physical Review B* 61 (2000) 14095-14107.

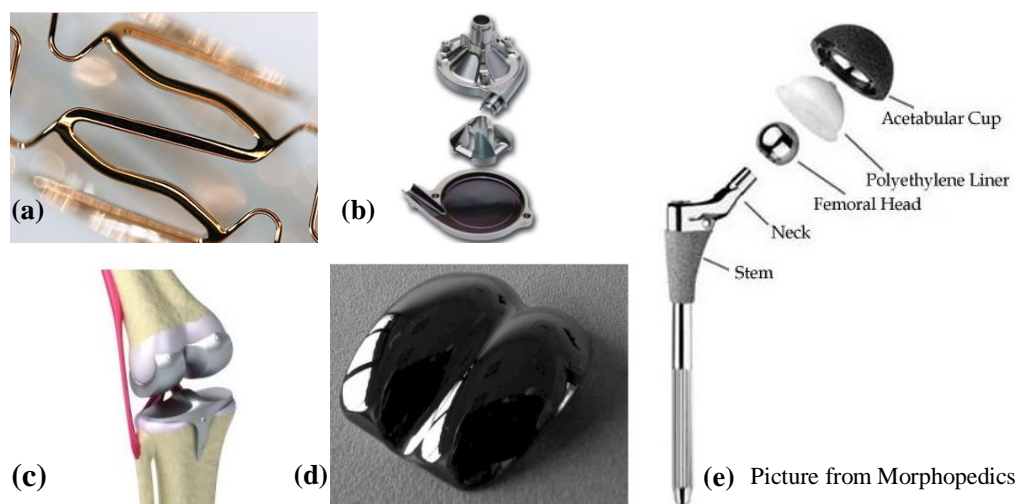
- 
- [6] G. Dearnaley, J.H. Arps, Biomedical applications of diamond-like carbon (DLC) coatings: A review, *Surface and Coatings Technology* 200 (7) (2005) 2518-2524.
- [7] J. Robertson, Diamond-like amorphous carbon, *Materials Science and Engineering R Reports: A Review Journal* 37 (2002) 129-281.
- [8] C. Casiraghi, A.C. Ferrari, J. Robertson, Raman spectroscopy of hydrogenated amorphous carbons, *Physical Review B* 73 (2005) 085401 1-14.
- [9] P. Koidl, C. Wagner, B. Dischler, J. Wagner, M. Ramsteiner, Plasma Deposition, Properties and Structure of Amorphous Hydrogenated Carbon Films, *Materials Science Forum* 52-53 (1990) 41-70.
- [10] J. Ristein, R. T. Stief, L. Ley, W. Beyer, A comparative analysis of a-C:H by infrared spectroscopy and mass selected thermal effusion, *Journal of Applied Physics* 84 (7) (1998) 3836-3847.
- [11] N.A. Morrison, S.E. Rodil, A.C. Ferrari, J. Robertson, W. I. Milne, High rate deposition of ta-C:H using an electron cyclotron wave resonance plasma source, *Thin Solid Films* 337 (1999) 71-73.
- [12] J.E. Field, *The properties of Diamond*, Academic Press, London, 1979.
- [13] B.T. Kelly, *Physics of Graphite*, Applied Science Publishers, London, 1981.
- [14] D.R. McKenzie, Tetrahedral bonding in amorphous carbon, *Reports on Progress in Physics* 59 (12) (1996) 1611-1664.
- [15] P.J. Fallon, V.S. Veerasamy, C.A. Davis, J. Robertson, G.A. Amaratunga, W.I. Milne, J. Koskinen, Properties of filtered-ion-beam-deposited diamondlike carbon as a function of ion energy, *Physical Review B* 48 (7) (1993) 4777-4782.
- [16] G.M. Pharr, D.L. Callahan, S.D. McAdams, T.Y. Tsui, S. Anders, A. Anders, J.W. Ager, I.G. Brown, C.S. Bhatia, S.R.P. Silva, J. Robertson, Hardness, elastic modulus, and structure of very hard carbon films produced by cathodic-arc deposition with substrate pulse biasing, *Applied Physics Letters* 68 (6) (1996) 779-781.
- [17] M. Weiler, S. Sattel, K. Jung, H. Ehrhardt, V.S. Veerasamy, J. Robertson, High tetrahedral, diamond-like amorphous hydrogenated carbon prepared from a plasma beam source, *Applied Physic Letters* 64 (21) (1994) 2797-2799.
- [18] M.F. Ashby, D.R.H. Jones, *Engineering Materials: An introduction to their properties and applications*, Pergamon Press, Oxford, England (1980).
- [19] A. Grill, V. Patel, Diamondlike carbon deposited by DC PACVD, *Diamond Films and Technology* 1 (1992) 219-233.
- [20] L.A. Thomson, F.C. Law, N. Rushton, J. Franks, Biocompatibility of diamond-like carbon coating, *Biomaterials* 12 (1) (1991) 37-40.
- [21] M. Allen, F. Law, N. Rushton, The effects of diamond-like carbon coatings on macrophages, fibroblasts and osteoblast-like cells in vitro, *Clinical Materials* 17 (1994) 1-10.
- [22] I. Dion, X. Roques, C. Baquey, E. Baudet, B.B. Cathalinat, N. More, Hemocompatibility of diamond-like carbon coating, *Biomedical Materials and Engineering* 3 (1) (1993) 51-55.

## 2.2 Applications of DLC coatings

As described in chapter 2.1, there is such a wide variety of different DLC coatings due to different structures so that they can have the different physical and chemical properties, which implies that DLC coatings are nowadays being used in various fields of industry. Firstly DLC coatings for the medical application will be discussed, because DLC coatings deposited in this work are mainly applied in the artificial hip joints of the biomedical field. Then the use in other fields will follow, for example, automotive, aerospace, electromagnetics, as well as optics and acoustics.

### 2.2.1 Biomedical applications

Diamond-like carbon (DLC), known as amorphous carbon, is a class of materials with excellent mechanical, tribological and biological properties, which makes them particularly attractive for biomedical applications, as shown in Fig. 2.4.



(a) Copyright © 2013 by Japan Stent Technology Europe GmbH. All rights reserved.

(b)(c) Copyright © 2013 by Nelson Publishing, Inc. All rights reserved.

Figure 2.4 DLC coated products (a) Stent [1] (b) Left ventricular assist device heart pump [2] (c) artificial joint [2] (d) Ankle joint [3] (e) Hip Joint [4]

#### (1) Bio- and haemo-compatibility

As is known, when one material is implanted into the human body, it has to be

---

biocompatible. So the implant of DLC coating used in biomedical applications has to withstand the corrosive environment and not cause any adverse effects on attached cells. That means, DLC coating must be biocompatible, which has been confirmed in vitro and in vivo in many papers [5-11]. Additionally, the biocompatibility of DLC can be improved from the viewpoint of its atomic structure (by varying the  $sp^2/sp^3$  ratio of carbon) and composition (by introduction of hetero-atoms such as Si, F, Ca and P to DLC) [12-15], as well as introducing both anodic and cathodic functional group to a DLC surface [16-18]. The haemo-compatible nature of DLC coating, not only its biocompatible property, is also reported in ref. [19-21], which makes DLC coatings available to be used for implants in direct contact with blood, for example artificial heart valves, blood pumps and stents. What's more, due to DLC's outstanding tribological properties, it is also widely used to reduce wear in the load bearing joints instead of the ultra-high molecular weight polyethylene (UHMWPE).

#### (2) Blood contacting applications

If one implant is in contact with blood directly, a key issue is to prevent thrombus formation which depends on the surface of the implant [3]. Due to the good haemo-compatibility and excellent tribological behavior of DLC coatings, several papers report in vitro that it may be a better coating for cardiovascular purposes because of the ability to suppress thrombus [7, 20]. In order to adjust the surface chemical behavior of DLC, the different elements are introduced into the DLC coatings, e.g. Si-DLC [21], Ti-DLC [19] and Cr-DLC [22]. These elements must also be biocompatible. Only few papers in vivo present the results of DLC-coated implants: stainless steel stents [23-24], blood pumps (made by Sun Medical Technology Research Corporation, Nagano, Japan) [25]. In addition, a few companies have produced some DLC-coated implants and make them available commercially, e.g. the Cardio Carbon Company, the Sorin Biomedica company and the company PHYTLS. Up to now, the blood-contacted applications are still in the state of development.

#### (3) Load bearing joints

DLC coating because of its low wear and low friction coefficient is used in load bearing joints. There are many reports about using DLC-coated femoral heads against UHMWPE implanted cups [26-35]. Metal-metal joints with one or both sides coated with DLC are also

studied in the laboratory [28, 36-37].

In the wear of DLC coated joint balls sliding against UHMWPE using pin-on-disk setup, the liquid lubricant used in tribological test has a crucial effect on the friction and wear values. With distilled water as a lubricant [26, 30-31], the wear of UHMWPE can be reduced by a factor of five or six, even by a factor of 10-100 in 1 wt. % NaCl water [27-29]. That's because the DLC is able to form a transfer layer on the softer counterpart when sliding in distilled water to protect it from wear [27]. By contrast, when the simulated body fluid or diluted calf serum is used in tribological test, there is no significant difference in the wear of the UHMWPE between the coated and the uncoated samples [32-35]. The different proteins like biomolecules (especially phospholipids, glycoproteins, albumin and hyaluronic acid), which are adsorbed on the surface of articulation, strongly influence the tribological behavior in the joints [38-39]. There is no transfer layer formed on the UHMWPE when sliding against DLC in biological media so that the UHMWPE wear could not be lowered [40]. Moreover, the lubricant is also playing a key role in the type of wear particles produced [38-39, 41].

However, according to ref. [24, 36] in metal/metal hip joints with both sides DLC coatings, very low wear rates below  $10^{-4}$  mm<sup>3</sup>/ year and  $10^{-3}$  to  $10^{-4}$  mm<sup>3</sup>/year (corresponding to a factor of about 10,000) can be obtained when it is tested with a hip joint simulator using bovine serum and NaCl(aq) as a lubricant, respectively. Furthermore, a 2- $\mu$ m-thick DLC (a-C:H)-coated steel ball sliding against a flat steel plate is tested by Shi et al. with bovine serum as lubricant and the wear rate is reduced by a factor of about 100 [37]. The results indicate that when DLC is articulating against DLC, a transfer layer may not be a main requirement for low wear [41]. At present, there is no in vivo experiment on DLC coated load bearing implants found in the literature. Comparing with other coatings, DLC because of its outstanding properties is a promising candidate in biomedical applications. Therefore much research work about DLC coatings is needed to do, especially some about DLC coated load bearing implants.

### 2.2.2 Other applications

Besides biomedical applications of DLC coatings as discussed above, DLC films are also

widely applied in other fields, for example cutting tools as protective coatings and composite additives, and thermal devices or optical devices and coatings, as well as electronic devices.

(1) Mechanical applications

Due to high hardness, low friction coefficient and good wear resistance, hard coatings, especially diamond-like carbon are widely applied in different mechanical applications reported in many literatures [42-43]. For example there are cutting tools as a protective coating [44-47], and automotive industry [48-49], bearings [50-51], gears [52-53], piston-rings and pins [54-55] and other components [56-57], as shown in Fig. 2.5 [58].



Figure 2.5 DLC coated products (a) End mill (b) Step drill (c) Engine piston (d) Gears (e) Engine tappets [58]

(2) Electromagnetic applications

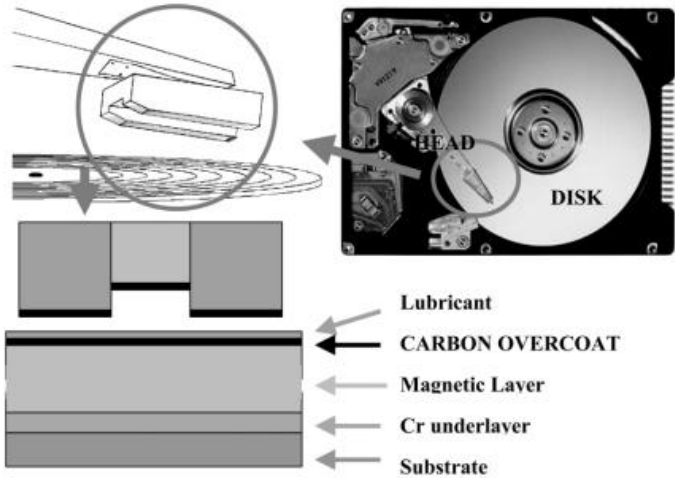


Figure 2.6 Hard disk architecture [59]

DLC coating is used as the protective layer in magnetic hard-disk drives due to its extremely smooth, continuous and chemically inert properties [59]. As is well known, the read/write head consists of many layers of thin films. Data are stored in a magnetic layer of Co-Cr-Pt alloy thin film [60-61]. A protective layer of DLC coating is applied over the Co layer, as shown in Fig. 2.6. One protective layer with ultra-smooth surface is required for smaller magnetic spacing as the storage density is increasing at a very rapid rate [46-47, 62]. Meanwhile, DLC coatings are also very attractive for field emission or doping applications [63-64].

### (3) Optical applications



Copyright © 2013 Diarkis LLC.

Figure 2.7 DLC coated IRST Dome [68]

Due to their IR transparency, DLC films can also be utilized in optical applications, such as the optical storage media as protective layers like in magnetic storage, and IR optics at a wavelength of 8-13  $\mu\text{m}$  made of Ge, ZnS, ZnSe [65-67]. DLC coated IRST Dome shows significant pitting (Fig. 2.7) [68]. In addition, DLCs are applied not only as protective optical coatings, but also as fabrication of optical components because DLCs are easily patterned by etching in oxygen plasmas [65].

### (4) Acoustical applications

High ratio of elastic modulus to mass density of DLC coating has also attracted much attention for the acoustical applications [69] using high acoustic wave velocity, e.g. speaker diaphragm and surface acoustic wave devices, as shown in Fig. 2.8. The DLC film with much superior elasticity and high surface propagating velocity can improve the characteristics of the conventional surface acoustic wave (SAW) [70].



Figure 2.8 Coaxial speaker (DLC-coated titanium centre cap) [71]

## References

- [1] [http://www.jstentech.de/eng/momo\\_dlc.html](http://www.jstentech.de/eng/momo_dlc.html) (2013.10.15)
- [2] <http://www.modernapplicationsnews.com/web/archives.php>  
Distributed by Pioneer Electronic Asia Centre Pte Ltd  
Diamond-like carbon biocompatible coatings ideal for medical applications,  
Modern Applications eNews 6(3) (2012).
- [3] R. Hauert, A review of modified DLC coatings for biological applications, *Diamond and Related Materials* 12 (2003) 583-589.
- [4] <http://morphopedics.wikidot.com/total-hip-arthroplasty> (2013.10.15)
- [5] L.A. Thompson, F.C. Law, N. Rushton, J. Franks, Biocompatibility of diamond-like carbon coating, *Biomaterials* 12 (1) (1991) 37-40.
- [6] M. Allen, F. Law, N. Rushton, The effects of diamond-like carbon coatings on macrophages, fibroblasts and osteoblast-like cells in vitro, *Clinical Materials* 17 (1994) 1-10.
- [7] R.S. Butter, A.H. Lettington, Diamond-like carbon for biomedical applications (review), *Journal of Chemical Vapor Deposition* 3 (3) (1995) 182-192.
- [8] H.J. Steffen, J. Schmidt, A. Gonzalez-Elipse, Biocompatible surfaces by immobilization of heparin on diamond-like carbon films deposited on various substrates, *Surface and Interface Analysis* 29 (2000) 386-391.
- [9] M. Allen, B. Myer, N. Rushton, In vitro and in vivo investigations into the biocompatibility of diamond-like carbon (DLC) coatings for orthopedic applications, *Journal of Biomedical Materials Research* 58 (2001) 319-328.
- [10] M. Mohanty, T.V. Anikumar, P.V. Mohanan, C.V. Muraleedharan, G.S. Bhuvaneshwar, F. Derangere, Y. Sampur, R. Suryanarayanan, Long term tissue response to titanium coated with diamond like carbon, *Biomolecular Engineering* 19 (2-6) (2002) 125-128.

- [11] A. Singh, G. Ehteshami, S. Massia, J. He, R.G. Storer, G. Raupp, Glial cell and fibroblast cytotoxicity study on plasma-deposited diamond-like carbon coatings, *Biomaterials* 24 (28) (2003) 5083-5089.
- [12] T.I.T. Okpalugo, A.A. Ogwu, P.D. Maguire, J.A.D. McLaughlin, D.G. Hirst, In-vitro blood compatibility of a-C: H: Si and a-C: H thin films, *Diamond and Related Materials* 13 (2004) 1088-1092.
- [13] S.C.H. Kwok, P.C.T. Ha, D.R. McKenzie, M.M.M. Bilek, P.K. Chu, Biocompatibility of calcium and phosphorus doped diamond-like carbon thin films synthesized by plasma immersion ion implantation and deposition, *Diamond and Related Materials* 15 (2006) 893-897.
- [14] T. Hasebe, A. Shimada, T. Suzuki, Y. Matsuoka, T. Saito, S. Yohena, A. Kamijo, N. Shiraga, M. Higuchi, K. Kimura, H. Yoshimura, S. Kuribayashi, Fluorinated diamond-like carbon as antithrombogenic coating for blood-contacting devices, *Journal of Biomedical Materials Research A* 76 (1) (2006) 86-94.
- [15] T. Hasebe, S. Yohena, A. Kamijo, Y. Okazaki, A. Hotta, K. Takahashi, T. Suzuki, Fluorine doping into diamond-like carbon coatings inhibits protein adsorption and platelet activation, *Journal of Biomedical Materials Research A* 83 (4) (2007) 1192-1199.
- [16] A. Mochizuki, T. Ogawa, K. Okamoto, T. Nakatani, Y. Nitta, Blood compatibility of gas plasma-treated diamond-like carbon surface-Effect of physicochemical properties of DLC surface on blood compatibility, *Materials Science and Engineering C* 31 (2011) 567-573.
- [17] T. Nakatani, K. Okamoto, Y. Nitta, A. Mochizuki, H. Hoshi, A. Homma, Surface engineering by plasma techniques of DLC for medical materials and Blood-compatibility, *Journal of Photopolymer Science and Technology* 21 (2) (2008) 225-230.
- [18] Y. Nitta, K. Okamoto, T. Nakatani, H. Hoshi, A. Homma, E. Tatsumi, Y. Taenaka, Diamond-like carbon thin film with controlled zeta potential for medical material application, *Diamond and Related Materials* 17 (11) (2008) 1972-1976.
- [19] R. Butter, M. Allen, L. Chandra, A.H. Lettington, R. Rushton, In vitro studies of DLC coatings with silicon intermediate layer, *Diamond and Related Materials* 4 (1995) 857-861.
- [20] M.I. Jones, I.R. McColl, D.M. Grant, K.G. Parker, T.L. Parker, Haemocompatibility of DLC and TiC/TiN interlayers on titanium, *Diamond and Related Materials* 8 (1999) 457-462.
- [21] T.I.T. Okpalugo, A.A. Ogwu, P.D. Maguire, J.A.D. McLaughlin, Adhesion of diamond to steel and copper with titanium interlayers, *Diamond and Related Materials* 13 (2004) 1549-1552.
- [22] N. All, Y. Kousar, J. Graclo, E. Titus, T.I. Okpalugo, V. Singh, M. Pease, A.A. Ogwu, E.I. Meletls, W. Ahmed, M.J. Jackson, Human microvascular endothelial cell seeding on Cr-DLC thin films for heart valve applications, *Journal of Materials Engineering and Performance*, 15 (2) (2006) 230-235.
- [23] I. De Scheerder, M. Szilard, H. Yanming, X.B. Ping, E. Verbeken, D. Neerinck, E. Demeyere, W. Coppens, F. Van de Werf, Evaluation of the biocompatibility of two new diamond-like stent coatings (Dylyn) in a porcine coronary stent model, *Journal of Invasive Cardiology* 12 (8) (2000) 389-394.
- [24] D. Antoniucci, A. Bartorelli, R. Valenti, P. Montorsi, G.M. Santoro, F. Fabbicchi, L. Bolognese, A. Loaldi, M. Trapani, D. Trabattoni, G. Moschi, S. Galli, Clinical and angiographic outcome after coronary arterial stenting with the carbostent, *American Journal of Cardiology* 85 (7) (2000) 821-825.

- 
- [25] K. Yamazaki, P. Litwak, O. Tagusari, T. Mori, K. Knon, M. Kameneva, M. Watach, L. Gordon, M. Miyaqishima, J. Tomioka, M. Umezu, F. Outa, J.F. Antaki, R.L. Kormos, H. Koyanaqi, B.P. Griffith, An implantable centrifugal blood pump with a recirculating purges system (Cool-Seal system), *Artificial Organs* 22 (6) (1998) 466-474.
- [26] D.P. Dowling, P.V. Kola, K. Donnelly, T.C. Kelly, K. Brumitt, L. Lloyd, R. Eloy, M. Therin, N. Weill, Evaluation of diamond-like carbon-coated orthopaedic implants, *Diamond and Related Materials* 6 (1997) 390-393.
- [27] H. Ronkainen, S. Varjus, K. Holmberg, Tribological performance of different DLC coatings in water-lubricated conditions, *Wear* 249 (3-4) (2001) 267-271.
- [28] V.-M. Tiainen, Amorphous carbon as a bio-mechanical coating – mechanical properties and biological applications, *Diamond and Related Materials* 10 (2) (2001) 153-160.
- [29] R. Lappalainen, H. Heinonen, A. Anttila, S. Santavirta, Some relevant issues related to the use of amorphous diamond coatings for medical applications, *Diamond and Related Materials* 7 (2-5) (1998) 482-485.
- [30] J.I. On˜ate, M. Comin, I. Braceras, A. Garcia, J.L. Viviente, M. Brizuela, N. Garagorri, J.L. Peris, J.I. Alava, Wear reduction effect on ultra-high-molecular-weight polyethylene by application of hard coatings and ion implantation on cobalt chromium alloy, as measured in a knee wear simulation machine, *Surface and Coatings Technology* 142-144 (2001) 1056-1062.
- [31] H. Dong, W. Shi, T. Bell, Potential of improving tribological performance of UHMWPE by engineering the Ti6Al4V counterfaces, *Wear* 225-229 (1) (1999) 146-153.
- [32] D. Sheeja, B.K. Tay, X. Shi, S.P. Lau, C. Daniel, S.M. Krishnan, L.N. Nung, Mechanical and tribological characterization of diamond-like carbon coatings on orthopedic materials, *Diamond and Related Materials* 10 (3-7) (2001) 1043-1048.
- [33] D. Sheeja, B.K. Tay, S.P. Lau, L.N. Nung, Tribological characterization of diamond-like carbon coatings on Co-Cr-Mo alloy for orthopaedic applications, *Surface and Coatings Technology* 146-147 (2001) 410-416.
- [34] V. Saikko, T. Ahlroos, O. Caloniuss, J. Keränen, Wear simulation of total hip prostheses with polyethylene against CoCr, alumina and diamond-like carbon, *Biomaterials* 22 (2001) 1507-1514.
- [35] S. Affatato, M. Frigo, A. Toni, An in vitro investigation of diamond-like carbon as a femoral head coating, *Journal of Biomedical Materials Research* 53 (3) (2000) 221-226.
- [36] R. Lappalainen, M. Selenium, A. Anttila, Y.T. Kontinen, S.S. Santavirta, Reduction of wear in total hip replacement prostheses by amorphous diamond coatings, *Journal of Biomedical Materials Research Part B: Applied Biomaterials* 66 B (2003) 410-413.
- [37] B. Shi, O.O. Ajayi, G. Fenske, A. Erdemir, H. Liang, Tribological performance of some alternative bearing materials for artificial joints, *Wear* 255 (2003) 1015-1021.
- [38] S.C. Scholes, A. Unsworth, A.A.J. Goldsmith, A frictional study of total hip joint replacements, *Physics in Medicine and Biology* 45 (2000) 3721-3735.
- [39] V. Saikko, T. Ahlroos, Phospholipids as boundary lubricants in wear tests of prosthetic joint materials, *Wear* 207 (1997) 86-91.

- [40] R. Hauert, DLC films in biomedical applications, *Tribology of Diamond-Like Carbon Films* (2008) 494-509.
- [41] T. Ahlroos, V. Saikko, Wear of prosthetic joint materials in various lubricants, *Wear* 211 (1997) 113-119.
- [42] M. Kalin, I. Velkavrh, J. Vižintin, L. Ožbolt, Review of boundary lubrication mechanisms of DLC coatings
- [43] J. Robertson, Diamond-like amorphous carbon, *Materials Science and Engineering R Reports: A Review Journal* 37 (2002) 129-281.
- [44] M. Dai, K. Zhou, Z. Yuan, Q. Ding, Z. Fu, The cutting performance of diamond and DLC-coated cutting tools, *Diamond and Related Materials* 9 (2000) 1753-1757.
- [45] T. Sato, T. Besshi, I. Tsutsui, T. Morimoto, Anti-galling property of a diamond-like carbon coated tool in aluminum sheet forming, *Journal of Materials Processing Technology* 104 (2000) 21-24.
- [46] J. Robertson, Ultrathin carbon coatings for magnetic storage technology, *Thin Solid Films* 383 (2001) 81-88.
- [47] P.R. Goglia, J. Berkowitz, J. Hoehn, A. Xidis, L. Stover, Diamond-like carbon applications in high density hard disc recording heads, *Diamond and Related Materials* 10 (2) (2001) 271-277.
- [48] M. Kano, I. Tanimoto, Wear mechanism of high wear-resistant materials for automotive valve trains, *Wear* 15 (1991) 229-243.
- [49] R. Cruz, J. Rao, T. Rose, K. Lawson, J.R. Nicholls, DLC-ceramic multilayers for automotive applications, *Diamond and Related Materials* 15 (2006) 2055-2060.
- [50] S.E. Franklin, J. Baranowska, Conditions affecting the sliding tribological performance of selected coatings for high vacuum bearing applications, *Wear* 263 (2007) 1300-1305.
- [51] A. Vanhulsel, F. Velasco, R. Jacobs, L. Eersels, D. Havermans, E.W. Roberts, I. Sherrington, M.J. Anderson, L. Gaillard, DLC solid lubricant coatings on ball bearings for space applications, *Tribology International* 40 (7) (2007) 1186-1194.
- [52] J.C. Jiang, W.J. Meng, A.G. Evans, C.V. Cooper, Structure and mechanics of W-DLC coated spur gears, *Surface and Coatings Technology* 176 (1) (2003) 50-56.
- [53] M. Kalin, J. Vižintin, The tribological performance of DLC-coated gears lubricated with biodegradable oil in various pinion/gear material combinations, *Wear* 259 (2005) 1270-1280.
- [54] S.C. Tung, H. Gao, Tribological characteristics and surface interaction between piston ring coatings and a blend of energy-conserving oils and ethanol fuels, *Wear* 255 (2003) 1276-1285.
- [55] I. Etsion, G. Halperin, E. Becker, The effect of various surface treatments on piston pin scuffing resistance, *Wear* 261 (2006) 785-791.
- [56] M. Kano, Super low friction of DLC applied to engine cam follower lubricated with ester-containing oil, *Tribology International* 39 (2006) 1682-1685.
- [57] J. Hershberger, O. Ozturk, J.B. Ajayi, J.B. Woodford, A. Erdemir, R.A. Erck, G.R. Fenske, Evaluation of DLC coatings for spark-ignited direct-injected fuel systems, *Surface and Coatings Technology* 179 (2004) 237-244.
- [58] <http://www.richterprecision.com/dlc-coatings.html> (2013.10.15)

- 
- [59] A.C. Ferrari, Diamond-like carbon for magnetic storage discs, *Surface and Coatings Technology* 180-181 (2004) 190-206.
- [60] M.F. Doerner, R.L. White, Materials issues in magnetic-disk performance, *MRS Bulletin*, (September) 28-34 (1996).
- [61] M.F. Doerner, K. Tang, T. Arnoldussen, H. Zeng, M.F. Toney, D. Weller, Microstructure and thermal stability of advanced longitudinal, *IEEE Transactions Magnetics* 36 (1) (2000) 43-47.
- [62] J. Robertson, Requirement of ultrathin carbon coatings for magnetic storage technology, *Tribology International* 36 (4-6) (2003) 405-415.
- [63] V.G. Litovchenko, A.A. Evtukh, R.I. Marchenko, N.I. Klyui, V.A. Semenovich, The enhanced field emission from microtips covered by ultrathin layers, *Journal of Micromechanics and Microengineering* 7 (1) (1997) 1-6.
- [64] A.I. Kosarev, V.V. Zhirnov, A.J. Vinogradov, M.V. Shutov, L.V. Bormatova, E.I. Givargizov, T.E. Felter, Field emission from low temperature carbon coated silicon tips, *Materials Research Society Symposium Proceedings* 509 (1998) 89-94.
- [65] A. Grill, Electrical and optical properties of diamond-like carbon. *Thin Solid Films* 355-356 (1999) 189-193.
- [66] C. Morsbach, C. Dubarry, M. Gabriel, M. Hoyer, S. Knappmann, F. Piazza, J. Robertson, R. Vullers, H.H. Gatzert, Flyable media for slider based ultra-high density optical recording, *IEEE Proceedings Science, Measurement Technology* 150 (5) (2003) 203-206.
- [67] A. Lettington, in: P. Koidl, P. Oelhafen (Eds.), *Amorphous Hydrogenated Carbon Films*, Proc. Eur. Mater. Res. Soc. Symp., Les Editions de Physique, Paris, 1987.
- [68] <http://diarkis.com/index.php/products/diamond-coatings/optical-coatings> (2013.10.15)
- [69] S.J. Cho, K.R. Lee, K. Y. Eun, J. H. Hahn, D.H. Ko, Determination of elastic modulus and Poisson's ratio of diamond-like carbon films, *Thin Solid Films* 341 (1999) 207-210.
- [70] I.T. Tang, H.J. Chen, W.C. Hwang, Y.C. Wang, M.P. Hwang, Y.H. Wang, Applications of piezoelectric ZnO film deposited on diamond-like carbon coated onto Si substrate under fabricated diamond SAW filter, *Journal of Crystal Growth* 262 (1-4) (2004) 461-466.
- [71] <http://www.sgarmart.com/products/overview.php?ID=402> (2013.10.15)

## **2.3 Deposition techniques of DLC coatings**

As described above, DLC coatings' applications in various fields rely on the coatings' properties, especially the biological reactions in biomedical applications. Although DLC as a class of materials has excellent mechanical, tribological and biological properties, it has to be noticed that control of film properties is strongly dependent on the chosen deposition system. With different deposition conditions, different properties including the chemical situation of the surface may be obtained. Therefore, any results about DLC should be correlated with an exact description of the deposition conditions, including materials and deposition process (the sample's pretreatment, deposition setup, deposition parameters and a detailed characterization of the coating).

Many methods have been developed for the deposition of DLC coatings in biomedical applications.

### **2.3.1 Physical vapor deposition of DLC coatings**

The physical vapor deposition (PVD) is widely employed to deposit wear-resistant thin-film coatings on different kinds of medical devices. By using PVD technology to deposit DLC, the coating material (carbon) is evaporated on the medical devices. In addition the underlying material properties, as well as biomechanical functionality are not varied, and just the surface properties of devices are modified. The main techniques available to evaporate carbon are: arc sources, electron beam guns as well as sputter sources.

- **Vacuum arc deposition**

One of the methods is vacuum arc deposition [1]. Firstly two cold electrodes are connected to the power supply with a low voltage (less than 100 V) and high current (more than 1 A) [2]. The chamber is pumped and reaches to a high vacuum which means residual gas in the chamber becomes rare. Then an arc is initiated by making two electrodes contacted and separated from each other. The electrodes are heated and become hot due to high contact resistance and high current at the contact point. At the moment of withdrawing the electrodes, the resistance and current are raised rapidly which leads to the fast increase of heat temperature, causing the electrode material is

---

evaporated. During this explosive emission process, the spot on the solid material target is formed. Meanwhile, very high electric field strength is formed at the small gap between cathode and anode resulting in strong field emission and gap breakdown, which is followed by the formation of vacuum arc.

As known, there are two types of the arc discharge: cathodic arc and anodic arc which depends on the source of the deposited material.

(1) Cathodic arc evaporation (CAE)

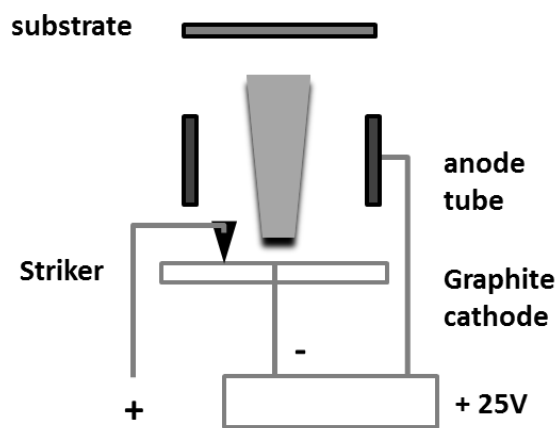


Figure 2.9 Schematic of cathodic vacuum arc [1]

If the vaporized material is originated from the cathode, this arc discharge is called cathodic arc which is a discrete continuous arc, and this deposition method is named by cathodic arc evaporation (CAE) which has been widely used in laboratory and industry [3-6]. When DLC coating is synthesized by CAE, carbon is vaporized from a graphite target as cathode by touching and separating it from anodic electrode. Usually the simplest anodic electrode is a small carbon striker and an arc forms on the cathode. The plasma with a high ion density of up to  $10^{13} \text{ cm}^{-3}$  is directly produced from localized small surface area of the solid material target which is called cathode spot ( $1\text{-}10 \text{ }\mu\text{m}$  and high current density of  $10^6\text{-}10^8 \text{ A cm}^{-2}$ ). The cathode spot exists in a short period of time, then self-extinguishes and reignites in a new area, which cause the motion of arc on the surface of a cold cathode and sustain the discharge. What's more, the macro particles (so-called droplets) are also deposited on the substrate because the explosive emission process happens so quickly that not all the target material has time to evaporate. This method is also widely

applied to deposit metals such as titanium in a nitrogen atmosphere reported in references [7-10]. If there is no gaseous atmosphere, the working gas is replaced by the vapor released from the cathode by action of the cathode spots. In evaporation process the substances from cathode surface are in form of  $Me^+$  (ions),  $Me$  (atoms), electrons ( $e^-$ ) and macro particles.

In this method the cathode spot emits not only the desired plasma particles but also macro particles of cathode materials that degrade coating performance and over all coating quality. To overcome this problem of macro particles, the use of techniques which can block macro particles or reduce the number of macro particles is required. Nowadays, many approaches to resolve this problem are reported, including use of different chamber configurations. The filtered cathodic vacuum arc (FCVA) process is developed to reject macro particles [11-17]. The filter has a focusing magnetic field and a steering field that separates the particles by mass, thus “filtering” them. The most common filtering designs include the linear duct filter [18], the 90 °filter [19] and 45 °filter [20], the 1/4 torus filter [8], the S-filter [21] and twist filter [22].

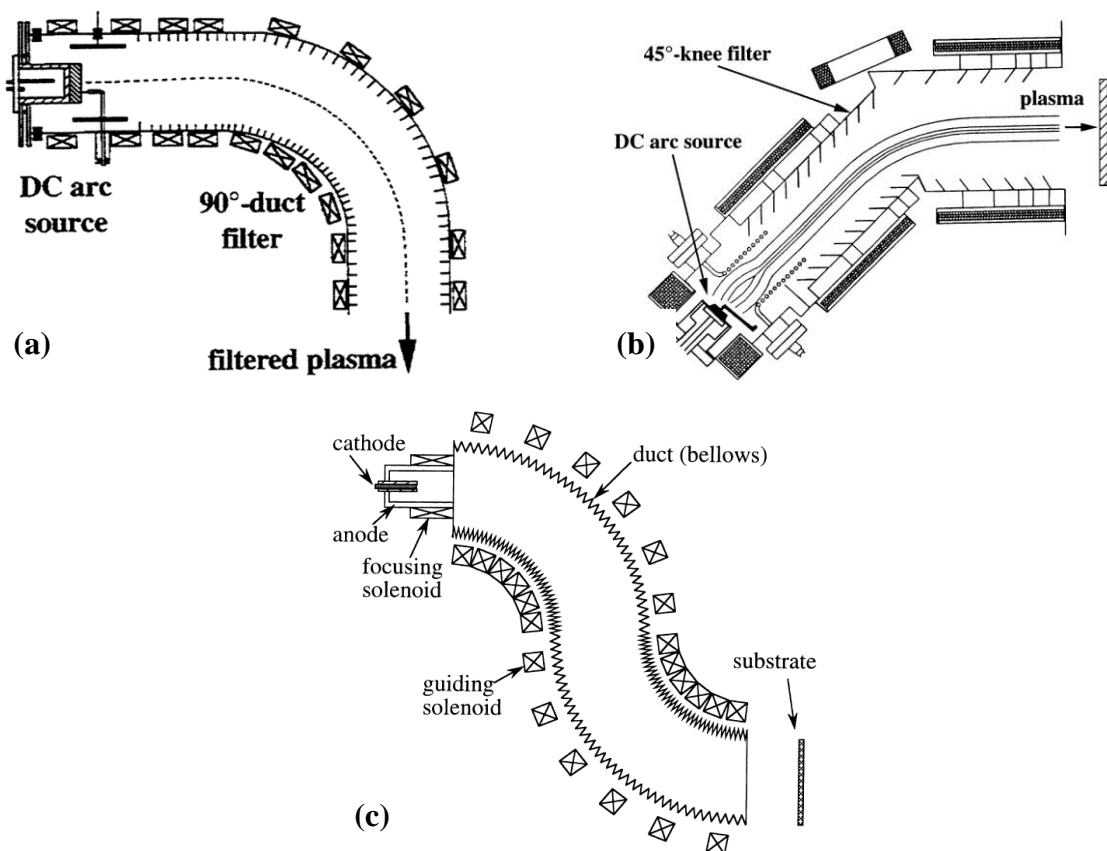


Figure 2.10 Schematic diagram of a various filters: (a) 90° filter (b) 45° filter (c) S-filter [23]

However, the drawback for these plasma filtering designs is the industrial disadvantage of increasing the technological complexity of the coating systems and hence the cost of the coated products [24]. These methods reduce the deposition rate as well. Above all, at low current, the cathodic mechanism of evaporating materials is not effective enough to overcome the rapid condensation on the surrounding walls [25]. Therefore, this type of arc is unstable and normally extinguishes in fractions of seconds [26]. That makes the evaporation of anode material interesting. The nature of the anode spot is different and characterized by lower temperatures.

### (2) Anodic arc evaporation deposition

If the evaporated material is originated from the anode, this arc discharge can be called anodic arc. The mechanisms of anode evaporation have been studied by [25, 27-30]. The anodic arc is a high current discharge that is sustained at least in part by material evaporating from a hot anode. The advantage of this type of arc is the absence of macro particles which are produced by the discrete arc [31]. Fig. 2.11 shows the schematic of anodic vacuum arc system.

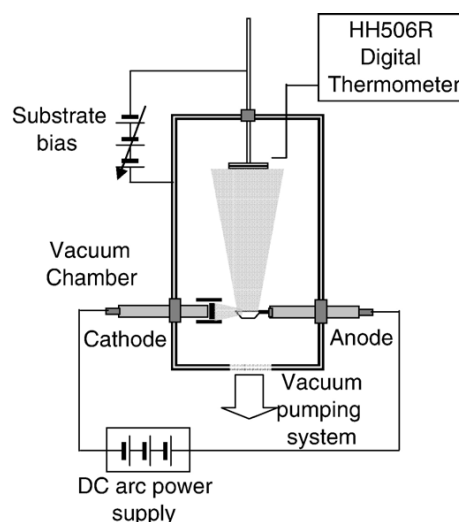


Figure 2.11 Schematic diagram of anodic vacuum arc deposition setup [32]

### (3) Transition between the cathodic arc and anodic arc

In vacuum the contact material transfer occurs during arcing. It is well known that sometimes this transfer cause the formation of a crater on the anode and a pip on the cathode [33]. There are two kinds of transfer: from the anode to the cathode and from the cathode to the anode, which is attributed to the anodic arc and the cathodic arc, respectively [34-35]. According to the reports

[36-40], the transition between the cathodic and anodic arc is associated with the metallic and gaseous phases of the arc. A transfer of material from the anode to the cathode is associated with the metallic phase, while the inverse transfer from the cathode to the anode was associated with the gaseous phase of the arc. However, N.B. Jemaa [33] performed testing under vacuum and concluded that it was independent of metallic and gaseous phases although the arc in vacuum was constantly in the metallic phase. The further work is needed for full confirmation. At present, few studies about the transition from the anodic arc to the cathodic arc have been done by measuring the evolution of material transfer with the arc lengthening, and show that the transition is independent of electrical and mechanical parameters [35, 41-42].

However, the transition from the cathodic to anodic arc in the deposition of DLC coatings has not been studied until now. In this work, DLC coatings are deposited by vacuum arc adjustable from anodic to cathodic operation mode. The transition between the cathodic and anodic arc can be realized by varying the anode-cathode diameter ratio of  $d_a/d_c$  with 1/3, 1/1 and 3/1.

- **Others physical vapor deposition**

DLC coatings can be also deposited by argon sputter deposition [43-44], direct or mass-selected ion beam deposition [45-47], as well as plasma beam deposition [48].

### 2.3.2 CVD and other deposition techniques of DLC coatings

Another deposition method for DLC coatings is chemical vapor deposition (CVD), involving the chemical reaction. Usually the hydrocarbon gases used for providing carbon ions ( $C^+$ ) in experiments are methane, ethane, acetylene and ethylene. In particular the plasma-enhanced CVD (PECVD) is popularly used in laboratory, in which the plasma is usually generated by radio frequency (RF) between two electrodes, e.g. electron-cyclotron wave resonance plasma chemical vapor deposition (ECWR plasma CVD) [49], radio-frequency CVD [50], plasma CVD combined with ion implantation [51].

Besides PVD and CVD, liquid electrochemical technique is also applied to deposit DLC coatings reported in literatures [52-54].

---

## References

- [1] J. Robertson, Diamond-like amorphous carbon, *Materials Science and Engineering R* 37 (2002) 129-281.
- [2] B. Jüttner, Cathode spots of electric arcs, *Journal of Physics D: Applied Physics* 34 (2001) R103-R123.
- [3] B.K. Tay, G.F. You, S.P. Lau, X. Shi, Plasma flow simulation in an off-plane double bend magnetic filter, *Surface and Coatings Technology* 133 (2000) 593-597.
- [4] M. Chowalla, J. Robertson, C.W. Chen, S.R.P. Silva, C.A. Davis, G.A.J. Amaratunga, W.I. Milne, Influence of ion energy and substrate temperature on the optical and electronic properties of tetrahedral amorphous carbon (ta-C) films, *Journal of Applied Physics* 81 (1997) 139-145.
- [5] A. Anders, A.V. Kulkarni, Synthesis of ultrathin ta-C films by twist-filtered cathodic arc carbon plasmas, *Materials Research Society Symposium Proceedings* 675 (2001) W111-12.
- [6] M.C. Polo, J.L. Andujar, J. Robertson, W.I. Milne, Preparation of tetrahedral amorphous carbon films by filtered cathodic vacuum arc deposition, *Diamond and Related Materials* 9 (3-6) (2000) 663-667.
- [7] I.G. Brown, Cathodic arc deposition of films, *Annual Review of Materials Sci.* 28 (1998) 243-269.
- [8] R.N. Tarrant, M.M.M. Bilek, T.W.H. Oates, J. Pigott, D.R. McKenzie, Influence of gas flow rate and entry point on ion charge, ion counts and ion energy distribution in a filtered cathodic arc, *Surface and Coatings Technology* 156 (2002) 110-114.
- [9] S.G. Harris, E.D. Doyle, Y.C. Wong, P.R. Munroe, J.M. Cairney, J.M. Long, Reducing the macroparticle content of cathodic arc evaporated TiN coatings, *Surface and Coatings Technology* 183 (2004) 283-284.
- [10] M. Ali, E. Hamzah, T. Abbas, M.R.Hj.M. Toff, I.A. Qazi, Macrodroplet reduction and growth mechanisms in cathodic arc physical vapor deposition of TiN films, *Surface Review and Letters* 15 (5) (2008) 653-659.
- [11] G. Dearnaley, J.H. Arps, Biomedical applications of diamond-like carbon (DLC) coatings: A review, *Surface and Coatings Technology* 200 (7) (2005) 2518-2524.
- [12] H.-S. Zhang, J.I. Endrino, A. Aders, Comparative surface and nano-tribological characteristics of nanocomposite diamond-like carbon thin films doped by silver, *Applied Surface Science* 255 (2008) 2551-2556.
- [13] A. Anders, W. Fong, A.V. Kulkarni, F.W. Ryan, C.S. Bhatia, Ultrathin diamond-like carbon films deposited by filtered carbon vacuum arcs, *IEEE Transactions on Plasma Science* 29 (5) (2001) 768-75.
- [14] B.F. Coll, D.M. Sanders, Design of vacuum arc-based sources, *Surface and Coatings Technology* 81 (1) (1996) 42-51.
- [15] G.M. Pharr, D.L. Callahan, D. McAdams, T.Y. Tsui, S. Anders, A. Anders, J.W. Ager, I.G. Brown, C.S. Bhatia, S.R.P. Silva, J. Robertson, Hardness, elastic modulus, and structure of very hard carbon films produced by cathodic-arc deposition with substrate bias, *Applied Physics Letters* 68 (6) (1996) 779-781.
- [16] R. Lossy, D.L. Pappas, R.A. Roy, J. J. Cuomo, V. H. Sura, Filtered arc deposition of amorphous diamond, *Applied Physics Letters* 61 (1992) 171-173.
- [17] R. Lossy, D.L. Pappas, R.A. Roy, J.P. Doyle, J. Bruley, Properties of amorphous diamond films prepared by a filtered cathodic arc, *Journal of Applied Physics* 77 (1995) 4750-4756.

- [18] D.A. Karpov, Cathodic arc sources and macroparticle filtering, *Surface and Coatings Technology* 96 (1997) 22-33.
- [19] I.I. Aksenov, V.A. Belous, V.G. Padalka, Apparatus to rid the plasma of a vacuum arc of macroparticles, *Instruments and Experimental Techniques* 21 (1978) 1416-1418.
- [20] D.A. Baldwin, S. Fallabella, Deposition processes utilizing a new filtered cathodic arc source, Proc. of the 38th Annual Techn. Conf., Society of Vacuum Coaters, Chicago, (1995) 309-316.
- [21] S. Anders, A. Anders, M.R. Dickinson, R.A. MacGill, I.G. Brown, S-shaped magnetic macroparticle filter for cathodic arc deposition, *IEEE Transactions on Plasma Science* 25 (1997) 670-674.
- [22] A. Anders, R. A. MacGill, Twist filter for the removal of macroparticles from cathodic arc plasmas, *Surface and Coatings Technology* 133-134 (2000) 96-100.
- [23] O. Filipov, Correlation of plasma fluxes and film properties deposited by vacuum arc, Doctoral Dissertation, Universität Duisburg-Essen (2013) 1-178.
- [24] A.W. Baouchi, A.J. Perry, A study of the macroparticle distribution in cathodic arc evaporated TiN films, *Surface and Coatings Technology* 49 (1991) 253-257.
- [25] H. Ehrich, The anodic vacuum arc. I. Basic construction and phenomenology, *Journal of Vacuum Science and Technology A* 6 (1) (1988) 134-138.
- [26] J.D. Cobine, G.A. Farrall, Experimental study of arc stability. I, *Journal of Applied Physics* 31 (1960) 2296-2304.
- [27] H. Ehrich, B. Hasse, M. Mausbach, K.G. Müller, R. Schmidt, The anodic vacuum arc. II. Experimental study of arc plasma, *Journal of Vacuum Science and Technology A* 6 (4) (1988) 2499-2504.
- [28] H.M. Katsch, M. Mausbach, K.G. Müller, Investigation of the expanding plasma of an anodic vacuum arc, *Journal of Applied Physics* 67 (8) (1990) 3625-3629.
- [29] H. Ehrich, B. Hasse, M. Mausbach, K. G. Müller, Plasma deposition of thin films utilizing the anodic vacuum arc, *IEEE Transactions on Plasma Science* 18 (6) (1990) 895-903.
- [30] H. Ehrich, B. Hasse, M. Mausbach, K.G. Müller, The anodic vacuum arc and its application to coating, *Journal of Science and Technology A* 8 (3) (1990) 2160-2164.
- [31] D.M. Sanders, D.B. Boercker, S. Falabella, Coating technology based on the vacuum arc-A review, *IEEE Transactions on Plasma Science* 18 (6) (1990) 883-894.
- [32] M.K. Sinha, S.K. Mukherjee, B. Pathak, R.K. Paul, P.K. Barhai, Effect of deposition process parameters on resistivity of metal and alloy films deposited using anodic vacuum arc technique, *Thin Solid Films* 515 (2006) 1753-1757.
- [33] N.B. Jemaa, L. Morin, Transition from the anodic arc phase to the cathodic metallic arc phase in vacuum at low DC electrical level, *IEEE Transactions on Components and Packaging Technologies* 25 (4) (2002) 651-655.
- [34] R. Holm, *Electric Contacts : Theory and Application*, 4th edition, Springer- Verlag 1967 334-337.
- [35] N. B. Jemaa, L. Morin, S. Benhenda, L. Nedelec, Anodic to cathodic arc transition according to break arc lengthening, *IEEE Transactions on Components and Packaging Manufacturing Technology Part A* 21 (4) (1998) 599-603.

- 
- [36] J. Swingler, J.W. McBride, The net zero erosion phenomena on opening switching contacts with AC loading, Proceeding of the 43<sup>rd</sup> IEEE Holm Conference on Electrical Contacts (1997) 238-245.
- [37] J. Swingler, J.W. McBride, The erosion and arc characteristics of Ag/CdO and Ag/SnO<sub>2</sub> contact materials under DC break conditions, IEEE Transactions on Components Packaging and Manufacturing Technology Part A 19 (3) (1996) 404-415.
- [38] Z.K Chen, K. Sawa, Particle sputtering and deposition mechanism for material transfer in breaking arcs, Journal of Applied Physics 76 (6) (1994) 3326-3331.
- [39] Z.K Chen, K. Sawa, Effect of arc behavior on material transfer: A Review, IEEE Transactions on Components Packaging and Manufacturing Technology Part A 21 (2) (1998) 310-322.
- [40] H. Sone, T. Takagi, Role of the metallic phase arc discharge on arc erosion in Ag contacts, I IEEE Transactions on Components Hybrids and Manufacturing Technology 13 (1) (1990) 13-19.
- [41] N.B. Jemaa, L. Morin, L. Lehfaoui, L. Nedelec, Effect of parameters on the transition from anodic to cathodic Arc, Proc. of the ICECT (1999) 173-179.
- [42] L. Morin, Experimental study of electric arcs and their consequences for contact materials. Application to automotive power switches (in English), Doctoral thesis, University of Rennes1, France, June 2000.
- [43] B. Wei, B. Zhang, K. E. Johnson, Nitrogen-induced modifications in microstructure and wear durability of ultrathin amorphous-carbon films, Journal of Applied Physics 83 (1998) 2491-2499.
- [44] S. Logothetidis, P. Patsalas, M. Gioti, A. Galdikas, L. Pranevicius, Growth kinetics of sputtered amorphous carbon thin films: composition studies and phenomenological model, Thin Solid Films 376 (2000) 56-66.
- [45] M.H. Sohn, S.I. Kim, Effects of interface mixing on adhesion of amorphous carbon films synthesized by variable-energy direct ion beam deposition, Journal of Vacuum Science and Technology A 18 (4) (2000) 1983-1986.
- [46] H.A. Durand, K. Sekine, K. Etoh, K. Ito, I. Kataoka, Dynamic behavior of carbon ultrathin film formation,
- [47] K. Yamamoto, T. Watanabe, K. Wazumi, F. Kokai, Y. Koga, S. Fujiwara, The sp<sup>3</sup> bond fraction in carbon films prepared by mass-separated ion beam deposition, Diamond and Related Materials 10 (2001) 895-899.
- [48] M.C.M. van der Sanden, R.J. Severens, R.F.G. Meulenbroeks, M.J. de Graaf, Z. Qing, D. K. Otobarev, R. Engeln, J.W.A.M. Gielen, J.A.M. van der Mullen, D.C. Schram, The role of hydrogen during plasma beam deposition of amorphous thin films, Surface and Coatings Technology 74-75 (1995) 1-9.
- [49] M. Weiler, K. Lang, E. Li, J. Robertson, Deposition of tetrahedral hydrogenated amorphous carbon using a novel electron cyclotron wave resonance reactor, Applied Physics Letters 72 (1998) 1314-1316.
- [50] A. Erdemir, I.B. Nilufer, O.L. Eryilmaz, M. Beschliesser, G.R. Fenske, Friction and wear performance of diamond-like carbon films grown in various source gas plasmas, Surface and Coatings Technology 120-121 (1999) 589-593.
- [51] F. Kenji, W. Koichiro, U. Kazuo, S. Tadashi, Preparation of highly adhesive diamond-like carbon films by plasma CVD combined with ion implantation, IHI Engineering Review 37 (1) (2004) 30-34.
- [52] T. Suzuki, Y. Manita, T. Yamazaki, S. Wada, T. Noma, Deposition of carbon films by electrolysis of a water-ethylene glycol solution, Journal of Materials Science 30 (1995) 2067-2069.

- [53] W.L. He, R. Yu, H. Wang, H. Yan, Electrodeposition mechanism of hydrogen-free diamond-like carbon films from organic electrolytes, *Carbon* 43 (9) (2005) 2000-2006.
- [54] Z. Sun, Y. Sun, X. Wang, Investigation of phases in the carbon films deposited by electrolysis of ethanol liquid phase using Raman scattering, *Chemical Physics Letters* 318 (2000) 471-475.

---

### 3. Hip joint replacement background

Nowadays, due to overaging of the population and increasing the average weight of people, even increasing number of accident injuries especially for young people, more and more load bearing joint replacements particularly hip joint replacements are required, what's worse, about 10% of the patients require second replacements. In addition, disease like arthritis can also require the replacement of joints due to worn cartilage. The normal hip displays the healthy articular cartilage and the diseased hip joint shows the damaged cartilage (see Fig. 3.1).

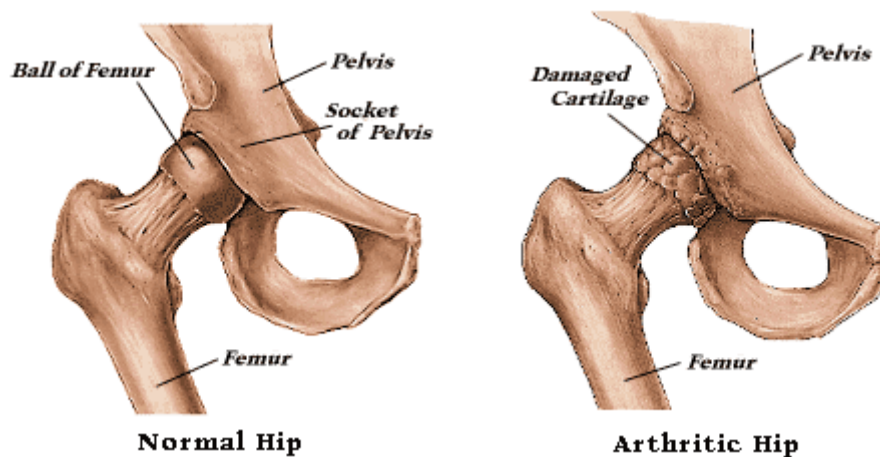


Figure 3.1 The normal hip joint and arthritic hip joint [1]

### 3.1 Introduction of normal hip joint and artificial hip joint

#### 3.1.1 Composition of hip joint

In human body, the normal hip joint mainly consists of femur, femoral head (ball), the cup-shaped acetabulum (cup) in the pelvis (see Fig. 3.2 left) [2], corresponding right in Fig. 3.2 is the structure of the artificial hip joint [3]. Ligaments as bands of tissue connect the femur to the acetabulum and help to keep them steady. Articular cartilage, the smooth and tough substance, covers the surfaces of the femoral head (ball) and the acetabulum (cup). Additionally, the cartilage cushions the bones like a shock absorber which allows smooth movement, so that the bones can move easily. The rest of surfaces of hip joint are covered by the synovial membrane which is a thin and smooth tissue liner. The synovial membrane produces a small amount of the synovial fluid that acts as a lubricant to reduce friction between bones each other. The capsule surrounds the joint and keeps the synovial fluid from leaking out [2].

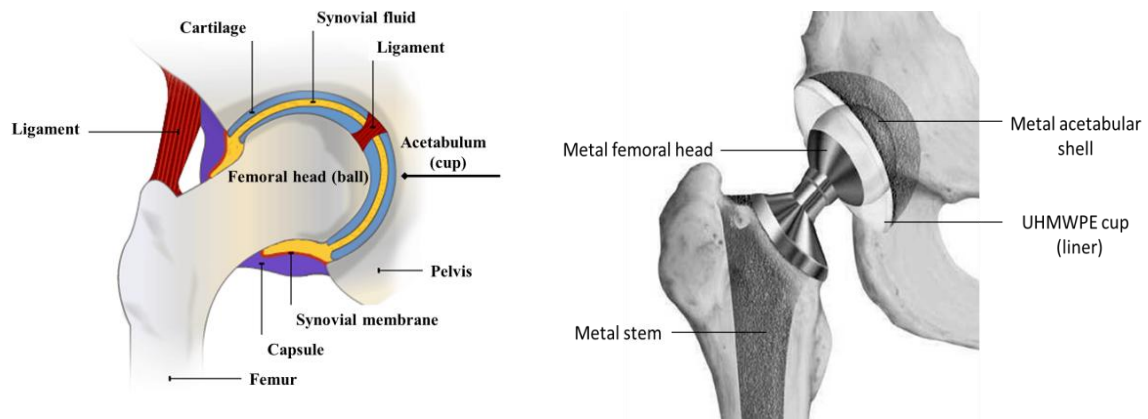


Figure 3.2 Schematic of a normal hip joint (left [2]), corresponding artificial hip joint (right [3])

The artificial hip joint consists of acetabular cup made of UHMWPE, steel, ceramic, or polyethylene inner, femoral head made of steel or ceramic, as well as femoral stem. UHMWPE acetabular cup is sometimes not covered with a metal shell. In joint prosthesis, polymers are used for one of the articulating surface components. Therefore, these polymers must have a low friction coefficient and low wear rate when they are in contact with the opposing surface, which is usually made of metal (e.g. cobalt-chromium alloys CoCrMo [4] or titanium alloys) or ceramics such as alumina ( $Al_2O_3$ ) and zirconia. These alloys are based on titanium, iron (surgical steel), cobalt, chromium, nickel (may cause allergies), zirconium, tantalum, the noble metals and carbon in its different forms [5].

### 3.1.2 Wear particles

Currently the life expectancy of such joints is about fifteen years [6], so it is urgent to extend the lifetime of the implants, in particular, for the patients aged < 50 years. However, it has been confirmed that the wear particle is the main factor for limiting the lifetime of the implants.

During the motion of joint, the wear particles are generated and shed into the surrounding synovial fluid and tissues, which initiate a macrophage-mediated inflammatory response, leading to osteoclast cells activation. The biological interaction with particles occurs. The body's immune system attempts to digest the wear particles as it would be a bacterium or virus, meanwhile enzymes are released that result in osteolysis. Over time, sufficient bone is resorbed around the implant to cause aseptic implant loosening [7-9].

---

If the particles are toxic, they will cause a series of morphological changes in macrophages, including retraction of pseudopodia, blebbing and smoothing of the surface, and finally cell destruction [10].

In ref. [11] it is concluded that if there are enough particles, macrophages phagocytosing foreign particles become activated and release mediators (soluble factors) that stimulate bone resorption even though there is no toxic effect, then the implant will loosen as its bony support will be lost, which indicate the importance of the amount of particles in implant loosening. Several studies have demonstrated that the composition and the volume of particles have the effect on the macrophage response to particles [12-16]. Meanwhile, few researchers propose that the size of particles is also one of the critical factors associated with aseptic loosening [15, 17], and demonstrate that submicron particles play a major role in wear particle-induced osteolysis [13]. Moreover, the large number of these particles, their size as well as their ability to adsorb endotoxins [18] can induce inflammatory reactions resulting in bone resorption. The onset of osteolysis is closely linked to both the volume and size of the wear debris produced [4]. The volume of debris generated is inversely proportional to the hardness of the materials, hence hard-on-hard bearings have also been investigated [19].

In ref. [20], it is the first time to present that particle size is able to affect the differentiation of macrophages into osteoclasts. The results show that the particles in the size range of 1  $\mu\text{m}$  ~ 10  $\mu\text{m}$  enhance the process of macrophage-osteoclast differentiation. According to ref. [21-23], it is known that phagocytosis can occur with particles in the size range of 0.5  $\mu\text{m}$  ~12  $\mu\text{m}$ . There are two different mechanisms to internalize foreign bodies: one is phagocytosis and another is pinocytosis. In contrast to phagocytosis, the particles with the size of 0.1  $\mu\text{m}$  are thought to be taken in by macrophages via pinocytosis, which is less active than phagocytosis [20]. Therefore, the particle size is also a very important factor for artificial hip joint loosening.

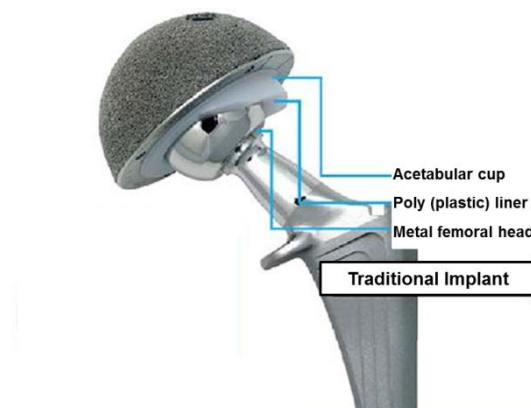
Research has shown that contact conditions and material parameters significantly influence the size and shape of the UHMWPE wear particles.

To date, different materials for joints are implanted with the different advantages and disadvantages. The forms of prosthetic hip replacements are mainly metal-on-UHMWPE, ceramic-on-UHMWPE, ceramic-on-ceramic or metal-on-metal.

## 3.2 Classification of artificial hip joint

### 3.2.1 Metal femoral heads articulating against UHMWPE cups

Traditional metal femoral heads articulating against ultra-high molecular weight polyethylene (UHMWPE) acetabular cup are widely employed in prosthetic hip replacements and most of them are successful clinically, as shown in Fig. 2.4 (e) and Fig. 3.3 [24-25]. However, about  $10^{10}$ - $10^{11}$  polyethylene wear particles with the size range of  $0.1 \mu\text{m} \sim 10 \mu\text{m}$  are generated, which weaken surrounding bone causing bone resorption, leading to the loosening of the prosthesis and ultimate failure [26-28]. In addition, the average wear rate of the polymer cup is in the range of  $20\text{-}60 \text{ mm}^3/\text{year}$  for metal-on-UHMWPE hip joint.



© 2013, BoneSmart. All Rights Reserved.

Figure 3.3 Metal-on-UHMWPE hip joint [25]

According to the ref. [29], cobalt-base alloys are the most commonly used metals for current metal-on-UHMWPE implants. The oxide surface layer on titanium alloy (Ti-6Al-4V) femoral heads result in high UHMWPE wear due to breakdown of titanium surface.

### 3.2.2 Ceramic femoral heads articulating against UHMWPE cups

Ceramic materials due to excellent biocompatibility and low friction coefficient have been used instead of a metallic femoral head for artificial joints [30]. Comparing to the traditional metal and polyethylene materials, the average wear rate of the UHMWPE can be decreased by 50 % when a ceramic femoral head articulates against UHMWPE [31]. Although ceramic

---

materials generate significantly less polyethylene debris when used in conjunction with polyethylene acetabular components in bearing couples, there is still a large number of particles. Additionally, the stress shielding due to the high elastic modulus of ceramic materials may be responsible for cancellous bone atrophy and loosening of the acetabular cup in older patients with senile osteoporosis or rheumatoid arthritis [32].



Figure 3.4 Ceramic-on-UHMWPE hip joint [25]

### 3.2.3 Metal femoral heads articulating against metal cups

As is well known, the wear particles produced during the motion of joint have been identified as the main factor limiting the lifetime of the implants, so the number of wear particles have attracted much researchers attention. As described above the volume of debris is inversely proportional to the materials hardness, thus hard-on-hard bearings have also been investigated [19].

By comparing with UHMWPE, metal-on-metal hip joints have a lower rate in the range of 1-5 mm<sup>3</sup>/year and the wear debris particles are decreased, smaller than those of UHMWPE in metal-on-UHMWPE and ceramic-on-UHMWPE implants (see Fig. 3.5) [28-29, 33]. The amounts of particles are about 10<sup>9</sup> (micrometer-size). The ball and cup are made of Co-Cr-Mo which is only in clinical use in Europe [29].

However, it is observed that the blood levels of metal ion releasing from the metal joint are increased, which may negatively influence the haemocompatibility of the surface and cause a delayed-type metal hypersensitivity [5, 34]. Additionally, the number of allergies is increasing at

a rate of about 10 % each year [34] and many people have allergies to implant metals or metallic particles. According to the report in ref. [35], patients with total hip replacements by implants of stainless steel or of Co-Cr alloys who experienced difficulties after two to fifteen years due to a loosening of the prosthesis and / or allergic reactions to Cr, Co or Ni were found to have an increased content of these elements in their urine, plasma and blood. Already fifteen months after removal the contents were excessive in these fluids. Moreover, a few elements (Cr, Co, Ni and V) have toxic effects. Ti and its alloys, Nb and Ta exhibit an inert behavior, nevertheless the steel 316L and the Co-Cr alloy are encapsulated by a tissue membrane and their behavior is not inert [36].

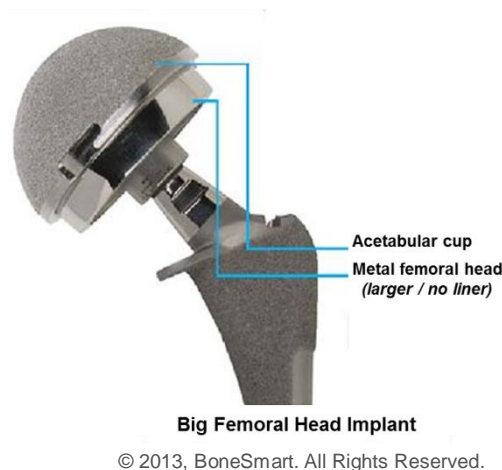


Figure 3.5 Metal-on-Metal hip joint [25]

#### 3.2.4 Ceramic femoral heads articulating against ceramic cups

Ceramic-on-ceramic hip joints, where an alumina femoral head is combined with an alumina acetabular cup, show very low wear in the range of  $0.05 \text{ mm}^3/\text{year}$  [31] and reduce wear rate of just  $0.032 \text{ mm}^3$  per million cycles. In addition, the use of ceramic-on-ceramic hip joint not only resolves the problems caused by wear debris, but also alleviates any concerns about metal ion release into the body, compared to other hip joint systems discussed above. Although ceramic-on-ceramic hip joint has these advantages, it is not in clinical use in the United States [29], because they may crack and release millions of hard particles which cannot all be removed surgically [34]. Actually, the best choice for ceramic hip joints is the type of

---

ceramic-on-ceramic, because ceramic particles are so hard that they can make metals or UHMWPE wear out quickly if they migrate onto the articulating surfaces.



© Copyright 2013 B. Braun Melsungen AG

Figure 3.6 Ceramic-on-Ceramic hip joint [37]

### 3.2.5 DLC coated artificial hip joint

In ref. [38], it was shown that polyethylene, cobalt-chromium or bone cement particles, introduced into implanted bone harvest chambers in rabbits, caused inflammatory reaction and reduced bone ingrowth.

As described above, in order to overcome the problem of wear particle generation in artificial implants, a new low wear material is required. The importance of the surface finish is reported by Dowson [31] in a comparative study of the performance of metallic and ceramic femoral heads. So coating is applied to the hip joint replacement because the implant surface can be modified by deposition. The advantages of DLC coatings used as material for joint have been discussed above in Chapter 2.

DLC coating, deposited on the metal substrate, can be used as a barrier to prevent leaching of metallic ions into the body. Additionally, the adhesion of DLC coating to substrate can be improved by interface layer, about which the details will be discussed in Chapter 4. Usually there are three different hip joints coated with DLC as reported by R. Hauert in ref. [34]: DLC-coated femoral heads against UHMWPE implanted cups, DLC-coated femoral heads against metal cups and DLC-coated femoral heads against metal DLC-coated cups. As described in biomedical

applications of DLC coatings in Section 2.2.1, these DLC-coated hip joints are studied in laboratory and still in process.

To date, the study of the amount of wear particles has attracted more and more researchers [11, 39-42]. However, reports about wear particle size distribution are rare to find, especially for DLC coatings in hip joints. In this work, the wear particle size distribution is studied in metal-on-metal joints with both sides coated with DLC.

### 3.3 Adhesion and interface layers in biomedical materials

As is well known, implantation of DLC coating into the human body also allows it to re-establish biological and mechanical functions, not just make it bio- and haemocompatible. Although the adhesion for a DLC-coated articulating joint is not the main point in this work, it is still a main concern which will influence the lifetime of DLC-coated implants. Due to poor adhesion, DLC coating delamination occurs under different conditions, which results in the failure of DLC-coated implants. Therefore the long-term adhesion has to be guaranteed to avoid premature replacements or revision of implants.

In this chapter, the review related to the adhesion of DLC coating in hip joint replacement is discussed as follows, in which much works are done including how to improve the adhesion. Especially, the failure mechanisms, analysis of the failure as well as tribological behavior of DLC-coated joint replacements have been investigated recently using Rockwell indentation setup by R. Hauert and U. Müller et al. [43-47].

#### (1) Adhesion of DLC coating and substrate

The adhesion of DLC to a range of prosthetic materials including 316 stainless steels [48-49], titanium [50] and Ti6Al4V [51] which is controlled by the interface is still an issue. Mainly the adhesion failure at the interface has to be attributed to the chemical stability of the interface. As described in the literature [52], the approaches for improving the adhesion of DLC coatings include: ① forming an intermediate layer between the substrate and the DLC coating such as interfacial metal-carbides [3] ② forming the gradient composition coatings inclined from the base material through the DLC coatings [53] for example silicon [54], titanium [55], chromium [56]

---

which must be biocompatible and amorphous, as well as multilayers  $TiN_x-TiC_y$  [50, 57-59], and ③ using an ion-mixing process based on ion-implantation technology [52, 60]. Actually, the problem of poor adhesion can, to an appreciable extent, be overcome by penetration of carbon atoms from the DLC coating to a substrate, the reaction of the carbon atoms with the substrate metal atoms and the formation of carbide. The interface reaction layer may also consist of metal-oxy carbide which is dependent on the precleaning and the conditions at the beginning of the DLC deposition process [34].

### (2) Failure mechanism of DLC coatings

During 1993-1995, a series of DLC coated Ti-Al-V femoral heads articulating against PE were studied in clinic and it was found that the coated implants had only a 54 % survival rate due to the delamination of the coatings after 8.5 years, causing severe wear of the PE counterpart [61]. Additionally, most delamination spots were round (more than 90 %). Therefore, it is necessary to analyze the failure mechanism and to estimate the adhesion lifetime for DLC coated implants. It was shown that mechanical failure is mainly caused by third body wear involving wear particles in simulator testing [43]. Besides mechanical failure, other delayed interface crack growth mechanisms including hydrogen embrittlement, galvanic, pitting, and crevice corrosion (CC) as well as stress corrosion cracking (SCC), also have to be considered, in which SCC and CC are related to the coating delamination since they are dependent on the stress and environment [43,45,62]. In these references it was shown that one failure of DLC-CoCrMo tested in synovial testing fluid took place due to CC of the adhesion promoting interlayer or SCC which may occur in a few nanometer thin reactively formed interface layer such as carbides.

### (3) Si interface layer

As is known, the different properties of different interface layers are obtained with different deposition conditions. These interface layers are very important for good adhesion, including not only the formation of interfacial carbides [45], also other additional materials introduced into the DLC coatings whose structures must be considered as amorphous rather than crystalline. According to ref. [34], it should be possible to tailor the biological reactions to any desired point between the properties of DLC and those of the added element. Moreover, it is reported that the biocompatibility can be improved by the addition of Si by some companies (Sulzer CarboMedics

and St. Jude Medical) in ref. [34]. Therefore, the cause of delamination of DLC/Si-DLC/CoCrMo was studied by C.V. Falub et al. [63] and was disclosed to be SCC of the interface material the same as DLC/CoCrMo. Furthermore, the threshold strain energy release rates for Si-DLC interlayer was improved by the factor of about 8 times compared to it for DLC coating without interlayer, which indicated that the interface layer can improve the adhesion of DLC coating to substrate.

However, the influence of testing environment on CC has been demonstrated by R. Hauert in 2012 [46]. It was found that the Si-rich interlayer appears to dissolve in Hyclone wear testing fluid, in contrast, no or only a few delamination was observed in phosphate-buffered saline (PBS), which indicates that the presence of proteins provide crevice corrosion conditions so that Si-based materials in contact with body fluid imposes a high risk of failure. Thus, the protective silicon oxide surface layer is not corrosion resistant in vivo.

#### (4) Ti interface layer

Ti and its alloys, Nb and Ta, which have a high polarization resistance, exhibit an inert behavior. The steel 316L and the CoCr alloy, which have a polarization resistance similar to that of titanium, are encapsulated by a tissue membrane and their behavior is not inert [36].

The biocompatibility on DLC-coated Ti samples was confirmed by Mohanty et al [64]. It was found that samples could stay in the skeletal muscle of rabbits for up to 1 year. Additionally, L. Lu reported that DLC adhered strongly to titanium and cobalt chrome as well as to polymers [59]. DLC coating with different concentrations of titanium have also been researched in vitro and found that the obtained surface was not only biocompatible, but also hard which can prevent the abrasion and scratching, enhancing bone ingrowth. According to ref. [34], the adsorbed proteins will subsequently have an effect on the cell attachment, cell proliferation and cell differentiation and even the tribological behavior probably. However the adsorption of different proteins in Ti-DLC coating, when Ti is exposed to a biological environment, can be controlled by the content of Ti [65]. Furthermore, the addition of Ti into the DLC can prevent the differentiation of bone marrow cells into bone resorbing cells, i.e. osteoclasts [66-67].

---

Due to the advantages of Ti introduced into DLC coating, titanium interface layer (~ 50 nm) is widely used in many industrial processes, including chromium interface layer or even multilayers. As is well known, the chemistry at an interface can be influenced and improved by the deposition of interface layers [34].

In previous work [56], chromium and titanium interface layers were deposited by cathodic arc vacuum on P2000 with the same deposition parameters. It was found that chromium adhered better on the austenite stainless steel P2000 than titanium, but DLC adhered better on titanium. However in this work, the focus lies on the wear particle size distribution of DLC coatings, not adhesion of it. In this work, Ti is used as interface layer and deposited by cathodic arc vacuum.

## References

- [1] [www.stryker.co.uk](http://www.stryker.co.uk), Patients, Hip, Hip replacement (2013 February).
- [2] [www.bbc.co.uk/bitesize/standard/](http://www.bbc.co.uk/bitesize/standard/), Biology, The body in action, Movement, revision, 3 (2013 February).
- [3] [Healthpages.org](http://Healthpages.org), Surgical Care, Having Hip Joint Replacement Surgery (2013 February).
- [4] C. Brockett, S. Williams, Z.M. Jin, G. Isaac, J. Fisher, Friction of total hip replacements with different bearings and loading conditions, *Journal of Biomedical Materials Research Part B: Applied Biomaterials* (2006) 508-515.
- [5] R. Hauert, A review of modified DLC coatings for biological applications, *Diamond and Related Materials* 12 (2003) 583-589.
- [6] H. Malchau, P. Herberts, Prognosis of total hip replacement, revision and re-revision rate in THR: a revision-risk study of 148 359 primary operations; 65<sup>th</sup> annual meeting of the american academy of orthopaedic surgeons 1998, New Orleans, USA.
- [7] S.B. Goodman, M. Lind, Y. Song, R.L. Smith, In vivo, in vitro, and tissue retrieval studies on particulate debris, *Clinical Orthopedics and Related Research* 352 (1998) 25-34.
- [8] K.J. Kim, J. Chiba, H.E. Rubash. In vivo and in vitro analysis of membranes from hip prostheses inserted without cement. *Journal of Bone and Joint Surgery* 76 (1994) 172-180.
- [9] W.J. Maloney, R.L. Smith. Periprosthetic osteolysis in total hip arthroplasty: the role of particulate wear debris, *Journal of Bone and Joint Surgery* 77 (9) (1995) 1448-1461.
- [10] M.D. Waters, D.E. Gardner, C. Aranyi, D.L. Coffin, Metal toxicity for rabbit alveolar macrophages in vitro, *Environmental Research* 9 (1) (1975) 32-47.
- [11] D.W. Murray, N. Rushton, Macrophages stimulate bone resorption when they phagocytose particles, *Journal of Bone and Joint Surgery British Volume* 72 (6) (1990) 988-992.
- [12] D.R. Haynes, S.D. Rogers, S. Hay, M.J. Percy, D.W. Howie, The differences in toxicity and release of bone-resorbing mediators induced by titanium and cobalt-chromium-alloy wear particles, *Journal of Bone and Joint Surgery* 75 (1993) 825-834.

- [13] Y. Kadoya, A. Kobayashi, H. Ohashi, Wear and osteolysis in total joint replacements, *Acta Orthopaedica Scandinavica Supplementum* 278 (1998) 1-16.
- [14] K.J. Kim, T. Itoh, M. Tanahashi, M. Kumeqawa, Activation of osteoclast-mediated bone resorption by the supernatant from a rabbit synovial cell line in response to polyethylene particles, *Journal of Biomedical Materials Research* 32 (1) (1996) 3-9.
- [15] A.S. Shanbhag, J.J. Jacobs, J. Black, J.O. Galante, T.T. Glant, Macrophage/particle interactions: Effect of size, composition and surface area, *Journal of Biomedical Materials Research* 28 (1) (1994) 81-90.
- [16] A.S. Shanbhag, J.J. Jacobs, J. Black, J.O. Galante, T.T. Glant, Human monocytes response to particulate biomaterials generated in vivo and in vitro, *Journal of Orthopedics Research* 13 (5) (1995) 792-801.
- [17] T.R. Green, J. Fisher, M. Stone, B.M. Wroblewski, E. Ingham, Polyethylene particles of a “critical size” are necessary for the induction of cytokines by macrophages in vitro, *Biomaterials* 19 (1998) 2297-2302.
- [18] A.U. Daniels, F.H. Barnes, S.J. Charlebois, R.A. Smith, Macrophage cykokine response to particles and lipopolysaccharide in vitro, *Journal of Biomedical Materials Research* 49 (4) (2000) 469-478.
- [19] H.P. Sieber, C.B. Reiker, P. K ötig, Analysis of 118 second-generation metal-on-metal retrieved hip implants, *Journal of Bone and Joint Surgery British Volume* 81 (1) (1999) 46-50.
- [20] T. Hirayama, Y. Fujikawa, I. Itonaga, R. Torisu, Effect of particle size on macrophage-osteoclast differentiation in vitro, *Journal of Orthopaedic Science* 6 (2001) 53-58.
- [21] T.T. Glant, J.J. Jacobs, G. Molnar, A.S. Shanbhag, M. Valyon, J.O. Galante, Bone resorption activity of particulate-stimulated macrophages, *Journal of Bone and Mineral Research* 8 (9) (1993) 1071-1079.
- [22] S.M. Horowitz, S.B. Doty, J.M. Lane, A.H. Burstein, Studies of the mechanism by which the mechanical failure of polymethylmethacrylate leads to bone resorption, *Journal of Bone and Joint Surgery American Volume* 75 (6) (1993) 802-813.
- [23] R.M. Steinman, I.S. Mellman, W.A. Muller, Z.A. Cohn, Endocytosis and the recycling of plasma membrane, *Journal of Cell Biology* 96 (1983) 1-27.
- [24] H. Malchau, P. Herberts, T. Eisler, G. Garellick, P. S öderman, The Swedish total hip replacement Register, *Journal of Bone and Joint Surgery* 84 (2002) 2-20.
- [25] <http://bonesmart.org/hip/hip-replacement-implant-materials/> (2013.10.18)
- [26] E. Ingham, J. Fisher, Biological reactions to wear debris in total joint replacement, *Proceeding of the Institution of Mechanical Engineers, Part H: Journal of Engineering in Medicine* 214 (2000) 21-37.
- [27] E. Ingham, J. Fisher, The role of macrophages in osteolysis of total joint replacement, *Biomaterials* 26 (11) (2005) 1271-1286.
- [28] J.L. Tipper, P.J. Firkins, A.A. Besong, P.S.M. Barbour, J. Nevelos, M.H. Stone, E. Ingham, J. Fisher, Characterisation of wear debris from UHMWPE on zirconia ceramic, metal-on-metal and alumina ceramic-on-ceramic hip prostheses generated in a physiological anatomical hip joint simulator, *Wear* 250 (1-12) (2001) 120-128.
- [29] M. Long, H.J. Rack, Titanium alloys in total joint replacement-A materials science perspective, *Biomaterials* 19 (18) (1998) 1621-1639.

- 
- [30] B.M. Wroblewski, P.D. Siney, D. Dowson, S.N. Collins, Prospective clinical and joint simulator studies of a new total hip arthroplasty using alumina ceramic heads and cross-linked polyethylene cups, *The Journal of Bone and Joint Surgery* 78-B (1996) 280-285.
- [31] D. Dowson, A comparative study of the performance of metallic and ceramic femoral head components in total replacement hip joints, *Wear* 190 (2) (1995) 171-183.
- [32] P. Christel, A. Meunier, J.M. Dorlot, J.M. Crolet, J. Witvolet, L. Sedel, P. Boritin, Biomechanical compatibility and design of ceramic implants for orthopedic surgery, *Bioceramics: Material Characteristics Versus In Vivo Behavior* 523 (1988) 234-256.
- [33] H.L. Anissian, A. Stark, A. Gustafson, V. Good, I.C. Clarke, Metal-on-metal bearing in hip prosthesis generate 100-fold less wear debris than metal-on-polyethylene, *Acta Orthop Scand* 70 (1999) 578-582.
- [34] R. Hauert, DLC films in biomedical application, C. Donnet, A. Erdemir (eds.), *Tribology of Diamond-like Carbon Films: Fundamentals and Applications*, (2008) 495-509.
- [35] H.F. Hildebrand, J.V. Mercier, A.M. Decaeslecker, P. Ostapzuk, U. Stoeppler, B. Roumazeille, J. Decloux, *Biomaterials*.
- [36] S.G. Steinemann, S.M. Perren, Titanium alloys as metallic biomaterials, in *Proc. of the 5th World Conference on Titanium 2* (1984) 1327-1334.
- [37] <http://www.shorthip-patients.com/cps/rde/xchg/ae-methapat-en-int/hs.xml/7345.html> (2013.10.18)
- [38] P. Aspenberg, A. Anttila, Y.T. Konttinen, R. Lappalainen, S.B. Goodman, L. Nordsletten, S. Santavirta, Benign response to particles of diamond and SiC: bone chamber studies of new joint replacement coating materials in rabbits, *Biomaterials* 17 (1996) 807-812.
- [39] A.G. Cobb, T.P. Schmalzreid, The clinical significance of metal ion release from cobalt-chromium metal on-metal hip joint arthroplasty, *Proceeding of the Institution of Mechanical Engineers, Part H: Journal of Engineering in Medicine* 220 (2) (2006) 385-398.
- [40] F.A. Müller, M. Hagymási, P. Greil, G. Zeiler, A. Schuh, Transfer of metallic debris after dislocation of ceramic femoral heads in hip prostheses, *Archives of Orthopaedic and Trauma Surgery* 126 (3) (2006) 174-180.
- [41] S. Affatato, M. Frigo, A. Toni, An in vitro investigation of diamond-Like carbon as a femoral head coating, *Journal of Biomedical Materials Research* 53 (3) (2000) 221-226.
- [42] G. Thorwarth, C.V. Falub, U. Müller, B. Weisse, C. Voisard, M. Tobler, R. Hauert, Tribological behavior of DLC-coated articulating joint implants, *Acta Biomaterialia* 6 (6) (2010) 2335-234.
- [43] K. Thorwarth, U. Müller, G. Thorwarth, C.V. Falub, M. Stiefel, Ch. Affolter, B. Weisse, C. Voisard, R. Hauert, Failure mechanisms of DLC coated joint replacements, *European Cell and Materials Suppl.* 19 (2) (2010) 24.
- [44] R. Hauert, G. Thorwarth, U. Müller, M. Stiefel, C.V. Falub, K. Thorwarth, T.J. Joyce, Analysis of the in-vivo failure of the adhesive interlayer for a DLC coated articulating metatarsophalangeal joint, *Diamond and Related Materials* 25 (2012) 34-39.
- [45] U. Müller, C.V. Falub, G. Thorwarth, C. Voisard, R. Hauert, Diamond-like carbon coatings on a CoCrMo implant alloy: A detailed XPS analysis of the chemical states at the interface, *Acta Materialia* 59 (2011) 1150-1161.

- [46] R. Hauert, C.V. Falub, G. Thorwarth, K. Thorwarth, Ch. Affolter, M. Stiefel, L.E. Podleska, G. Taeger, Retrospective lifetime estimation of failed and explanted diamond-like carbon coated hip joint balls, *Acta Biomaterialia* 8 (2012) 3170-3176.
- [47] S. Equey, S. Roos, U. Müller, R. Hauert, N.D. Spencer, R. Crockett, Reactions of zinc-free anti-wear additives in DLC/DLC and steel/steel contacts, *Tribology International* 41 (2008) 1090-1096.
- [48] R.L.C. Wu, Synthesis and characterization of diamond-like carbon films for optical and mechanical applications, *Surface and Coatings Technology* 51 (1992) 258-266.
- [49] N. Yoshino, Y. Shibuya, K. Naoi, T. Nanya, Deposition of a diamond-like carbon film on a stainless steel substrate: studies of intermediate layers, *Surface and Coatings Technology* 47 (1991) 84-88.
- [50] C. Dumkum, D.M. Grant, I.R. McColl, A multilayer approach to high adhesion diamond-like carbon coatings on titanium, *Diamond and Related Materials* 6 (1997) 802-806.
- [51] S.S. Perry, J.W. Ager III, G.A. Somorjai, R.J. McClelland, M.D. Drory, Interface characterization of chemically vapor deposited diamond on titanium and Ti-6Al-4V, *Journal of Applied Physics* 74 (1993) 7542-7550.
- [52] F. Kenji, W. Koichiro, U. Kazuo, S. Tadashi, Preparation of highly adhesive diamond-like carbon films by plasma CVD combined with ion implantation, *IHI Engineering Review* 37 (1) (2004) 30-34.
- [53] K. Miyoshi, B. Pohlchuck, K. W. Street, J. S. Zabinski, J. H. Sanders, A. A. Voevodin, R.L.C. Wu, Sliding wear and fretting wear of diamond-like carbon-based, functionally graded nanocomposite coatings, *Wear* 225 (1) (1999) 65-73.
- [54] R. Butter, M. Allen, L. Chendra, A.H. Lettington, N. Rushton, In vitro studies of DLC coatings with silicon intermediate layer, *Diamond and Related Materials* 4 (5-6) (1995) 857-861.
- [55] Y. Ren, I. Erdmann, B. K ü z ü n, F. Deuerler, V. Buck, Effect of deposition parameters on wear particle size distribution of DLC coatings, *Diamond and Related Materials* 23 (2012) 184-188.
- [56] B. Stamm, B. K ü z ü n, O. Filipov, S. Reuter, I. Erdmann, F. Deuerler, D. Krix, K. Huba, H. Nienhaus, V. Buck, Adjustment of wear particle size distribution of DLC coatings for tribological metal-on-metal pairing in artificial hip joints, *Mat.-wiss. und Werkstofftech* 40 (1-2) (2009) 98-100.
- [57] D.P. Monaghan, D.G. Teer, P.A. Logan, I. Efeoglu, R.D. Arnell, Deposition of wear resistant coatings based on diamond like carbon by unbalanced magnetron sputtering, *Surface and Coatings Technology* 60 (1993) 525-530.
- [58] J. Narayan, W.D. Fan, R.J. Narayan, P. Tiwari, H.H. Stadelmaier, Diamond, diamond-like and titanium nitride biocompatible coatings for human body parts, *Materials Science and Engineering: B* 25 (1) (1993) 5-10.
- [59] L. Lu, M.W. Jones, R.L.C. Wu, Diamond-like carbon as biological compatible material for cell culture and medical application, *Biomedical Materials and Engineering* 3 (4) (1993) 223-228.
- [60] S. Miyake, T. Saitoh, S. Watanabe, M. Kanou, Y. Yasuda and Y. Mabuchi, Effects of ion implantation on scratching properties of diamond-Like carbon and boron carbide films, *Japanese Journal of Tribology* 45 (3) (2000) 283-296.

- 
- [61] G. Taeger, L.E. Podleska, B. Schmidt, M. Ziegler, D. Nast-Kolb, Comparison of diamond-like-carbon and alumina-oxide articulating with polyethylene in total hip arthroplasty, *Mat. -wiss. und Werkstofftech* 34 (12) (2003) 1094-1100.
- [62] C.V. Falub, U. Mueller, G. Thorwarth, M. Parlinska-Wojtan, C. Voisard, R. Hauert, In vitro studies of the adhesion of diamond-like carbon thin films on CoCrMo biomedical implant alloy, *Acta Materialia* 59 (2011) 4678-4689.
- [63] C.V Falub, G. Thorwarth, C. Affolter, U. Mueller, C. Voisard, R. Hauert, A quantitative in vitro method to predict the adhesion lifetime of diamond-like carbon thin films on biomedical implants, *Acta Biomaterialia* 5 (2009) 3086-3097.
- [64] M. Mohanty, T.V. Anilkumar, P.V. Mohanan, C.V. Muraleedharan, G.S. Bhuvaneshwar, F. Derangere, Y. Sampeur, R. Suryanarayanan, Long term tissue response to titanium coated with diamond like carbon, *Biomolecular Engineering* 19 (2002) 125-128.
- [65] R. Hauert, L. Knoblauch-Meyer, G. Francz, A. Schroeder, E. Wintermantel, Tailored a-C: H coatings by nanostructuring and alloying, *Surface and Coatings Technology* 120-121 (1999) 291-296.
- [66] A. Schroeder, G. Francz, A. Bruinink, R. Hauert, J. Mayer, E. Wintermantel, Titanium containing amorphous hydrogenated carbon films (a-C: H/Ti): surface analysis and evaluation of cellular reactions using bone marrow cell cultures in vitro, *Biomaterials* 21 (2000) 449-456.
- [67] G. Francz, A. Schroeder, R. Hauert, Surface analysis and bioreactions of Ti- and V-containing a-C: H, *Surface and Interface Analysis* 28 (1) (1999) 3-7.

## **4. Experimental methods for characterization of DLC coatings**

### **4.1 Morphology and structure of DLC coatings**

#### **4.1.1 Coating thickness and roughness**

The coating thickness was measured in this work by Dektak 6M stylus profiler [1] which is a semi-manual instrument as one contacting gauge. The Dektak 6M provides profile data of a sample by detecting the vertical dropping of a stylus which is moved horizontally across the step on the sample surface.

In this work, the thickness of DLC coating deposited on Si wafer, where the step was made by a marker, was used to represent it deposited on P2000 with interface layer due to the same deposition parameters. By means of thickness and weight, the density of DLC coating could be obtained. As is well known, DLC coating possesses the broad range of density  $1.2 \text{ g/cm}^3 \sim 3.1 \text{ g/cm}^3$  depending on the content of  $\text{sp}^3$  [2-6]. Moreover, the DLC coating deposition rate is given by the thickness over deposition time.

The Mitutoyo SJ-301 [7] with cut-off wavelength of 2.5 mm was used to observe the surface roughness of the film characterized by the arithmetic average roughness Ra. The value of Ra is the average roughness after testing at three different positions of each sample. Prior to the measurement, the samples needed to be cleaned in the ethanol solution for 10 min then dried with  $\text{N}_2$ .

#### **4.1.2 Scanning electron microscopy (SEM)**

Scanning electron microscopy (SEM) can be utilized for high magnification imaging of almost all materials. The surface morphology of the coatings could be observed by SEM. SEM consists of three main components: the vacuum system, the electron beam system and the imaging system [8]. Fig. 4.1 shows the schematic diagram of scanning electron microscope.

The principle of SEM is based on the interaction between the electron and substance. The primary electrons emitted from an electron gun pass through a combination of condenser lenses to

produce a fine electron beam with extremely narrow energy spread. The electron beam hits the surface of specimen and interacts with it, which will produce a number of signals including secondary electrons (SE), Auger electrons, back-scattered electrons (BSE), characteristic X-rays, continuum X-rays, elastically scattered electrons and transmission electrons as shown in Fig. 4.2 [9]. Actually the electron beam interacts not only with the surface atoms of specimen, but also with them in a certain thickness of specimen, which is called “interaction volume”. The thickness of interaction volume is different for the different signals. For SE due to their low energy ( $\leq 50$  eV) they are within a few nanometers from the specimen surface [10]. However for X-rays they are originated from few micrometers.

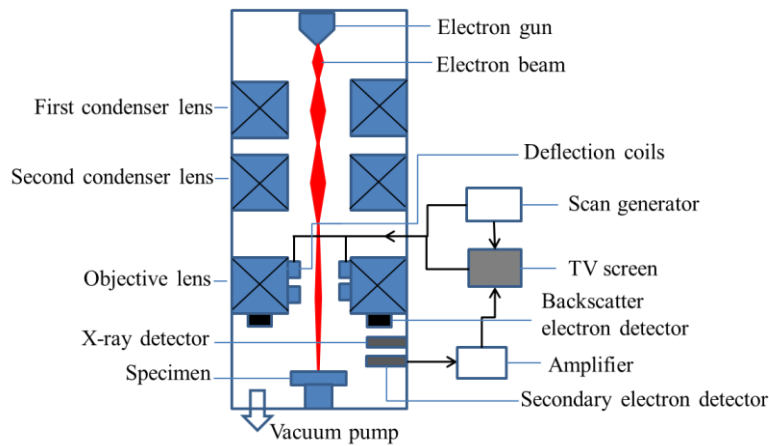


Figure 4.1 Schematic diagram of scanning electron microscope (SEM)

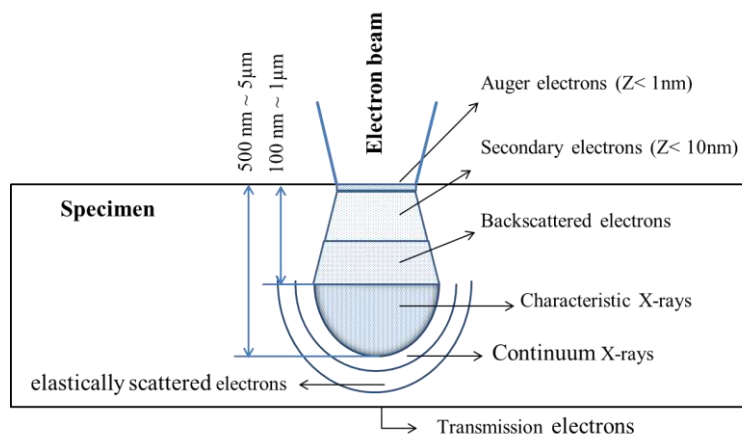


Figure 4.2 Interaction between electron beam and surface layer of the specimen

These signals from interaction can provide diverse physical and chemical information about the specimen itself, for example the morphology, components and structure, and so on. Which information can be obtained is dependent on the detection mode. Different detectors are necessary for different signals. The SE signal is collected by secondary electron detectors which contribute to the formation of SEM images.

The SEM (Zeiss DSM 960) used in recent work has an acceleration voltage (in the range) of 0.5 kV to 30 kV and the resolution is 5 nm at 30 kV (tungsten cathode). The magnification ranges from  $15\times$  to  $200\,000\times$  at a working distance of 7 mm, nevertheless the real value was  $50000\times$  at small contrast and the 23 mm working distance.

Here SEM was carried out in the observation of the morphologies of worn surface and wear particles (or wear debris) after tribological testing. It was also possible to find out the wear mechanism for DLC sliding against DLC in the disc-on-disc wear test setup by analyzing SEM images of worn surface and wear debris. Furthermore, the particle size and shape could be observed directly by SEM images of wear particles, especially the agglomeration of particles.

For the observation of worn surface of DLC coating deposited on P2000, the sample was just mounted on the specimen holder then placed in the chamber directly, whereas, the wear particles could not be used directly in SEM. As is well known, the specimen should be conductive and completely dry for the standard SEM equipment. Therefore, the wear particles collected in suspension in deionized water after tribological test were filtered with a membrane of  $0.2\ \mu\text{m}$  pore size and dried first. The dry particles were mounted on the holder using the conductive double-sided adhesive tape, and then sputtered with gold. Finally, they were located into the chamber.

### **4.1.3 Energy dispersive X-ray spectroscopy (EDX)**

Usually energy dispersive X-ray spectroscopy (EDX) is used for the elemental analysis or chemical characterization of a sample in combination with SEM. Characteristic X-rays generated in a region about  $2\ \mu\text{m}$  in depth (SEM) are emitted by interaction between the electron beam and the specimen surface and detected by the X-ray detector and give information about the elemental

---

composition of the material. The data are acquired in the form of spectra which display the X-ray intensity (I) or number of X-rays as a function of the X-ray energy (E). The intensity of a peak in EDX spectrum is proportional to the content of the corresponding element in the sample. Each element has a unique atomic structure allowing unique set of peaks on its X-ray spectrum [11]. Elements of low atomic number are difficult to detect by EDX. The detection of elements below an atomic number of 11 (Na) was prevented, which resulted from the absorption of the soft X-rays by the Be-window.

Here EDX (Link Analytical Pentafet, Model: 5778) with the Lithium drifted Silicon (SiLi) detector (area of 10 mm<sup>2</sup>) was carried out in conjunction with SEM, and a Beryllium window was used to protect the SiLi detector in the EDX system. The SiLi detector must be operated at liquid nitrogen temperature and the bias of -500 V. The resolution is 143 eV.

In order to determine whether the interface layer was destroyed or not during the tribological testing, the elements of worn area were analyzed combined with SEM images. In this work, the deposited coating was DLC, so carbon of low atomic number was difficult to detect by EDX. However elements from interface layer (Ti) and P2000 substrate were viewed by the EDX spectrum.

#### **4.1.4 Raman spectroscopy**

Raman spectroscopy is a scattering spectroscopy used to analyze the molecular structure of a sample by observing the vibrational and rotational mode. Especially as a fast and nondestructive tool it is also widely used in the characterization of crystalline, nanocrystalline, and amorphous carbon. Much information about samples from Raman spectroscopy can be obtained, for example compositions of material determined by Raman frequencies, stress or strain state correlated to change in frequency of Raman peak, quality of crystal depended on width of Raman peak, and amount of material (thickness of transparent coating) influenced by the intensity of Raman peak [12-13].

When light irradiates a transparent sample and interacts with it, most of light pass through the sample, while a small part can also be scattered in each direction. The scattered light is divided into Rayleigh scattering (elastic scattering) and Raman scattering (inelastic scattering), for which the

vibrational energy level is shown in Fig. 4.3 [14]. In Rayleigh scattering there is no energy exchange but the direction can be changed due to the elastic scattering. That means, the photon is absorbed to a higher virtual level and is instantly scattered elastically back to the initial level. However for Raman scattering not only the direction is changed, when the inelastic collision takes place between the photons and molecular of sample, but also the energy is exchanged. In addition, there are two types of Raman scattering: Stokes scattering and anti-Stokes scattering. The photons emitted by Stokes-Raman scattering usually have a lower energy and frequency than that of the photons absorbed and these photons are inelastically scattered, transferring some of their energy to the molecule. The reverse is also possible; the photons emitted have a higher energy and frequency than the photons absorbed. This is called Anti-Stokes-Raman, but it is not likely at room temperature as electrons prefer to be in the ground state [14].

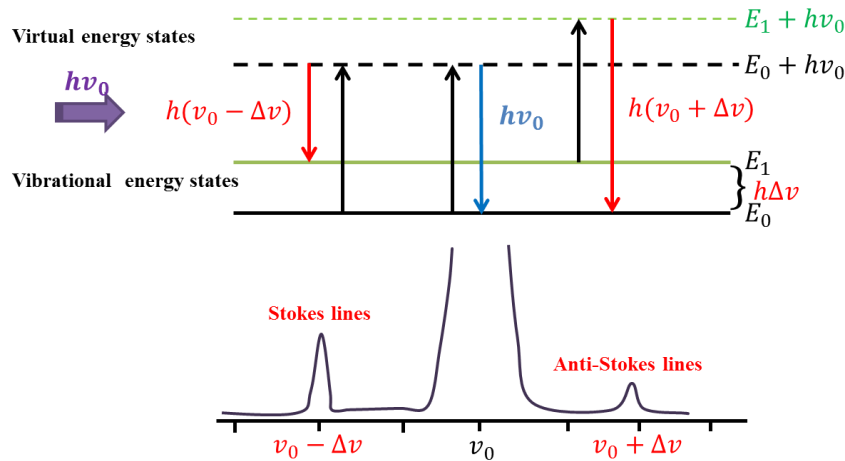


Figure 4.3 Vibrational energy level diagram of Rayleigh scattering and Raman scattering

Upon interaction with matter, a photon excites the molecule from the original state to a virtual energy state. At room temperature, almost all molecules are in the ground state, so the intensity of Stokes lines is more than that of anti-Stokes lines. In Raman spectroscopy Stokes lines are recorded. Raman shift ( $\Delta\nu$ ) is expressed typically in wave number ( $\text{cm}^{-1}$ ) plotted on the abscissa in Raman spectrum. The formula is described as:

$$\Delta\nu = \frac{1}{\lambda_0} - \frac{1}{\lambda_1} \quad (1)$$

where  $\lambda_0$  is the excitation wavelength and  $\lambda_1$  is the Raman spectrum wavelength.

For the different substance, the photons emitted have unique wavelength because each molecule has a different set of vibrational energy levels. The value of  $\Delta\nu$  is dependent on the molecule structure, not related to the excitation wavelength  $\lambda_0$ . Other values, e.g. peaks and intensity in the spectrum also rely on the vibrational and rotational modes of molecule in substance.

In this work, the material is DLC coating deposited by vacuum arc. The internal structure of the coating was investigated using a micro-Raman system of JOBIN YVON with the visible excitation of the  $514.5\text{ nm Ar}^+$  laser line. Usually the visible Raman spectroscopy is carried out at the commonly available wavelengths in the blue-green spectral region (488-514.5 nm), which is 50-230 times more sensitive to  $sp^2$  sites [12, 15] than the  $sp^3$  phase as visible photons preferentially excite their  $\pi$  states [13]. The shortest excitation wavelength (typical UV excitation of 244 nm) with the highest resolution and higher photon energy of 5.1 eV can excite both the  $\pi$  and the  $\sigma$  states corresponding to the  $sp^2$  and  $sp^3$  sites [13, 16-18]. Different kind of carbon has different Raman spectrum as shown in Fig. 4.4 [19-20].

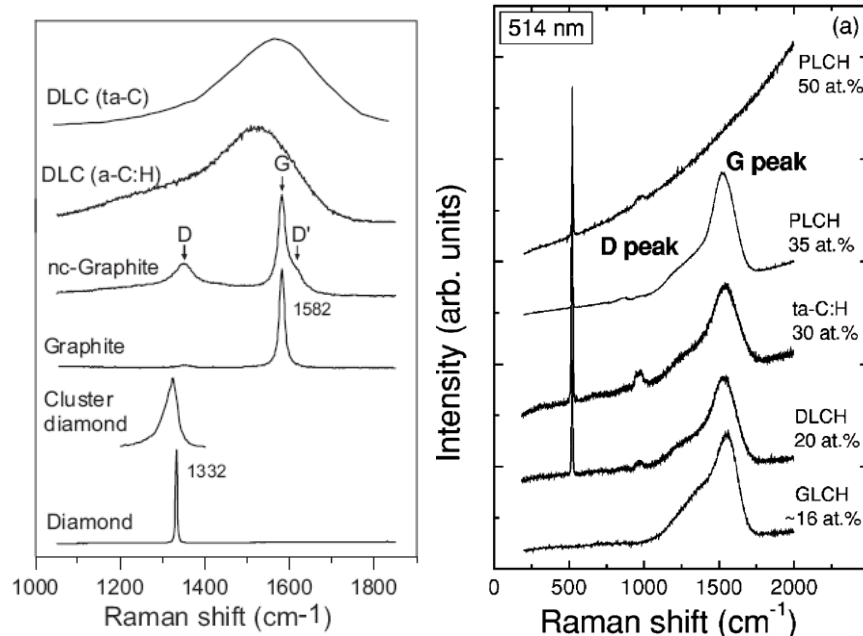


Figure 4.4 Characteristic Raman spectra of some carbon-based materials at 514.5 nm [19,20]

The Raman spectrum of diamond is  $1332\text{ cm}^{-1}$  due to the zone center phonons of  $T_{2g}$  symmetry mode [21]. The G peak of  $1575\text{ cm}^{-1}$  represents the Raman spectrum of graphite due to

$E_{2g}$  C(sp<sup>2</sup>)-C(sp<sup>2</sup>) stretching mode [22]. D peak around 1355 cm<sup>-1</sup> is assigned to A<sub>1g</sub> symmetry mode. The G and D peaks are due to sp<sup>2</sup> sites only. The G peak belongs to the bond stretching modes of all pairs of sp<sup>2</sup> atoms in both rings and chains. So this mode does not need the presence of sixfold rings. However, the D peak is correlated to the breathing modes of sp<sup>2</sup> sixfold aromatic rings, and this mode only becomes active in the presence of disorder [13].

The T peak at around 1060 cm<sup>-1</sup> due to C-C sp<sup>3</sup> bonding can be observed only in UV excitation [13, 16, 17, 23]. In nano-crystalline diamond (NCD) or ultra nano-crystalline diamond (UNCD), the 1150 cm<sup>-1</sup> peak is always accompanied with the peak of ~1450 cm<sup>-1</sup> and shows the strong dispersion, which is not related to the diamond grains (sp<sup>3</sup>-bonded carbon) assigned to the  $\bar{\nu}_1$  and  $\bar{\nu}_3$  modes of a contamination in the grain boundaries by transacetylene [24-25]. The origin of peaks at ~1150 cm<sup>-1</sup> and ~1450 cm<sup>-1</sup> in nanocrystalline diamond were reported by A.C. Ferrari [24, 26]. Furthermore, J. Birrell [26] reported that these two peaks of ~1150 cm<sup>-1</sup> and ~1450 cm<sup>-1</sup> in the Raman spectrum of UNCD maybe due to carbon-hydrogen bonds in the grain boundaries.

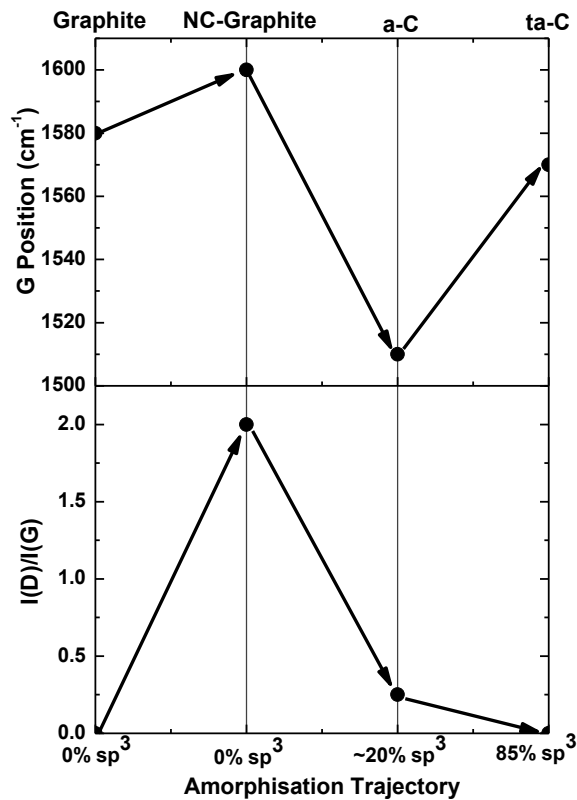


Figure 4.5 Amorphization trajectory [13]

---

For different amorphous carbon coatings, the Raman peak position is correlated to the structure of coating itself dependent on the deposition process. It was reported by Tarrant [27] that more than one G peak appeared in Raman spectrum of DLC films deposited by pulsed substrate bias, which was assigned to A peak at  $1550\text{ cm}^{-1}$  determined by the range and population of non-hexagonal  $sp^2$  bonded groupings. The G peak can be shifted to frequency above  $1575\text{ cm}^{-1}$  when DLC (ta-C) is very hard with high content of  $sp^3$  shown in Fig. 4.4 [19]. As well known the visible Raman spectrum depends fundamentally on the order of  $sp^2$  sites and only indirectly on the fraction of  $sp^3$  sites [13].

However, Raman scattering is sometimes used to probe the  $sp^2/sp^3$  fraction in DLC's by the  $I_D/I_G$  ratio. According to the phenomenological three-stage model presented by A.C. Ferrari et al. [9], a schematic variation of the G position and  $I_D/I_G$  ratio in visible Raman spectra is shown in Fig. 4.5. In Fig. 4.5 the possible role of hydrogen on the spectrum is not taken into consideration because the C-H stretching modes have no detectable contribution in the G and D peaks of visible Raman spectra.

In ref. [19] the role of hydrogen in a-C:H coatings are discussed. On the one hand, hydrogen changes the carbon network by converting C=C groups into  $sp^3$  bonded CH-CH groups. On the other hand, the background luminescence increases because the optical gap is increased resulting from the number of  $sp^3$  sites with increased hydrogen content. The C-H stretching modes lie outside the D and G regions above  $3000\text{ cm}^{-1}$  which can only be observed in UV excitation due to the overwhelming cross section of  $sp^2$  sites in visible excitation [28].

The Raman spectrum of DLC which is more disordered is considered to depend on clustering of the  $sp^2$  phase, bond disorder, the presence of  $sp^2$  rings or chains and the  $sp^2/sp^3$  fraction as shown in Fig. 4.6 [13]. The G and D peak positions and the  $I_D/I_G$  ratio in the Raman spectra change more or less according to the different kinds of amorphous carbon due to the introduction of a series of defects: bond-angle disorder, bond-length disorder and hybridization.

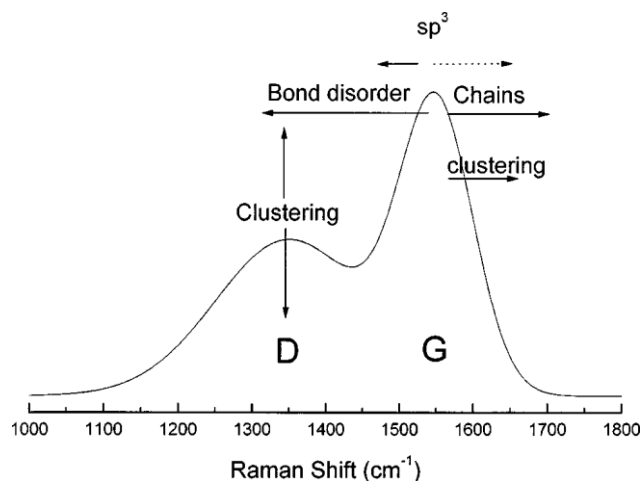


Figure 4.6 Schematic diagram of influence on the Raman spectra

A dotted arrow marks the indirect influence of the  $sp^3$  content on increasing G positions [13].

The clustering and disorder of the  $sp^2$  phase are the main factor affecting peak positions, width, and intensity [20]. The  $I_D/I_G$  ratio is a measurement of the size of the  $sp^2$  phase organized in rings [13]. If the  $I_D/I_G$  ratio is near zero, the  $sp^2$  phase is mainly organized in chains, or, even if rings are present, the  $\pi$  bonds are not fully delocalized on the rings [13]. Another Raman parameter is the full width at half maximum of the G peak, FWHM (G), which examines those  $sp^2$  clusters resonant at particular excitation energy as a single wavelength parameter. That means, clusters have the similar size at a given excitation wavelength. Actually FWHM (G) is mainly a measurement of structural disorder caused by bond angle and bond length distortions. At a given cluster size, FWHM (G) is increased with the increase of bond length and bond angle disorder [20]. In contrast the size and shape distribution of  $sp^2$  cluster resulting in topological disorder can be probed by G peak dispersion, Disp(G). The G peak dispersion results from the resonant selection of  $sp^2$  chains of different sizes at different excitation energies [28-29].

For DLC coatings, one broad Raman peak appears in the range between  $1000\text{ cm}^{-1}$  and  $1800\text{ cm}^{-1}$ , which can be fitted by Gaussians or Lorentzians on a linear background. It is discussed in detail about multi-peak fitting analysis of Raman spectra at  $514.5\text{ nm}$  in chapter 6.1.

---

## 4.2 Tribological evaluation of DLC coatings

Tribology is the science and technology of contacting surfaces having a relative motion against each other. This means that tribology deals with the phenomena of friction and wear of surface with and also without lubrication. In several fields of technical application, e.g., in the automotive or aircraft industries, the reduction of friction and wear is a very important aspect with respect to longer lifetimes. What's more, it is also important and has become a true clinical problem in biomedical applications, especially for artificial hip joints.

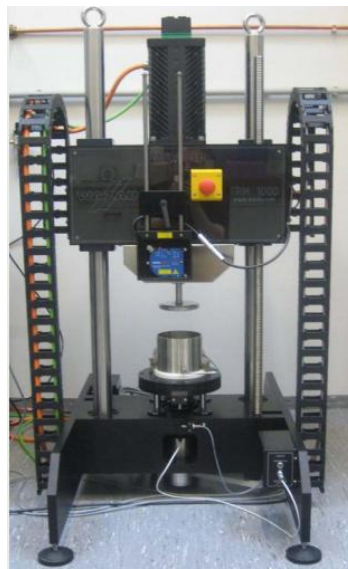


Figure 4.7 The tribological test setup [30]

The main mechanical properties, such as friction coefficient and wear rate are measured here by a Wazau TRM 1000 tribometer (Berlin, Germany) using the disc-on-disc test as shown in Fig. 4.7 [30]. Meanwhile, the wear particles are generated by this tester, where a rotary disc is located above and pressed against a stationary disc with a defined normal force. Deionized water is used as lubrication. During tests with high values of friction torque leading to a temperature rise of the lubricant, the temperature of the lubricant can be measured. Usually it is kept at room temperature. The test is conducted at the defined direction. The normal force is set by means of a drive-spindle system adjustable from 5 ~ 1000 N. Actually the normal force is dependent on the properties of samples. If the DLC coating deposited is harder, the normal force must be increased in order to get enough wear particles. The minimum of normal force used in this work is 50 N for the

disc-on-disc setup. The velocity of circulation or rotational speed can be set, and here 0.01 m/s as velocity is chosen. The radius of 15.5 mm or 16 mm is set dependent on the diameter of sample. The other value is automatically calculated by the equation:

$$v = 2 \cdot \pi \cdot r \cdot n / (60 \cdot 1000) \quad (2)$$

where  $v$  = velocity [m/s]

$r$  = radius [mm]

$n$  = rotational speed [ $\text{min}^{-1}$ ].

The value of friction coefficient at rotating movement is calculated satisfying the following equation:

$$\mu = M \cdot 1000 / F_N \cdot r \quad (3)$$

where  $\mu$  = friction coefficient

$M$  = friction torque [Nm]

$F_N$  = normal force [N].

The wear rate can be calculated from the wear amount and the time.

After tribological test, not only the mechanical properties of coatings can be obtained, but also the wear particles can be produced. For the analysis of the wear particle size distribution, the particles must be collected. It is difficult to collect all wear particles. In addition one must take care that the particle concentration is not too low, and also ensure that the material collected is representative of the most particles collective. The detail about particles collection will be discussed in Section 6.4.

### 4.3 Cavitation erosion test

Cavitation is the process of rupturing a liquid by decrease in pressure at roughly constant liquid temperature. It involves the formation, growth and rapid collapse of cavities or bubbles and occurs in flowing liquid. When cavities collapse close to a solid surface, it may result in high velocities, pressures, and temperatures which can cause the material damage. Besides the effects of vibration and damage, cavitation can produce the effects of noise and erosion even corrosion because of the presence of a liquid environment frequently [31-32].

In the laboratory an ultrasonic equipment of ASTM G32-98 [33] is used with vibratory apparatus for cavitation erosion of DLC coatings (Fig. 4.8), by which the adhesion of DLC coatings to substrate can be investigated, combined with the quantitative images analysis. The frequency vibration of the sonotrode (frequency of 20 kHz) causes a cavitation bubble field in front of the substrate surface originated by the pressure fluctuations at the tip of the sonotrode [34-36]. The occurrence of cavitation is in flowing liquid systems where hydrodynamic effects result in regions of the flow where the pressure falls below the vapor pressure [32]. Therefore, the surface of sample is destroyed by the repeated treatment of the gas and fluid cavities implosion. In addition, the high energetic fluid jets with about the diameter of  $\sim 1\mu\text{m}$ , where the pressure of  $10^5$  bar can be obtained, cause the surface disruption by fatigue [35].

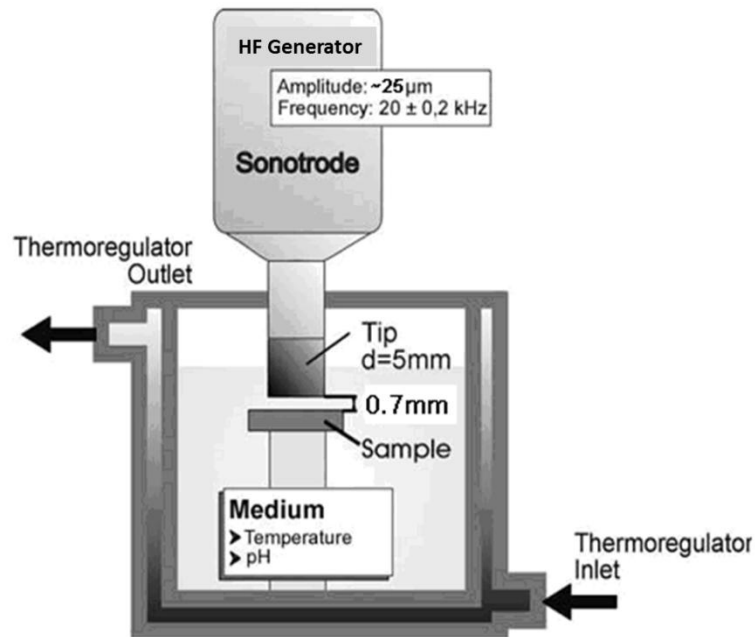


Figure 4.8 Cavitation equipment [35]

In order to compare all samples well, all cavitation charging must be tested with the constant parameters, for example, 5 mm diameter of sonotrode, 0.7 mm distance between the sonotrode and the substrate, water with  $27^\circ\text{C}$ . The vessel is filled up to 2 cm below the edge of the pool with the cavitation, and the sonotrode is to adjust so that 8-16 mm of sonotrode will be immersed in the cavitation medium according to ASTM G32-98 [35]. In Section 6.3 it is described clearly that how and why to choose appropriate parameters for certain materials prior to the cavitation test.

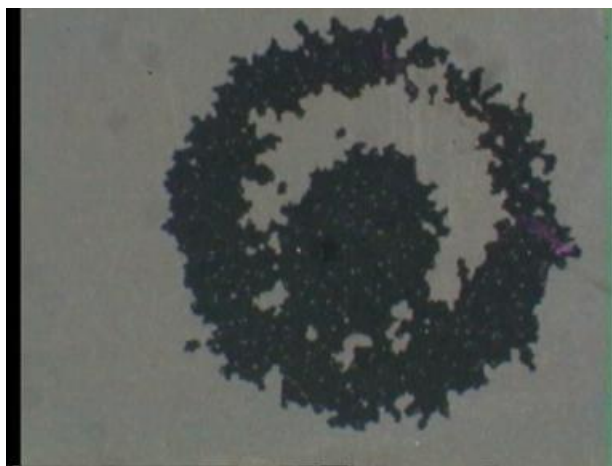


Figure 4.9 Wear damage by cavitation erosion of DLC coatings

At an incubation period of cavitation charging there is no any measurable wear, then the wear of DLC coating starts with the test duration. After cavitation erosion test, the quality was analyzed by light microscopic investigation. The change of the surface area is converted into the surface damage by means of quantitative evaluation through quantitative image analysis (see Fig. 4.9). The high black and white contrast of the light microscope, which resulted from the small depth of focus, allows a separation between undamaged and worn coating areas. The percentage of worn area can be calculated automatically by the application software (named Color World programmed by Jialiang Guan). The properties of coatings and substrate could be optimized by comparison of the adhesion of all samples by means of different proportions of the surface damage mass.

#### 4.4 Particle size distribution analysis

The wear particles are collected in suspension in the deionized water, then measured using a laser scattering particle size analyzer Horiba LA-950 with 17 channels per decade as shown in Fig. 4.10 [37]. In this equipment Mie scattering theory is used. The widest dynamic range of  $0.01 \mu\text{m} \sim 3000 \mu\text{m}$  which is determined by Laser light diffraction spectrometry makes it possible to perform precise particle size measurements on a wide scale in many different industries.

According to the ref. [38], there are two reasons which influence the result of distribution. One is different physical properties used in characterizing the “size” of individual particles.

Another is different types and different measures of quantity chosen. Here the volume cumulative distribution  $Q_3(x)$  and the volume density distribution  $q_3(x)$  are chosen to characterize the size of particles. All values are measured in certain size intervals.



Figure 4.10 The equipment of particle size distribution analyzer [37]

The volume cumulative distribution  $Q_3(x_i)$ , the range from 0 to 1, represents the concentration of particles equal to or smaller than a given particle size  $x_i$ . The density distribution (the frequency distribution)  $q_3(x_i)$  which is the first derivative or the slope of  $Q_3(x)$  represents the amount of particles of a given particle size  $x_i$ , relative to the entire particle size distribution:

$$q_3(x_i) = \frac{dQ_3(x)}{dx} \quad (4)$$

As formula (4) shows, it should be noted that the density distribution has the dimension of an inverse length and represents amounts of particles that fall within the interval size. According to the cumulative distribution and density distribution, other various parameters can be determined, including the median value  $x_{50}$ , the modal value  $x_{\text{mod}}$  and the mean value  $\bar{x}$ . The median value means 50% of the total particle collective is smaller than  $x_{50}$ ,  $Q_3(x) = 0.5$ . The modal value that occurs most often, is the particle size at which the density distribution  $q_3(x_i)$  exhibits a maximum.

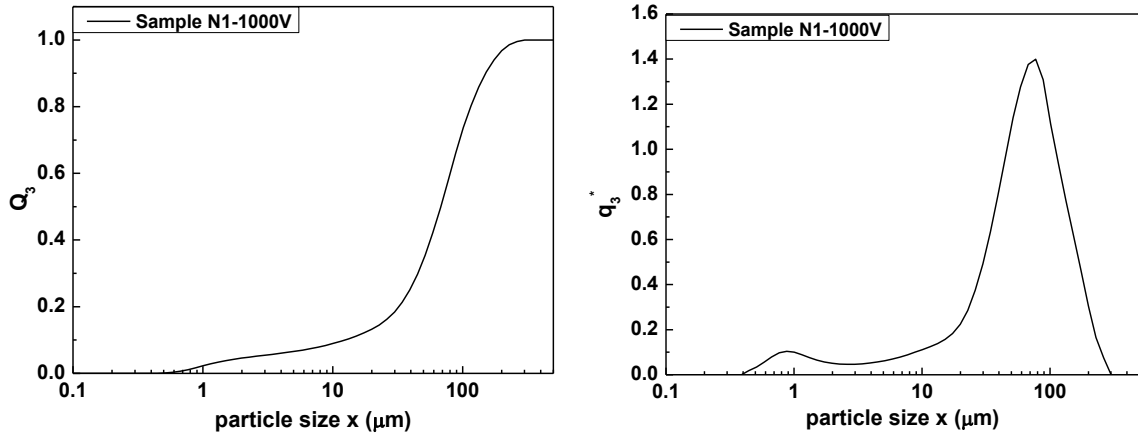


Figure 4.11 Cumulative distribution and transformed frequency distribution of sample N1 deposited with an anode-cathode diameter ratio of  $d_a/d_c = 3/1$  at a DC bias of  $-1000$  V

By means of particle size analyzer Horiba LA-950, the cumulative distribution  $Q_3(x)$  and the transformed frequency distribution  $q_3^*(x)$  of samples can be directly obtained as shown in Fig. 4.11. Actually the value of  $q_3^*(x)$  can be determined by  $Q_3(x)$ :

$$q_3^*(x) = \frac{dQ_3(x)}{d \log x} \quad (5)$$

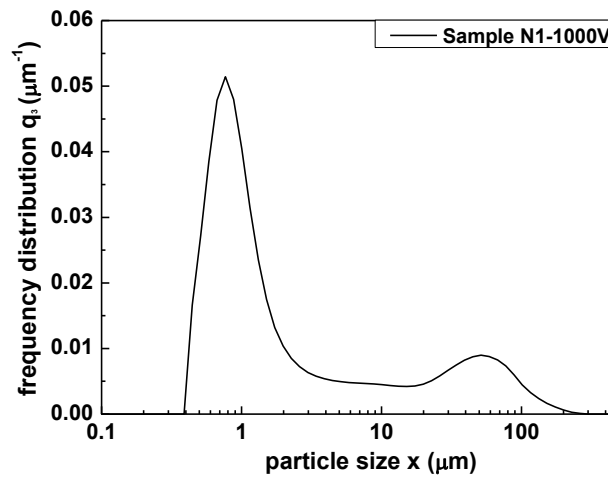


Figure 4.12 Frequency distribution  $q_3(x)$  of sample N1 deposited with an anode-cathode diameter ratio of  $d_a/d_c = 3/1$  at a DC bias of  $-1000$  V

In these experiments, the frequency (density) distribution  $q_3(x)$  as one representation of particle size analysis is illustrated in Fig. 4.12, which is totally different from the transformed frequency distribution  $q_3^*(x)$  shown in Fig. 4.11.

---

When the particle size analyzer Horiba LA-950 is used, many parameters need to be set prior to analysis. It is very important to select appropriate analysis parameters for one certain sample, for example the refractive index of sample and solvent, the speed of the circulation pump and ultrasonic as dispersion conditions, even including the particle collection. In this work 1.952 of carbon is chosen as the refractive index and demineralized water (refractive index  $n_c=1.333$ ) is the dispersion medium. The details about parameters can be seen in Section 6.4.

## References

- [1] C. Kowalski, Dektak 6M Manual, Digital Instruments Veeco Metrology Group, 2002.
- [2] P. Koidl, C. Wagner, B. Dischler, J. Wagner, M. Ramsteiner, Plasma deposition, properties and structure of amorphous hydrogenated carbon films, *Materials Science Forum* 52-53 (1990) 41-70.
- [3] D.R. McKenzie, Tetrahedral bonding in amorphous carbon, *Reports on Progress in Physics* 59 (12) (1996) 1611-1664.
- [4] P.J. Fallon, V.S. Veerasamy, C.A. Davis, J. Robertson, G.A. Amaratunga, W.I. Milne, J. Koskinen, Properties of filtered-ion-beam-deposited diamondlike carbon as a function of ion energy, *Physical Review B* 48 (7) (1993) 4777-4782.
- [5] G.M. Pharr, D.L. Callahan, S.D. McAdams, T.Y. Tsui, S. Anders, A. Anders, J.W. Ager, I.G. Brown, C.S. Bhatia, S.R.P. Silva, J. Robertson, Hardness, elastic modulus, and structure of very hard carbon films produced by cathodic-arc deposition with substrate pulse biasing, *Applied Physics Letters* 68 (6) (1996) 779-781.
- [6] M. Weiler, S. Sattel, K. Jung, H. Ehrhardt, V.S. Veerasamy, J. Robertson, High tetrahedral, diamond-like amorphous hydrogenated carbon prepared from a plasma beam source, *Applied Physics Letters* 64 (21) (1994) 2797-2799.
- [7] Surface measurement surftest SJ-301, Mitutoyo Europe GmbH, Neuss, Germany PRE 1211 (3).
- [8] R.E. Lee, *Scanning electron microscopy and X-ray microanalysis*, Prentice-Hall (QH212S3L44) for undergraduate students (1993) 93-95.
- [9] L. Reimer, *Scanning electron microscopy-physics of image formation and microanalysis*, Second Edition, *Measurement Science and Technology* 11 (12) (2000).
- [10] B. Jaehne, H. Haussecker, P. Geissler, *Handbook of Computer Vision and Applications Volume 1 Sensors and Imaging*, San Diego, London, Boston, New York, Sydney, Tokyo, Toronto, Academic Press(1999) 364-367.
- [11] J. Goldstein, *Scanning Electron Microscopy and X-Ray Microanalysis*. Springer. ISBN 978-0-306-47292-3 (2003) Retrieved 26 May 2012.
- [12] S. R. Salis, D.J. Gardiner, M. Bowden, J. Savage, D. Rodway, Monitoring the quality of diamond films using Raman spectra excited at 514.5 nm and 633 nm, *Diamond and Related Materials* 5 (6-8) (1996) 589-591.

- [13] A.C. Ferrari, J. Robertson, Interpretation of Raman spectra of disordered and amorphous carbon, *Physical Review B* 61 (2000) 14095-14107.
- [14] D.C. Harris, M.D. Bertolucci, *Symmetry and spectroscopy: an introduction to vibrational and electronic spectroscopy*, New York Dover Publications (1989).
- [15] N. Wada, P. J. Gaczi, S.A. Solin, "Diamond-like" 3-fold coordinated amorphous carbon, *Journal of Non-Crystalline Solids* 35-36 (1980) 543-548.
- [16] K.W.R. Gilkes, H.S. Sands, D.N. Batchelder, J. Robertson, W.I. Milne, Direct observation of  $sp^3$  bonding in tetrahedral amorphous carbon using ultraviolet Raman spectroscopy, *Applied Physics Letters* 70 (15) (1997) 1980-1982.
- [17] V.I. Merkulov, J.S. Lannin, C.H. Munro, S.A. Asher, V.S. Veerasamy, W.I. Milne, UV studies of tetrahedral bonding in diamondlike amorphous carbon, *Physical Review Letters* 78 (25) (1997) 4869-4872.
- [18] D. W. Pohl, W. Derik, M. Lanz, Optical stethoscopy: Image recording with resolution  $\lambda/20$ , *Applied Physics Letters* 44 (7) (1984) 651-653.
- [19] G. Irmer, A. Dorner-Reisel, Micro-Raman studies on DLC coatings, *Advanced Engineering Materials* 7 (8) (2005) 694-705.
- [20] C. Casiraghi, A.C. Ferrari, J. Robertson, Raman spectroscopy of hydrogenated amorphous carbons, *Physical Review B* 73 (2005) 085401 1-14.
- [21] D.S. Knight, W.B. White, Characterization of diamond films by Raman spectroscopy, *Journal of Materials Research* 4 (1989) 385-393.
- [22] F. Tuinstra, J.L. Koenig, Raman spectrum of graphite, *Journal of Chemical Physics*, 53(3) (1970) 1126-1130.
- [23] M. Rybachuk, J.M. Bell, Growth of diamond-like carbon films using low energy ion beam sputter-bombardment deposition with Ar ions, *Journal of Physics: Conference Series* 100 (2008) 082009 1-4.
- [24] A.C. Ferrari, J. Robertson, Origin of the  $1150\text{-cm}^{-1}$  Raman mode in nanocrystalline diamond, *Physical Review B* 63 (2001) 121405(R) 1-4.
- [25] R. Pfeiffer, H. Kuzmany, P. Knoll, S. Bokova, N. Salk, B. Guenther, Evidence for trans-polyacetylene in nano-crystalline diamond films, *Diamond and Related Materials* 12 (2003) 268-271.
- [26] J. Birrell, J.E. Gerbi, O. Auciello, J.M. Gibson, J. Johnson, J.A. Carlisle, Interpretation of the Raman spectra of ultrananocrystalline diamond, *Diamond and Related Materials* 14 (2005) 86-52.
- [27] R.N. Tarrant, D.R. McKenzie, M.M.M. Bilek, Raman characterization of PIII multilayer carbon films, *Diamond and Related Materials* 13 (2004) 1422-1426.
- [28] A.C. Ferrari, J. Robertson, Resonant Raman spectroscopy of disordered, amorphous, and diamondlike carbon, *Physical Review B* 64 (2001) 075414 1-13.
- [29] S. Piscanec, F. Mauri, A.C. Ferrari, M. Lazzeri, J. Robertson, Ab initio resonant Raman spectra of diamond-like carbons, *Diamond and Related Materials* 14 (3-7) (2005) 1078-1083.

- 
- [30] Manual Tribometer Type TRM 1000, Dr. -Ing. Georg Wazau Mess- + Prüfsystem GmbH, Berlin, Germany, (2007) 1-69.
- [31] B.J. Briscoe, M.J. Adams (eds), Tribology in Particulate Technology, 1987
- [32] C.E. Brennen, Cavitation and bubble dynamics, CHAPTER 3, Cavitation bubble collapse, Oxford University Press 1995.
- [33] [ASTM G 32-98/1998] Standard Test Method for Cavitation Erosion Using Vibratory Apparatus.
- [34] F. Deuerler, H. Gruner, M. Pohl, L. Tikana, Wear mechanisms of diamond-coated tools, Surface and Coatings Technology 142-144 (2001) 674-680.
- [35] F. Deuerler, O. Lemmer, M. Frank, M. Pohl, C. Heßing, Diamond films for wear protection of hard metal tools, International Journal of Refractory Metals & Hard Materials 20 (2002) 115-120.
- [36] F. Deuerler, M. Pohl, C. Heßing, Micro- and nanostructured diamond films under wear charging in cavitation test, Surface and Coatings Technology 174-175 (2003) 732-737.
- [37] Partikelgrößenanalyse mit Statischer Laserlichtstreuung, HORIBA LA-950, Retsch Technology GmbH Haan, Germany 99.950.0001/D-11-2010.
- [38] K. Leschonski, Representation and evaluation of particle size analysis data. Part. Charact. I (1984) 89-95.

## 5. Experiments for deposition of interface layer and DLC coatings

### 5.1 Deposition of interface layer (Ti) by cathodic arc evaporation

#### 5.1.1 Deposition setup (Cathodic arc evaporation)

The interface layers were deposited on the P2000 discs by vacuum arc from the titanium cathode with DC bias voltage. The schematic diagram of the deposition system used in this study was shown in Fig. 5.1. The cathodic target is located in the chamber with a water cooling system and connected to the power supply which has a low voltage and high current supply ranged from 0 ~ 40 V and 0 ~ 100 A, respectively. Another small electrode is a carbon striker. The vacuum arc is initiated by touching the titanium cathode with a small carbon striker electrode and withdrawing the striker mechanically.

In order to get the higher current to maintain a vacuum arc, the power supply is operated in parallel with another unit which permits one “master” supply to control the other supplies. Here two TCR 3 phase power supplies LAMBDA EMI with 4 kW maximum output power are used [1].

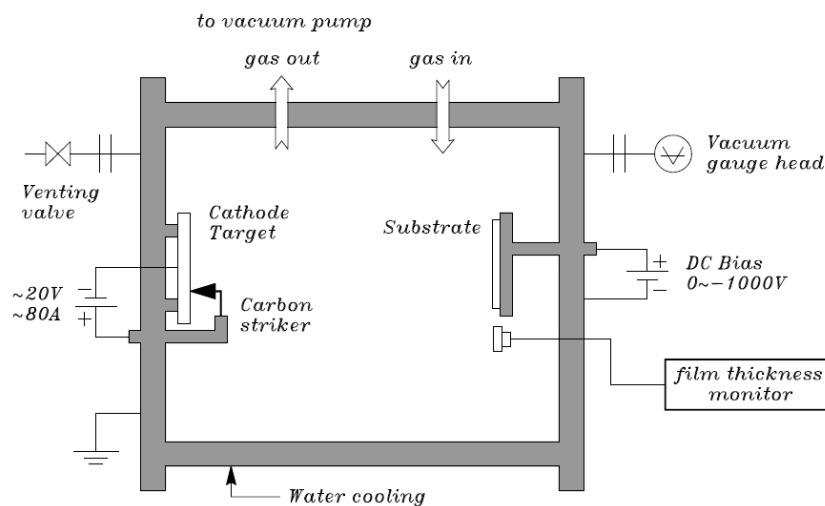


Figure 5.1 Schematic diagram of cathodic vacuum arc deposition system for interface layer

The bias supply connected to the substrate is MAGPULS QP-1000/10/20 bp by Magtron with the maximum frequency of 33 KHZ [2]. The applied voltage, duty cycle and frequency could

be adjusted from 0 to 1000 V, 0 to 100 % and 0.05 to 33 kHz, respectively. However, in this work, the chosen mode is the DC bias not pulse bias.

### 5.1.2 Deposition Process

In this work, discs of 31 mm diameter and 4 mm thickness were used as substrates made of P2000. P2000 is a Cr-Mn-Mo-N-steel as shown in Table 5.1 for high technological components remelted under high pressure (DIN-Code: 1.4452) [3]. This material is developed by the company Energietechnik Essen and passed the bio-compatibility test according to DIN ISO 10993-5 [3], with hardness of 380 HV30 [4-5].

Table 5.1 Chemical analysis of P2000 [3]

[Co. %]	C	Si	Mn	P	N	Al	Cr	Mo	Ni	V	Nb
Min.	--	--	12.00	--	0.75	--	16.00	2.50	--	--	--
Max.	0.15	1.00	16.00	0.05	1.00	0.10	20.00	4.20	0.30	0.20	0.25

For optimum tribological performance, controlling the initial nucleation density of DLC is the key to obtain uniform and continuous DLC films which must be deposited onto highly polished surfaces. The most widely used surface pretreatments involve modification of the substrate surface either by abrading the surface with diamond particles [6] or bombarding the surface with diamond particles by immersing the substrate in a diamond suspension by ultrasonic agitation [7]. In these experiments, the surfaces of discs were polished with diamond suspension by a factory. After polishing, the substrates are treated in an ultrasonic bath with an isopropanol solution for 10 min, and then blown dry with N<sub>2</sub>. Before deposition the weights of the samples are measured.

Pre-cleaned discs were placed onto the stainless steel substrate holder. The pure titanium target as the cathode was disc-shaped. The inside of chamber was necessary to clean with vacuum cleaner first then the wall with ethanol. After cleaning the chamber the cathode and the substrate holder were installed into it and made them stationary. When the process chamber was in a high vacuum, the DC bias supply was turned on first to make sure the surface of substrate was clean, and then the arc power supply was switched on. At last the button of controlling the small carbon

## 5. Experiments for interface layer characterization of DLC coatings

striker was pressed to make it contacted and separated with the cathode quickly. Then the arc formed on the cathode and the cathodic material (Ti) was evaporated. Meanwhile, the plasma was produced in the vapor of the vaporized material (Ti). In this work, the interface layer deposition was carried out without any gases.

Table 5.2 Deposition process parameters for interface layers

Deposition parameters	Conditions
Arc current	40 A - 80 A
Arc voltage	20 V - 40 V
Deposition time	5 min
Substrate	P2000

The deposition time was 5 min. During the deposition of titanium, the DC bias applied to the substrate was changed with time. At the beginning the DC bias of  $-1000$  V was set, which was after 30 s continuously reduced within 4 min and 30 s to  $-100$  V. The deposition pressure was increased first when an arc was initiated and then decreased with decreasing the bias slowly. The temperature of the cathode and the substrate holder was controlled by water cooling. Experimental parameters are summarized in Table 5.2.

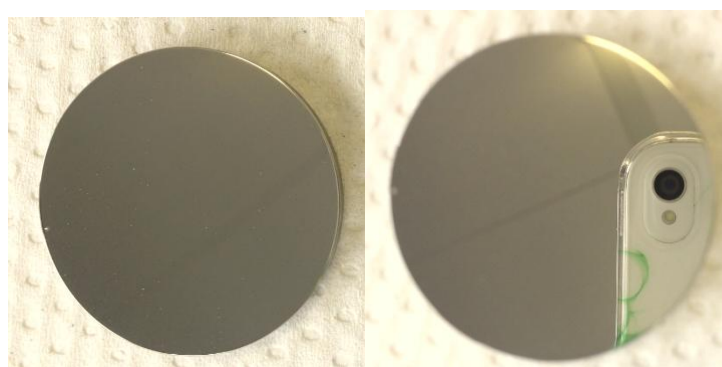


Figure 5.2 Interface layer of Ti deposited on P2000

After deposition, the chamber needed some time to cool down, so the cooling water must run in the whole deposition process. Usually the deposited interface layer of Ti showed the silver color and looked like a mirror as shown in Fig. 5.2.

---

## 5.2 Relationship between deposition pressure and arc voltage and current

As described above, the working pressure during the deposition of Ti was not constant. Usually the deposited interface layer of Ti showed the silver color. When Ti was grown at the pressure of  $2 \sim 4 \times 10^{-2}$  mbar (base pressure of  $1 \times 10^{-3}$  mbar), the film displayed the diverse color which indicated the nonuniformity of coating. What's more, the arc current and voltage changed with the pressure, kept at  $40 \text{ A} \sim 60 \text{ A}$  and  $30 \text{ V} \sim 40 \text{ V}$  respectively. There seemed to be some relationship between deposition pressure and arc voltage and current. In addition, in order to get low-pressure gas ambient further vacuum pump was connected to the system. After that a base chamber pressure of less than  $7 \times 10^{-4}$  mbar was achieved.

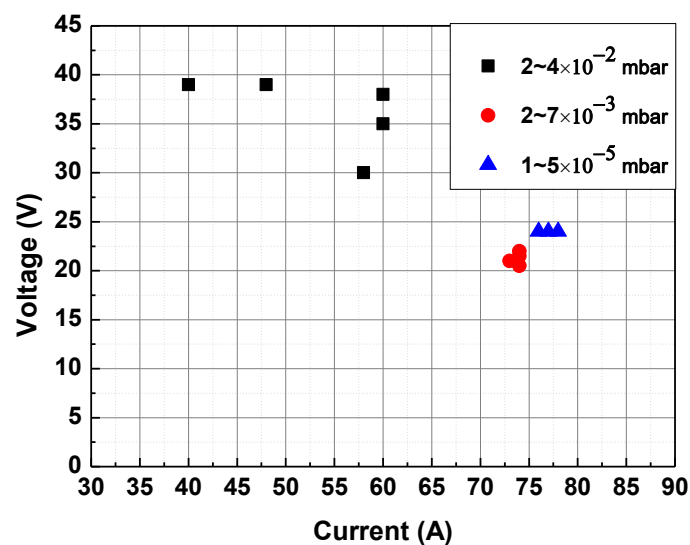


Figure 5.3 Relationship between voltage and current at the different deposition pressure

Argon was added to establish a stable chamber pressure and the arc was stable. Just for the study of the relation between pressure and arc voltage and current there was no sample in chamber and no bias voltage applied to the substrate. The chamber pressure controlled by the argon gas flow rate was varied from  $5.5 \times 10^{-3}$  mbar to  $6.4 \times 10^{-6}$  mbar, with which the voltage and current were changed in the range of  $20 \text{ V} \sim 25 \text{ V}$  and  $70 \text{ A} \sim 80 \text{ A}$ , respectively.

The relationship was observed by plotting the arc voltage and current as a function of the chamber pressure as shown in Fig. 5.3. It was found that the arc voltage and current were increased with decreasing the chamber pressure.

The titanium was deposited on P2000 as the process described above. During the deposition argon was used to adjust the deposition pressure. When the DC bias was applied to the substrate, the relation between deposition pressure and the characteristic of arc was different from it without bias. By comparison, at the same deposition pressure the arc current was increased, but the arc voltage was kept at the constant when the bias was introduced to the substrate as shown in Table 5.3.

Table 5.3 Comparison of effect of the bias on the arc characteristic

Deposition pressure / mbar	No DC bias to the substrate		With DC bias to the substrate	
	Voltage / V	Current / A	Voltage / V	Current / A
$2\sim7\times 10^{-3}$	21	70	21	74
$1\sim5\times 10^{-5}$	24	73	24	77

During the whole deposition of Ti, the voltage and current were changed with the working pressure as shown in Fig. 5.3. At the higher pressure of  $\sim 10^{-2}$  mbar the higher voltage and lower current were obtained. With decreasing the pressure to  $\sim 10^{-3}$  mbar, the voltage was reduced to  $\sim 20$  V and the current was increased to  $\sim 74$  A. When the chamber vacuum reached to  $\sim 10^{-5}$  mbar, the voltage and current were increased slightly comparing with the values at the pressure of  $\sim 10^{-3}$  mbar. In addition, it was found that the values of voltage and current were not stable and changed in a broad range at the higher deposition pressure, which resulted in the nonuniformity of Ti film. In contrast, at lower pressure the values were more stable, which was of advantage to deposit the interface layer of high quality by cathodic arc vacuum evaporation.

---

## 5.3 Deposition of DLC coatings by new vacuum arc equipment

### 5.3.1 Deposition setup (Transition between the cathodic arc and anodic arc)

As described in chapter 2.3.1, there are two types of the arc discharge: cathodic arc and anodic arc which depends on the source of the deposited material. If the evaporated material is originated from the anode, this arc discharge can be called anodic arc. The type of the arc discharge plays an important role in properties of coating during deposition. Here the transition from cathodic to anodic arc can be achieved by adjusting an anode-cathode diameter ratio in the DLC coatings deposition system. The schematic diagram of the deposition setup was shown in Fig. 5.4.

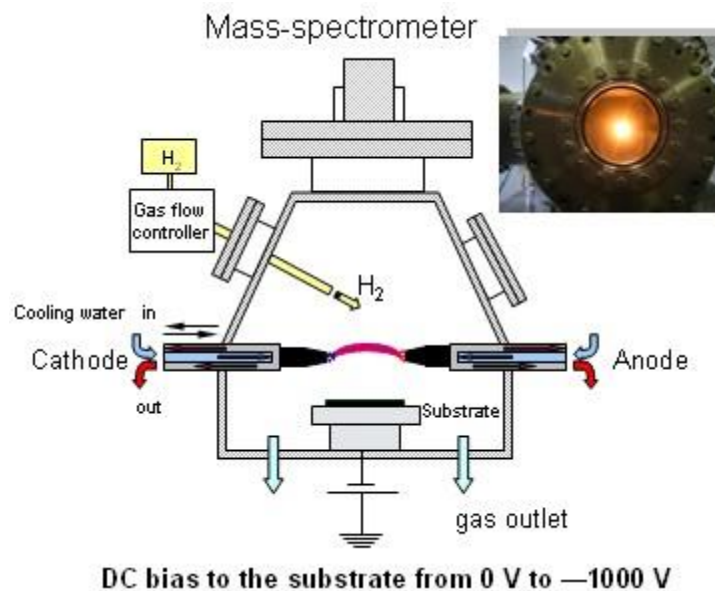


Figure 5.4 Schematic diagram of vacuum arc deposition system for DLC coatings

In this system the hydrogen can be introduced into the deposition chamber. But in this work, there was not any source of hydrogen used, so the DLCs deposited were hydrogen-free a-C coatings.

Two electrodes were manufactured from Ringsdorff spectroscopic carbon (Type RW 003) consisting of pure graphite cylinder and must be cooled with water during the deposition. In the experiments, the electrode diameter ratio of  $d_a/d_c$  was varied from 1/3 to 3/1.

Two TCR 3 phase power supplies LAMBDA EMI [1] with 4 kW maximum output power were used in series. The voltage and current were in the range of 0 ~ 40 V and 0 ~ 100 A,

respectively. The bias supply applied to the substrate was Magpuls QP-1000/10/20 BP [2], which was the same equipment described in Chapter 5 for the deposition of Ti. The mode was also DC negative bias. The deposition conditions were monitored with the Quadrupole Mass Spectrometer (QMS-200 Prisma™) [8].

### 5.3.2 Deposition Process

After deposition of interface layer Ti on P2000, two discs as the substrates were taken out from the chamber, and subjected to an ultrasonic bath with acetone solution for 10 min, and then blown dry with N<sub>2</sub>. The weight was measured by a balance. At the same time, double-side polished silicon wafer (100) was cut into piece of 20 mm × 10 mm and used as another substrate. Silicon wafer was also treated ultrasonically in isopropanol solution for 10 min, and then dried with pure nitrogen. After cleaning, the silicon substrate was lined using one marker for measuring the film thickness. Finally all samples consisting of two discs and one Si wafer were fixed on the substrate holder and the silicon wafer was positioned in the middle of two discs.

Table 5.4 Deposition process parameters for DLC coatings

Deposition parameters	Conditions
Deposition pressure	$2 \times 10^{-3}$ mbar
Arc current	80 A
Arc voltage	20 V
Deposition time	3 min
DC bias to substrate	0, -250, -500, -750, -1000 V
$d_a/d_c$	1/3, 1/1, 3/1

Firstly the deposition chamber needed to be cleaned with vacuum cleaner. Secondly the substrate holder and electrodes were mounted in the deposition chamber. Prior to closing the chamber it was important to make sure that the cathode and anode were contacted to each other. The chamber was evacuated to a base pressure of  $1.5 \times 10^{-5}$  mbar. The DC bias supply was turned on and the certain negative bias was inputed first. Then the power supply was switched on and the

---

electrodes were heated. When the voltage was increased slowly to 10 V and the current was a constant of 80 A, the sufficient electrode temperature was obtained. At this time, the carbon plasma was produced by separating the graphite electrodes in this high vacuum. The voltage was kept at about 20 V by adjusting the distance of 5 mm between two electrodes. The DLC coatings were deposited on P2000 substrates with Ti as interface layer by vacuum arc method with an anode-cathode mode. A more detailed list of deposition process parameters is given in Table 5.4.

After DLC coatings deposition, the power supply and bias supply were switched off in sequence. The samples were not taken out until the chamber was cooled down to room temperature. The Si wafer with marker was cleaned ultrasonically in acetone and ethanol solution, respectively. When the marker was removed and the step was formed, the Si wafer was blown dry with N<sub>2</sub> and the thickness of the DLC coating was measured by the contacting gauge. Two discs were taken out and weighed directly. The weight of the DLC coating could be obtained by the weight difference before and after DLC coating deposition.

## References

- [1] Instruction manual for TCR 3 PHASE POWER SUPPLY, LAMBDA EMI, 83-467-001 Revision B.
- [2] Y.Y. He, Deposition of diamond-like carbon films by liquid electrochemical technique (dissertation), Universit ät Duisburg-Essen (2011) 1-139.
- [3] DIN-Code: 1.4452, DIN ISO 10993-5, Stainless austenitic steel, Energietechnik Essen P2000 X13 CrMnMoN 18-14-3 (2003) 1-9.
- [4] S. Reuter, B. Weßkamp, R. B üscher, A. Fischer, B. Barden, F.L öer, V. Buck, Correlation of structural properties of commercial DLC-coatings to their tribological performance in biomedical applications, *Wear* 261 (2006) 419-425.
- [5] B. Stamm, B. K üz ün, O. Filipov, S. Reuter, I. Erdmann, F. Deuerler, D. Krix, K. Huba, H. Nienhaus, V. Buck, Adjustment of wear particle size distribution of DLC coatings for tribological metal-on-metal pairing in artificial hip joints, *Mat.-wiss. u. Werkstofftech* 40 (1-2) (2009) 98-100.
- [6] J.C. Arnault, L. Demuynck, C. Speisser, F.Le Normand, Mechanisms of CVD diamond nucleation and growth on mechanically scratched Si (100) surfaces, *The European Physical Journal B* 11 (1999) 327-343.
- [7] E. Anger, A. Gicquel, Z.Z. Wang, M.F. Ravet, Chemical and morphological modifications of silicon wafers treated by ultrasonic impacts of powders: consequences on diamond nucleation, *Diamond and Related Materials* 4 (5-6) (1995) 759-764.
- [8] Operating instructions, QMS 200 Prisma TM 80 Quadrupole mass spectrometer, BG 805 204 BE/B (0203).

## 6. Parameters of analysis of Raman spectra and wear tests

### 6.1 Analysis of Raman spectra

Raman spectrum fitting is used to get the intensity ratio of the D and G bands in the analyzed diamond-like carbon (DLC). As reference [1] shows, for the same carbon coatings, different Raman spectra can be obtained with different excitation wavelengths. This thesis is referred to Raman data at 514 nm.

Usually there are two fits: a Lorentzian fit and a Gaussian fit. The simplest fit for Raman spectra of DLC: two Gaussians [2-4], two Lorentzians or a fit with a Breit-Wigner-Fano (BWF) line for the G peak and a Lorentzian for the D peak (BWF + Lorentzian fits) [5-9], in which two Gaussians fitting is widely used in Raman spectra as reference [10] shows. Most papers focus on the G and D peaks as two prominent features, neglecting other features that sometimes are present, such as those at 1100~1200 and 1400~1500  $\text{cm}^{-1}$ . Therefore, in order to be fitted very well on a linear background, other peaks must be considered. For example, “T” peak at around 1060  $\text{cm}^{-1}$  is due to CC  $\text{sp}^3$  bonding and appears only for UV excitation [5-6,11-12], which can't be observed in visible excitation. However, a simple two symmetric-line fit for different kinds of carbon films is not always suitable in visible Raman spectra.

In the year 2009, F.C. Tai used three-peak fitting of visible Raman spectra of as-deposited hydrogenated diamond-like carbon (DLCH) film under Gaussian function for D1(~ 1450  $\text{cm}^{-1}$ ), D2(~ 1280  $\text{cm}^{-1}$ ) and G peaks or D, G1(~1530  $\text{cm}^{-1}$ ) and G2(~ 1600  $\text{cm}^{-1}$ ) peaks [13], and found that the  $I_D/I_G$  ratio was inconsistent. In one doctoral thesis [14], the author discussed the visible Raman spectra of amorphous carbon by using two-Gaussian, three-Gaussian, two-Lorentzian and three-Lorentzian fitting. More three-peak fitting can be seen from references [15-19] with full Gaussian function, in which the peak position consisted of two peaks (D2, D1) for D peaks and two peaks (G1, G2) for G peaks: ~ 1180  $\text{cm}^{-1}$  (nanocrystalline diamond), ~1350  $\text{cm}^{-1}$  (microcrystalline or nanocrystalline graphite), ~ 1490  $\text{cm}^{-1}$  (disordered graphite) and ~ 1580  $\text{cm}^{-1}$  (ordered graphite), respectively. However, according to the Raman curve fitting made by Nakao [18] and F.C. Tai et al. [13], several assumptions have been made on the multi-peak intensity

calculations:  $D=D_1+D_2$ ,  $G=G_1+G_2$ ,  $D_2<D_1$  and  $G_2<G_1$ . So it is very important to choose appropriate numbers and positions of peak before fitting the Raman spectrum. Because of the different values, for example the peak position, the ratio of  $I_D/I_G$  and so on, can be obtained using different numbers and positions of peak, which will reflect the characterization of coatings' structure.

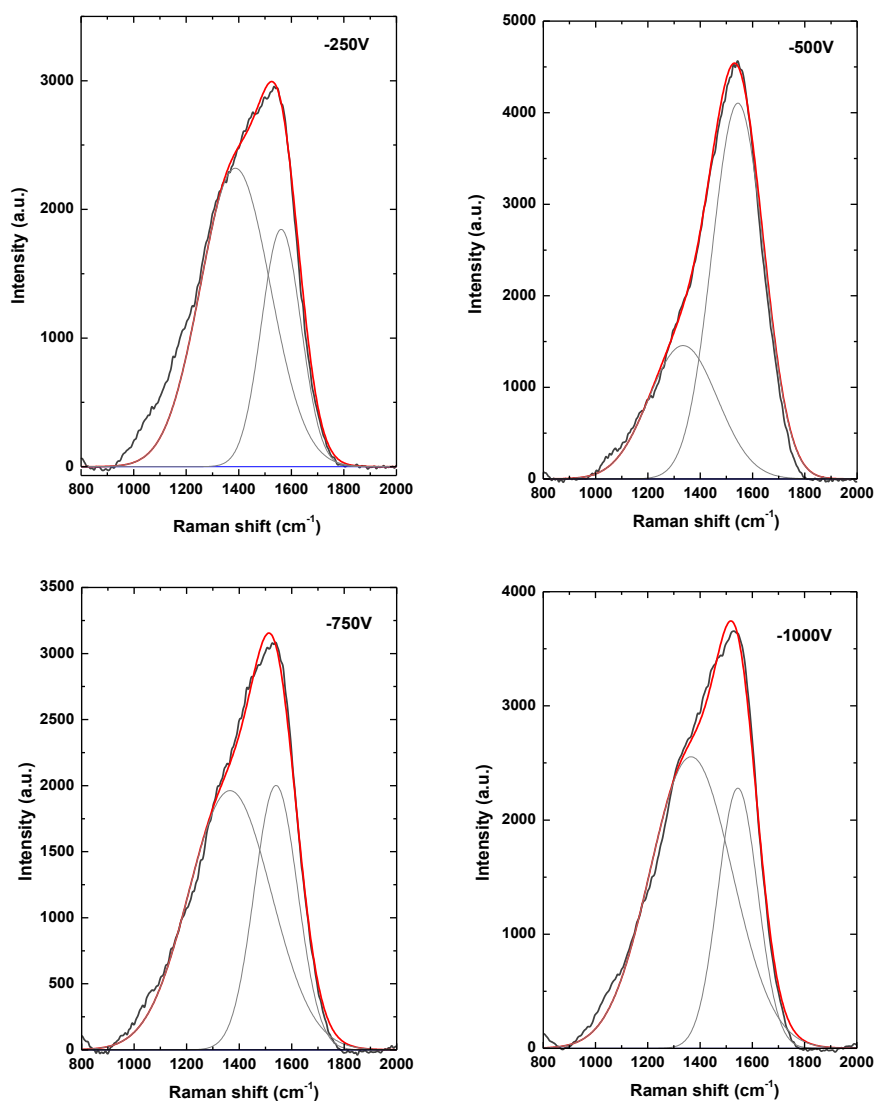


Figure 6.1 Raman spectra fitted with two-Gaussian fits of DLC synthesized at the DC bias of  $-250\text{ V}$  to  $-1000\text{ V}$  (the red line represents the fitted curve)

- Deposition of DLC coatings

DLC coatings were deposited on steel (P2000) by a vacuum arc adjustable from anodic to cathodic operation mode, with an anode-cathode diameter ratio of  $d_a/d_c = 1/1$  at a DC bias of  $-250$

V to  $-1000$  V. The details of deposition processing and parameters were shown in the reference [20]. A micro-Raman system of HORIBA Jobin Yvon with the visible excitation of the  $514.5$  nm  $\text{Ar}^+$  laser line was used. Most coatings deposited by arc showed weak peaks at  $\sim 1100$   $\text{cm}^{-1}$  in visible Raman spectra. A linear background was subtracted before fitting the spectra.

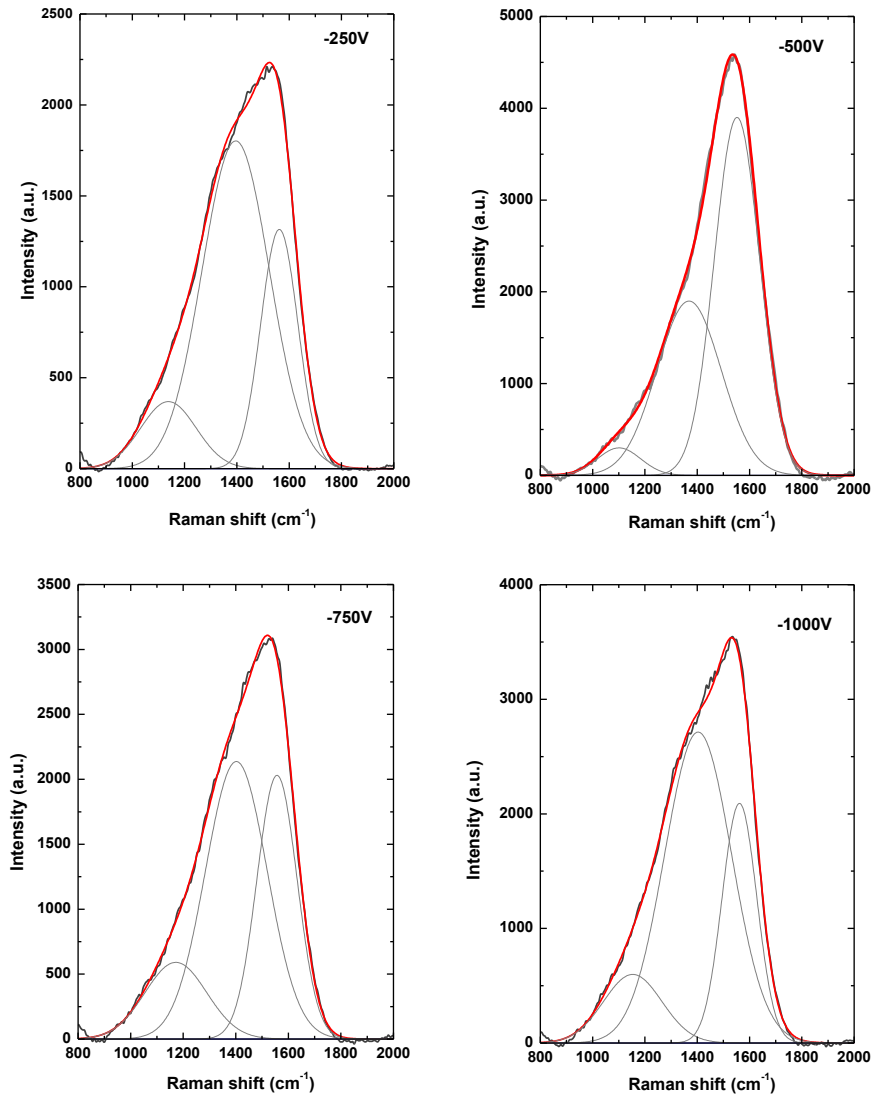


Figure 6.2 Raman spectra fitted with three-Gaussian of DLC synthesized at a DC bias of  $-250$  V to  $-1000$  V

- Two-peak fitting analysis of visible Raman spectra of DLC coatings

Fig. 6.1 shows that Raman spectra were fitted by Gaussian curves using two general peaks (D peak and G peak). It was found that there was no match at the lower frequency ( $<1200$   $\text{cm}^{-1}$ ) with original Raman spectrum when fitting spectrum with two Gaussian functions. The fitted curves

(red lines in Fig. 6.1) were a little bit higher than the measured data at the highest peak, because a weak peak at  $\sim 1400\text{ cm}^{-1}$  appeared between D peak ( $1350\text{ cm}^{-1}$ ) and G peak ( $1570\text{ cm}^{-1}$ ). When D peak and G peak were matched well, the fitted curves about  $1400\text{ cm}^{-1}$  were lower than the original curve. So two-Gaussian fitting was not suitable to characterize the structure of the samples.

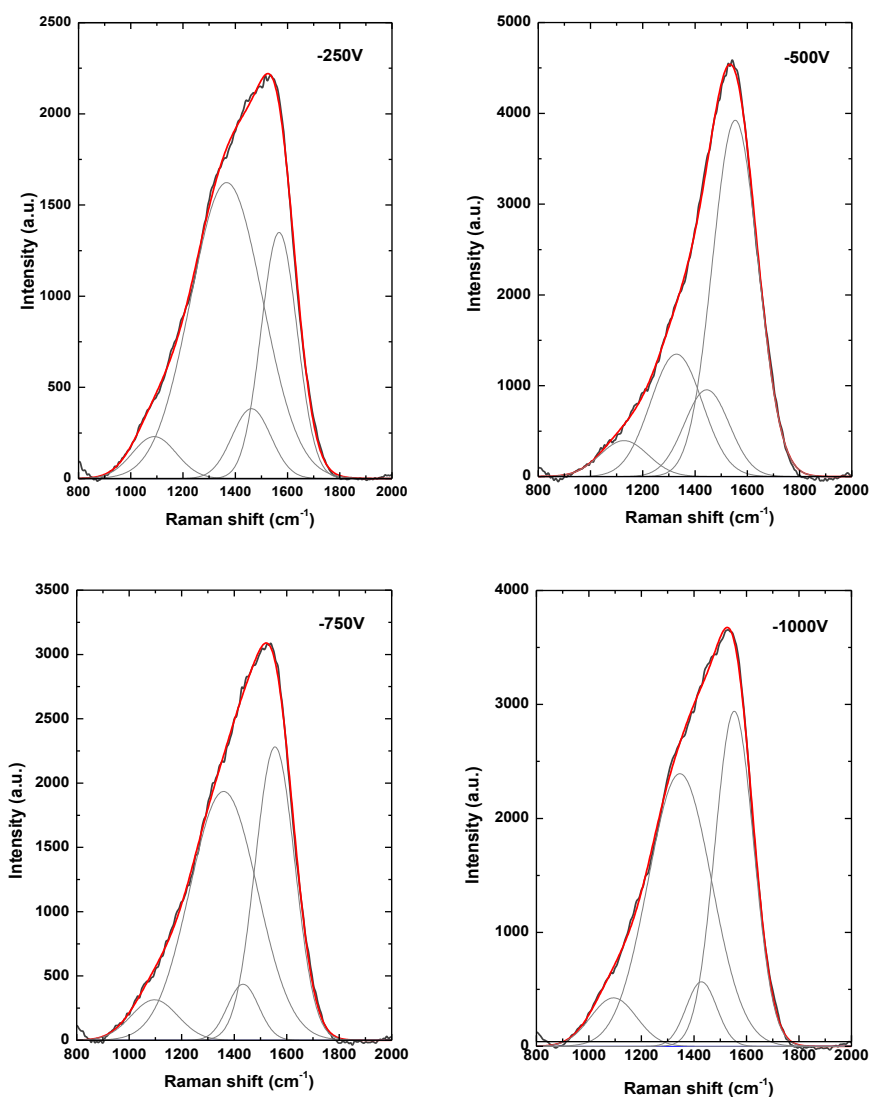


Figure 6.3 Raman spectra fitted with four-Gaussian of DLC synthesized at a DC bias of  $-250\text{ V}$  to  $-1000\text{ V}$

- Three-peak fitting analysis of visible Raman spectra of DLC coatings

Fig. 6.2 shows that Raman spectra were fitted by Gaussian curves using three peaks (D2, D1 and G peaks). For D2, D1 and G three-peak model, the peak positions are  $\sim 1100$ ,  $\sim 1350$  and  $\sim 1580\text{ cm}^{-1}$ , respectively.

To use three-peak fitting was much better than two-peak fitting as shown in Fig. 6.2, but a

weak peak at  $\sim 1400 \text{ cm}^{-1}$  was not fitted well if using only three peaks, especially for the Raman spectra at a bias of  $-250 \text{ V}$  and  $-1000 \text{ V}$ .

- Four-peak fitting analysis of visible Raman spectra of DLC coatings

Fig. 6.3 shows that Raman spectra were fitted by Gaussian curves using four peaks (D2, D1, G2 and G1 peaks). A four-peak fitting of the Raman spectrum has two peaks for D peaks: D2 ( $\sim 1100 \text{ cm}^{-1}$ ), D1 ( $\sim 1350 \text{ cm}^{-1}$ ) and two peaks for G peaks: G2 ( $\sim 1400 \text{ cm}^{-1}$ ), G1 ( $\sim 1580 \text{ cm}^{-1}$ ).

When four-peak fitting was used to deconvolve the Raman spectra (see Fig. 6.3), it was found that the measured data were fitted very well compared with using two-Gaussian (Fig. 6.1) and three-Gaussian (Fig. 6.2).

- Discussion

Therefore, with different fittings of Raman spectra, different values of D, G position, as well as the  $I_D/I_G$  ratio can be obtained as shown in Fig. 6.4.

$I_D/I_G$  is the ratio of peak heights. Usually the intensities of D and G peaks refer to the intensities of these two peaks: “ $\sim 1350 \text{ cm}^{-1}$ ” and “ $\sim 1580 \text{ cm}^{-1}$ ”, which means the ratio of  $I_{D1}/I_{G1}$  stands for  $I_D/I_G$ . So there will be two different  $I_D/I_G$  values needed to be discussed. For three-peak fitting, there are  $I_{D1}/I_G$  and  $I_{(D1+D2)}/I_G$ . The values of  $I_{D1}/I_{G1}$  and  $I_{(D1+D2)}/I_{(G1+G2)}$  are considered in four-peak fitting.

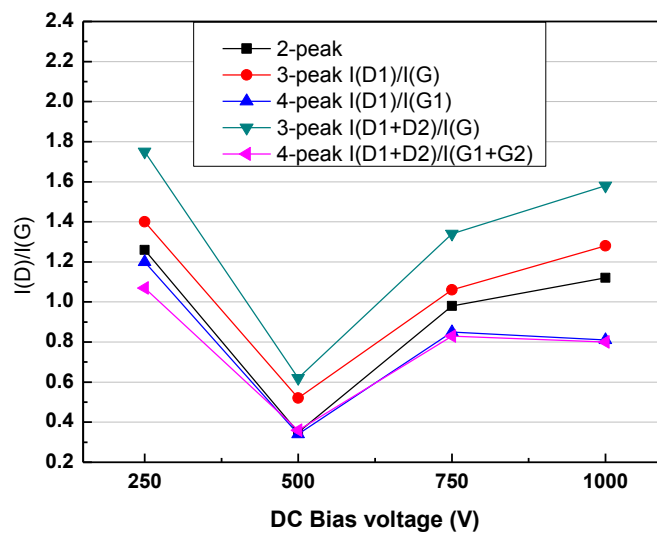


Figure 6.4  $I_D/I_G$  ratio of DLC synthesized at a DC bias of  $-250 \text{ V}$  to  $-1000 \text{ V}$  under different fitting function

---

Fig. 6.4 shows the corresponding value of  $I_D/I_G$  at the two-peak fitting, three-peak fitting and four-peak fitting, respectively. It was shown that the  $I_D/I_G$  ratio of all fitting functions for Raman spectra had the same tendency to change with the biases. According to Raman spectra fittings, the most widely used two-Gaussian function was absolutely not suitable to the Raman spectra on DLC films deposited by vacuum arc adjustable from anodic to cathodic operation mode, so the intensity ratio of D and G peak was not exact and will not be discussed here. However, by comparing with the ratio of  $I_D/I_G$  of two-peak fitting function, the three-peak Gaussian function had higher  $I_D/I_G$  ratio and the four-peak Gaussian function exhibited a lower one, no matter what kind of D and G peak was used in calculation of  $I_D/I_G$ . In three-peak fitting function, it was obviously observed that the  $I_{(D1+D2)}/I_G$  value was higher than the ratio of  $I_{D1}/I_G$  due to D2 peak. For four-peak Gaussian function, values of  $I_D/I_{G1}$  and  $I_{(D1+D2)}/I_{(G1+G2)}$  were nearly the same.

- Conclusion

Raman spectra using four peaks can be fitted very well to analyze DLC films deposited on P2000 steel substrates by vacuum arc adjustable from anodic to cathodic operation mode, instead of the typical two-Gaussian fitting. By comparing with multi-peak Gaussian function, three-peak Gaussian function had the largest  $I_D/I_G$  ratio and four-peak fitting had a smaller  $I_D/I_G$  ratio. In addition, the intensity ratio of D and G bands obtained was almost not affected by the calculation formula. The results of  $I_{D1}/I_{G1}$  and  $I_{(D1+D2)}/I_{(G1+G2)}$  of four-peak Gaussian function were consistent nearly. This will be very important for the choice of fitting function for Raman spectra of DLC coatings deposited by vacuum arc.

## 6.2 Parameters of tribological test

The importance of tribology in the field of artificial hip joints is well known. The tribological property of DLC coatings is determined by a very large number of factors that have an extremely complex influence, which is a property of the whole tribological system not a material property. But some factors are very obvious like materials, relative speed, pressure, temperature, surrounding medium, and surface topography.

- The normal force

In a normal healthy hip joint (see chapter 3), the surfaces of the femoral head and socket

(acetabulum) are covered by a smooth, tough material called articular cartilage, which cushions the bones and let them move easily. In a diseased hip joint, it shows worn cartilage. During walking or running, two cartilage layers exert contact pressure on each other. This pressure has been a notable parameter to evaluate the physical conditions inside the hip joint. High pressures are shown to be in association with soft tissue damage within the hip joint. Therefore, to measure the contact pressure within the hip joint is crucial for estimating joint pressure, which is also important for the determination of load in tribological testing. The measurements of contact pressure in vivo or in vitro have been performed parallel to the development of predictive tools, for example, finite element methods (FEM) and a statistical model [21-23].

According to ref. [22], it was estimated that the average pressure was in the range of 2.0-3.0 MPa at threefold body-weight load. At 2.6 body-weight force at the hip, the peak local cartilage stress is 6.78 MPa, with a mean pressure of 2.14 MPa. So here the contact pressures of 2~6 MPa were chosen. The normal force is also dependent on the wear testing setup. For traditional disc-on-pin of wear testing setup, the load of 5 N was applied to the pin and initial contact pressure of 370 MPa was produced via Hertzian theory [24].

The same disc-on-pin tribological equipment and same parameters as reported by S. Reuter et al. [24] were used in the first set of experiments. However, the wear particles generated were not enough for analyzing the particle size distribution although the diameter of pin fitted in the pin holder screwed in the bottom of the container can be adjusted. What's more important is that some dirty things from the surrounding environment will fall into the container during adjusting the diameter of pin every time, which will pollute the results of wear particle size distribution. In a word, there are some restrictions in analysis of wear particle size with the traditional disc-on-pin wear testing setup.

To overcome this problem, the disc-on-disc of wear testing setup was used in the tribological test. It is the area contact for the surface, not point or line contact. So it is not suitable to analyze the normal force via the contact stress using Hertzian theory. In the experiments, the load of 50 N, 80 N, 100 N and 120 N was chosen. With the lower load the wear particles can't be produced and it is not available for use in hip joints, whereas, with the higher load the wear particles from the

---

interface layer or substrate will influence the results of the distribution.

- Other parameters

Deionized water was used as lubrication for testing the DLC coatings in order not to induce any artificial facts from corrosion (as expected from Synovia, Ringer's solution and the bovine serum, etc. [25-28]). The sliding velocity of 0.01 m/s was chosen. The sliding time in the experiments was varied depending on the properties of DLC coatings. Actually for some coatings the load must added up to more than 120 N due to high hardness.

- Experiments

Two DLC coatings (sample 1 and 2) were deposited on the substrate of P2000 with an anode-cathode diameter ratio of  $d_a/d_c = 1/1$  at a DC bias of  $-250$  V and  $-1000$  V, having a thickness of 1450 nm and 348 nm, as well as a density of  $1.73$  g/cm<sup>3</sup>,  $1.93$  g/cm<sup>3</sup>, respectively. Ti as interface layer was deposited by cathodic vacuum arc evaporation (see chapter 5.1).

The tribological conditions were at the room temperature, other parameters were as described above, deionized water was used and the rotation speed was 0.01 m/s. After 1h disc-on-disc testing in deionized water the surface morphology of sample 1 was measured by scanning electron microscope (SEM) as shown in Fig. 6.5 and Fig. 6.6. For sample 2, the testing time was 15 h, the corresponding SEM images were shown in Figs. 6.7 and 6.8. According to the morphology of worn surface observed by SEM, several wear mechanisms could be found [29].

Fig. 6.5 shows the SEM image of the surface destroyed after tribological test using 100 N as load. The wear tracks included two parts: black and white parts. It was observed visually that the white parts (see SEM 2) were destroyed more seriously than the black parts (see SEM 1), which was confirmed by the corresponding EDX spectra of the areas indicated in Fig. 6.5.

The EDX spectrum (1) shows higher intensity of Ti coming from the titanium interface layer than of Fe coming from the steel substrate. That indicates that the interface layer was not damaged or less damaged, and probably little of the DLC coating was left. It was found that the surfaces were more or less destroyed (white parts as seen in SEM 2) still keeping the titanium interface layer although the intensity of titanium decreases as the intensity of iron (P2000) increases.

Other loads for tribological test have been used to generate particles, for example: 50 N, 80 N and 120 N. However, it was found that a few particles can be obtained after a long time when 50 N

## 6. Parameters of analysis of Raman spectra and wear tests

and 80 N were loaded, and to use 120 N as a load which can produce more particles, but the coatings were destroyed seriously, including the interface layers and even the substrates. This indicates that the parameters for tribological testing, the load of 100 N and sliding velocity of 0.01 m/s etc., were appropriate to generate wear particles.

After one hour of wear testing of sample 1, the color of worn surface was changed from dark to brown. There were grooves observed obviously in the form of concentric circles, especially in the center of discs, which can be defined as abrasive wear resulting from a hard damage may due to the presence of hard particles.

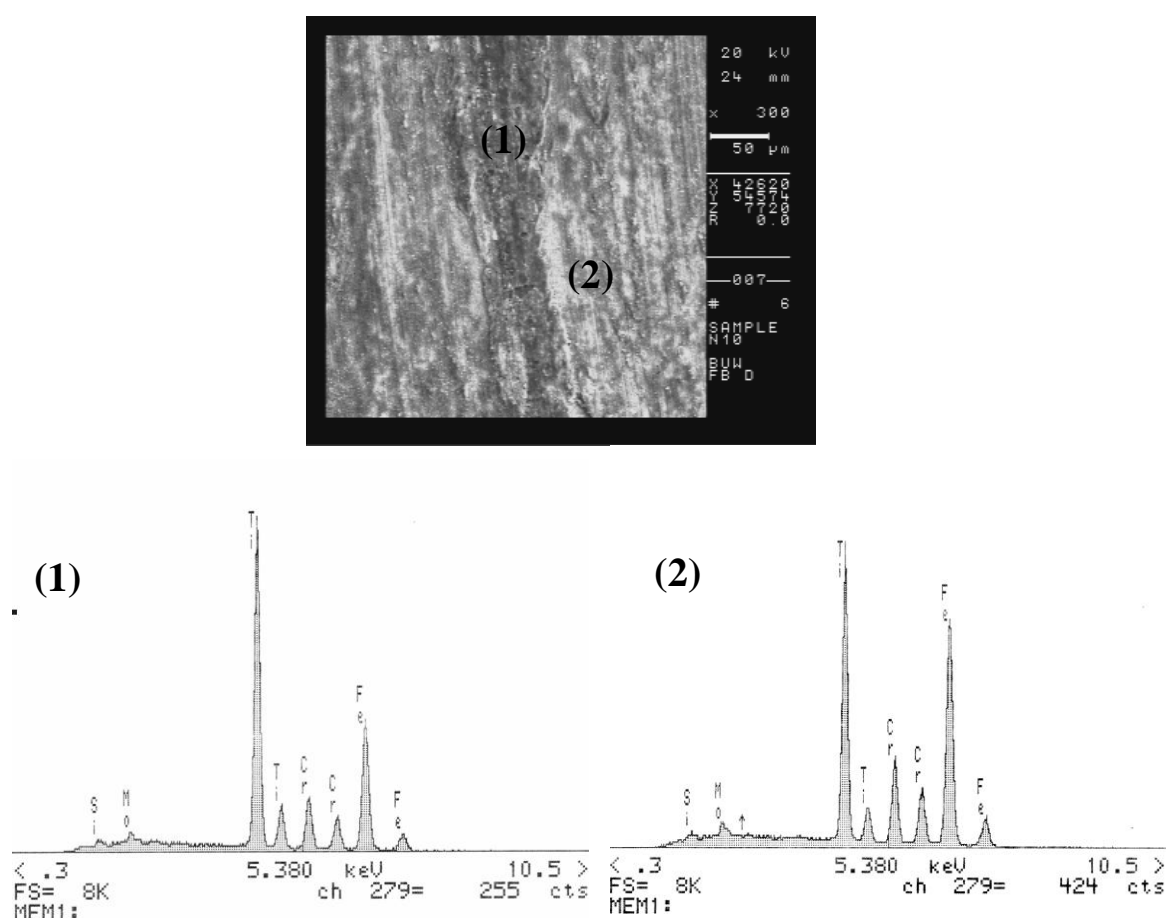


Figure 6.5 SEM image of the center of worn surfaces and the corresponding EDX spectra (sample 1: 1450 nm and -250 V)

However, Fig. 6.6 shows different morphology of wear surface. It was found that there was no obvious groove on the edge of worn surface (see Fig. 6.6) and consisted of three parts. Part (1) was DLC film left without damage, so the corresponding EDX spectrum shows lower intensity of

Fe, Cr and Mo from P2000 substrate compared to the intensity of Ti of interface layer due to the DLC film thickness of 1450 nm (see Fig. 6.6 (1) ). When the DLC coating was destroyed, the intensity of elements from substrate was increased as shown in Fig. 6.6 (2) and (3). In part (1) of SEM image it was observed that the shape of edge of DLC coating was not induced by scratch, whereas it was caused by crack resulted in plastic deformation. That means, the wear testing exfoliated the coating near the edge of sample 1. So the wear mechanism should belong to the typical delamination wear [29], which was confirmed by the SEM image of particle size. It was found that there was large wear debris in form of sheets.

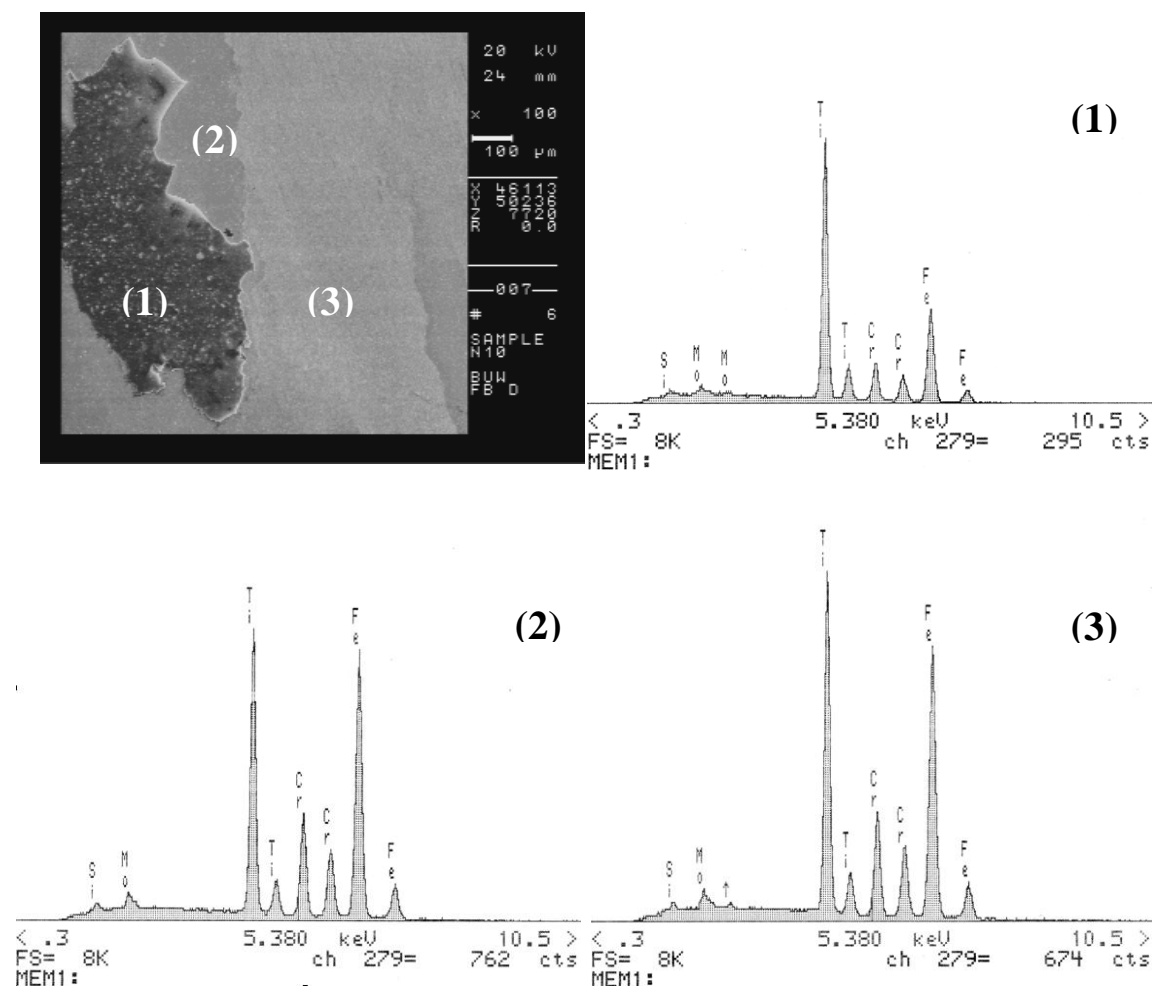


Figure 6.6 SEM image of the edge of worn surfaces and the corresponding EDX spectra (sample 1: 1450 nm and -250 V)

DLC coating of sample 2 was deposited by the bias of -1000 V. After one-hour tribological test, there was no wear track, so the time was increased to 15 h. The SEM images and EDX spectra

were shown in Fig. 6.7 and Fig. 6.8. The EDX spectrum in Fig. 6.7 shows that the intensity of Ti was nearly zero. It was confirmed that on few parts of surface the interface layer was destroyed along with DLC coating during the longtime testing. There were much multi-axial scratches on the surface in SEM image of Fig. 6.7.

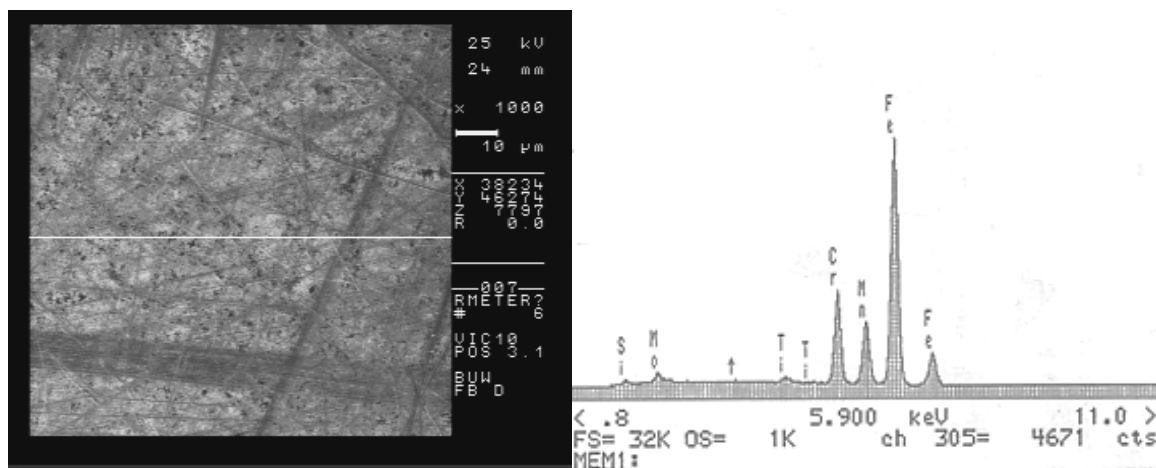


Figure 6.7 SEM image of the worn surfaces and the corresponding EDX spectra (sample 2: 348 nm and -1000 V)

Most grooves were clearly visible on worn surface as shown in Fig. 6.8, the similar to Fig. 6.6. The white part was scratched and the interface layer was still left according to the intensity of Ti on the corresponding EDX spectrum. In SEM image some dark parts came from smaller wear particles generated by rubbing surfaces themselves in disc-on-disc setup. In the experiments one common phenomenon is that some fine brown wear particles appear between the moving counter-surfaces as shown in Fig. 6.8. They were DLC coatings from themselves or the transfer from one surface to another surface during relative motion.

Usually DLC has the ability to form a transfer layer on the softer counterpart protecting it from wear during sliding against certain materials in ambient atmosphere [30]. It was reported in ref. [30-31] that the lubricant was also important so that DLC can form a transfer layer for sliding against UHMWPE when using distilled water as a lubricant, but no transfer layer found in biological media. The transfer layer might play the role of the low shear stress surface which account for low friction at the DLC-DLC interface as Jia, Li, Fisher and Gallois reported in ref.

[32]. However, according to the research of Ronkainen et al. in 1996 [33] for DLC articulating against DLC, it seems that the transfer layer may not be a main requirement for low wear, in addition, the biotribological behavior does not change significantly in the presence of proteins in lubricant. So it is still not so clear about the effect of transfer layer at the interface of DLC sliding against DLC on the tribological behavior. Maybe it is not the main factor, but the adhesive wear is characterized by the transfer. Accordingly, the mechanism of wear of sample 2 shown in Fig. 6.8, besides abrasive wear, was adhesive wear which has been denoted as being the most commonly detected mechanism of wear [29].

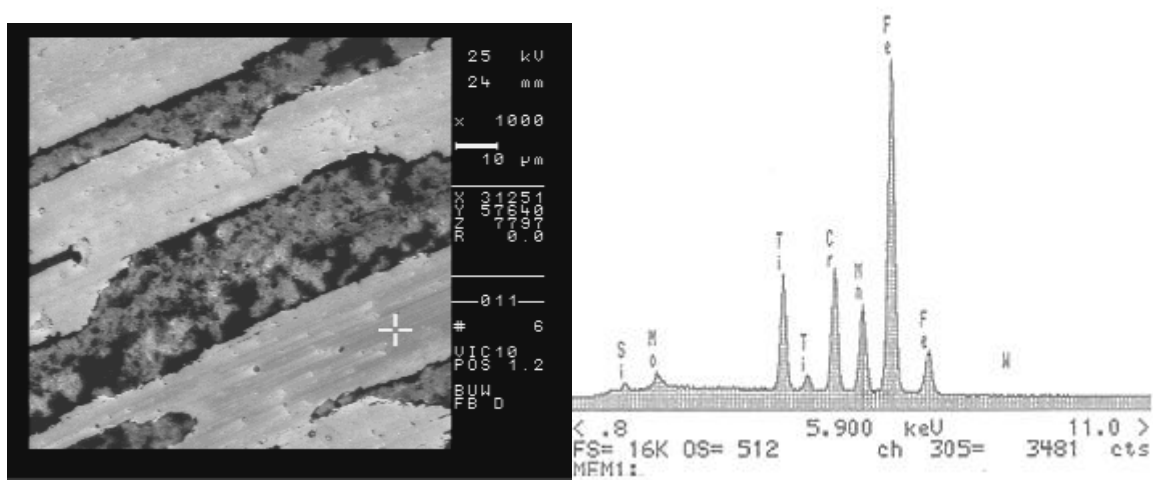


Figure 6.8 SEM image of the worn surfaces and the corresponding EDX spectra (sample 2: 348 nm and -1000 V)

## ● Conclusion

For the DLC coatings deposited by vacuum arc with  $d_a/d_c = 1/1$ , disc-on-disc testing at the load of 100 N was found to produce sufficient amount of wear particles to determine particle size distribution. The DLC coating, deposited with different parameters, has different tribological properties. Especially in order to get enough wear particles, some parameters of testing must be changed, e.g. the running time. The normal force and velocity also need to be increased when the sample was deposited at a bias of -750 V.

As is known, the wear and frictional properties of materials are dependent on the tribological conditions of the tribosystem. When the anode-cathode diameter ratio was changed, for example,  $d_a/d_c = 1/3$  or  $3/1$ , the normal force was varied in disc-on-disc setup according to the properties of

DLC coatings. Although it is sometimes impossible to avoid the impurity from environment, it was tried to make sure the interface layer will not be damaged so that almost all particles come from the DLC coating whatever load used.

Many mechanisms will be involved in the process of wear. For DLC sliding against DLC, the main mechanisms are adhesive wear and abrasive wear, sometimes combined with delamination wear. Due to thicker DLC coatings, the films have high stress or poor adhesion which results in the phenomenon of delamination.

### 6.3 Parameters of cavitation erosion test

- Amplitude and distance

The setup of cavitation test was shown in chapter 4.3. On the basis of ASTM G32-98 [34] the vibration amplitude of the sonotrode should be  $25 \mu\text{m} \pm 5\%$ . Actually it can be adjusted by means of the power regulator on the ultrasonic generator in the used test setup. In addition, according to the handbook of cavitation test it is possible to change the range of amplitude from 0 to  $33 \mu\text{m}$ , nevertheless it should be noted that the amplitude characteristic is non-linear for power control on the ultrasound generator as shown in Table 6.1 [34-35]. So it is very important to choose appropriate amplitude for certain material prior to the cavitation test.

Table 6.1 Relationship of amplitude and percentage controlled in ultrasound generator

%	30	40	50	60	70	80	90	100
$\mu\text{m}$								
Amplitude	13.5	16.5	19.0	21.5	25.0	28.0	30.5	33.0

As the distance from the substrate surface to the sonotrode, a gap of 0.65 mm was proven based on plenty of experiments in terms of the operating instructions of cavitation testing setup. A tolerance of  $\pm 0.01$  mm setting is allowable. In experiments it was found that the distance of the sample from the sonotrode impacted on the stress of sample. In a range from 0.60 mm to 0.70 mm, the smallest change of load was observed in the setting deviations. However in ref. [36-38], 0.5

---

mm was chosen as the distance from the substrate although the similar equipment for cavitation testing was used. The distance chosen will be related to the properties of sample. Here it was confirmed that 75% and 0.7 mm were appropriate for the samples by the following experiments in following section.

- Other parameters

When the ambient medium of the sonotrode of air changes to water, the amplitude is adjusted automatically, and the oscillation frequency is kept well at  $20 \pm 0.3$  kHz. In the water the cavitation corrosion may occur besides the cavitation erosion for stainless steels. There is no big difference between distilled water and tap water [35]. Before the sample is immersed in the water, it is necessary to run sonotrode for 5 min at least in order to stabilize the gas content of cavitation medium. To avoid the influence of the liquid erosion (abrasive wear particles dissolved in the liquid) on cavitation, the cavitation medium needs to be replaced and the vessel also need to be cleaned after one test.

It was found that there was no effect of temperature in the range of  $22.1 \sim 33.1$  °C in one part of the diploma work [35]. For better reproducibility, the temperature of the water is  $25 \sim 27$  °C.

- Experiments

DLC films were deposited on the substrate of P2000 with the different anode-cathode diameter ratio of  $d_a/d_c = 3/1$  and  $1/3$  at a DC bias of 0 V, -250 V and -750 V. Ti as interface layer was deposited by cathodic vacuum arc evaporation. The sample was fixed in the substrate holder immersing in the water with 27 °C. The sonotrode was used with a diameter of 5 mm and a frequency of 20 kHz.

Many experiments were done for choosing appropriate parameters of cavitation test. When the distance was kept at 1 mm and 0.5 mm, there was no damage on the surface of sample with increasing the amplitude from 45% to 60%. According to ASTM G32-98 and Table 6.1 shown in operating instructions [34-35], the range of distance and amplitude discussed here were 0.6 mm ~ 0.7 mm and 45% ~ 75%. DLC coating was deposited with  $d_a/d_c = 3/1$  at the different bias. The damaged surface area was changed with the distance of sample to the sonotrode after the cavitation testing with 75% of amplitude for 30 s as shown in Fig. 6.9 and Fig. 6.10.

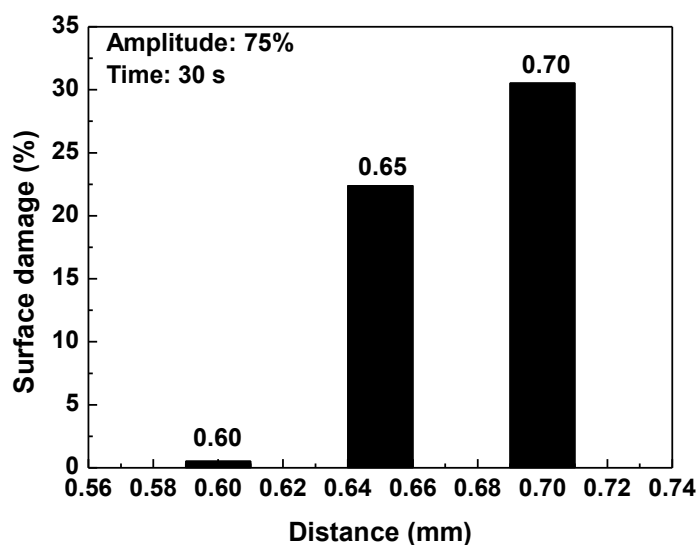


Figure 6.9 Wear damage by cavitation erosion of DLC coatings deposited with  $d_a/d_c = 3/1$  at 0 V

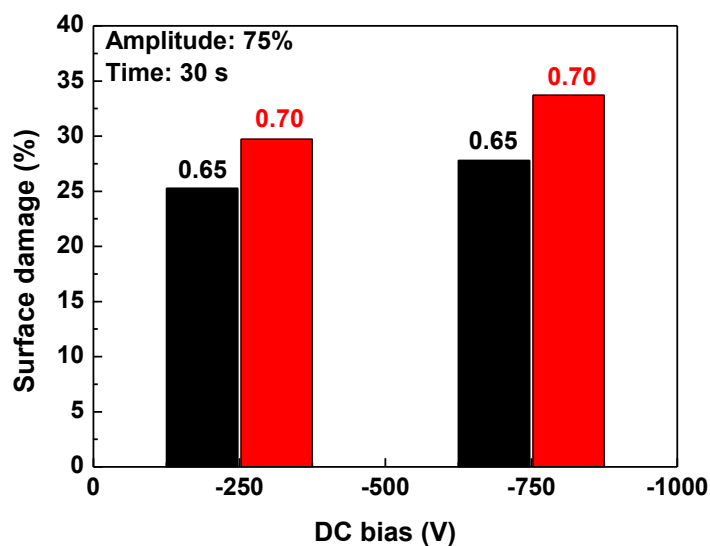


Figure 6.10 Wear damage by cavitation erosion of DLC coatings deposited with  $d_a/d_c = 3/1$  at -250 V and -750 V

Fig. 6.9 shows the surface damage of DLC coating deposited without bias. It was found that the surface area was increased with increasing the distance of sample from the sonotrode. Only 0.5% of surface area was destroyed when the distance was kept at 0.6 mm. However, the percentage of surface damage was raised more than 40 times when the distance was 0.65 mm as against 0.60 mm. With further increasing the distance from 0.65 mm to 0.70 mm, the damaged area was increased

---

from 23 % to 30%.

Fig. 6.10 shows the percentage of surface damage by cavitation test of DLC coatings deposited at  $-250$  V and  $-750$  V. The effect of the distance of 0.65 mm and 0.70 mm on the surface damage was studied. It was found that more areas were destroyed with 0.70 mm than 0.65 mm for the same DLC coatings, but the difference was less than 10% when the distance was kept at 0.70 mm as compared with 0.65 mm, according with the result shown in Fig. 6.9. Therefore, it was indicated that the surface damage (% of charged area) was increased with increasing the distance which was in a range of 0.60 mm ~ 0.70 mm. By comparing with 0.60 mm and 0.65 mm, 0.70 mm was the best choice to get more damaged area.

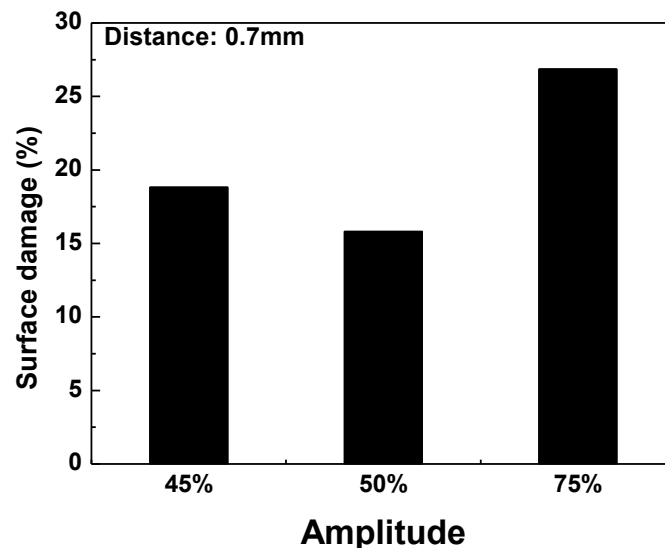


Figure 6.11 Wear damage by cavitation erosion of DLC coatings deposited with  $d_a/d_c = 1/3$  at 0 V

According to Fig. 6.9 and Fig. 6.10, it was found that 0.7 mm as the distance was appropriate to produce a high ratio of damaged surface. The effect of amplitude on the surface damage of DLC coating deposited with  $d_a/d_c = 1/3$  at 0 V was shown in Fig. 6.11. The cavitation erosion was done with 0.7 mm distance from the substrate for 10 min, and the amplitude was varied in a range of 45% to 75%. For the amplitude of 45% - 50%, there was no surface disruption at the beginning of 30 s. However after 10 min cavitation charging, about 20% of surface area was destroyed. No material is available which withstands the attack of cavitation charging in the long run [38]. For higher amplitude (75%) worn surface was more than for lower amplitude of 45% and 50%.

- Conclusion

DLC coatings, deposited with an anode-cathode diameter ratio of  $d_a/d_c = 3/1$  at a DC bias of 0 V, -250 V and -750 V respectively, were used to study the influence of distance from the sample to the sonotrode and the amplitude on the cavitation erosion test. The damaged coating area was observed more or less after 30 s of cavitation charging in a range of 0.60-0.70 mm, on the contrary, there was no damage under the same test duration when the distance exceeded this range.

Furthermore the surface damage (% of charged area) was increased with increasing the distance under this range. More areas of coatings were destroyed at 0.70 mm which parameter was suitable for DLC coatings deposited by vacuum arc.

In addition, the effect of amplitude on the cavitation erosion test of DLC coating prepared with  $d_a/d_c = 1/3$  at 0 V was investigated. It was found that after the long test duration of 10 min the surface was destroyed no matter which amplitude was used in the range of 45% to 75%, although there was no damaged area observed after 30 s of cavitation charging. The different proportions of the surface damage were dependent on the test duration, under condition that other parameters were constant (e.g. distance and amplitude). When the test duration was kept at constant, the damaged surface area was increased with increasing the amplitude. It was indicated that 75% (25  $\mu\text{m}$  - 28  $\mu\text{m}$ ) as the amplitude was appropriate. As a result, 0.70 mm and 75% chosen as the distance and amplitude were suitable for DLC coatings deposited by vacuum arc in the experiments.

## 6.4 Parameters of particle size distribution analysis

- Ultrasound for deagglomeration

During particles collection it is found that many particles in the deionized water are adsorbed onto the plastic container. When the glass container instead of plastic container is used, it's better but the phenomena of adsorption still take place. In order to overcome this problem, the container made of Polytetrafluoroethylene (PTFE) called no-stick coating is the best choice due to the lower surface energy [39-40].

However, wear particles in the container are aggregated due to van der Waals forces and the

---

wetting angle of the solid-liquid interface, dependent on the properties of wear particles and solvent. Especially for nano-particles, they have strong tendency to agglomerate because of van der Waals forces acting over a reduced area and resulting in greater interparticle attraction [41]. Therefore, the particles need to be dispersed prior to the analysis of particle size distribution, unless one intends to measure the size distribution of the agglomerates. For efficient dispersion, adhesion bridges between the particles must be broken (without destroying the particles) and the particles must be evenly distributed in a fluid [42]. Wet preparation is advantageous in lowering the adhesion forces between particles [43]. In this work, the particles are suspended in deionized water. So the break-up of agglomerates can be assisted by the physical and chemical method. The physical method consists of stirring, shaking and ultrasound. Adding dispersion agents as the chemical method is also widely used in wet preparation. Dispersion agents adsorb on the particles' surface, causing the wettability, zeta potential and van der Waals forces to be modified [44-46].

Here the deagglomeration is assisted by ultrasound for 2 min during the measurement of particle size distribution which has been proved by the following experiments.

- Other parameters

In some cases the optical properties of the particles, such as the refractive index  $n$  and the absorption index  $\kappa$ , must be known in order to apply laser light diffraction spectrometry successfully [47]. In addition, light diffraction in disperse systems not only depends on the material properties of the particles, the refractive index of the continuous phase  $n_c$  is also important [42]. So the analysis conditions must be selected before measurement, e.g. the refractive indexes of the particles and continuous phase. The demineralized water with refractive index  $n_c = 1.333$  is used as the continuous phase in this work. For wear particles of DLC coatings, there are two refractive indexes which can be chosen: carbon (1.920) and diamond (2.410). Finally 2 and 1.920 are selected as the speed of the circulation and the refractive index of particles, respectively.

- Experiments

DLC coatings of sample 4 and sample 10 were deposited with an anode-cathode diameter ratio of  $d_a/d_c = 1/1$  at a DC bias of  $-500$  V and  $-1000$  V for 3 min. Ti as interface layer was deposited by cathodic vacuum arc evaporation. The wear particles of DLC coating were generated by tribological test with disc-on-disc and collected in deionized water in the PTFE container. The

wear particle size distribution was measured using a particle size analyzer Horiba LA-950 with 17 channels per decade [48]. The speed of circulation was 2 unit. The volume cumulative distribution and the volume density distribution were chosen to characterize the size of particles.

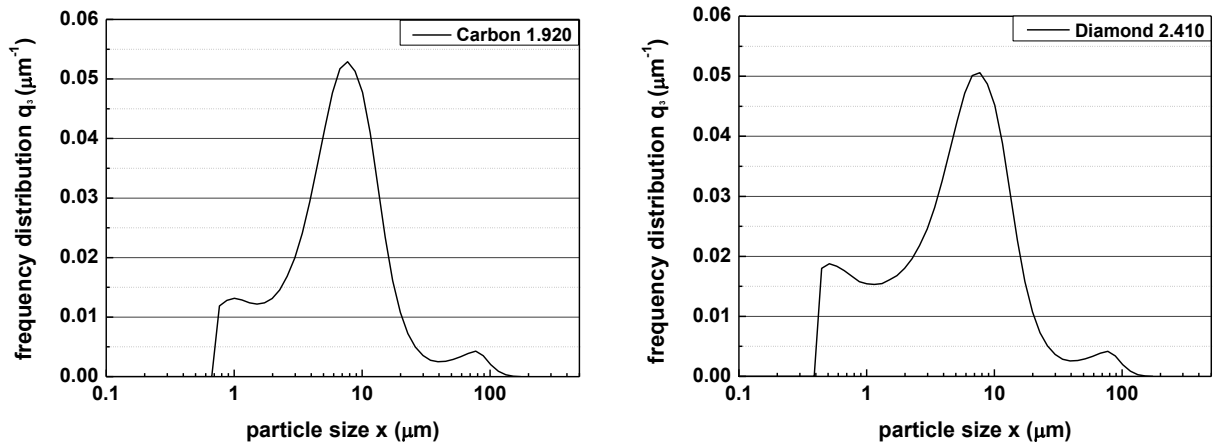


Figure 6.12 Frequency distribution of sample 4 without ultrasonic with different refractive index: 1.920 of carbon (left) and 2.410 of diamond (right)

Fig. 6.12 shows the frequency distribution of sample 4 with the different refractive index without ultrasonic. Left is with the refractive index of carbon (1.920) and right is with the refractive index of diamond (2.410).

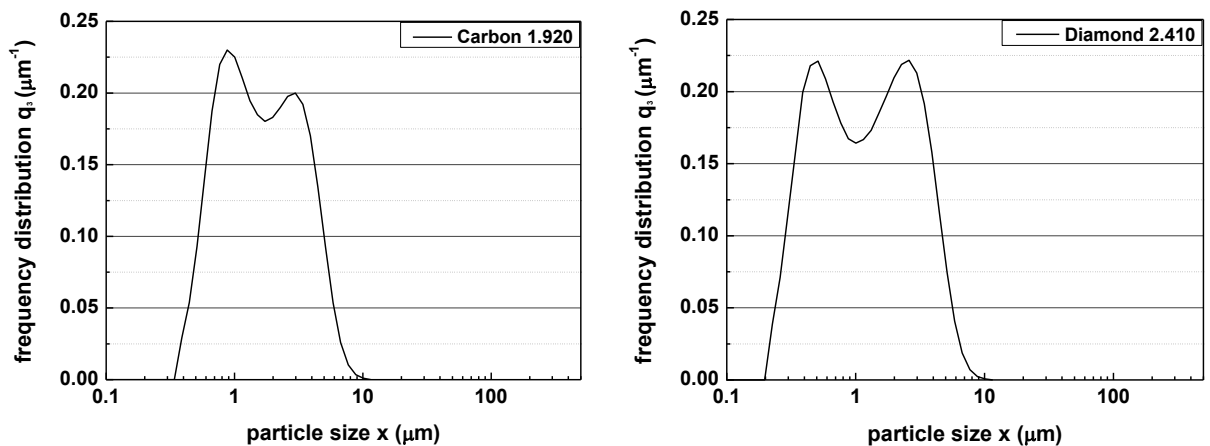


Figure 6.13 Frequency distribution of sample 4 with 2 min-ultrasonic with different refractive index: 1.920 of carbon (left) and 2.410 of diamond (right)

The results show that there was nearly the same particle size distribution in the range of 0.04 ~ 200  $\mu\text{m}$  where three peaks were distributed no matter which refractive index was used in Fig. 6.12.

Only slight difference existed in the peak height. It was found that the height of peak around 10  $\mu\text{m}$  was a little higher with the refractive index of carbon than with diamond. By contrast, the value of peak about 1  $\mu\text{m}$  was higher with the diamond as the refractive index. However, the frequency distribution of  $\sim 100 \mu\text{m}$  did not vary with the refractive index.

As discussed above, for larger particles, the frequency distribution of particle size was not influenced by the refractive index. The larger particles were from the agglomerate due to interparticle adhesion which was confirmed in Fig. 6.13.

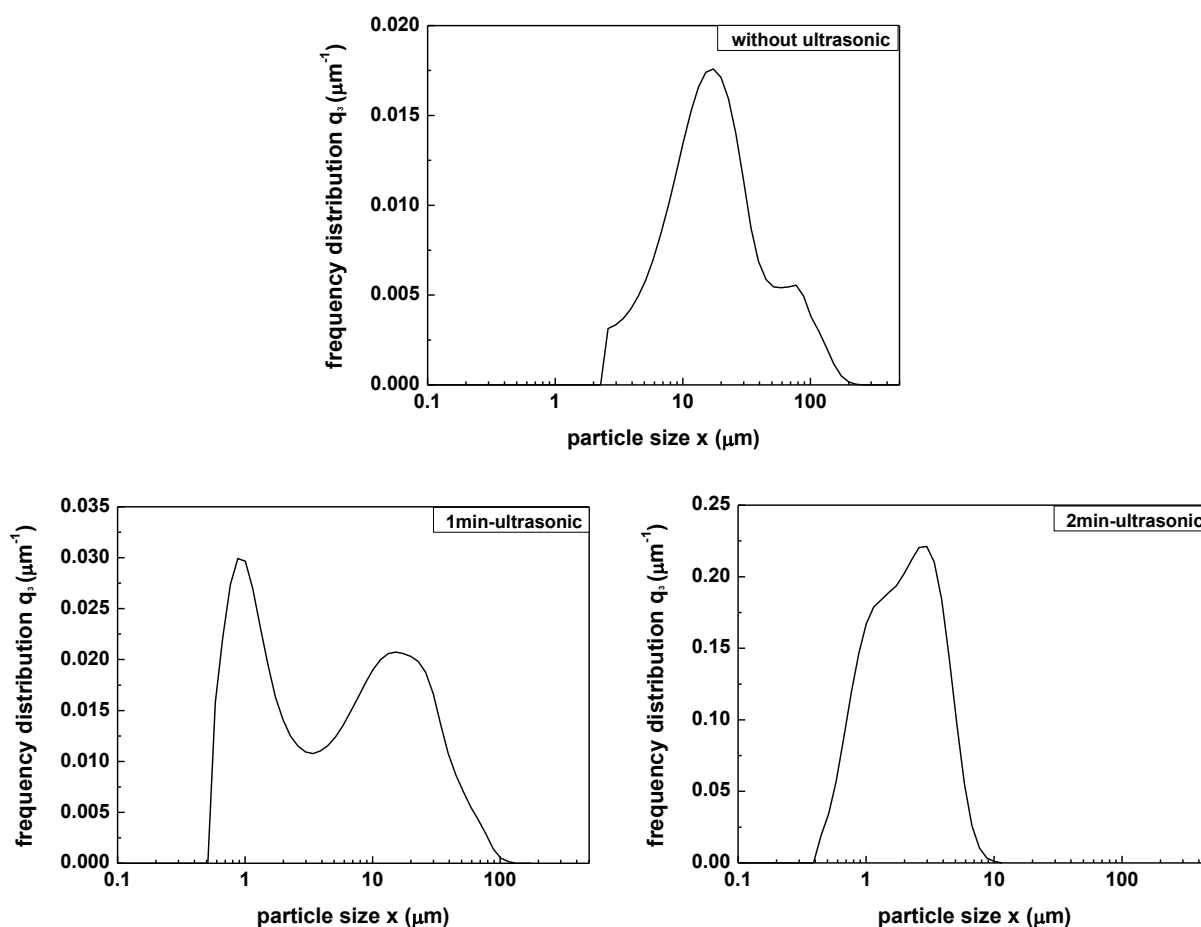


Figure 6.14 Frequency distribution of sample 10 analyzed with the refractive index of carbon by (1) no-ultrasonic (2) 1 min-ultrasonic (3) 2 min-ultrasonic

There was shown the frequency distribution of sample 4 assisted by 2 min-ultrasonic with different refractive index. It was found that the source of larger particles observed in Fig. 6.12 was from agglomerate which was broken by using 2 min-ultrasonic. Furthermore, Fig. 6.13 displayed the bimodal distribution in the range of 0.1  $\sim 10 \mu\text{m}$  no matter which refractive index was used, but

show different peak values. It was difficult to choose which refractive index was appropriate for the DLC coatings. However, according to the ref. [49] it was reported that the refractive index of DLC was 1.8 ~ 2.2. So in the following experiments, the carbon's refractive index 1.920 was used as the optical property of the particles in this work.

By comparing Fig. 6.12 and Fig. 6.13, it was indicated that the ultrasonic is useful during analyzing the particle size distribution, whereas, it is also important to choose the appropriate time for ultrasonic. If different duration of ultrasonic is used, the different result can be obtained as shown in Fig. 6.14. When no any agents and method for disperse was used, the particle size was distributed in the range of 2 ~ 200  $\mu\text{m}$  and a weak peak presented around larger particle size of ~100  $\mu\text{m}$  (Fig. 6.14 (1)).

When ultrasonic was utilized as the dispersion condition, the particle size distribution showed a downward tendency, which moved to smaller particles. Another peak appeared at the smaller size of about 1  $\mu\text{m}$  when the particle size distribution was analyzed with 1min-ultrasonic (Fig. 6.14 (2)). With increasing the time of ultrasonic from 1 min to 2 min, the broad peak at 10 ~ 100  $\mu\text{m}$  vanished so that the whole particle size distribution was in the range of 0.4 ~ 10  $\mu\text{m}$  (Fig. 6.14 (3)), which indicated that to use 1 min-ultrasonic was not enough to disperse the agglomerates completely. What's more, it was found that with increasing the time of ultrasonic the ordinate value of frequency distribution was increased which resulted from the break-up of agglomerates causing the increase of smaller particles due to efficient disperse.

#### ● Conclusion

DLC coatings were deposited with an anode-cathode diameter ratio of  $d_a/d_c = 1/1$  at a DC bias of -500 V and -1000 V respectively. The wear particles were produced by tribological test of disc-on-disc. For preventing from the phenomena of adsorption, PTFE container was used to collect the particles. The effect of parameters of particle size distribution analysis on the frequency distribution was investigated. The higher value of  $q_3(x)$  was obtained at the maximal peak with the refractive index of carbon (1.920) than diamond (2.410) although other characters of these two curves were the same.

During analyzing the particle size distribution, ultrasonic was necessary to disperse the

---

agglomerates. In order to make the particles evenly distributed in the water, the time for ultrasonic was also very important. By comparing with 1 min-ultrasonic, it was confirmed that with 2 min-ultrasonic the agglomerates can be dispersed completely into the smaller particles. Therefore, the refractive index of carbon and 2 min-ultrasonic are the appropriate parameters of particle size distribution analysis in my work.

## References

- [1] A.C. Ferrari, J. Robertson, Resonant Raman spectroscopy of disordered, amorphous, and diamondlike carbon, *Physical Review B* 64 (2001) 075414 1-13.
- [2] O. Durand-Drouhin, M. Lejeune, M. Benlahsen, Growth and bonding structure of hard hydrogenated amorphous carbon thin films deposited from an electron cyclotron resonance plasma, *Journal of Applied Physics* 91 (2002) 867-873.
- [3] M.A. Tamor, W.C. Vassell, Raman “fingerprinting” of amorphous carbon films, *Journal of Applied Physics* 76 (6) (1994) 3823-3830.
- [4] Rusli, S.F. Yoon, H. Yang, J. Ahn, Q. Zhang, Y. S. Wu, W.L. New, Influence of process pressure on the growth of hydrocarbon films under direct dc bias in an electron cyclotron resonance plasma, *Journal of Applied Physics* 84 (9) (1998) 5277-5282.
- [5] A.C. Ferrari, J. Robertson, Interpretation of Raman spectra of disordered and amorphous carbon, *Physical Review B* 61 (2000) 14095-14107.
- [6] K.W.R. Gilkes, H.S. Sands, D.N. Batchelder, J. Robertson, W.I. Milne, Direct observation of  $sp^3$  bonding in tetrahedral amorphous carbon using ultraviolet Raman spectroscopy, *Applied Physics Letters* 70 (15) (1997) 1980-1982.
- [7] D.G. McCulloch, S. Praver, A. Hoffman, Structural investigation of xenon-ion-beam-irradiated glassy carbon, *Physical Review B* 50 (1994) 5905-5917.
- [8] D.G. McCulloch, S. Praver, The effect of annealing and implantation temperature on the structure of C ionbeamirradiated glassy carbon, *Journal of Applied Physics* 78 (1995) 3040-3047.
- [9] S. Praver, K.W. Nugent, Y. Lifshitz, G.D. Lempert, E. Grossman, J. Kulik, I. Avigal, R. Kalish, Systematic variation of the Raman spectra of DLC films as a function of  $sp^2$  :  $sp^3$  composition, *Diamond and Related Materials* 5 (3-5) (1996) 433-438.
- [10] P.K. Chu, L. Li, Characterization of amorphous and nanocrystalline carbon films, *Materials Chemistry and Physics* 96 (2006) 253-277.
- [11] V.I. Merkulov, J.S. Lannin, C.H. Munro, S.A. Asher, V.S. Veerasamy, W.I. Milne, UV studies of tetrahedral bonding in diamondlike amorphous carbon, *Physical Review Letters* 78 (25) (1997) 4869-4872.
- [12] M. Rybachuk, J.M. Bell, Growth of diamond-like carbon films using low energy ion beam sputter – bombardment deposition with Ar ions, *Journal of Physics: Conference Series* 100 (2008) 082009 1-4.
- [13] F.C. Tai, S.C. Lee, J. Chen, C. Wie, S.H. Chang, Multippeak fitting analysis of Raman spectra on DLCH film, *Journal of Raman Spectroscopy* 40 (2009) 1055-1059.

- [14] A.L. Shen. On the data analytic method applied to the 532 nm visible Raman spectra of sputtered amorphous carbon and the related researches of diamond-like carbon (Dissertation).
- [15] B. Oral, R. Hauert, U. Müller, K.H. Ernst, Structural changes in doped a-C:H films during annealing, *Diamond and Related Materials* 4 (4) (1995) 482-487.
- [16] M. Iwaki, H. Watanabe, Analyses of Raman spectra for Na-ion implanted polyacetylene, *Nuclear Instruments and Methods in Physics Research Section B: Beam Interactions with Materials and Atoms* 141 (1-4) (1998) 206-210.
- [17] H. Watanabe, K. Takahashi, M. Iwaki, Structural characterization of ion implanted pyrolytic graphite, *Nuclear Instrument and Methods in Physics Research Section B: Beam Interactions with Materials and Atoms* 257 (1-2) (2007) 549-553.
- [18] S. Nakao, J. Choi, J. Kim, S. Miyagawa, Y. Miyagawa, M. Ikeyama, Effects of positively and negatively pulsed voltages on the microstructure of DLC films prepared by bipolar-type plasma based ion implantation, *Diamond and Related Materials* 15 (4-8) (2006) 884-887.
- [19] J. Schwan, S. Ulrich, V. Batori, H. Ehrhardt, S.R.P. Silva, Raman spectroscopy on amorphous carbon films, *Journal of Applied Physics* 80 (1) (1996) 440-447.
- [20] Y. Ren, I. Erdmann, B. Kützün, F. Deuerler, V. Buck, Effect of deposition parameters on wear particle size distribution of DLC coatings, *Diamond and Related Materials* 23 (2012) 184-188.
- [21] E. Arbabi, S. Chegini, R. Boulic, S.J. Ferguson, D. Thalmann, Estimating hip joint contact pressure from geometric features. N. Magnenat-Thalmann et al. (eds.), *Recent Advances in the 3D Physiological Human*, DOI 10.1007/978-1-84882-565-9\_11, © Springer-Verlag London Limited (2009) 166-177.
- [22] W.A. Hodge, R.S. Fijan, K.L. Carlson, R.G. Burgess, W.H. Harris, R.W. Mann, Contact pressures in the human hip joint measured in vivo, *Proceeding of the National Academy of Sciences of the United States of America* 83 (1986) 2879-2883.
- [23] M.E. Russell, K.H. Shivanna, N.M. Grosland, D.R. Pedersen, Cartilage contact pressure elevations in dysplastic hips: a chronic overload model, *Journal of Orthopaedic Surgery and Research* 1 (6) (2006) 1-11.
- [24] S. Reuter, B. Weßkamp, R. Büscher, A. Fischer, B. Barden, F. Lör, V. Buck, Correlation of structure properties of commercial DLC-coatings to their tribological performance in biomedical applications, *Wear* 261 (2006) 419-425.
- [25] V. Saikko, T. Ahlroos, O. Caloniun, J. Keränen, Wear simulation of total hip prostheses with polyethylene against CoCr, alumina and diamond-like carbon, *Biomaterials* 22 (2001) 1507-1514.
- [26] S.C. Scholes, A. Unsworth, A.A.J. Goldsmith, A frictional study of total hip joint replacements, *Physics In Medicine and Biology* 45 (12) (2000) 3721-3735.
- [27] V. Saikko, T. Ahlroos, Phospholipids as boundary lubricants in wear tests of prosthetic joint materials, *Wear* 207 (1997) 86-91.
- [28] M.A. Wimmer, J. Loos, R. Nassutt, M. Heitkemper, A. Fischer, The acting wear mechanisms on metal-on-metal hip joint bearings: in-vitro results, *Wear* 250 (1-2) (2001) 129-139.

- 
- [29] M. LaBerge, Chapter 7 WEAR. J. Black and G. Hastings (Eds.), London: Chapman & Hall. ISBN 0 412 60330 Handbook of Biomaterial Properties (1998) 365-401.
- [30] R. Hauert, DLC films in biomedical applications. C. Donnet and A. Erdemir (Eds.), Tribology of Diamond-like Carbon Films: Fundamentals and Applications (2008) 500-502.
- [31] H. Ronkainen, S. Varjus, K. Holmberg, Tribological performance of different DLC coatings in water-lubricated conditions, *Wear* 249 (2001) 267-271.
- [32] K. Jia, Y.Q. Li, T.E. Fischer, B. Gallois, Tribology of diamond-like carbon sliding against itself, silicon nitride and steel, *Journal of Materials Research* 10 (6) (1995) 1403-1410.
- [33] H. Ronkainen, J. Likonen, J. Koskinen, S. Varjus, Effect of tribofilm formation on the tribological performance of hydrogenated carbon coatings, *Surface and Coatings Technology* 79 (1996) 87-94.
- [34] [ASTM G 32-98/1998] Standard Test Method for Cavitation Erosion Using Vibratory Apparatus.
- [35] J. Nebel, *Handbuch Kavitationstest* 2004.
- [36] F. Deuerler, H. Gruner, M. Pohl, L. Tikana, Wear mechanisms of diamond-coated tools, *Surface and Coatings Technology* 142-144 (2001) 674-680.
- [37] F. Deuerler, O. Lemmer, M. Frank, M. Pohl, C. Heßing, Diamond films for wear protection of hardmetal tools, *International Journal of Refractory Metals & Hard Materials* 20 (2002) 115-120.
- [38] F. Deuerler, M. Pohl, C. Heßing, Micro- and nanostructured diamond films under wear charging in cavitation test. *Surface and Coatings Technology* 174-175 (2003) 732-737.
- [39] Q. Zhao, Y. Liu, E.W. Abel, Effect of Cu content in electroless Ni-Cu-P-PTFE composite coatings on their anti-corrosion properties, *Mater. Chem. Phys.* 87 (2004) 332-335.
- [40] J.S. Hadley, L.E. Harland, Electroless nickel/PTFE composite coatings, *Met. Finish.* 85 (1987) 51.
- [41] R.J. Zeng, L.F. Chen: *J. Xiamen University (Natural Science)*, 1998, 37 (1), 88. (in Chinese)
- [42] U. Teipel, J.K. Bremser, Chapter 8: Particle Characterization, *Energetic materials: particle processing and characterization*, Wiley-VCH Verlag GmbH & Co. KGaA (2005) 293-332.
- [43] H. Krupp, Particle adhesion: theory and experiment, *Advan. Colloid Interface Sci.* 1 (1967) 111-239.
- [44] J.N. Israelachvili, *Intermolecular and Surface Forces*, Academic Press, London (1992).
- [45] J. Lyklema, *Fundamentals of Interface and Colloid Science*, Academic Press, San Diego, CA (1993).
- [46] R.D. Nelson, *Dispersion of Powders in Liquids*, Elsevier, Amsterdam (1988).
- [47] U. Förter-Barth, U. Teipel, Characterization of particles by means of laser light diffraction and dynamic light scattering, *Eur. J. Mech. Environ. Eng.* 46 (2001) 11-14.
- [48] Partikelgrößenanalyse mit Statischer Laserlichtstreuung, HORIBA LA-950, Retsch Technology GmbH Haan, Germany 99.950.0001/D-11-2010.
- [49] Y.W. Yang, J. Yang, H.W. Gu, H.Z. Liu, H. Zhang, W. Jin, Properties, processing and application of diamond-like carbon film, *Bulletin of the Chinese Ceramic Society* 27 (1) (2008) 119-126 (in Chinese).

## 7. Influence of substrate bias on the particle size distribution of DLC coatings

### 7.1 Anode-cathode diameter ratio of $d_a/d_c = 1/3$

The DLC coatings were deposited with an anode-cathode diameter ratio of  $d_a/d_c = 1/3$  and ion density of  $7.163 \times 10^{11} \text{ cm}^{-3}$  at a DC bias of  $-250 \text{ V}$ ,  $-500 \text{ V}$ ,  $-750 \text{ V}$  and  $-1000 \text{ V}$  for 3 minutes each. The austenite stainless steel P2000 (see chapter 5.1) was used as substrate material for the deposition of carbon coatings. In order to improve the adhesion of DLC coating to substrate, Ti as interface layer was deposited by cathodic vacuum arc evaporation prior to the deposition of DLC coating. During the deposition of carbon coatings an arc current of 80 A and an arc voltage of 20 V were used. Each sample consisted of two P2000 discs, and each disc was coated with the same parameters. Si (100) wafer was marked on the surface with a marker for the purpose of film thickness measurement, and then also placed on the substrate holder with P2000 substrate.

At the beginning, the work was just focused on the wear particle size distribution of DLC coatings. So in order to get the detail about the DLC coatings deposited, for example the density and deposition rate of DLC coatings, the experiments were done repeatedly.

#### 7.1.1 Density and deposition rate of DLC coatings

In Fig. 7.1 the results of deposition rate and density as a function of bias voltage are shown. The deposition rate turned out to ascend with the bias, although it appeared to be lower at  $-750 \text{ V}$  than at  $-500 \text{ V}$ . When the bias was increased to  $-1000 \text{ V}$ , more carbon atoms/ ions were deposited on the substrate so that the deposition rate was very fast and reached to the maximum value of 9.0 nm/sec as Fig. 7.1 (a) shown.

However, according to the curve of density with the bias in Fig. 7.1 (b), the DLC coating deposited at  $-1000 \text{ V}$  had the lowest density. As can be seen in Fig. 7.1 (b) the density varied between  $1.55 \text{ g/cm}^3$  and  $2.25 \text{ g/cm}^3$  and with the bias increasing from  $-250 \text{ V}$  to  $-750 \text{ V}$  the density was gradually increased from  $1.8 \text{ g/cm}^3$  to  $2.2 \text{ g/cm}^3$ , then decreased to  $1.65 \text{ g/cm}^3$  at higher bias of  $-1000 \text{ V}$ . The results indicated that the negative bias can make the DLC coatings

denser and may cause the deposition rate ascend which was totally different compared to the results in Y.S. Park's report [1,2]. Usually, the films became denser resulting from the increase of high ion impingement energies because it decreased voids from the penetration of the ions, which can result in the decrease of deposition rate [1].

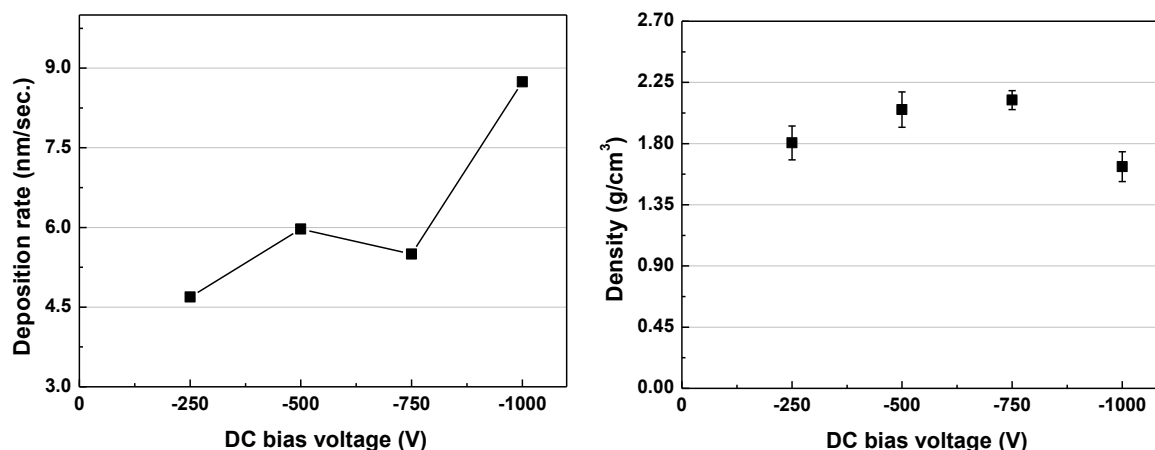


Figure 7.1 Deposition rate (a) and density (b) as a function of bias voltage

However, according to the result obtained by Y.S. Park et al. [2], the DC bias voltage was in the range of 0~200 V and the deposition rate trended upwards slightly at -200 V. So it was deduced that the deposition rate maybe increased with increasing the bias from -200 V. What's more, as Fig. 7.1 (b) shows, with increasing the DC bias voltage from -250 V to -750 V not only there was no decreasing of deposition rate, but also the density of DLC coating was increased. In contrast to the density of coating at -750 V, the DLC coating had lower density at -1000 V. So the higher bias of -1000 V applied to the substrate, although it can improve the deposition rate, can influence the structure of DLC coatings.

### 7.1.2 Raman spectra of DLC coatings

Fig. 7.2 shows Raman spectra of DLC coatings at different DC bias voltage between -250 V and -1000 V. It appeared that there was no obvious changes in all the spectra, the same peak position, one broad peak at  $\sim 1580 \text{ cm}^{-1}$  and one weak peak at  $\sim 1350 \text{ cm}^{-1}$ , assigned to G and D band (corresponding to  $\text{sp}^2$  sites), respectively. Another weak peak can be observed at  $\sim 1200 \text{ cm}^{-1}$ . Raman spectrum fitting (see Section 6.1) is used to analyze the structure of DLC coatings as shown in Fig. 7.3. Because two Gaussian curves are sometimes not suitable for all carbon coatings,

especially DLC coatings deposited by vacuum arc, so other features, such as the weak peaks at  $1100 \sim 1200 \text{ cm}^{-1}$  and  $1400 \sim 1500 \text{ cm}^{-1}$ , must be considered, except for G and D peaks present in Fig. 7.3.

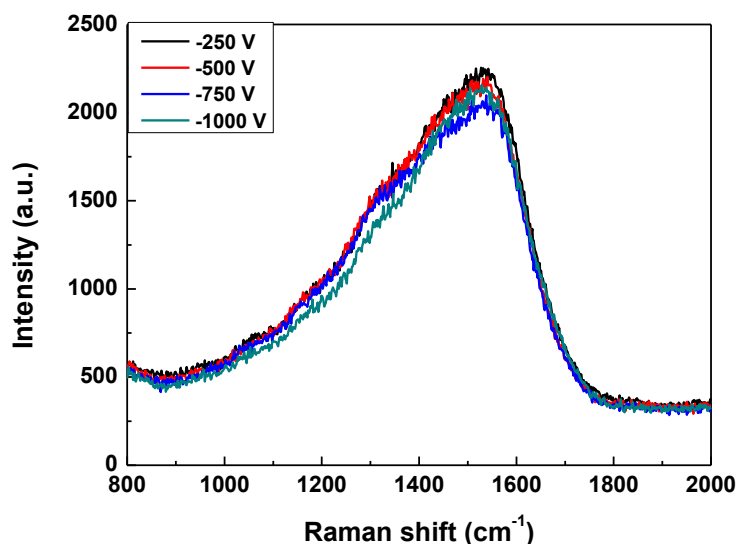


Figure 7.2 Raman spectra of DLC coatings with DC bias voltage

A linear background was subtracted before fitting the spectra with Gaussian curves. The Raman spectrum of DLC coatings deposited at different DC bias voltages was fitted very well using four peaks as seen in Fig. 7.3. The third peak, around  $1400 \sim 1500 \text{ cm}^{-1}$ , decreased with increasing DC bias voltage, and disappeared when the bias was increased to  $-1000 \text{ V}$ , which indicated G band became more symmetrical at  $-1000 \text{ V}$  than at other bias voltages.

Fig. 7.4 plots the peak positions and the intensity ratios of D and G band. The D band was around  $1355 \text{ cm}^{-1}$ , in the range of  $1350 \sim 1365 \text{ cm}^{-1}$  when the DC bias was increased from  $-250 \text{ V}$  to  $-750 \text{ V}$ . And then it was shifted to higher frequencies up to  $1400 \text{ cm}^{-1}$  with the DC bias increasing to  $-1000 \text{ V}$ . Another feature was the shift of G band from  $1546$  to  $1554 \text{ cm}^{-1}$ . The G peak position was almost constant, especially at the bias of  $-500 \text{ V}$ ,  $-750 \text{ V}$  and  $-1000 \text{ V}$ , with a very slight tendency to increase with the DC bias voltage. But it was decreased comparing to G band of graphite at  $1580 \text{ cm}^{-1}$  due to increasing bond-angle and bond-bending disorder and the presence of nonsixfold rings softening the vibrational density of states (VDOS) [3, 4].

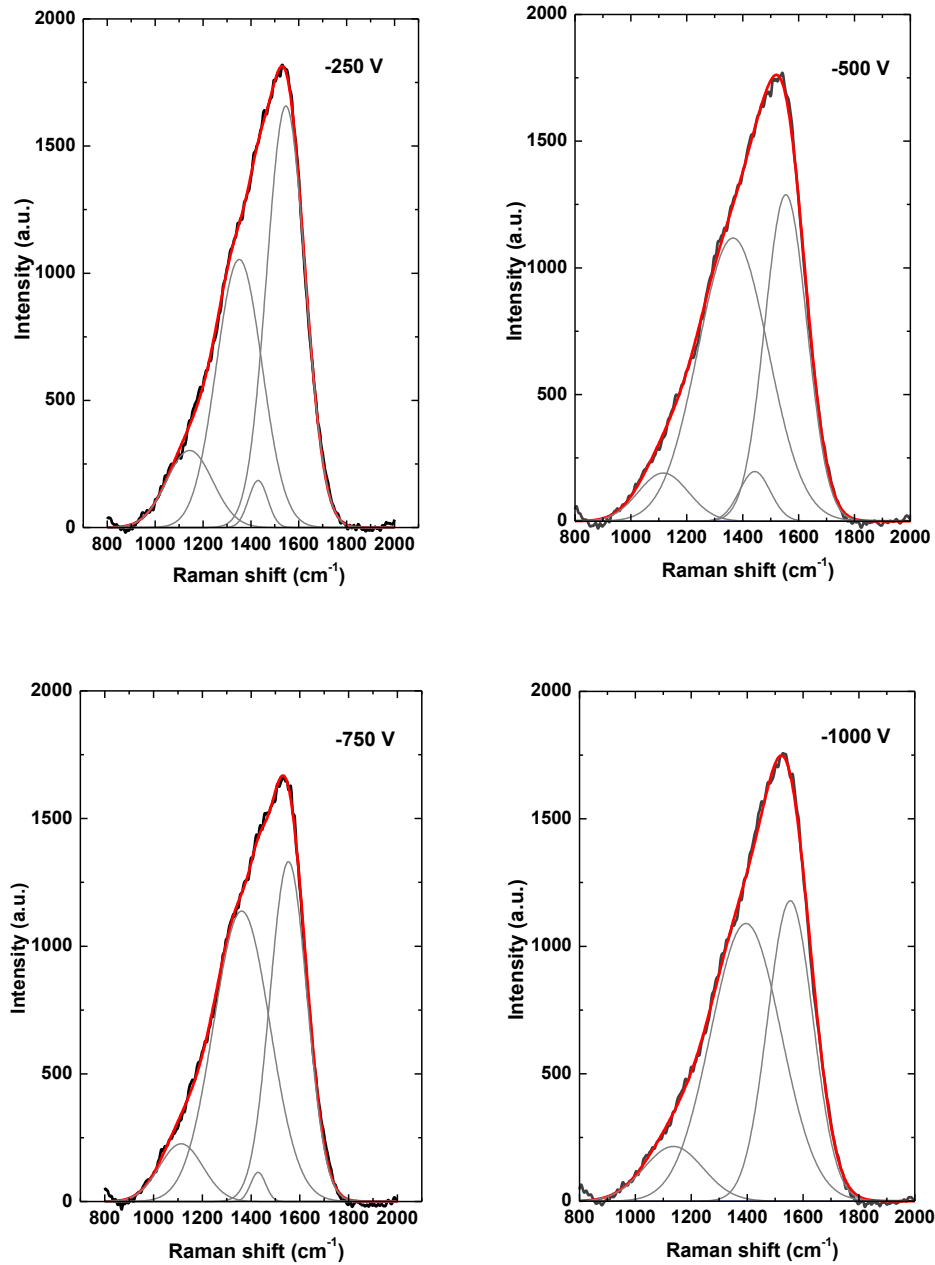


Figure 7.3 Raman spectra fittings of DLC coatings with different DC bias voltage

The ratio of  $I_D/I_G$  was increased with the DC bias voltage increasing and the minimum value was 0.63 at  $-250$  V, corresponding to Fig. 7.3, which shows that DLC coating deposited using  $-250$  V as the substrate bias had a higher  $sp^3$  content compared with other bias voltages. As the bias increases from  $-500$  V to  $-1000$  V, the intensity ratio of D and G band was almost constant, 0.85~0.95.

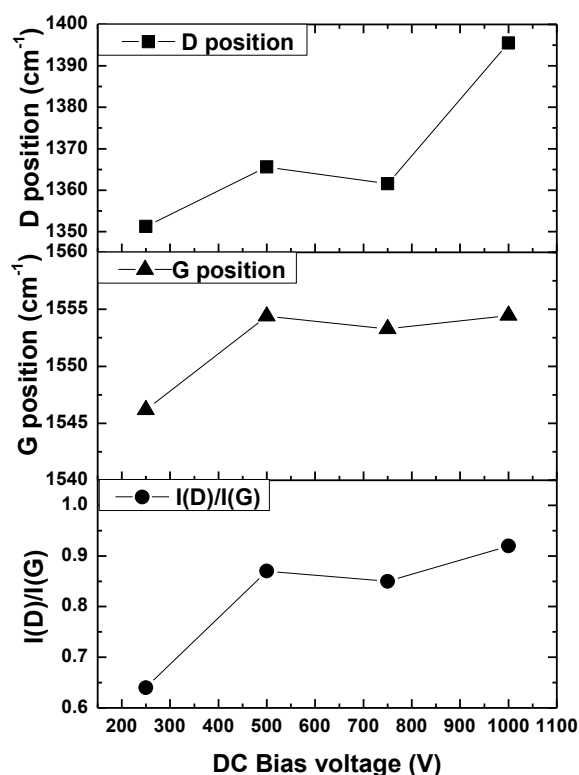


Figure 7.4 Variation of D and G positions and  $I_D/I_G$  ratio as a function of DC bias voltage

### 7.1.3 Tribological properties of DLC coatings

Disc-on-disc tests (see chapter 6.2) are performed in the normal force of 80 N with the temperature of 21.5 °C in deionized water. Common relative speed is 0.01 m/s. After a running time of 0.5 h, all samples were worn. What's more, the coating at the edge of all samples was peeled off more or less maybe due to the compressive stress of DLC coatings resulting from the thicker film. According to the ref. [5], with the thickness of film increasing from 3 nm to 50 nm the stress of films was increased first, then decreased slightly at thickness of  $> 50$ nm. The compressive stress began to increase again at 190 nm, at which the film starts to delaminate. The samples deposited with an anode-cathode diameter ratio of  $d_a/d_c = 1/3$  had higher deposition rate as Fig. 7.1(a) shown. The films with the thickness of  $\sim 800$  nm at least after 3 min deposition were much thicker than that in ref. [5].

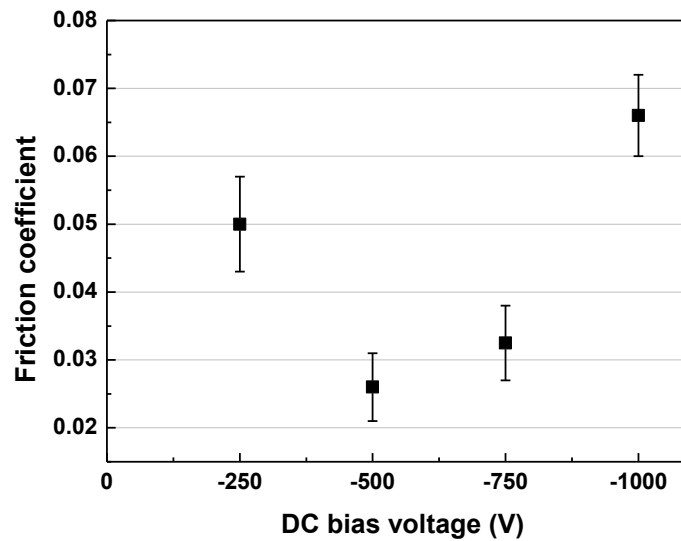


Figure 7.5 Friction coefficient of DLC coatings deposited at various DC bias voltages

Fig. 7.5 shows the variation of the friction coefficient of DLC coatings as a function of DC bias voltage. It was observed that the coatings at the bias of  $-500$  V and  $-750$  V exhibited the lower friction coefficient of  $0.02 \sim 0.04$ . The relatively higher coefficient of friction shown at the higher bias of  $-1000$  V might be the influence of interface layer of Ti. This interpretation was based on the fact that after tribological test there was no DLC coating left around the wear track which just appeared on the surface of interface layer or the substrate, which indicated that the peeling-off coating was due to higher compressive stress resulting from the thicker coating.

#### 7.1.4 Particle size distribution of DLC coatings

The graphical representation of particle size analysis data is shown in Fig. 7.6~7.8. Fig. 7.6 shows the cumulative distribution  $Q_3(x)$  with an anode-cathode diameter ratio of  $d_a/d_c = 1/3$  at a DC bias of  $-250$  V,  $-500$  V,  $-750$  V and  $-1000$  V. Each individual point of  $Q_3(x)$  represents the relative amount of particles equal to or smaller than a certain particle size  $x$ . The results shown that almost 10% particles of coatings deposited at  $-250$  V and  $-750$  V were smaller than  $10 \mu\text{m}$ , whereas 20% at  $-500$  V and  $-1000$  V. Nearly 50% particles were smaller than  $50 \mu\text{m}$  (Fig. 7.6), and 90% smaller than  $100 \mu\text{m}$ .

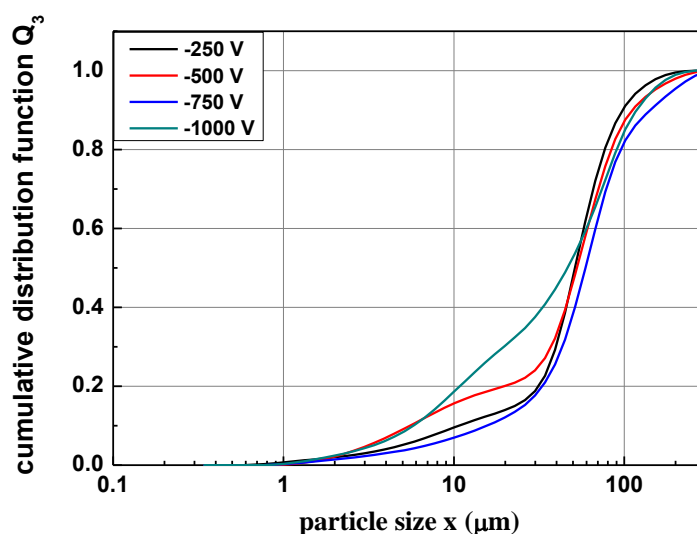


Figure 7.6 Cumulative distribution by volume  $Q_3(x)$ : comparison of substrate biases of  $-250$  V,  $-500$  V,  $-750$  V and  $-1000$  V ( $d_a/d_c = 1/3$ )

Fig. 7.7 is the curve of the volume density distribution as a function of particle size. The density distribution  $q_3(x)$  which represents the amount of particles of a given particle size  $x$ , relative to the entire particle size distribution, can be obtained from

$$q_3(x_i) = \frac{dQ_3(x)}{dx} \quad (7.1)$$

The main peaks found in each of the curves are assigned to the modal values  $x_{\text{mod}}$ . That means these particle sizes  $\sim 1$ ,  $\sim 5$ , and  $\sim 50$   $\mu\text{m}$  occur most often when the DLC coatings were deposited at the bias of  $-250$ ,  $-750$  and  $-1000$  V. There were two main peaks at the bias of  $-500$  V, which means two maximums of the curve in the range of particle size distribution. With the bias increasing, the peak height at  $\sim 50$   $\mu\text{m}$  was decreased, from which can be estimated that it is possible to make the maximum of frequency distribution shift to lower than  $10$   $\mu\text{m}$ , even  $1$   $\mu\text{m}$  at the higher bias.

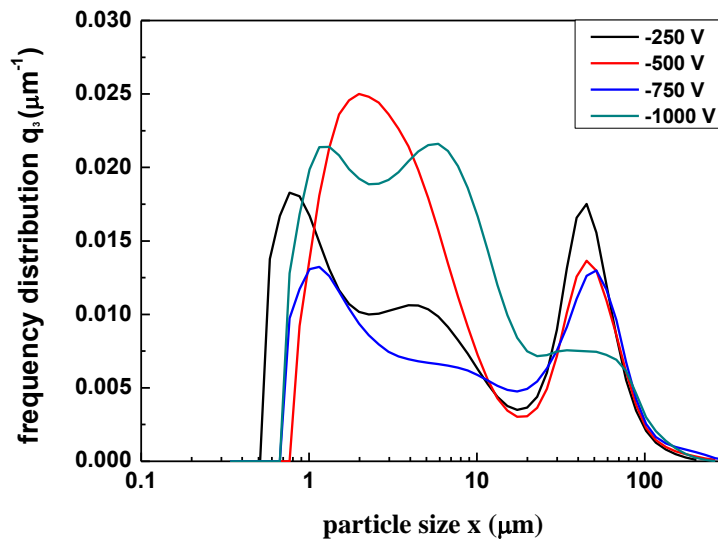


Figure 7.7 Volume density distribution  $q_3(x)$ : comparison of substrate biases of  $-250$  V to  $-1000$  V

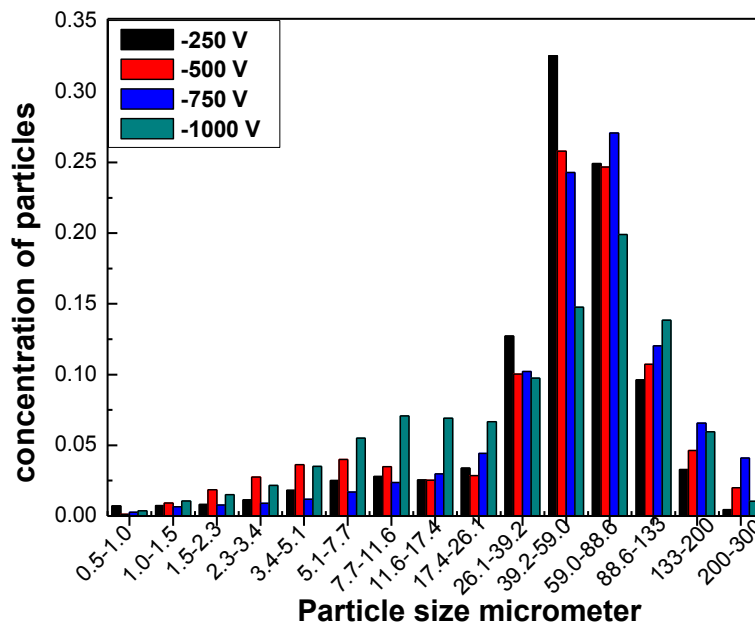


Figure 7.8 Particles size distribution: comparison of substrate biases of  $-250$  V to  $-1000$  V

In order to get the details about the particle size distribution in the different interval size, the concentration histogram of particles was drawn in the different range of particle size (see Fig. 7.8), because amounts that fall within a given particle size interval were referenced to the interval size according to the formula (7.1). It was shown that all particles were distributed in the range of  $0.45 \sim 300 \mu\text{m}$ , and the maximum concentration of particles was distributed in the larger range of  $39.23$

~ 58.95  $\mu\text{m}$  and 58.95~88.58  $\mu\text{m}$ . It was found that just only 10.5%, 16.8%, 8.1% and 21.2% of all particles were smaller than 11.57  $\mu\text{m}$  when the bias was -250, -500, -750 and -1000 V, respectively, as also shown in Fig. 7.8. Few amounts of larger particles maybe came from the peeling-off films, another from the wear debris or impurity and contamination which was difficult to avoid. As discussed above, the DLC coating deposited at -250 V with the minimum ratio of  $I_D/I_G$  has the highest  $\text{sp}^3$  content, however almost 90% of all particles generated are larger than 11.57  $\mu\text{m}$ .

### **7.1.5 Conclusion**

The DLC coatings were deposited on P2000 substrates with Ti as interface layer by vacuum arc method with an anode-cathode diameter ratio of  $d_a/d_c=1/3$ . Although all samples deposited at different negative bias take place the same delamination phenomenon after 0.5 h-tribological testing, the negative bias applied to the substrate has effect on the structure and properties of DLC coatings. It can improve the deposition rate and the density of coatings. The DLC coating deposited at -250 V had the lowest value of  $I_D/I_G$ , but the density was just about 1.8  $\text{g/cm}^3$ . At a bias of -500 V and -750 V, the density reached the range of 2.00  $\text{g/cm}^3 \sim 2.25 \text{g/cm}^3$  and the lowest friction coefficient of 0.02 ~ 0.04. When the bias was increased to -1000 V, the DLC coating had the lowest density, higher ratio of  $I_D/I_G$  and highest friction coefficient compared with films deposited at other biases. Meanwhile, the wear particle size distribution was influenced by the negative bias. With increasing the bias the maximum of frequency distribution of wear particles had the trend towards the smaller particle of ~ 10  $\mu\text{m}$ . It has been estimated that the peak around ~ 50  $\mu\text{m}$  in frequency distribution of wear particles would disappear when the DLC coatings were deposited at higher negative bias of > 1000 V. These results show that by varying the process parameters especially DC bias during DLC deposition the properties and the wear particles size distribution of DLC coatings can be modified.

## 7.2 Anode-cathode diameter ratio of $d_a/d_c = 1/1$

The DLC coatings were deposited with an anode-cathode diameter ratio of  $d_a/d_c = 1/1$  and ion density of  $1.47 \times 10^{12} \text{ cm}^{-3}$  at a DC bias of  $-250 \text{ V}$ ,  $-500 \text{ V}$ ,  $-750 \text{ V}$  and  $-1000 \text{ V}$  for 3 minutes each. During the deposition an arc current of  $80 \text{ A}$  and the arc voltage of  $20 \text{ V}$  were used. Each sample consisted of two discs (P2000 with titanium), and each disc was coated with the same parameters.

At the beginning, the focus lays on the wear particle size distribution of DLC coatings. So in order to get the details about the DLC coatings deposited, for example the density and deposition rate of DLC coatings, the experiments were done repeatedly.

### 7.2.1 Density and deposition rate of DLC coatings

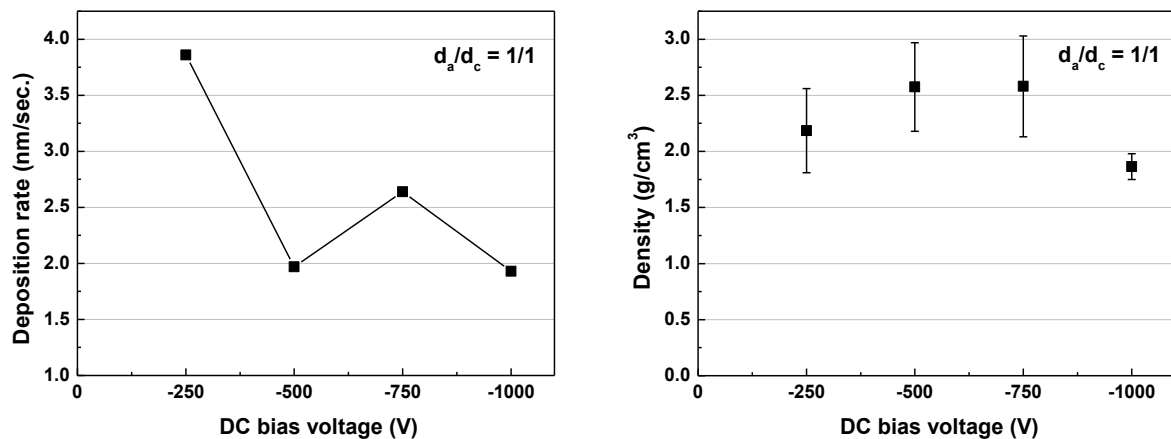


Figure 7.9 Deposition rate (a) and density (b) as a function of bias voltage

Fig. 7.9 shows the different deposition rate and density of DLC coatings on the various DC bias voltages at the condition of working pressure of  $2 \times 10^{-4} \text{ mbar}$ . The results showed clearly that the deposition rate decreased with increasing DC bias voltage from  $-250 \text{ V}$  to  $-500 \text{ V}$ , then slightly increased at the bias of  $-750 \text{ V}$ . However when the bias reached to the highest voltage of  $-1000 \text{ V}$ , the deposition rate reached the minimum value.

The plasma sheath expands from the substrate after a short period of the negative DC bias voltage [2]. As a result, ion flux from the plasma to the substrate decreases abruptly [6]. This behavior resulted in the decrease of the flux from the plasma and as a consequence the deposition rate decreases.

What's more, it was found that the density was in a range of  $1.6 \text{ g/cm}^3 \sim 3.1 \text{ g/cm}^3$ . With increasing the bias the density was increased to the maximum at the bias of  $-750 \text{ V}$ , decreased to the minimum of  $1.8 \text{ g/cm}^3$  when the bias reached to the maximum of  $-1000 \text{ V}$ . Usually, with increasing the DC bias the deposition rate decreases, which means the coating becomes denser. Because the bias applied to the substrate can improve the nucleation density and provide mobility to the atoms/ions being deposited so that dense and void free films are deposited. That means, the density should be the maximum when the deposition rate decreases to the minimum at the bias of  $-1000 \text{ V}$ . However, here the result is definitely contrary. It seems that high bias will cause repulse adsorption of carbon ions which result from the large charge accelerating toward to the substrate due to higher bias.

### 7.2.2 Raman spectra of DLC coatings

Fig. 7.10 shows the Raman spectra of DLC coatings deposited with various DC bias voltages and the corresponding peak positions of D and G and the ratio of  $I_D/I_G$  (b) after the Raman deconvolution as shown in Fig. 7.11. A linear background was subtracted before fitting the spectra. Although the visible Raman spectra of DLC films mainly come from the ordering of the  $sp^2$  bonded carbon in the films and only indirect from the  $sp^3$  fraction in the films, it can be applied in a restricted range of film properties to derive information about the  $sp^3/sp^2$  ratio. The applicability of the Raman spectroscopy was proven by comparison with different analytical methods which determine the  $sp^3/sp^2$  ratio more directly like electron energy loss and NMR spectroscopy [7]. Especially the three stage model by Ferrari and Robertson is a very well accepted and helpful method to estimate the  $sp^3/sp^2$  ratio in the carbon films from the G peak position and the  $I_D/I_G$  ratio taken from visible Raman spectra [8].

The spectra show two broad peaks, at approximately  $1560 \text{ cm}^{-1}$  and  $1360 \text{ cm}^{-1}$ , attributed to G-band and D-band, respectively. The G and D peaks are due to  $sp^2$  sites only. Another weak peak was found around  $1000 \text{ cm}^{-1} \sim 1200 \text{ cm}^{-1}$ .

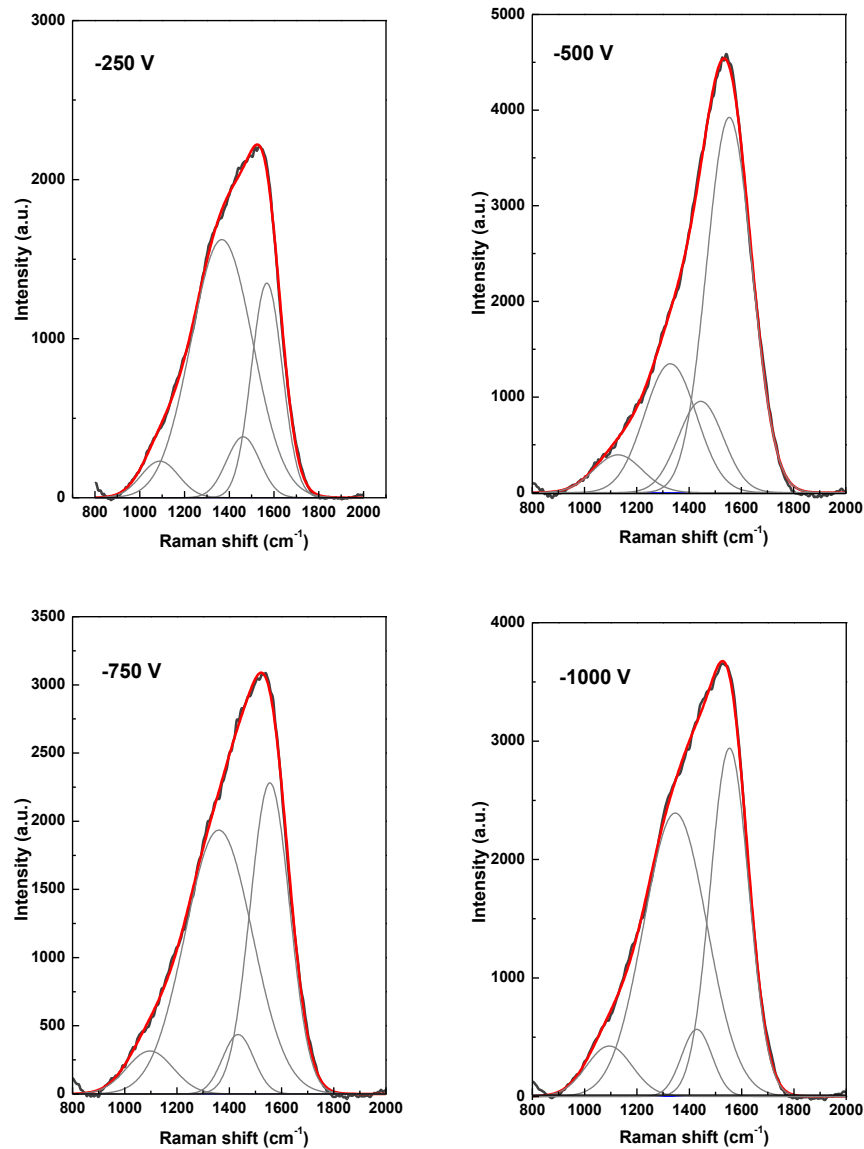


Figure 7.10 Raman spectra fittings of DLC coatings with different DC bias voltage

Raman spectrum fitting is used to measure the intensity ratio of the D and G bands in order to analyze the  $sp^3/sp^2$  ratio of DLC coatings. Usually two Gaussian functions for the G peak are widely used in most papers [7, 9-10] just focusing on the G and D peaks. In paper [9], the researchers neglected other features that are sometimes present, such as those at  $1100\text{ cm}^{-1} \sim 1200\text{ cm}^{-1}$  and  $1400\text{ cm}^{-1} \sim 1500\text{ cm}^{-1}$ . Comparing with different Raman spectra fittings using two peaks, three peaks and four peaks in chapter 6.1, it was found that Raman spectrum with four peaks could be fitted very well. So other peaks present in Fig. 7.10 around  $1100\text{ cm}^{-1} \sim 1200\text{ cm}^{-1}$  and  $1400\text{ cm}^{-1} \sim 1500\text{ cm}^{-1}$ , must be considered. A Gaussian fit of the D and G peak positions and the ratio of  $I_D/I_G$  are shown in Fig. 7.11.

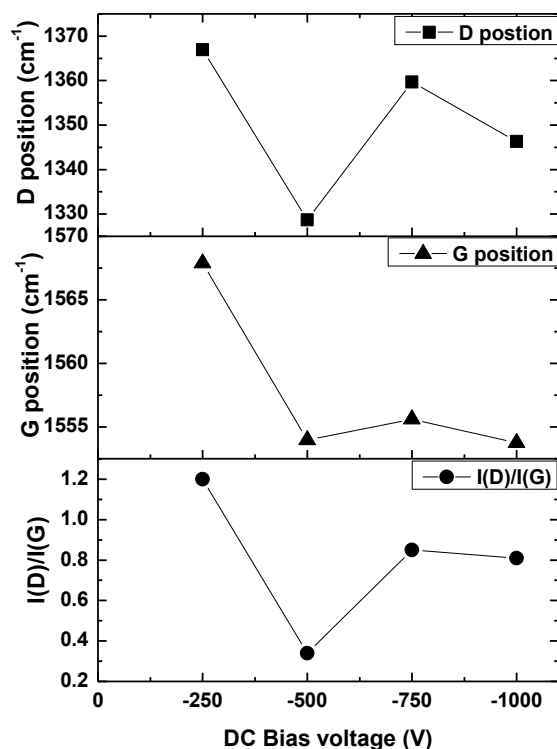


Figure 7.11 Variation of D and G positions and  $I_D/I_G$  ratio as a function of DC bias voltage

Variation of the D, G peak positions and  $I_D/I_G$  ratio with DC bias voltage between  $-250$  V and  $-1000$  V can be described obviously as a curve of “V”. It was observed that the G peak frequency downshifted to lower than  $1580$   $\text{cm}^{-1}$  and G band is in the range of  $1553$   $\text{cm}^{-1} \sim 1567$   $\text{cm}^{-1}$ , because the weak bonds caused by the topological disorder introduced to the graphite layer soften the vibrational modes. With DC bias voltage increasing to  $-500$  V the G peak positions and the intensity ratios of the D and G bands all decreased to the lowest value at  $1553$   $\text{cm}^{-1}$  and 0.3, respectively. This indicates that higher content of  $\text{sp}^3$ -bonded carbon can be obtained when the DLC coating is deposited at  $-500$  V compared to other bias voltages. Then, with increasing the DC bias voltage from  $-500$  V to  $-1000$  V, it was found that the G peak position and  $I_D/I_G$  increased at  $-750$  V but at a lower level than at  $-250$  V. However, there was no obvious change of values at a bias of  $-750$  V and  $-1000$  V.

As known, the  $\text{sp}^3/\text{sp}^2$  ratio is an important parameter for DLC studies, and it is related to the peak positions and the ratio of  $I_D/I_G$ . The intensity of D peak, correlated with the breathing modes

of rings, is proportional to the number of  $sp^2$ -clusters of graphite. It can be confirmed that with DC bias increasing from  $-250$  V to  $-500$  V, the cluster size and number decreased which resulted in the decrease of the peak positions and the intensity ratio of the D and G bands, which was in accord with the result reported by Irmer [7].

According to a phenomenological three-stage model [8,9] used to interpret the Raman spectra of amorphous carbons, the coatings deposited belong to stage 2: from nano-crystalline graphite to a-C.

### 7.2.3 Tribological properties of DLC coatings

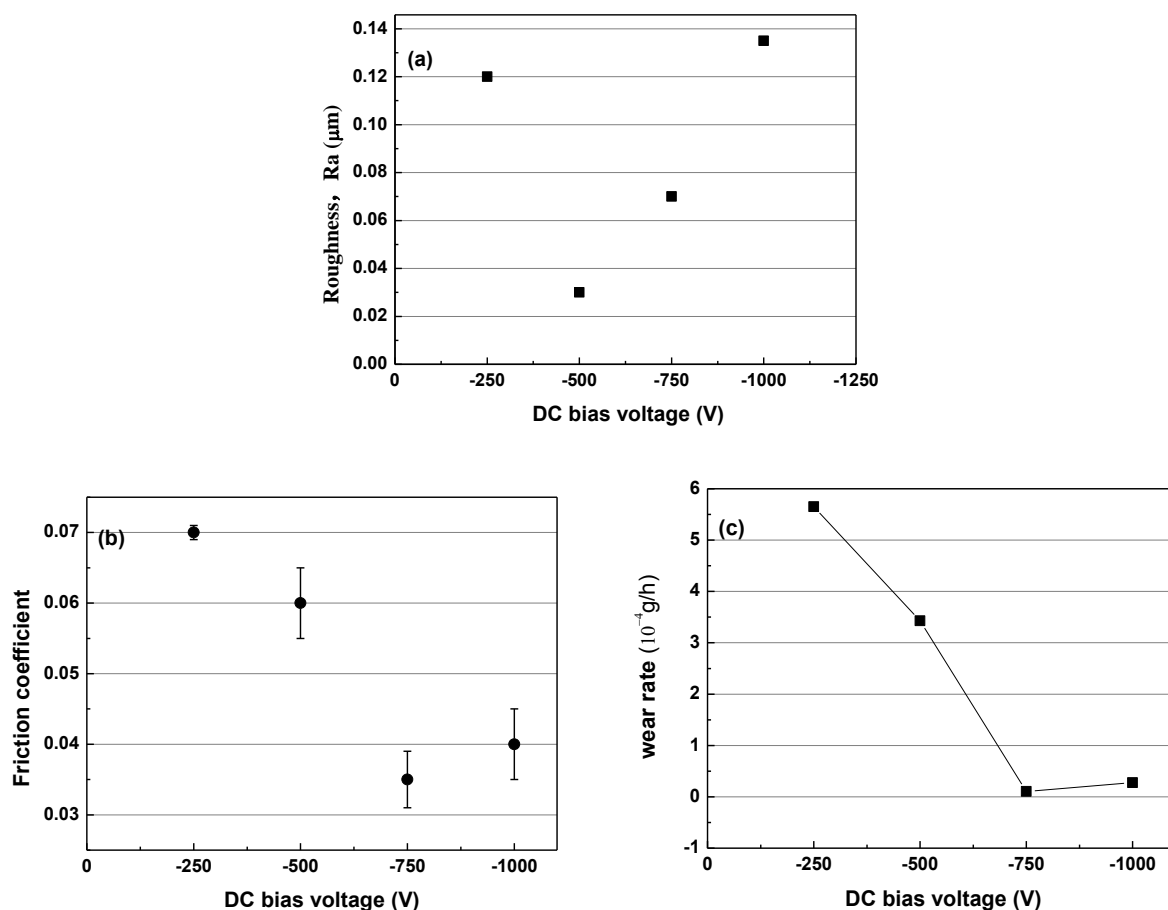


Figure 7.12 Roughness ( $R_a$ ) (a), friction coefficient (b) and wear rate (c) of DLC coatings deposited at various DC bias voltages

Fig. 7.12 presents the experimental results of average roughness ( $R_a$ ), coefficient of friction and wear rate as a function of substrate bias voltage. The friction coefficient and wear rate of the film was measured by a tribometer with the temperature of  $21.5$  °C in deionized water. Fig. 7.12

shows lowest surface roughness of 30 nm at  $-500$  V, however, higher friction coefficient. It was found that the surface roughness has a maximum of 135 nm at  $-1000$  V, but the lower friction coefficient.

According to the references [11-13], the coefficient of friction depends on the force applied and the surface energy, in addition the surface roughness values are inversely related to the average friction coefficient. The same results which had the lowest Ra value and highest coefficient of friction were illustrated by Zhang et al. [11].

The friction coefficient varied between 0.03 and 0.07. It decreased with increasing bias to a minimum of 0.035 at  $-750$  V, and then increased to 0.04 at higher bias ( $-1000$  V). It was observed that the wear rate presented the same change trend with the friction coefficient as Fig. 7.12(b) and (c) show.

With increasing the bias the wear rate was reduced. The DLC coating deposited at  $-750$  V has the lowest wear rate, which is very important in the application of hip joint implants. Actually, the tribological properties of a given coating do not only depend on the coating itself, but also on the surroundings, e.g. lubricated environment, load, velocity and so on. So in these experiments load of 100 N and speed of 0.01 m/s were chosen. For the sample deposited at  $-750$  V, after a running time of 5 h, there was no wear track. In an attempt to get the wear particles, the load and velocity were increased to 120 N and 0.06 m/s, respectively, but still no wear track after 10 h. Finally, the additional tests were carried out at the load of 300 N and the velocity of 0.1 m/s for 55 h, the color of DLC coating became dark but no delamination observed. According to the Fig. 7.9 (b) it had the highest density of  $3.03 \text{ g/cm}^3$ , which was close to  $3.1 \text{ g/cm}^3$  of ta-C coating reported in ref. [14-16]. It was confirmed that the DLC coating deposited at the bias of  $-750$  V has good tribological properties.

#### **7.2.4 Particle size distribution of DLC coatings**

As described above, the deposition parameters e.g. DC bias voltages had an effect on the DLC coating structures. Therefore it is very important to study the effect of bias on the particles size distribution. The wear particles were collected in suspension in deionized water, then

measured using a particle size analyzer. Here the volume cumulative distribution and the volume density distribution were chosen to characterize the size of particles. The graphical representation of particle size analysis data is shown in Fig. 7.13~7.14. The curve plotted in Fig. 7.13 shows the density distribution of the particles size of DLC coatings after tribological tests. The curve plotted in Fig. 7.14 shows the concentration of particles collected in different size distribution.

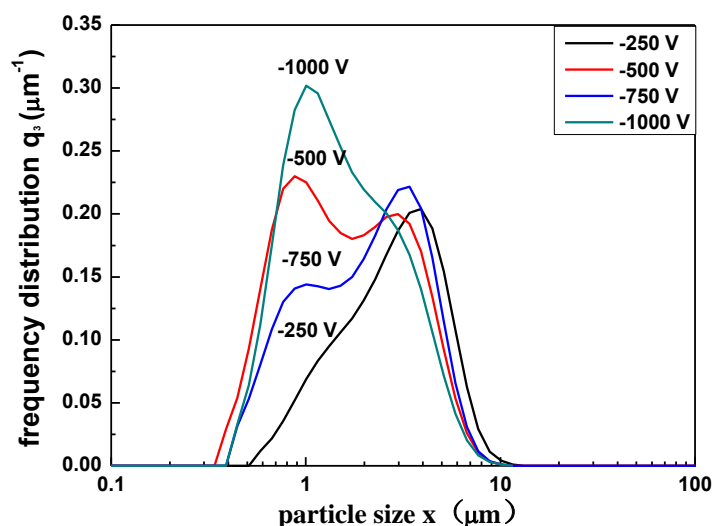


Figure 7.13 Volume density distribution  $q_3(x)$ : comparison of substrate biases of  $-250$  V to  $-1000$  V

Fig. 7.13 showed that all particles generated were distributed in the range of  $0.3$   $\mu\text{m}$  to  $10$   $\mu\text{m}$  and there were two maximums of each curve in the range of particle size distribution. However, the maximum in Fig. 7.13 does not mean that the large amount of particles was distributed in this range, because the frequency distribution in Fig. 7.13 has the dimension of an inverse length. Amounts that fall within a given particle size interval were referenced to the interval size.

It was found that almost 80 % of all particles were smaller than  $6$   $\mu\text{m}$  (Fig. 7.14). All samples showed the highest concentration at the same particle size distribution of  $3.41$  to  $5.12$   $\mu\text{m}$  (Fig. 7.14), not around  $\sim 1$   $\mu\text{m}$  as to be seen in Fig. 7.13. The frequency distribution of particles reached the maximum when the bias voltage was at  $-1000$  V, the minimum at  $-250$  V, presenting the converse curve of “V” (see Fig. 7.12 (b)). At DC bias voltages of  $-250$  V and  $-750$  V, the largest amount of particles was found at  $> 5.12$   $\mu\text{m}$ , while, on the contrary, at  $-500$  V and  $-1000$  V it was distributed in a range  $< 5.12$   $\mu\text{m}$ . It was obviously shown that the concentration of particles at –

1000 V was distributed more equally in a whole range.

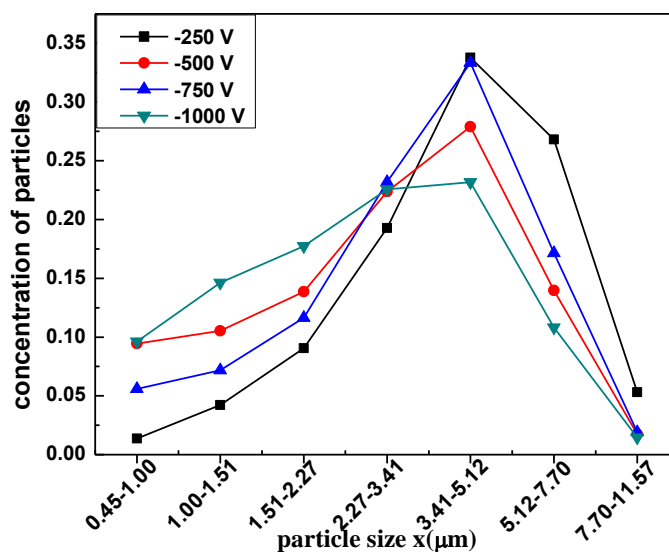


Figure 7.14 Particles size distribution: comparison of substrate biases of -250 V to -1000 V

## 7.2.5 Conclusion

The DLC coatings were deposited on P2000 substrates with Ti as interface layer by vacuum arc method with an anode-cathode diameter ratio of  $d_a/d_c = 1/1$ . The effect of DC bias voltage on the distribution of wear particle size generated by disc-to-disc tests was investigated. Disc-on-disc testing at the load of 100 N was found to produce sufficient amount of wear particles to determine particle size contribution. The lowest friction coefficient of 0.035 was attained at a bias of -750 V. The DLC coating deposited at -500 V has the lowest Ra and higher  $sp^3$  content. All particle size distributions were in a range of 0.3 μm to 10 μm and most of the particles appeared around 3.41 μm to 5.12 μm. With increasing bias from -250 V to -1000 V the wear particle size decreased and the largest amount of particles was smaller than 5.12 μm. For medical reasons it is necessary to adjust the structure of DLC coatings and wear particle size distribution. These results show that by varying the process parameters during DLC deposition the properties and wear particles size distribution can be modified.

### 7.3 Anode-cathode diameter ratio of $d_a/d_c = 3/1$

Discs as substrates, the diameter of 31 mm and thickness of 4 mm, were made of stainless steel (P2000). Titanium was chosen to be as interface layer better than chromium to improve the adhesion of the DLC film to P2000. The interface layers were synthesized using titanium cathode. The DLC coatings were deposited at different DC biases using an anode-cathode diameter ratio of  $d_a/d_c = 3/1$ . A more detailed list of deposition process parameters is given in Table 7.1. Here, in the first group experiments, the bias of  $-700$  V was used instead of  $-750$  V.

Table 7.1 Deposition process parameters of DLC coatings of  $d_a/d_c = 3/1$

Ion density	$2.59 \times 10^{12} \text{ cm}^{-3}$
Arc voltage	20 V
Arc current	80 A
Deposition pressure	$2 \times 10^{-3}$ mbar
Deposition time	3 min
Substrate bias voltage	$-250$ V, $-500$ V, $-750$ V ( $-700$ V), $-1000$ V

#### 7.3.1 Density and deposition rate of DLC coatings

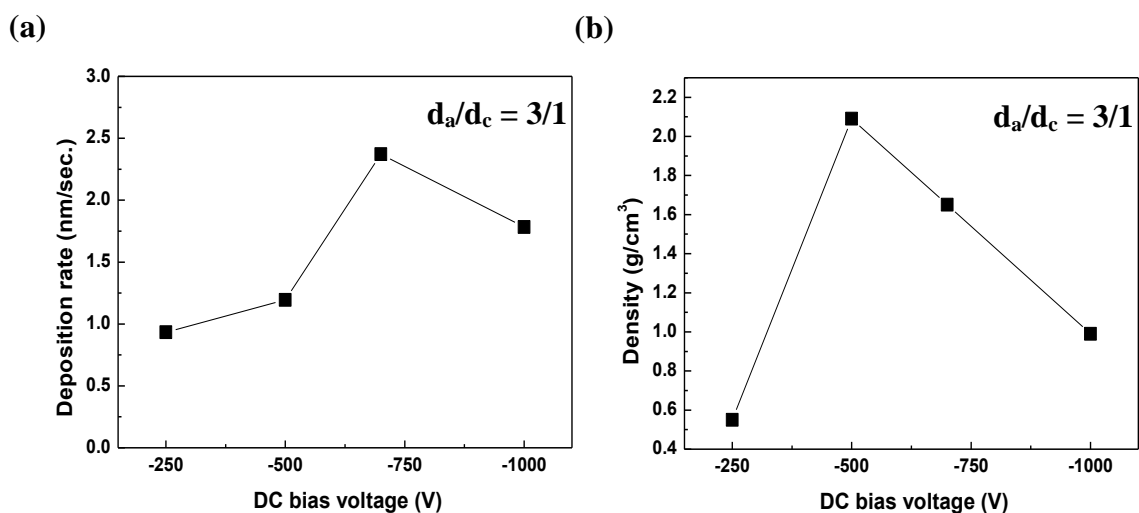


Figure 7.15 Deposition rate (a) and density (b) of DLC coatings deposited at various DC bias voltages

Fig. 7.15 shows different deposition rate and density of DLC coatings grown with  $d_a/d_c = 3/1$  at different DC bias voltage. It was found that with increasing bias from  $-250$  V to  $-1000$  V the deposition rate was increased to the maximum of  $2.4$  nm/sec at  $-700$  V, then decreased to  $1.8$  nm/sec at  $-1000$  V, which indicated that more carbon ions are accelerated to the substrate with the increase of the negative bias voltage. However, when the bias increased to the higher level ( $-1000$  V), accompanied by the higher energy, the energy of the bombarding ions on the substrate increased, which resulted in resputtering of the growing films and decrease of deposition rate.

In Fig. 7.15 (b), it was shown that at  $-500$  V the density of coating reached the maximum of  $2.09$  g/cm<sup>3</sup> with the deposition rate of  $1.2$  nm/sec, then began to reduce to  $1.0$  g/cm<sup>3</sup> with the bias increased to  $-1000$  V. This indicated that the certain bias supplied to the substrate provides mobility of the atoms / ions being deposited so that dense DLC coatings were deposited. At higher bias the density of film decreased. The results confirmed that the bias voltage could affect the number of carbon ions arriving on the surface and the properties of DLC coatings, which was in accordance with the report of Jin-Bao Wu [17].

### 7.3.2 Raman spectra of DLC coatings

Fig. 7.16 (a) shows the Raman spectra of the DLC coatings deposited at various DC bias voltage with an anode-cathode diameter ratio of  $d_a/d_c = 3/1$ . It was found that there were two main peaks: one broad peak at  $1580$  cm<sup>-1</sup> and another weak peak around  $1350$  cm<sup>-1</sup>, assigned to G band and D band, respectively. These two peaks are due to  $sp^2$  sites only. The visible Raman spectroscopy is more sensitive to the  $sp^2$  than to  $sp^3$  phase ( $50 \sim 250$  times for  $514.5$  nm) [8].

It was shown that the width of G band broadened with increasing the bias. That was accompanied by the decreasing of the peak height. Fig. 7.16 shows great differences in the Raman peak intensity with different DC bias. The peak intensity decreased with increasing bias from  $-250$  V to  $-700$  V, then increased when the bias voltage increased to  $-1000$  V, which had the contrary tendency with the deposition rate as a function of bias voltage (seen in Fig. 7.15 (a)). That was not accordant with the report of Varanasi et al. in the reference [18]. Varanasi proposed a method for measuring the thickness of carbon coatings on sliders using the Raman band intensity, because the

Raman peak intensity was proportional to the thickness of DLC coatings (seen in Fig. 7.16 (b)).

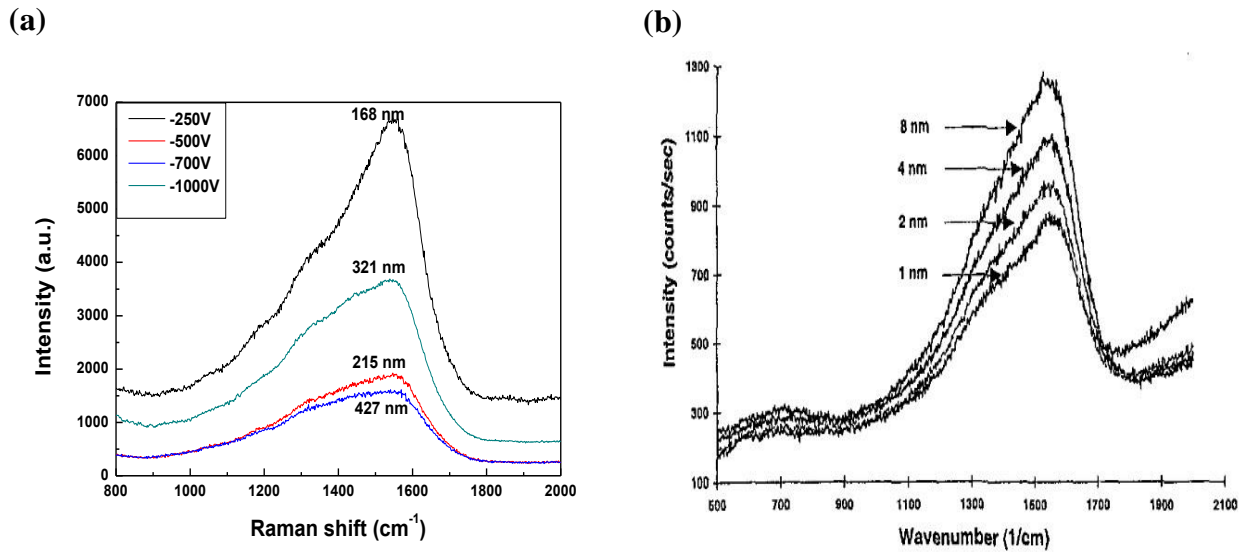


Figure 7.16 Raman spectrum of (a) the DLC coatings deposited at various DC bias voltage and (b) the sputtered DLC coatings deposited with different thicknesses (Varanasi et al. [18])

However, here the Raman intensity was different due to the bias voltage supplied to the substrate which influences the properties of DLC coatings as Fig. 7.15 and Fig. 7.16 (a) shown. By comparing with Raman spectrum in Fig. 7.16, it seemed that the Raman intensity was directly dependent to the DLC coating properties.

Other features, such as at  $\sim 1200 \text{ cm}^{-1}$  and  $\sim 1450 \text{ cm}^{-1}$ , although they are some minor modulations, are present and should be considered in order to fit the spectrum very well. In previous study [19], Raman spectrum that was reported could be fitted very well using four-Gaussians ( $\sim 1100 \text{ cm}^{-1}$ ,  $\sim 1350 \text{ cm}^{-1}$ ,  $\sim 1400 \text{ cm}^{-1}$  and  $\sim 1580 \text{ cm}^{-1}$ ). Here the same method of Raman spectrum fitting was used (see Fig. 7.17), and the corresponding information after a Gaussian fit, for example D and G positions and the ratio of  $I_D/I_G$ , was shown in Fig. 7.18.

In Fig. 7.17, a linear background was subtracted before fitting the spectra. These four peaks were assigned at  $1350 \text{ cm}^{-1} \sim 1370 \text{ cm}^{-1}$  for D peak,  $1545 \text{ cm}^{-1} \sim 1560 \text{ cm}^{-1}$  for G peak, which was obviously different from the true graphitic G peak at about  $1582 \text{ cm}^{-1}$ . However, according to the report of Tarrant et al. [20] a peak at  $1550 \text{ cm}^{-1}$  was referred to as the amorphous carbon “A peak”. The position and the width of the Gaussian A peak seems to be largely determined by the range and

## 7. Influence of substrate bias on the particle size distribution of DLC coatings

population of non-hexagonal  $sp^2$  bonded groupings. Another two peaks at  $\sim 1150\text{ cm}^{-1}$  and  $\sim 1450\text{ cm}^{-1}$  due to the origin of peaks in nano-crystalline diamond [21]. Until now the assignation of the observed peaks, especially for those weak peaks, is still not clear, so it is the subject of future studies.

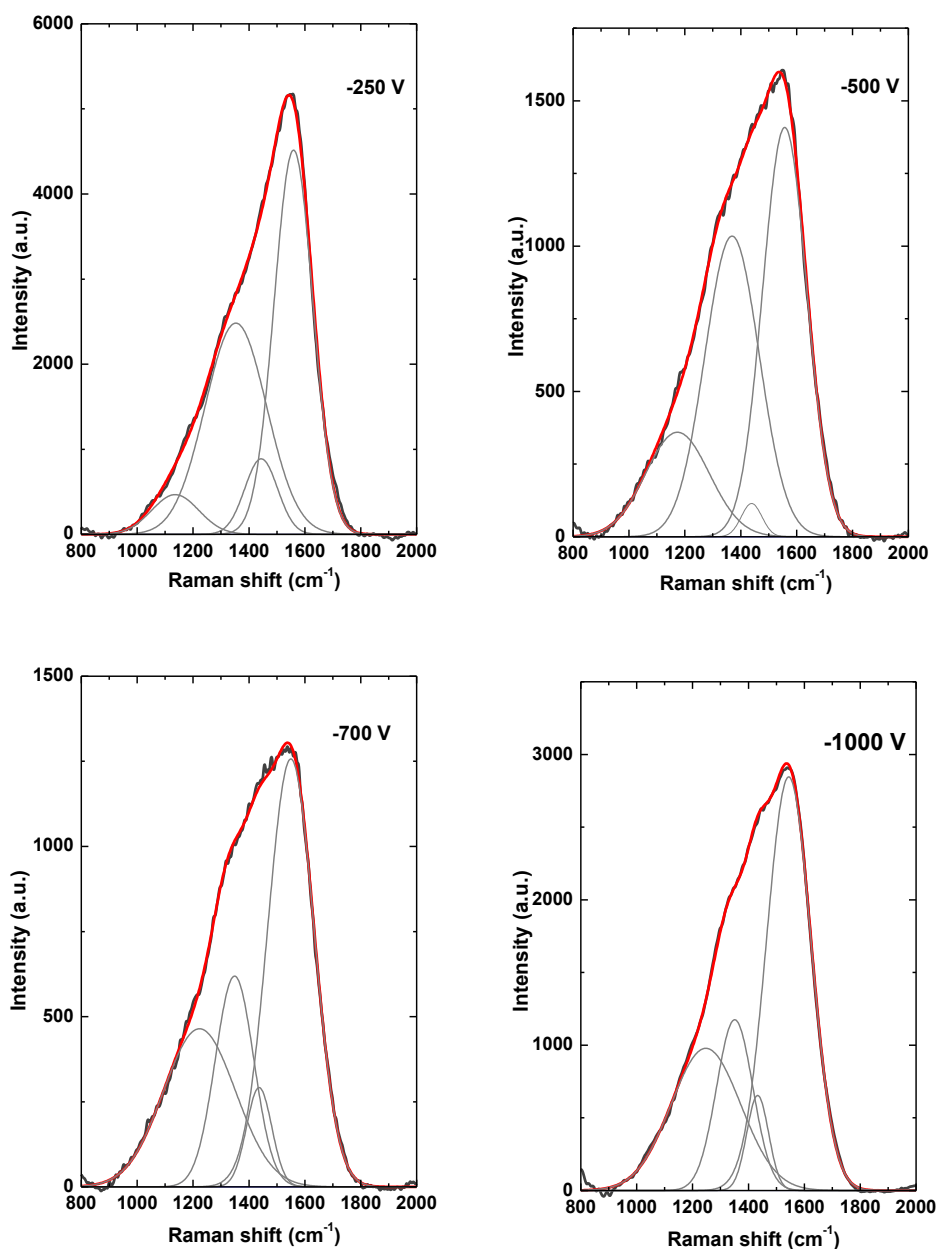


Figure 7.17 Fitted Raman spectrum of the DLC coatings deposited at various DC bias voltages

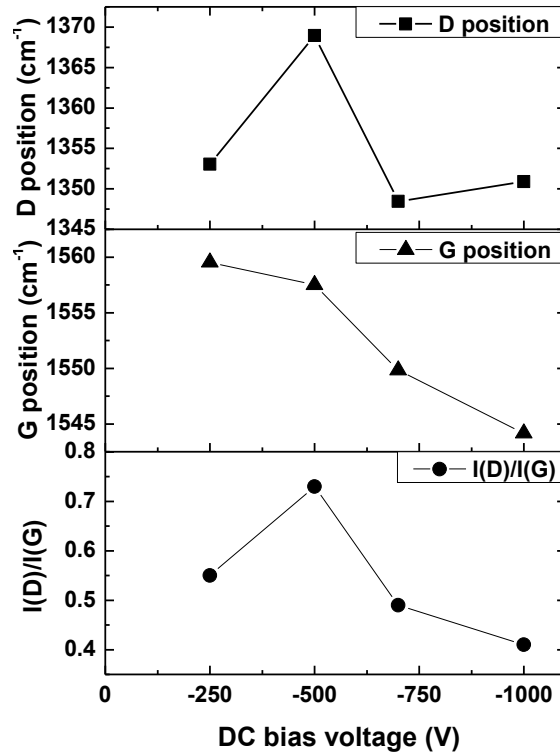


Figure 7.18 Variation of D position, G position and  $I_D/I_G$  ratio with DC bias voltage

The crucial property of interest in DLC is the  $sp^2/sp^3$  fraction which is related to the  $I_D/I_G$  ratio obtained after a Gaussian fit. Fig. 7.18 shows the D, G position and the relative intensity ratio of D and G peaks. Usually there are two ways to calculate the intensity ratio of D and G band: the ratio of the peak heights or peak areas. Here is referred to  $I_D/I_G$  as the ratio of peak heights. As Fig. 7.18 shows with increasing the bias, the ratio of  $I_D/I_G$  was increased first and reached to the maximum of 0.75 at  $-500$  V, then decreased to the minimum of 0.4 at  $-1000$  V. The ratio of  $sp^2/sp^3$  was increased with decreasing  $I_D/I_G$  ratio. That means the DLC coating deposited with  $d_a/d_c = 3/1$  at  $-1000$  V had the highest  $sp^3$  content because of the minimum ratio of  $I_D/I_G$ .

The G peaks at the higher bias ( $> 500$  V) were much broader (seen in Fig. 7.16), but shifted to lower frequencies from  $1560$   $cm^{-1}$  to  $1545$   $cm^{-1}$  with increasing the bias voltage (seen in Fig. 7.18) due to a series of defects (bond disorder) and the presence of  $sp^3$  sites into structures which softens the vibrational density of states (VDOS) resulting from finite-crystal-size effects. The broadening of peaks was also correlated to a distribution of clusters with different orders and dimensions [9].

### 7.3.3 Tribological properties of DLC coatings

Fig. 7.19 shows the roughness  $R_a$  and friction coefficient of DLC coatings deposited with  $d_a/d_c = 3/1$  as a function of DC bias voltage. The value of  $R_a$  was the average roughness after testing at three different positions of each sample. The lowest surface roughness of 30 nm was obtained at  $-250$  V. When the bias increased to  $-500$  V,  $R_a$  reached the maximum which indicated the surface was the roughest. It was found that with increasing the bias from  $-500$  V to  $-1000$  V the roughness decreased linearly to 70 nm (see Fig. 7.19 (a)).

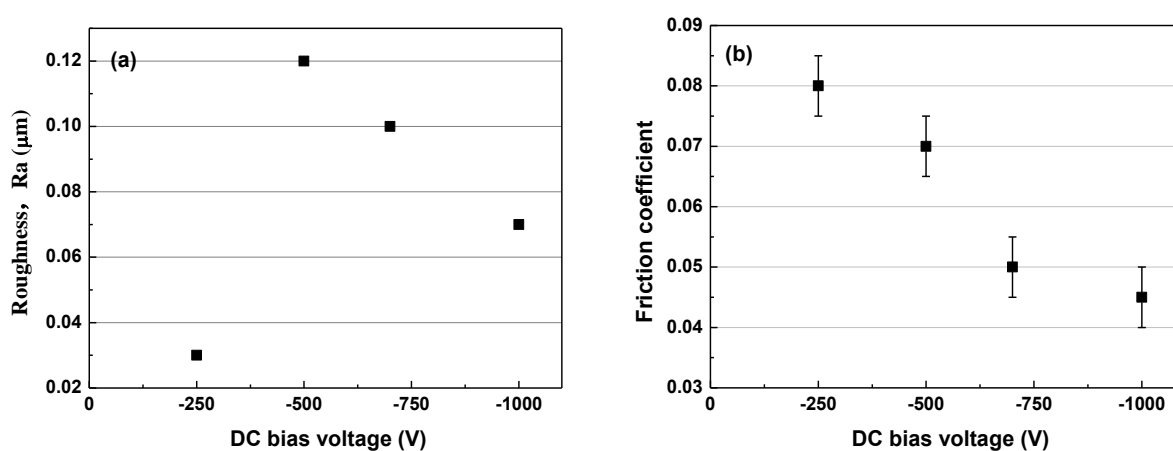


Figure 7.19 Roughness ( $R_a$ ) (a) and wear rate (b) of DLC coatings deposited at various DC bias voltages

Fig. 7.19 (b) shows that the friction coefficient decreased gradually from 0.08 to 0.045 with increasing the bias. Although the DLC coating deposited at the bias of  $-250$  V had the lowest  $R_a$  of 30 nm, it had the largest coefficient of friction comparing it with other bias. During the tribological testing, for the coating deposited at the bias of  $-250$  V, the wear track can be seen easily with the load of 50 N and the velocity of 0.01 m/s after one hour-testing. However, when the bias was increased to  $-500$  V,  $-700$  V and  $-1000$  V, the load of 50 N was so low that no wear track was observed few hours later. Then the load and the time of testing must be increased to 120 N and 20 h, respectively. The surface of coating was destroyed just for DLC coatings deposited at  $-500$  and  $-1000$  V. Even using the same tribological parameters of 120 N, 0.01 m/s and 20 h, there was no sign of wear for the coating deposited at  $-700$  V. The velocity was up to 10 cm/s, the particles were obtained after 5 h. It was confirmed that with increasing the bias the hardness of coating was

---

improved which resulted from lower ratio of  $I_D/I_G$  (the higher  $sp^3$  content) at higher bias as shown in Fig. 7.18.

### 7.3.4 Particle size distribution of DLC coatings

The wear particles were generated by a disc-on-disc test and collected in suspension in deionized water. The properties of particles depend strongly on their size and shape which can be observed by SEM after filtering with a membrane of  $0.2\ \mu\text{m}$  pore size, drying and sputtering (seen in Fig. 7.20). The morphology of the original membrane without particles is shown in Fig. 7.20 (a). Compared with Fig. 7.20 (a), it is shown in Fig. 7.20 (b) that particles with different size and irregular shape are distributed on the filter membrane, consisting of smaller particles ( $< 1\ \mu\text{m}$ ) and the wear debris of about  $75\ \mu\text{m}$ . It was difficult to evaluate the particle size distribution by SEM because of mainly irregularly shaped particles. The characterization of the particle size distribution varies depending on the measurement method used.

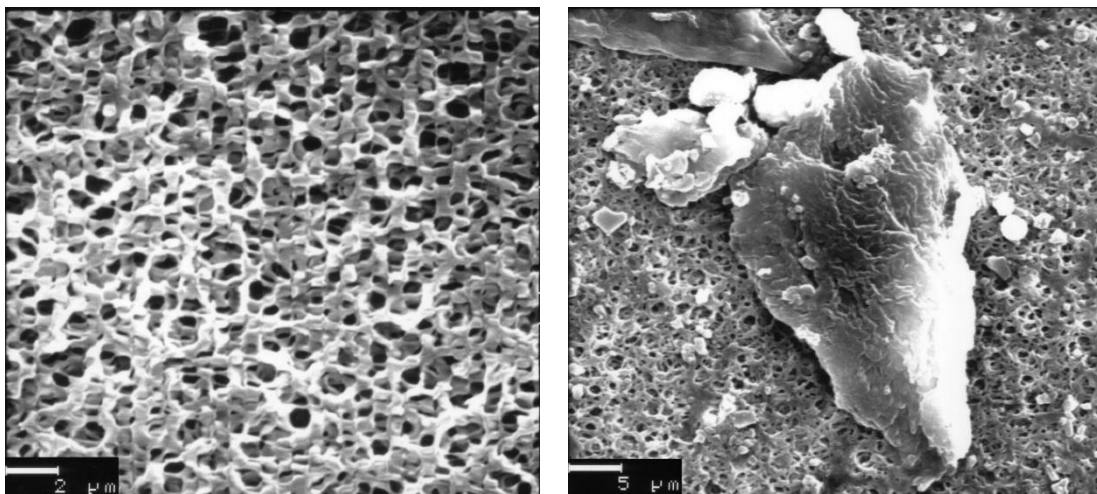


Figure 7.20 SEM images of (a) original filter membrane and (b) typical particles on filter membrane

Here the volume density distribution  $q_3(x)$  was chosen to characterize the size of particles, which represents the amount of particles of a given particle size  $x$  relative to the entire particles size distribution, as shown in Fig. 7.21.

The modal value  $x_{\text{mod}}$ , the particle size at which the density distribution  $q_3(x)$  exhibits a maximum, can be obtained by the particle collective from the measured size distribution  $q_3(x)$ . Fig. 7.21 shows that when the DLC coatings were deposited with  $d_a/d_c = 3/1$ , the wear particles

## 7. Influence of substrate bias on the particle size distribution of DLC coatings

collected were in the range of 0.3  $\mu\text{m}$  to 200  $\mu\text{m}$ . It was found that there were two peaks in volume density distribution no matter which bias was applied. One peak was distributed at  $\sim 1 \mu\text{m}$  ( $x_{1_{\text{mod}}}$ ), another was at  $\sim 50 \mu\text{m}$  ( $x_{2_{\text{mod}}}$ ). That means the most particles were distributed in the range of smaller particles and larger particles.

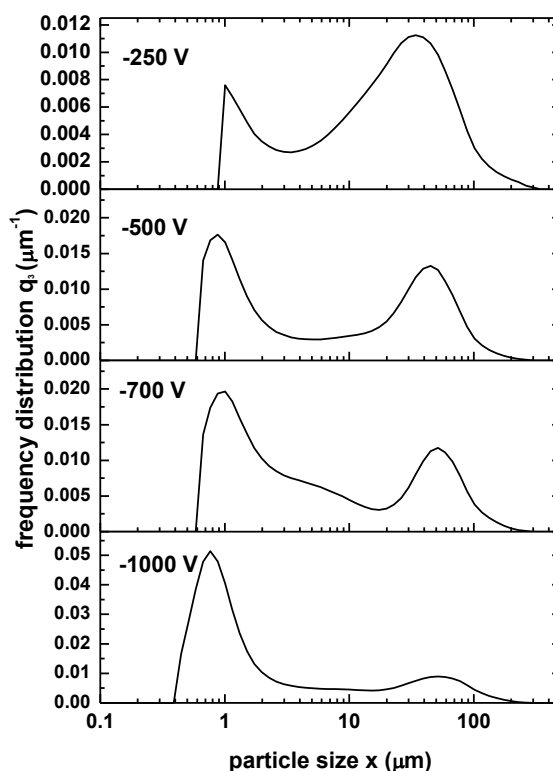


Figure 7.21 Volume density distribution  $q_3(x)$  at the DC bias from  $-250 \text{ V}$  to  $-1000 \text{ V}$  with the anode-cathode diameter ratio of  $d_a/d_c = 3/1$

In Fig. 7.21, it was observed that two peak heights, representing the density distribution of  $x_{1_{\text{mod}}}$  and  $x_{2_{\text{mod}}}$ ,  $q_3(x_{1_{\text{mod}}})$  and  $q_3(x_{2_{\text{mod}}})$ , respectively changed with the bias. Fig. 7.21 showed that the curve had the same tendency with the bias. The maximum of the curve was shifted from  $\sim 50 \mu\text{m}$  to  $\sim 1 \mu\text{m}$  when the bias was increased from  $-250 \text{ V}$  to  $-1000 \text{ V}$ .

The relative density distribution ratio of  $x_{2_{\text{mod}}}$  and  $x_{1_{\text{mod}}}$  is shown in Fig. 7.22. In there, it was obviously observed that the ratio of  $q_3(x_{2_{\text{mod}}})$  and  $q_3(x_{1_{\text{mod}}})$  decreased from 1.5 to 0.1 regularly with increasing bias from  $-250 \text{ V}$  to  $-1000 \text{ V}$  as a curve of Bezier, which indicated that the maximum of the frequency distribution can be shifted to below  $1 \mu\text{m}$  at higher bias. According to

Bezier curve equation, I tried to get the approximation of bias at which the  $q_3(x_{2_{mod}})/q_3(x_{1_{mod}})$  ratio eventually nears zero. It was found that the wear particle size could be reduced and the frequency distribution would be downshifted to below 1  $\mu\text{m}$  when the bias is about  $-1100\text{ V}$  (see red plotted line in Fig. 7.22).

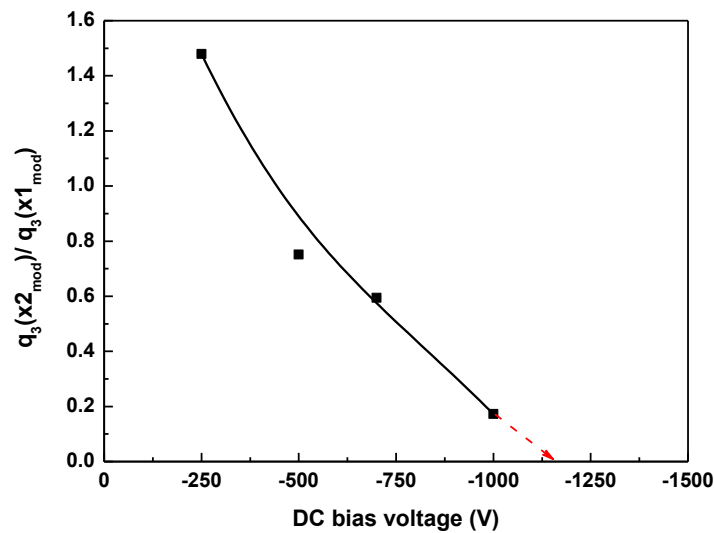


Figure 7.22 Variation of  $q_3(x_{2_{mod}})/q_3(x_{1_{mod}})$  ratio with DC bias voltage

### 7.3.5 Conclusion

Amorphous carbon (a-C) films were synthesized on P2000 substrates by vacuum arc technique using an anode-cathode diameter ration of  $d_a/d_c = 3/1$  with the application of a DC bias to the substrate from  $-250\text{ V}$  to  $-1000\text{ V}$ . The most typical wear particles were irregular and composed of smaller particles (even  $< 1\ \mu\text{m}$ ) and a few debris about  $\sim 75\ \mu\text{m}$ . The influence of  $d_a/d_c$  and the substrate bias on the wear particle size distribution were investigated. The roughness and density of a-C films increase first then decrease with DC bias voltage. A lowest surface roughness of  $30\text{ nm}$  at  $-250\text{ V}$  and the high value of density ( $2.09\text{ g/cm}^3$ ) at  $-500\text{ V}$  are obtained. The lowest friction coefficient of  $0.045$  can be obtained with increasing the bias to  $-1000\text{ V}$ . The wear particle size of a-C coatings deposited with  $d_a/d_c = 3/1$  is distributed in the range of  $0.3\ \mu\text{m}$  to  $200\ \mu\text{m}$ . There are two peaks in the curve of the frequency distribution. The maximum of the frequency distribution can be downshifted gradually with increasing bias, below  $1\ \mu\text{m}$  at  $-1000\text{ V}$ . It is estimated that all wear particles can be distributed in the range of  $\sim 1\ \mu\text{m}$  when the bias was

increased approximately to  $-1100$  V.

## References

- [1] Y.S. Park, B. Hong, Tribological properties of hydrogenated amorphous carbon thin films by close field unbalanced magnetron sputtering method, *Journal of the Korean Physical Society* 45 (2004) S824-S28.
- [2] Y.S. Park, H.S. Myung, J.G. Han, B. Hong, Tribological properties of amorphous carbon thin films grown by magnetron sputtering method, *Surface and Coatings Technology* 180-181 (2004) 218-221.
- [3] Th. Köhler, Th. Frauenheim, G. Jungnickel, Stability, chemical bonding, and vibrational properties of amorphous carbon at different mass densities, *Physical Review B* 52 (16) (1995) 11837-11844.
- [4] D. Beeman, J. Silverman, R. Lynds, M.R. Anderson, Modeling studies of amorphous carbon, *Physical Review B* 30 (2) (1984) 870-875.
- [5] D. Sheeja, B.K. Tay, K.W. Leong, C.H. Lee, Effect of film thickness on the stress and adhesion of diamond-like carbon coatings, *Diamond and Related Materials* 11 (2002) 1643-1647.
- [6] X.L. Peng, Z.H. Baber, T.W. Clyne, Surface roughness of diamond-like carbon films prepared using various techniques, *Surface and Coatings Technology* 138 (1) (2001) 23-32.
- [7] G. Irmer, A. Dorner-Reisel, Micro-Raman studies on DLC coatings, *Advanced Engineering Materials* 7 (8) (2005) 694-705.
- [8] A.C. Ferrari, Determination of bonding in diamond-like carbon by Raman spectroscopy, *Diamond and Related Materials* 11 (2002) 1053-1061.
- [9] A.C. Ferrari, J. Robertson, Interpretation of Raman spectra of disordered and amorphous carbon, *Physical Review B* 61 (2000) 14095-14107.
- [10] H.S. Zhang, K. Komvopoulos, Direct-current cathodic vacuum arc system with magnetic-field mechanism for plasma stabilization, *Review of Scientific Instruments* 79 (2008) 073905 1-7.
- [11] H.S. Zhang, J.I. Endrino, A. Aders, Comparative surface and nano-tribological characteristics of nanocomposite diamond-like carbon thin films doped by silver, *Applied Surface Science* 255 (5) (2008) 2551-2556.
- [12] F.W. Delrio, M.P. De Boer, J.A. Knapp, E.D. Reedy Jr, P.J. Clews, M.L. Dunn, The role of van der Waals forces in adhesion of micromachined surfaces, *Nature Materials* 4 (2005) 629-634.
- [13] S.J. Timpe, K. Komvopoulos, An Experimental Study of Sidewall Adhesion in Microelectromechanical Systems, *Journal of Microelectromechanical Systems* 14 (6) (2005) 1356-1363.
- [14] D.R. McKenzie, Tetrahedral bonding in amorphous carbon, *Reports on Progress in Physics* 59 (1996) 1611-1664.
- [15] P.J. Fallon, V.S. Veerasamy, C.A. Davis, J. Robertson, G.A.J. Amaratunga, W.I. Milne, J. Koskinen, Properties of filtered-ion-beam-deposited diamondlike carbon as a function of ion energy, *Physical Review B* 48 (1993) 4777-4782.

- 
- [16] G.M. Pharr, D.L. Callahan, S.D. McAdams, T.Y. Tsui, S. Anders, A. Anders, J.W. Ager, I.G. Brown, C.S. Bhatia, S.R.P. Silva, J. Robertson, Hardness, elastic modulus, and structure of very hard carbon films produced by cathodic-arc deposition, *Applied Physics Letters* 68 (1996) 779-781.
- [17] J.B. Wu, J.J. Chang, M.Y. Li, M.S. Leu, A.K. Li, Characterization of diamond-like carbon coatings prepared by pulsed bias cathodic vacuum arc deposition, *Thin Solid Films* 516 (2007) 243-247.
- [18] S.S. Varanasi, J.L. Lauer, F.E. Talke, G. Wang, J.H. Judy, Friction and wear studies of carbon overcoated thin film magnetic sliders: application of Raman microspectroscopy, *Journal of Tribology* 119 (3) (1997) 471-475.
- [19] Y. Ren, I. Erdmann, B. Kützler, F. Deuerler, V. Buck, Effect of deposition parameters on wear particle size distribution of DLC coatings, *Diamond and Related Materials* 23 (2012) 184-188.
- [20] R.N. Tarrant, D.R. McKenzie, M.M.M. Bilek, Raman characterisation of PIII multilayer carbon films, *Diamond and Related Materials* 13 (2004) 1422-1426.
- [21] A.C. Ferrari, J. Robertson, Origin of the 1150 cm<sup>-1</sup> Raman mode in nanocrystalline diamond, *Physical Review B* 63 (2001) R121405-R121408.

## 8. Influence of $d_a/d_c$ on the particle size distribution of DLC coatings

As discussed in chapter 2.3.1, there are mainly two types of the arc discharge: cathodic arc and anodic arc. Additionally, these two kinds of arc will transfer each other from the cathode to the anode or from the anode to the cathode. In ref. [1] this transfer mode was discussed and the mass difference of each electrode before and after deposition was plotted in Fig.8.1.

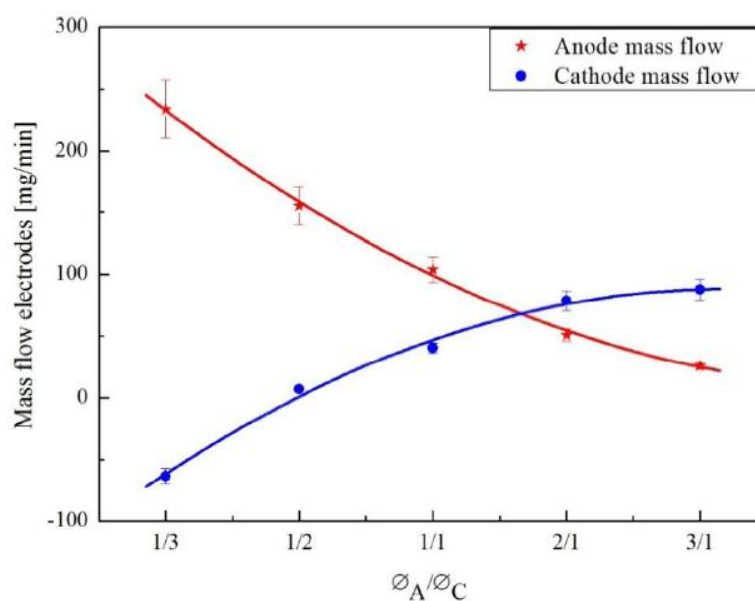


Figure 8.1 Electrodes mass flow as a function of the vacuum arc mode [1]

It was found that the transfer mode of  $d_a/d_c = 1/3$  was called anodic because the weight of the cathode before deposition was much more than after deposition which indicated much anode material was evaporated and the cathode electrode was covered by the anode material after deposition at this mode. With increasing the diameter ratio of  $d_a/d_c$  more cathode electrode was evaporated. However, the anode material was reduced more or less no matter which mode was used even  $d_a/d_c = 3/1$ .

In O. Filipov's doctoral thesis [1], the influence of transition between the cathodic and anodic arc in the deposition of DLC coatings on the ion energy and ionization was investigated in detail. In this work, all DLC coatings were deposited by vacuum arc adjustable from anodic to cathodic operation mode by varying the anode-cathode diameter ratio of  $d_a/d_c$  with 1/3, 1/1 and 3/1. The ion

density varied with the ratio of  $d_a/d_c$ , was  $7.163 \times 10^{11}$ ,  $1.47 \times 10^{12}$  and  $2.59 \times 10^{12}$ , corresponding to 1/3, 1/1 and 3/1, respectively. In this section, the influence of  $d_a/d_c$  on the properties and particle size distribution of DLC coatings were studied when the substrate bias was constant.

## 8.1 Substrate bias at $-250$ V

### 8.1.1 Density and deposition rate of DLC coatings

The DLC coatings were deposited at  $-250$  V for 3 min with the anode-cathode diameter ratio of 1/3, 1/1 and 3/1. After deposition, the density and deposition rate were calculated by the weight and the film thickness as shown in Fig.8.2. It was found that the density of the DLC coating reached to the maximum of about  $2.2 \text{ g/cm}^3$  at  $d_a/d_c = 1/1$ , and the value of density was reduced with increasing anode-cathode diameter ratio to 3/1. The deposition rate as a function of  $d_a/d_c$  showed the decreasing trend with increasing the diameter of anode electrode. At the diameter ratio of 1/3, more DLC coatings with the density of about  $1.8 \text{ g/cm}^3$  were deposited on the substrate.

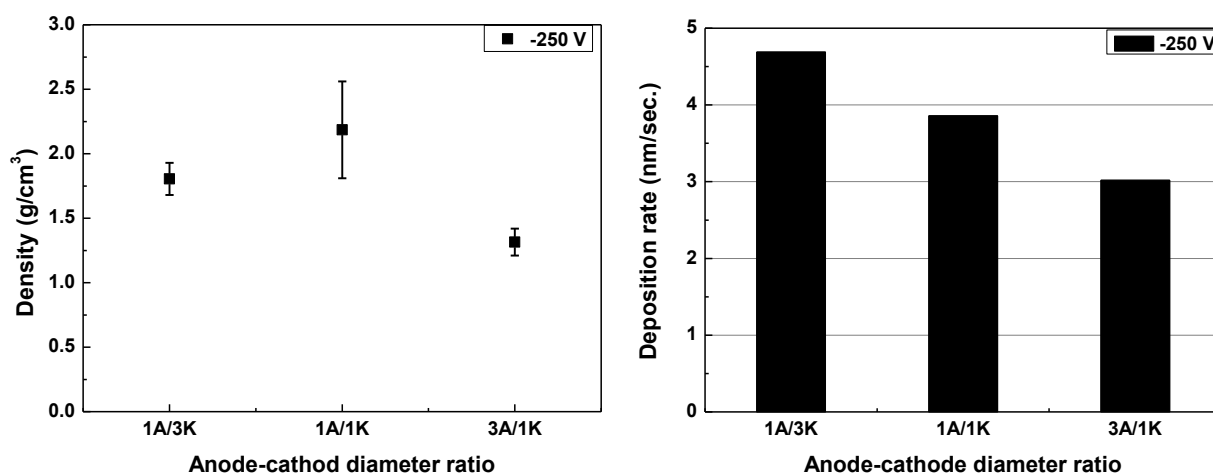


Figure 8.2 Density and deposition rate of DLC coatings deposited at  $-250$  V with different  $d_a/d_c$

### 8.1.2 Raman spectra of DLC coatings

Raman spectra of DLC coating deposited at  $-250$  V with different  $d_a/d_c$  were shown in Fig.8.3. It was found there were two broad peaks at about  $1575 \text{ cm}^{-1}$  and  $1355 \text{ cm}^{-1}$ , assigned to G and D band. According to four-peak fitting with full Gaussian function discussed in chapter 6.1, after fitting the values of G peak position,  $I_D/I_G$ , as well as FWHM (G) were obtained (see Table

8.1). Besides D and G peaks, there were another two weak peaks:  $\sim 1150 \text{ cm}^{-1}$  and  $\sim 1450 \text{ cm}^{-1}$  which were attributed to the grain boundaries of nano-crystalline samples and not related to  $\text{sp}^3$ -bond carbon [2-4]. It was shown in Fig.8.3 the G peak intensity increased with increasing  $d_a/d_c$ . As Table 8.1 shows, G peak shifted down lower than  $1575 \text{ cm}^{-1}$  resulting from introduction of the bond disorder.

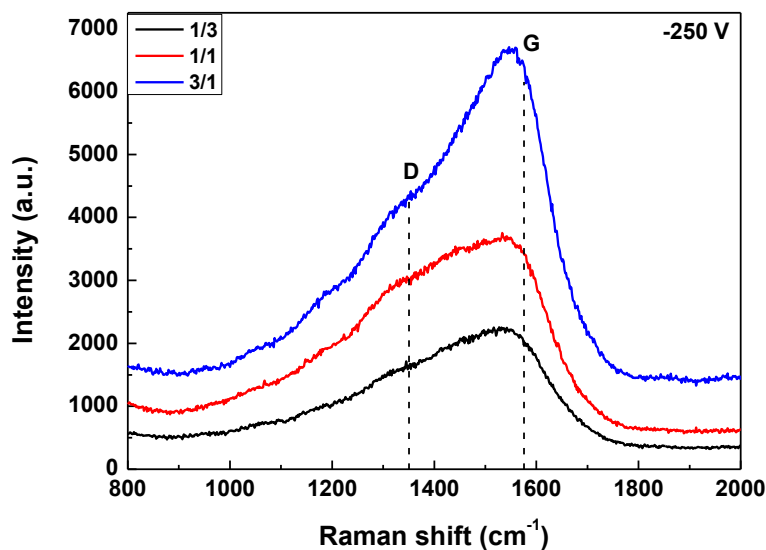


Figure 8.3 Raman spectrum of DLC coatings deposited at  $-250 \text{ V}$  with different  $d_a/d_c$

Table 8.1 Variation of G position, FWHM and the  $I_D/I_G$  ratio of DLC coatings deposited at  $-250 \text{ V}$  with different  $d_a/d_c$

$d_a/d_c$	G position / $\text{cm}^{-1}$	$I_D/I_G$	FWHM (G)
1A/3K	1546	0.64	188
1A/1K	1567	1.2	162
3A/1K	1559	0.55	163

Combined with the value of FWHM (G) caused by bond angle and bond length distortions, it was found that with increasing the diameter ratio from 1/3 to 1/1 the FWHM decreased. When the diameter ration was raised to 3/1, the value was nearly constant comparing with 1/1. It was indicated DLC coating deposited with  $d_a/d_c = 1/3$  at  $-250 \text{ V}$  had most of bond length and bond angle disorder. Although the value of FWHM was the same at 1/1 and 3/1, the intensity ratio of D

and G peaks was totally different. When DLC coating was deposited with 3/1, the Raman spectrum had the higher and sharper G peak as shown in Fig.8.3 (blue curve) by comparing with other Raman spectra in Fig. 8.3. That's because the defect of not only bond disorder was introduced, but also clustering of the  $sp^2$  phase which resulted in decreasing the D peak height and increasing its width.

### 8.1.3 Particle size distribution of DLC coatings

The anode-cathode diameter ratio of  $d_a/d_c$  also influenced the wear particle size distribution of DLC coatings. The frequency distribution of wear particle size generated by tribological test using a disc-disc setup is shown in Fig. 8.4.

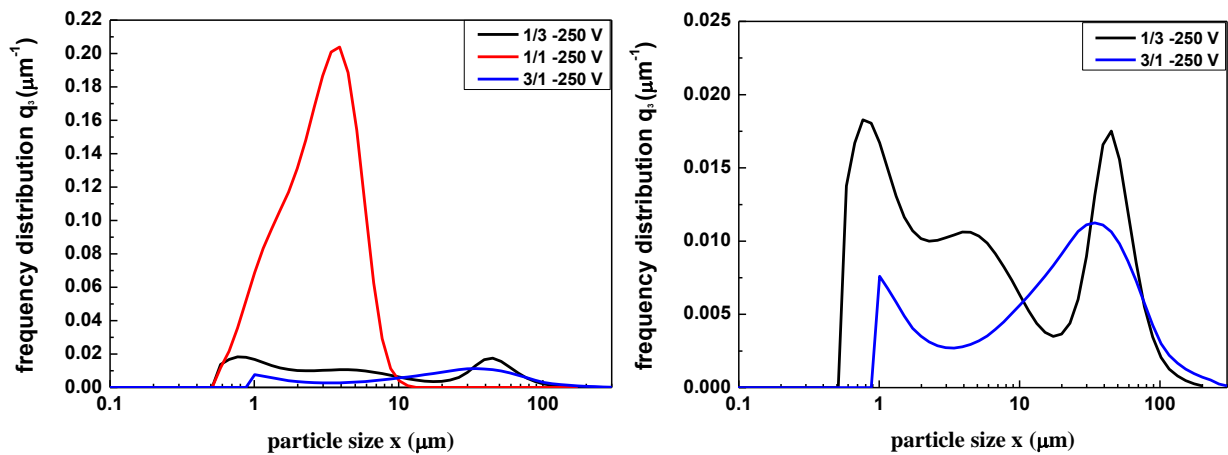


Figure 8.4 Volume density distribution  $q_3(x)$  at  $-250$  V with different  $d_a/d_c$

Fig. 8.4 (left) shows great differences in particle size distribution resulting from the varied anode-cathode diameter ratio. When DLC coatings were deposited with  $d_a/d_c = 1/1$ , all particles generated are in the range of  $0.3 \mu\text{m} \sim 10 \mu\text{m}$ , smaller than the range of  $0.45 \mu\text{m} \sim 300 \mu\text{m}$  obtained with  $d_a/d_c = 1/3$  and  $3/1$ . Additionally, it was observed obviously that the value of ordinate (frequency distribution  $q_3(x)$ ) with  $1/1$  was larger than that with  $1/3$  or  $3/1$ . That means, when DLC coatings were deposited at  $-250$  V with  $d_a/d_c = 1/1$  the amount of generated particles of a given particle size were more than that of particles using  $1/3$  or  $3/1$ . Actually, these results were not just for the coatings deposited at  $-250$  V, but also suitable for coatings deposited at other substrate biases, e.g.  $-500$  V,  $-750$  V and  $-1000$  V shown in the following sections.

In order to disguise the volume density distribution of coatings deposited with 1/3 and 3/1, another figure was drawn in Fig. 8.4 (right). It was observed that with the smaller  $d_a/d_c$  (1/3) the whole frequency distribution downshifted and it had larger amount of particles, comparing with the larger  $d_a/d_c$  (3/1), furthermore, there were three peaks in the whole range. However for the coatings with the larger anode-cathode diameter ratio of 3/1, the curve plotted in Fig. 8.4 (right) show the bimodal distribution, and the particles produced were not too much.

### 8.1.4 Conclusion

The DLC coatings were deposited at  $-250$  V with the anode-cathode diameter ratio of  $d_a/d_c = 1/3, 1/1$  and  $3/1$ . When the diameter ratio of  $1/1$  was used, the particle size distribution was in the range of  $0.3 \mu\text{m} \sim 10 \mu\text{m}$ , moreover, the deposited DLC coating had the highest  $I_D/I_G$  of  $1.2$  although it had the maximum density of  $2.2 \text{ g/cm}^3$ . For the DLC coating deposited with  $d_a/d_c = 1/3$  or  $3/1$ , the wear particles generated were distributed in the broad range of  $0.45 \mu\text{m} \sim 300 \mu\text{m}$ , and two peaks appeared at smaller size of  $\sim 1 \mu\text{m}$  and the larger size of  $\sim 50 \mu\text{m}$ . For  $d_a/d_c = 1/3$ , two peak heights were nearly the same and the DLC coating with the density of  $\sim 1.8 \text{ g/cm}^3$  had the smaller  $I_D/I_G$  of  $0.64$  compared with  $1.2$  of  $d_a/d_c = 1/1$ . However, the deposition rate for  $d_a/d_c = 1/3$  reached to the maximum of about  $5 \text{ nm/sec}$ . With increasing the anode-cathode ratio to  $3/1$ , the amount of wear particles generated was decreased and the peak height at larger size was higher than that at smaller size. In addition, the DLC coating deposited with  $d_a/d_c = 3/1$  had the minimum of  $1.3 \text{ g/cm}^3$ , but the ratio of  $I_D/I_G$  was smallest value of  $0.55$ .

## 8.2 Substrate bias at $-500$ V

### 8.2.1 Density and deposition rate of DLC coatings

The DLC coatings were deposited at  $-500$  V with the anode-cathode diameter ratio of  $1/3, 1/1$  and  $3/1$  for  $3 \text{ min}$ , respectively. After deposition, the density and deposition rate obtained by means of thickness and weight of DLC coatings were shown in Fig. 8.5.

At  $-500$  V, all densities of coatings synthesized were about  $2.0 \text{ g/cm}^3$ , when the diameter ratio of  $1/1$  was used, the density could reach to the highest value of  $3.0 \text{ g/cm}^3$ . With increasing the ratio

to 3/1, the coating had the density of 2.3 g/cm<sup>3</sup>. Although when using the smallest diameter ratio of 1/3 the density measured was the minimum of 2.0 g/cm<sup>3</sup>, the deposition rate was so fast that about 1 μm thick DLC coating could be deposited after 3 min. For other diameter ratios, by contrast, the deposition rate of 2 nm/sec was much smaller than that of about 6 nm/sec.

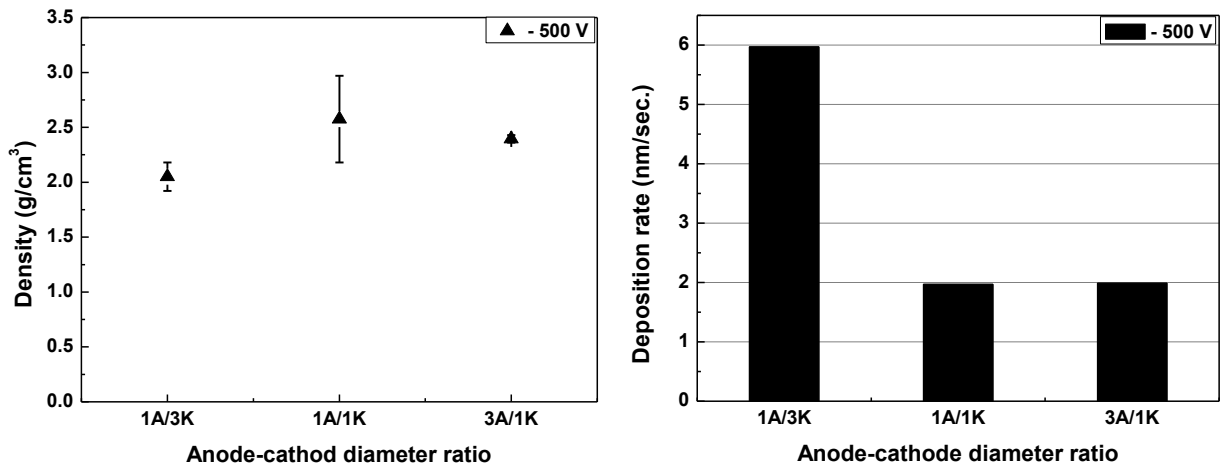


Figure 8.5 Density and deposition rate of DLC coatings deposited at -500 V with  $d_a/d_c = 1/3, 1/1$  and  $3/1$

## 8.2.2 Raman spectra of DLC coatings

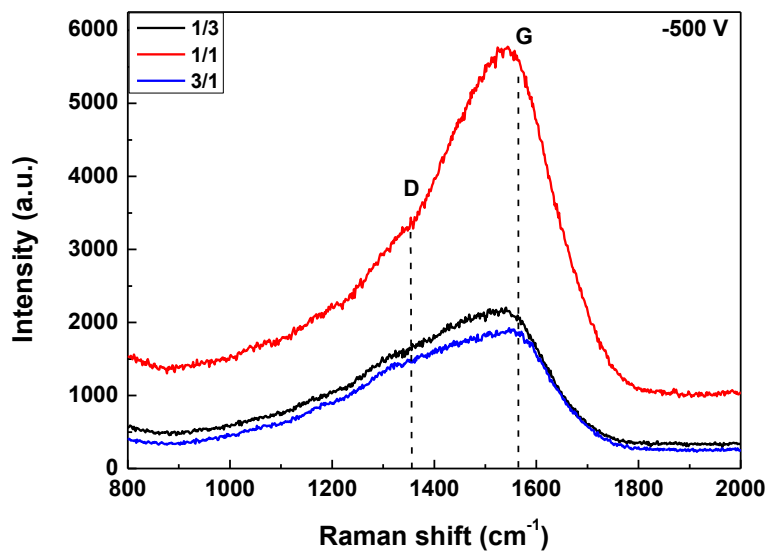


Figure 8.6 Raman spectrum of DLC coatings deposited at -500 V with different  $d_a/d_c$

Raman spectroscopy was widely used to analyze the molecular structure of DLC coatings.

Fig. 8.6 shows the Raman spectra of DLC coatings deposited at  $-500$  V by vacuum arc with different anode-cathode diameter ratio of 1/3, 1/1 and 3/1. One broad G peak at  $\sim 1575$   $\text{cm}^{-1}$  and another weak D peak around  $\sim 1350$   $\text{cm}^{-1}$  were seen in Fig. 8.6, as discussed above for  $-250$  V. The G peak position, the intensity ratio of the D and G bands and FWHM after Raman spectrum fitting with Gaussian curves were obtained in Table 8.2.

Table 8.2 Variation of G position, FWHM and the  $I_D/I_G$  ratio of DLC coatings deposited at  $-500$  V with different  $d_a/d_c$

$d_a/d_c$	G position / $\text{cm}^{-1}$	$I_D/I_G$	FWHM (G)
1A/3K	1554	0.87	177
1A/1K	1554	0.34	205
3A/1K	1557	0.73	186

For DLC coating deposited with  $d_a/d_c = 1/1$ , the G peak intensity in Raman spectra (red curve) was highest and it had the lowest  $I_D/I_G$  of 0.34, as well as the largest value of FWHM seen in Table 8.2. However, the positions of G peaks of coatings with different  $d_a/d_c$  were at  $\sim 1554$   $\text{cm}^{-1}$ . As is well known, although the visible Raman spectra of DLC coatings mainly came from the order of  $\text{sp}^2$  bond carbon, the  $\text{sp}^2/\text{sp}^3$  fraction could be probed by Raman scattering [5].

In addition, according the amorphization trajectory described by Ferrari and Robertson [5], the  $\text{sp}^3$  content of DLC coatings can be estimated from G position and  $I_D/I_G$ . Thus, it was indicated that it belonged to the stage 2: from graphite to nano-crystalline graphite when the DLC coatings were deposited at  $-500$  V. Moreover, with increasing  $d_a/d_c$  the  $\text{sp}^3$  content was increased first then reduced. When using  $d_a/d_c = 1/1$ , the higher content of  $\text{sp}^3$ -bonded carbon could be obtained, and the DLC coating had the highest density as shown in Fig. 8.5.

### 8.2.3 Particle size distribution of DLC coatings

After tribological test, the collected wear particles were measured using the particle size analyzer. Here the volume density distribution was used to characterize the size of particles. When DLC coatings were deposited at  $-500$  V with different  $d_a/d_c$ , the results of wear particle size

distribution were shown in Fig. 8.7. With the diameter ratio of 1/1, although the smaller particles ( $< 10 \mu\text{m}$ ) could be obtained, a larger number of wear particles were generated compared with the amount of wear particles with  $d_a/d_c = 1/3$  or  $3/1$  (Fig. 8.7 left).

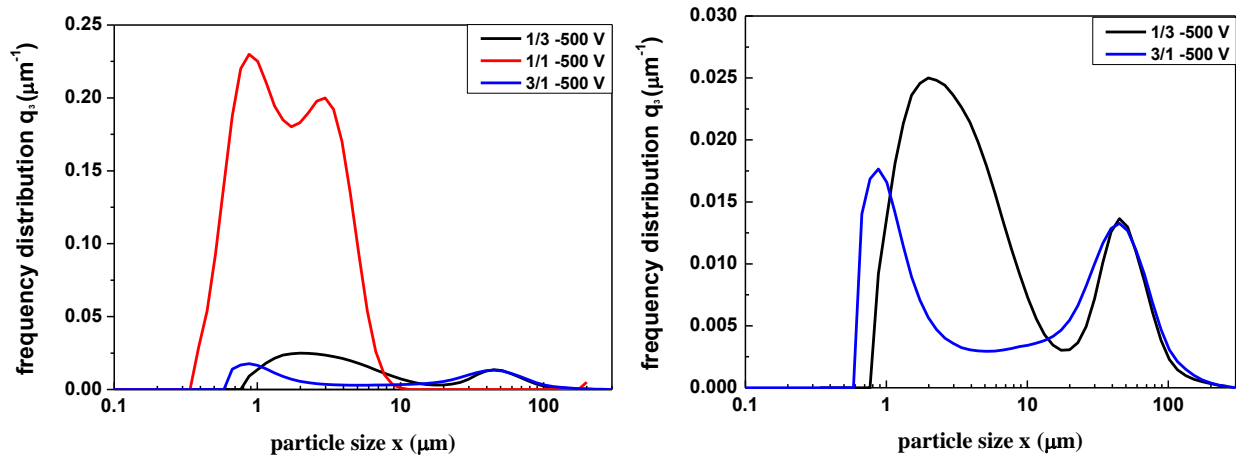


Figure 8.7 Volume density distribution  $q_3(x)$  at  $-500 \text{ V}$  with different  $d_a/d_c$

In Fig. 8.7 (right), it was found that the wear particle size distribution was bimodal no matter which anode-cathode diameter ratio was chosen. At one peak of  $\sim 50 \mu\text{m}$ , for  $d_a/d_c = 1/3$  and  $3/1$ , they had almost the same amount of particles due to the same peak height. Another peak was distributed  $\sim 3 \mu\text{m}$  for  $d_a/d_c = 1/3$ . However with increasing the ratio to  $3/1$ , another peak position was shifted from  $\sim 3 \mu\text{m}$  to  $\sim 1 \mu\text{m}$  and the amount of particles was reduced. Therefore, when the substrate bias was at  $-500 \text{ V}$ , using the ratio of  $3/1$  will be propitious to get the smaller size and quantity of wear particles.

## 8.2.4 Conclusion

The DLC coatings were deposited at  $-500 \text{ V}$  with the anode-cathode diameter ratio of  $d_a/d_c = 1/3$ ,  $1/1$  and  $3/1$ . All density values of coatings were larger than  $2.0 \text{ g/cm}^3$ . The DLC coating with the higher density of about  $2.5 \text{ g/cm}^3$ , deposited with  $d_a/d_c = 1/1$ , was obtained. In addition, the deposited coating had the smallest ratio of  $I_D/I_G$  of  $0.34$ , which indicated that the coating also had higher  $\text{sp}^3$  content. Furthermore, the wear particles of coatings deposited with  $d_a/d_c = 1/1$  were smaller than  $10 \mu\text{m}$  and there was the presence of bimodal peak at  $\sim 1 \mu\text{m}$  and  $5 \mu\text{m}$ . When  $d_a/d_c$  was  $1/3$  and  $3/1$ , there was no big difference in the density and  $I_D/I_G$ , even the distribution range of wear particles of  $0.45 \mu\text{m} \sim 200 \mu\text{m}$  is similar, which was larger than it for  $d_a/d_c = 1/1$ .

Additionally, in the particle size distribution the peak height at smaller size was higher than the peak height at larger size. Therefore, when the DLC coating was deposited at  $-500$  V, the larger anode-cathode diameter ratio of 3/1 was better than smaller one of 1/3 for reducing the wear particle size.

### 8.3 Substrate bias at $-750$ V

#### 8.3.1 Density and deposition rate of DLC coatings

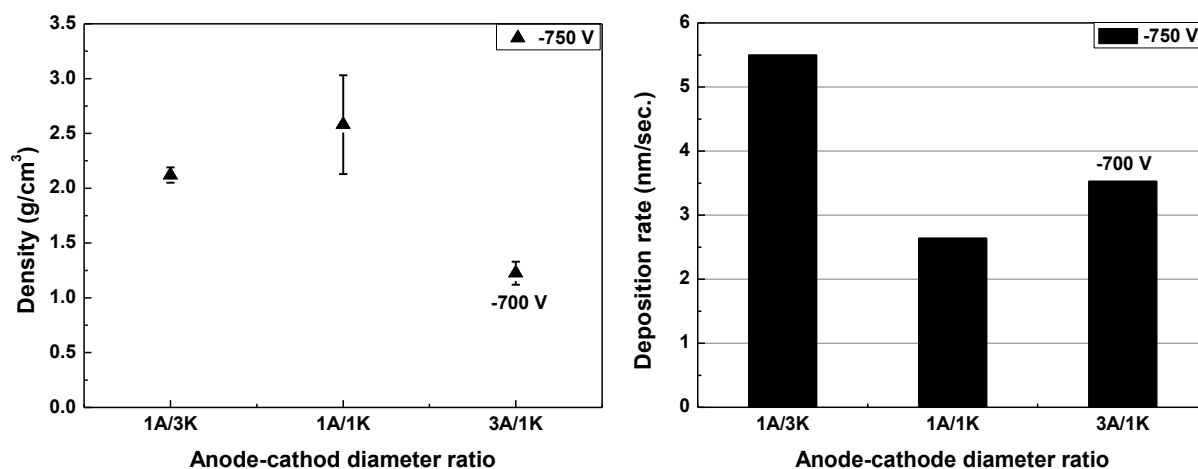


Figure 8.8 Density and deposition rate of DLC coatings deposited at  $-750$  V with  $d_a/d_c = 1/3, 1/1$  and  $3/1$  ( $-700$  V)

In this group, a negative bias of  $-750$  V was used to apply to the substrate. There were two samples for each ratio. Here it must be noted that when DLC coating was deposited with  $d_a/d_c=3/1$ , the substrate bias was  $-700$  V not  $-750$  V. The influence of the anode-cathode diameter ratio on the density and deposition rate of DLC coatings is shown in Fig. 8.8.

With increasing the electrode diameter ratio from  $d_a/d_c = 1/3$  to  $3/1$ , the density of DLC films was increased first then decreased to  $1.2$  g/cm<sup>3</sup> at  $3/1$ . When the ratio of  $1/1$  was used, the DLC coating deposited at  $-750$  V had the highest density of  $2.5$  g/cm<sup>3</sup>. When DLC coating was deposited with anodic arc, e.g.  $1/3$ , the density was  $2.1$  g/cm<sup>3</sup> and the deposition rate was faster comparing with cathodic arc, e.g.  $1/1$  and  $3/1$ .

### 8.3.2 Raman spectra of DLC coatings

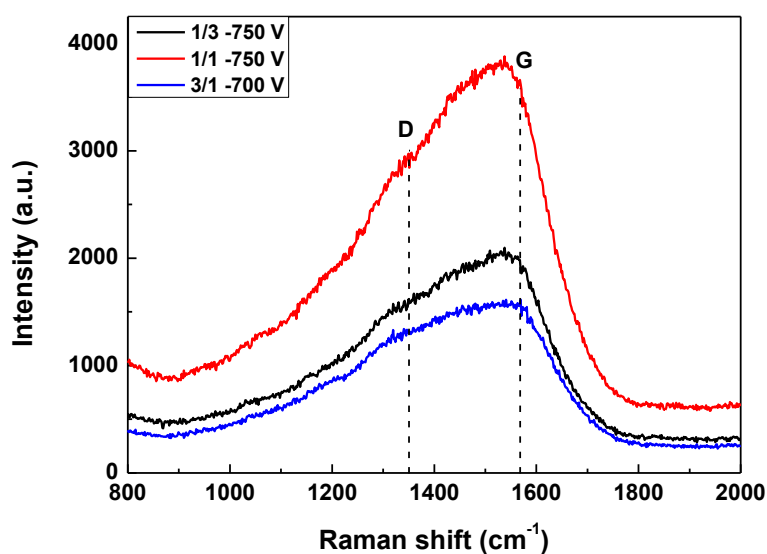


Figure 8.9 Raman spectrum of DLC coatings deposited at  $-750$  V with different  $d_a/d_c$

Raman spectra of DLC coatings deposited at  $-750$  V with different anode-cathode diameter ratio of 1/3, 1/1 and 3/1 were shown in Fig. 8.9. The corresponding G peak positions, the ratios of  $I_D/I_G$  and FWHM (G) after Raman deconvolution were shown in Table 8.3. Before fitting the spectra, a linear background was subtracted. In Fig. 8.9 one broad peak appeared at  $\sim 1550$   $\text{cm}^{-1}$  lower than the true G band due to the bond disorder. Another weak peak at  $\sim 1350$   $\text{cm}^{-1}$  is found assigned to D band arising from aromatic rings [5].

Table 8.3 Variation of G position, FWHM and the  $I_D/I_G$  ratio of DLC coatings deposited at  $-750$  V with different  $d_a/d_c$

$d_a/d_c$	G position / $\text{cm}^{-1}$	$I_D/I_G$	FWHM (G)
1A/3K	1553	0.85	179
1A/1K	1556	0.85	178
3A/1K (700 V)	1550	0.49	195

When the DLC coating was deposited at  $-700$  V with 3/1, the ratio of  $I_D/I_G$  was the minimum of 0.49 and the FWHM was the maximum resulting from more bond length and bond angle disorder. Although the Raman spectra of DLC coatings with 1/3 and 1/1 were completely different

(see Fig. 8.9), after fitting they had the same  $I_D/I_G$  and FWHM, even similar G position (see Table 8.1). Actually the intensity of G peak for 1/1 was higher than that for 1/3 obviously, so that's indicated that the intensity of D peak for 1/1 was lower than it for 1/3. Additionally, the ratio of  $I_D/I_G$  was increased when decreasing the anode-cathode diameter ratio, which indicated that more disorder was introduced into the coatings at anodic arc.

### 8.3.3 Particle size distribution of DLC coatings

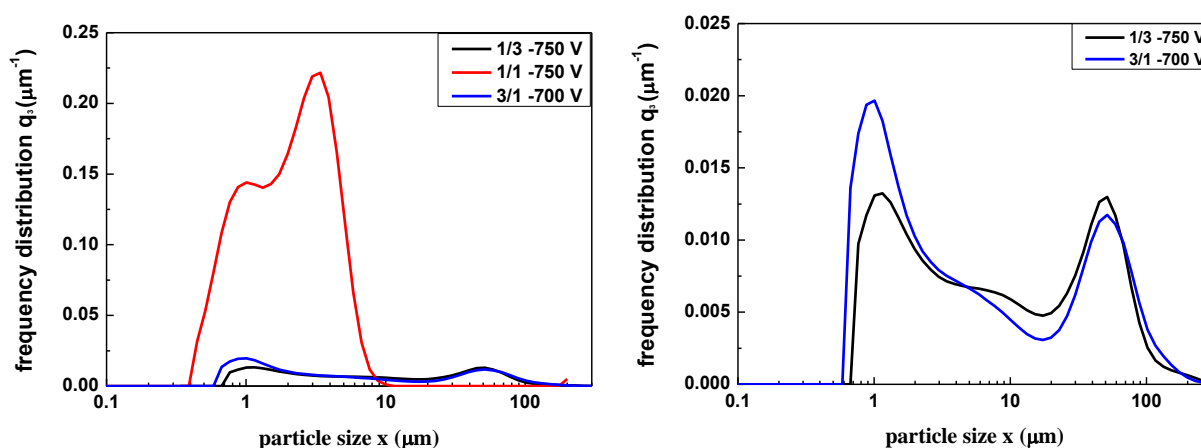


Figure 8.10 Volume density distribution  $q_3(x)$  at  $-750$  V with different  $d_a/d_c$

Fig. 8.10 shows the particle size distribution of DLC coatings deposited at  $-750$  V. It was found that with varied anode-cathode diameter ratio the different distribution curve was plotted. Especially for  $d_a/d_c = 1/1$ , the particles distributed in the range of  $0.3 \mu\text{m} \sim 10 \mu\text{m}$  and most particles were distributed at  $\sim 1 \mu\text{m}$  and  $5 \mu\text{m}$ . Although the size of particles of coatings deposited with  $d_a/d_c = 1/1$  was smaller, the larger amount of particles was generated, compared with other anode-cathode diameter ratios of 1/3 and 3/1.

Due to big peak height of 1/1, the particle size distributions of 1/3 and 3/1 must be plotted separately in Fig. 8.10 (right). It was found that the height of bimodal peak was the same when the DLC coating was deposited with  $d_a/d_c = 1/3$  and 3/1, nevertheless, the height of peak at  $\sim 1 \mu\text{m}$  was higher than that of peak at  $\sim 50 \mu\text{m}$  for  $d_a/d_c = 3/1$ . Additionally, with increasing the ratio from 1/3 to 3/1, the height of peak at  $\sim 1 \mu\text{m}$  was increased and the height at  $\sim 50 \mu\text{m}$  was reduced.

### 8.3.4 Conclusion

DLC coatings were deposited at  $-750$  V with the anode-cathode diameter ratio of  $d_a/d_c = 1/3$ ,  $1/1$  and  $3/1$  ( $-700$  V). There were two peaks in the curve of volume density distribution  $q_3(x)$  of all DLC coatings. With increasing  $d_a/d_c$  from  $1/3$  to  $3/1$ , it was found that the frequency distribution was shifted down to the smaller size. When the ratio of  $1/1$  was used, the particle size distribution was in the range of  $0.3 \mu\text{m} \sim 10 \mu\text{m}$ , much smaller than those of  $1/3$  and  $3/1$  which were distributed in the range of  $0.45 \mu\text{m} \sim 200 \mu\text{m}$ . Furthermore, the intensity ratio of D and G bands was decreased with increasing the anode-cathode diameter ratio. Therefore, when the substrate bias of  $-750$  V was chosen, DLC coating was deposited with  $d_a/d_c = 3/1$  better than with  $1/3$ .

## 8.4 Substrate bias at $-1000$ V

### 8.4.1 Density and deposition rate of DLC coatings

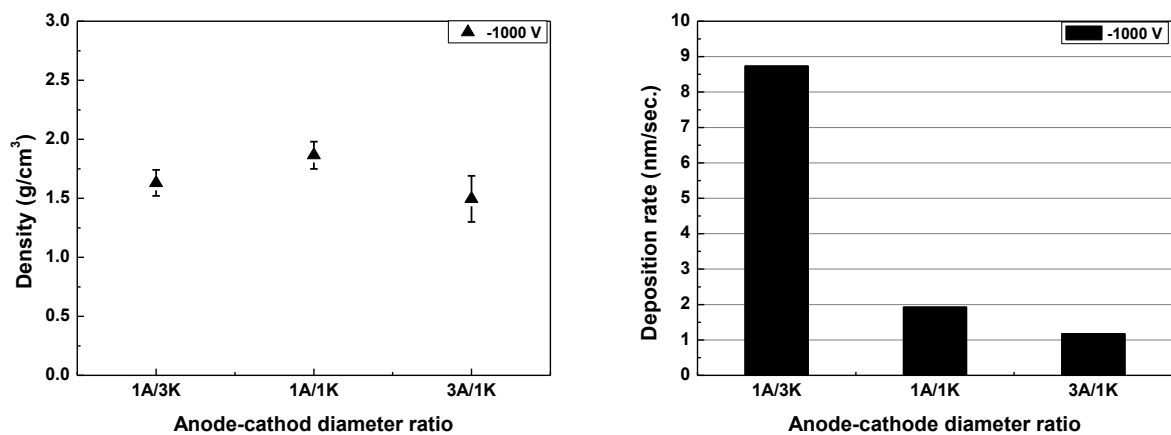


Figure 8.11 Density and deposition rate of DLC coatings deposited at  $-1000$  V with different  $d_a/d_c$

Fig. 8.11 shows the density and deposition rate of DLC coatings deposited at  $-1000$  V with the anode-cathode diameter ratio of  $1/3$ ,  $1/1$  and  $3/1$ . There were two samples for each ratio. It was found that the density was lower than  $2.0 \text{ g/cm}^3$ . The deposition rate was decreased with increasing the anode-cathode diameter ratio. When the ratio of  $1/3$  was used, the deposition rate quite fast reached to the maximum of nearly  $9 \text{ nm/sec}$ , comparing with the other ratios of  $1/1$  and  $3/1$ .

### 8.4.2 Raman spectra of DLC coatings

After deposition, the structure of DLC coatings was analyzed using Raman with the visible excitation of 514 nm. The Raman spectra of DLC coatings deposited at  $-1000$  V were shown in Fig. 8.12. There were two broad peaks at  $\sim 1575$   $\text{cm}^{-1}$  of G band and  $\sim 1355$   $\text{cm}^{-1}$  of D band due to all  $\text{sp}^2$  sites. The other main Raman parameters to monitor carbon bonding are values of  $I_D/I_G$  and FWHM (G), which can be obtained using Raman fitting as shown in Table 8.4.

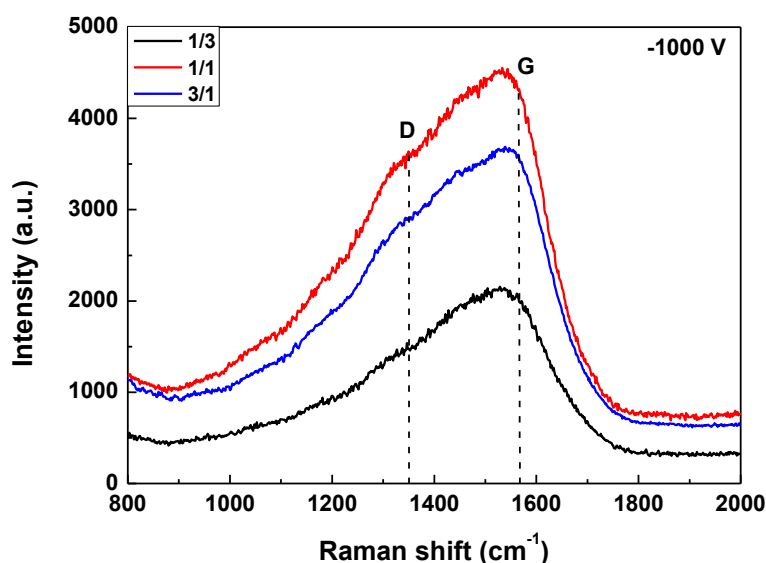


Figure 8.12 Raman spectrum of DLC coatings deposited at  $-1000$  V with different  $d_a/d_c$

Table 8.4 Variation of G position, FWHM and the  $I_D/I_G$  ratio of DLC coatings deposited at  $-1000$  V with different  $d_a/d_c$

$d_a/d_c$	G position / $\text{cm}^{-1}$	$I_D/I_G$	FWHM (G)
1A/3K	1554	0.92	192
1A/1K	1554	0.81	173
3A/1K	1544	0.41	187

According to ref. [5]  $I_D/I_G$  is a measure of the size of the  $\text{sp}^2$  phase organized in rings in amorphous carbons. With increasing the anode-cathode diameter ratio, the ratio of  $I_D/I_G$  was decreased to 0.41 at 3/1. The  $\text{sp}^2$  phase was mainly organized in rings for the DLC coating deposited with the smaller anode-cathode diameter ratio. When the larger ratio of 3/1 was chosen,

the  $sp^2$  phase in rings was raised, more than it in chains.

In addition, FWHM had higher value when the DLC coating was deposited at  $-1000$  V with  $d_a/d_c = 1/3$ , which resulted from a higher bond length and bond angle disorder for a given cluster size. In this work, the excitation energy for Raman was constant so clusters in the coatings deposited have nearly same size [6].

### 8.4.3 Particle size distribution of DLC coatings

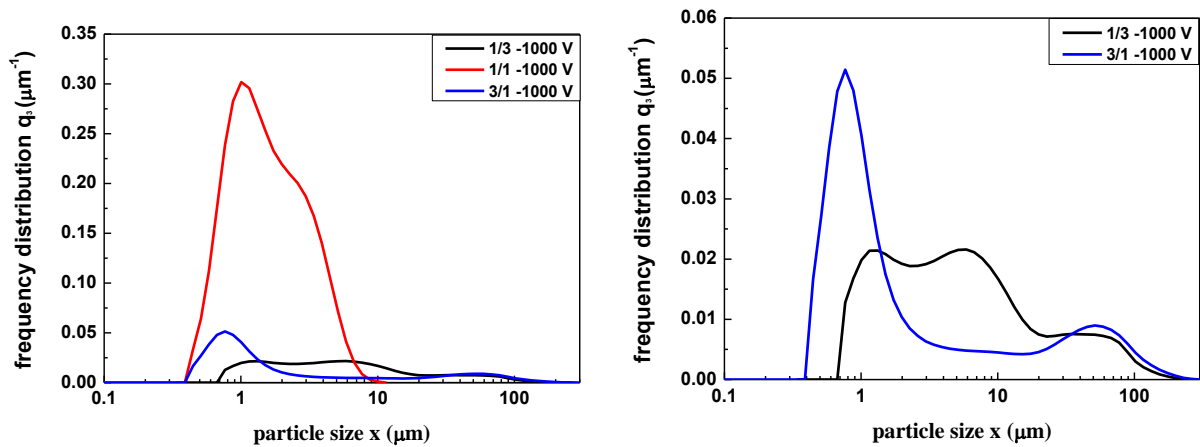


Figure 8.13 Volume density distribution  $q_3(x)$  at  $-1000$  V with different  $d_a/d_c$

The wear particles were collected in the deionized water after tribological test, and then measured by the particle size analyzer. Fig. 8.13 shows the volume density distribution of DLC coatings deposited at  $-1000$  V. It was found that for  $d_a/d_c = 1/1$  the particle size distribution was in the range of  $0.3 \mu\text{m} \sim 10 \mu\text{m}$  and large amount of particles distributed at the smaller size of  $\sim 1 \mu\text{m}$  (Fig. 8.13 (left)). In Fig. 8.13 (right), the distribution curves of particles for  $d_a/d_c = 1/3$  and  $3/1$  were separated from Fig. 8.13 (left). It was observed obviously the peak height at smaller size was higher than that at larger size of  $\sim 50 \mu\text{m}$ . For the diameter ratio of  $3/1$ , large amount of particles distributed in the smaller size of  $\sim 1 \mu\text{m}$ , however for  $1/3$ , most particles were in the range of  $1 \mu\text{m} \sim 10 \mu\text{m}$ .

### 8.4.4 Conclusion

The DLC coatings were deposited at  $-1000$  V with the anode-cathode diameter ratio of  $d_a/d_c = 1/3, 1/1$  and  $3/1$ . With increasing  $d_a/d_c$  the deposition rate was decreased and the density was

increased first and then decreased to the minimum at the diameter ratio of 3/1. For bimodal distribution of wear particle size, the peak for  $q_3(x)$  around the smaller size of  $\sim 1 \mu\text{m}$  was higher than it around the larger size of  $\sim 50 \mu\text{m}$ . In addition, the ratio of  $I_D/I_G$  was decreased to 0.41 with increasing the anode-cathode diameter ratio to 3/1. The curve of wear particle size distribution downshifted to the smaller than  $1 \mu\text{m}$  when the DLC coating was deposited with  $d_a/d_c = 3/1$ .

## References

- [1] O. Filipov, Correlation of plasma fluxes and film properties deposited by vacuum arc, Doctoral Dissertation, Universität Duisburg-Essen 2013 1-178.
- [2] A.C. Ferrari, J. Robertson, Origin of the  $1150\text{-cm}^{-1}$  Raman mode in nanocrystalline diamond, Physical Review B 63 (2001) 121405(R) 1-4.
- [3] R. Pfeiffer, H. Kuzmany, P. Knoll, S. Bokova, N. Salk, B. Guenther, Evidence for trans-polyacetylene in nano-crystalline diamond films, Diamond and Related Materials 12 (2003) 268-271.
- [4] J. Birrell, J.E. Gerbi, O. Auciello, J.M. Gibson, J. Johnson, J.A. Carlisle, Interpretation of the Raman spectra of ultrananocrystalline diamond, Diamond and Related Materials 14 (2005) 86-52.
- [5] A.C. Ferrari, J. Robertson, Interpretation of Raman spectra of disordered and amorphous carbon, Physical Review B 61 (2000) 14095-14107.
- [6] C. Casiraghi, A.C. Ferrari, J. Robertson, Raman spectroscopy of hydrogenated amorphous carbons, Physical Review B 73 (2005) 085401 1-14.

---

## 9. Influence of substrate bias and $d_a/d_c$ on adhesion (Cavitation erosion)

### 9.1 Anode-cathode diameter ratio of $d_a/d_c = 1/3$

The DLC coatings were deposited with an anode-cathode diameter ratio of  $d_a/d_c = 1/3$  and ion density of  $7.163 \times 10^{11} \text{ cm}^{-3}$  at a DC bias of  $-250 \text{ V}$ ,  $-500 \text{ V}$ ,  $-750 \text{ V}$  and  $-1000 \text{ V}$  for 3 minutes each. Austenite stainless steel P2000 was used as substrate material for the deposition of carbon coatings. In order to improve the adhesion of DLC coating to substrate, Ti as interface layer was deposited by cathodic vacuum arc evaporation prior to the deposition of DLC coating (see chapter 5.1 for details).

- Wear experiments by cavitation erosion

After deposition of DLC coatings, samples were placed on the substrate holder of cavitation testing setup, and immersed in the water ( $27 \text{ }^\circ\text{C}$ ). The ultrasonic equipment (see chapter 4.3) was used for cavitation erosion of DLC coatings with a sonotrode of the frequency of  $20 \text{ kHz}$  and a diameter of  $5 \text{ mm}$ . The distance of  $0.7 \text{ mm}$  from substrate to sonotrode was constant. The vibration amplitude, which can be adjusted, was kept at  $75 \%$ . The duration of cavitation erosion testing was dependent on the properties of samples. Every sample of DLC coating, deposited by different bias, was treated by wear experiments by means of cavitation treatment with different time from  $30 \text{ s}$  up to  $1800 \text{ s}$ . After cavitation testing, the surface damage was measured by means of quantitative image analysis.

- Results and discussion

As shown in Fig. 9.1, the surface damage (% of charged area) by cavitation treatment of up to  $360 \text{ s}$  was observed with quantitative image analysis for DLC coating deposited at  $-500 \text{ V}$ . The diameter of the worn areas at the insert surface (about  $5 \text{ mm}$ ) corresponded to the tip of the sonotrode in the cavitation equipment. The image showed a small spot with the diameter of about  $1 \text{ mm}$  when the surface was treated under cavitation erosion for  $30 \text{ s}$  and  $60 \text{ s}$ . With increasing the time of cavitation charging from  $120 \text{ s}$  to  $300 \text{ s}$ , the images were characterized by concentric rings in the damaged area as shown in left side of the image insert in Fig. 9.1. After  $180 \text{ s}$  of cavitation

9. Influence of substrate bias and  $d_a/d_c$  on adhesion (Cavitation erosion)

charging, the surface damage of the DLC coating increased linearly with cavitation duration. When the duration was up to 360 s, nearly 60 % of surface was damaged.

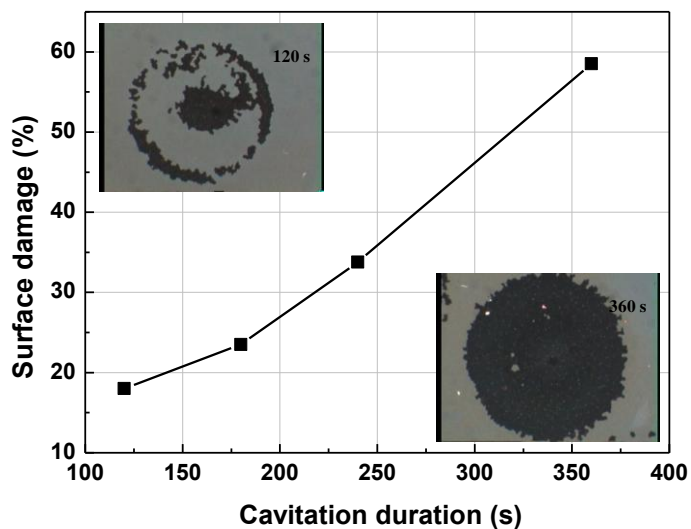


Figure 9.1 Wear damage of cavitation erosion of DLC coating deposited with  $d_a/d_c = 1/3$  at  $-500$  V

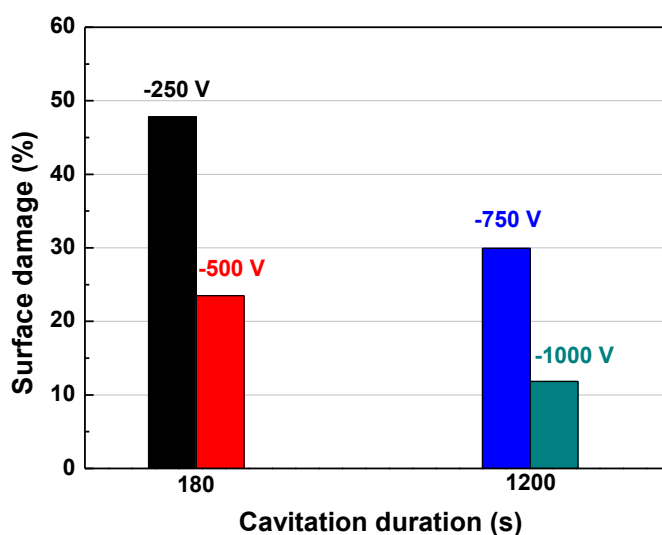


Figure 9.2 Wear damage by cavitation erosion of DLC coatings

The wear damage (% of charged area) by cavitation erosion of all DLC coatings with the bias of  $-250$  V,  $-500$  V,  $-750$  V and  $-1000$  V is shown in Fig. 9.2. At  $-250$  V, nearly 50 % of surface

---

was destroyed by cavitation erosion after 180 s (see Fig. 9.2). With increasing the bias to  $-500$  V, the surface damage halved to about 25 % compared with the DLC coating deposited at  $-250$  V. When the bias was increased to  $-750$  V and  $-1000$  V, no damaged surface was found on the surface of samples after 180 s cavitation.

When the DLC coating was deposited at the bias of  $-750$  V, at the beginning of 300 s of cavitation charging, there was no worn area on the surface. With increasing the charging time up to 600 s, the color started to change. About 30 % of surface area was destroyed after 1200 s. However, for DLC coating at  $-1000$  V no damage could be seen with naked eyes even though the sample was done by cavitation treatment of up to 600 s. When the cavitation duration was up to 1200 s, there was less damage on the surface, approximately 12 %, than the worn area of DLC coating at  $-750$  V. It was indicated obviously that the worn surface area destroyed by cavitation erosion was decreased with increasing the bias from  $-250$  V to  $-1000$  V, which means that the adhesion of DLC coating on the substrate was improved with increasing DC bias voltage, especially at  $-750$  V and  $-1000$  V.

As discussed in chapter 7.1.1, with increasing of the DC bias voltage to  $-750$  V the density of DLC coatings was increased. As is known, under high ion impingement energies, the ions became implanted beneath the surface, where the impact energy was less efficient in promoting surface diffusion [1-3]. That means the high ion energy decreased voids from the penetration of the ions which made the film denser. What's more, the high ion impingement energies improve the ability of chemical reaction so that it increased the adhesion of amorphous carbon coating with the Ti interface layer [4].

- Conclusion

The DLC coatings were produced by vacuum arc deposition with an anode-cathode diameter ratio of  $d_a/d_c = 1/3$  by the different DC bias from  $-250$  V to  $-1000$  V. Due to the bad adhesion of DLC coating on P2000, the metallic interface layer (Ti) was produced prior to the deposition of DLC coating. In order to study the effect of the DC bias on the adhesion of DLC coating to the interface layer, the cavitation erosion test was used. It was found that the incubation time of cavitation charging was different for DLC coatings deposited by different bias. The incubation time was increased with increasing the bias. After incubation period, the surface damage (%)

charged area) was dependent on the cavitation time, and increased linearly.

With increasing the bias, the damaged surface examined by quantitative image analysis was decreased. The adhesion can be improved by increasing the DC bias voltage due to high ion impingement energies.

## 9.2 Anode-cathode diameter ratio of $d_a/d_c = 1/1$

The DLC coatings were deposited with an anode-cathode diameter ratio of  $d_a/d_c = 1/1$  and ion density of  $1.47 \times 10^{12} \text{ cm}^{-3}$  at a DC bias of  $-250 \text{ V}$ ,  $-500 \text{ V}$ ,  $-750 \text{ V}$  and  $-1000 \text{ V}$  for 3 minutes each. Discs of P2000 stainless steel were used as substrates for the deposition of carbon coatings. In order to improve the adhesion between substrate and DLC coating, Ti as interface layer was deposited by cathodic vacuum arc evaporation prior to the deposition of DLC coating. The vacuum was pumped below  $1.5 \times 10^{-5} \text{ mbar}$ , and the deposition pressure was kept at  $1 \times 10^{-3} \text{ mbar} \sim 2 \times 10^{-4} \text{ mbar}$ . For more details see the chapter 5.3.

Here it must be noted that during the arc process the distance between the two electrodes were increased with evaporating them. So in order to maintain the arc, the distance of the two electrodes must be adjusted during the deposition. However, when DLC coating was deposited at  $-250 \text{ V}$ , the deposition had to be ended at 2 min 22 s because the two electrodes could not be closer resulting in the arc was not initiated again. Therefore, the deposition time for DLC coating at  $-250 \text{ V}$  was just 2 min 22 s and the density was  $1.98 \text{ g/cm}^3 \sim 2.16 \text{ g/cm}^3$ . Moreover, it was found that after 17 h storage of sample deposited at  $-750 \text{ V}$ , a few parts of DLC coatings on the edge of sample peeled off before cavitation test, which maybe resulted from the internal stress due to the thicker coating or quick cooling.

- Wear experiments by cavitation erosion

DLC coated samples were placed on the substrate holder of cavitation testing setup, and immersed in the water ( $27 \text{ }^\circ\text{C}$ ). The ultrasonic equipment was used for cavitation erosion of DLC coatings with the sonotrode of the frequency of 20 kHz and the diameter of 5 mm. The distance of 0.7 mm from substrate to sonotrode was constant. 75 %, as the vibration amplitude which can be adjusted, was used in this work. Every sample of DLC coating, deposited by different bias, was

treated by wear experiments with different time which depended on the properties of the samples. Usually the incubation period of cavitation charging was about few seconds, at which there was no measurable wear. After cavitation testing, the surface damage was measured by means of quantitative image analysis and analysis software.

- Results and discussion

The damaged surfaces' images of DLC coatings were made by light microscopy after cavitation. Although the surface image of DLC coating deposited at  $-250\text{ V}$  was not so clear that there was no good contrast and it was difficult to analyze the surface damage (% charged area) by application software, the worn coating areas were visible to the naked eye. It was observed obviously that a few small spots appeared after 10 s of cavitation treatment and with increasing the charging time to 30 s the surface area was in the form of homocentric circles. When the cavitation duration was 60 s, the damaged area was roughly circular in shape with the diameter of 5 mm corresponding to the tip size of the sonotrode. The value of the damaged area estimated by comparing with other microscopy images was approximately 60 %.

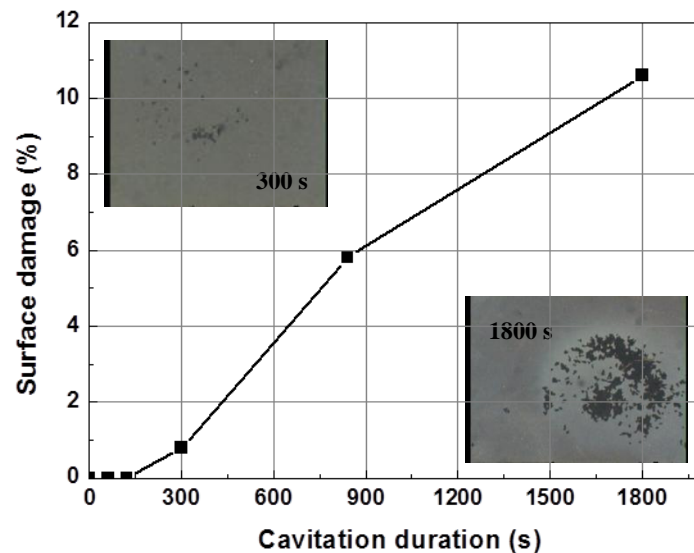


Figure 9.3 Wear damage of cavitation erosion of DLC coating deposited with  $d_a/d_c = 1/1$  at  $-500\text{ V}$

When the DLC coating deposited at  $-500\text{ V}$  was treated by cavitation test, the surface damage as a function of cavitation duration was shown in Fig. 9.3. It was found that there was not any worn surface before 120 s and some small spots (only 1 % damaged surface) were observed after 300 s.

With increasing the duration of cavitation test to 1800 s, more spots appeared as image shows in Fig. 9.3 and about 11 % of area was destroyed.

- When DLC coating was deposited at  $-750$  V, a few parts of coating on the edge of disc peeled off before cavitation test due to internal stress as described above. Therefore, the surface in the middle of disc was chosen for wear experiments. The worn surface was observed after 420 s of cavitation charging (see Fig. 9.4), and the percentage of damaged surface was about 7 % calculated by analysis software. However, the cavitation charging also speeded up the peeling of coating on the edge of sample, which resulted in a large number of wear debris peeled off and dissolved in the water causing the liquid erosion during cavitation test. Thus, 7 % of charged area was attributed to not only the repeated treatment of the gas and fluid cavities implosion, but also the abrasive wear debris. Actually when the coating on substrate was destroyed, even though a little surface was damaged, it was still not appropriate to be used for the cavitation test. For this kind of sample, it is difficult to analyze the adhesion of coating on the substrate via the cavitation erosion.

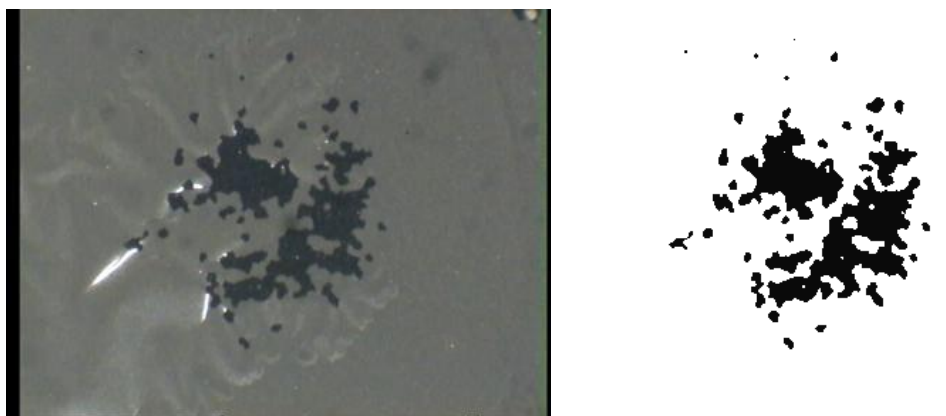


Figure 9.4 Light microscopy image of worn surface and corresponding analytical image by software after 420 s-cavitation charging of DLC coating deposited with  $d_a/d_c = 1/1$  at  $-750$  V

However, for the DLC coating deposited at  $-1000$  V, after 1200 s of cavitation erosion no spot or any damaged area was visible to the naked eye. When the cavitation time was increased to 2400 s, it was found that the surfaces' color was changed a little but no area was destroyed. At least the damaged surface could not be observed by the naked eyes.

---

- Conclusion

In order to investigate the influence of the substrate bias on the adhesion of coating and the substrate, a series of DLC coatings were produced by vacuum arc deposition with an anode-cathode diameter ratio of  $d_a/d_c = 1/1$  at the different DC bias from  $-250$  V to  $-1000$  V. As is well known, due to the poor adhesion of DLC coating on P2000 steel, the DLC coating will not be deposited directly on the substrate. Usually the interface layer was used prior to the deposition of DLC coating, here Ti was chosen as interface layer.

As discussed above, after 60 s of cavitation erosion, for DLC coating deposited at  $-250$  V the whole circular area with the diameter of 5 mm (60 %) was destroyed totally, by contrast, there was no damage observed on the surface of DLC coating deposited at  $-500$  V,  $-750$  V and  $-1000$  V after 120 s, 180 s and 1200 s, respectively. It was indicated obviously with increasing the bias from  $-250$  V to  $-1000$  V, the incubation time of cavitation charging was increased. In addition at  $-750$  V about 7 % of surface area was destroyed after 420 s of cavitation duration, but for DLC coating deposited at  $-500$  V to obtain the same damaged area the twice time of cavitation charging was required. Here it was still difficult to confirm that the adhesion of DLC coating deposited at  $-500$  V was better than that of DLC coating deposited at  $-750$  V which had some peeling before the cavitation test. However the DLC coating at  $-1000$  V had the best adhesion compared with those at other biases.

### 9.3 Anode-cathode diameter ratio of $d_a/d_c = 3/1$

Austenite stainless steel P2000 was used as substrate material for the deposition of carbon coatings. In order to improve the adhesion between substrate and DLC coating, Ti as interface layer was deposited by cathodic vacuum arc evaporation prior to the deposition of DLC coating. The DLC coatings were deposited with an anode-cathode diameter ratio of  $d_a/d_c = 3/1$  and ion density of  $2.59 \times 10^{12} \text{ cm}^{-3}$  at a DC bias of  $-250$  V,  $-500$  V,  $-750$  V and  $-1000$  V for 3 minutes each (see chapter 5.3 for more details).

Fig. 9.5 shows the deposition rate and density of DLC coatings deposited with  $d_a/d_c = 3/1$  at different substrate bias. It was found that at  $-750$  V more carbon ions were deposited on the substrate so that it had the maximum of deposition rate about 3.5 nm/sec compared with other bias,

but the minimum value of density. On the contrast, the DLC coating had the maximal density of  $2.3 \text{ g/cm}^3$  when it was deposited at  $-500 \text{ V}$ . It was indicated that the substrate bias had a big influence on the properties of DLC coatings. Therefore, in next section it will be discussed about the effect of the bias on the adhesion between DLC coating and substrate by cavitation erosion test.

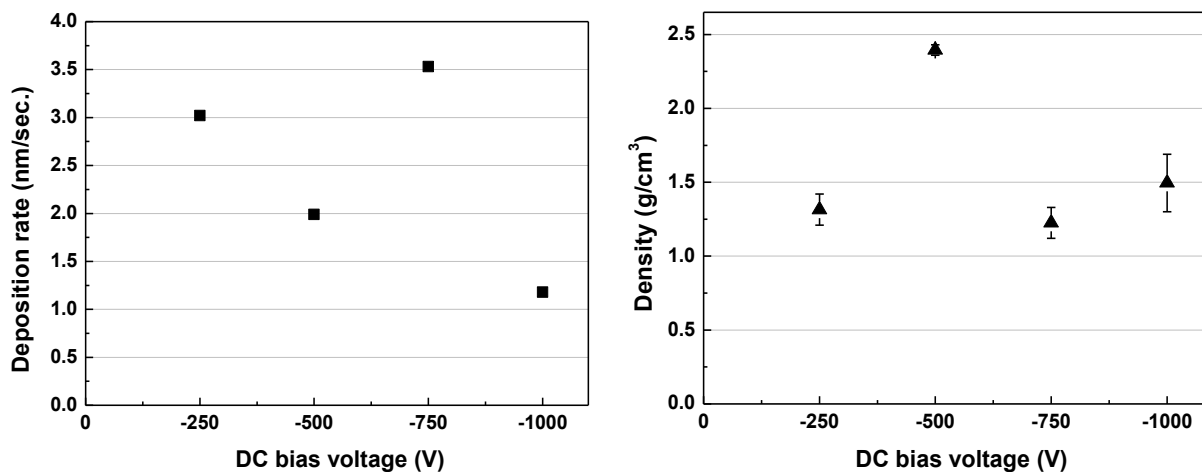


Figure 9.5 Deposition rate and density of DLC coating deposited with  $d_a/d_c = 3/1$  as a function of bias voltage

- Wear experiments by cavitation erosion

The ultrasonic equipment (see also chapter 4.3) was used for cavitation erosion of DLC coatings with a sonotrode of the frequency of 20 kHz and a diameter of 5 mm. Firstly, the test parameters should be fitted. The distance of 0.7 mm from substrate to sonotrode was constant. The vibration amplitude, which can be adjusted, was kept at 75 % in this work. Samples with DLC coatings were placed on the substrate holder of cavitation testing setup. In order to stabilize the gas content of cavitation medium, it is necessary to run the sonotrode for 5 min before the samples are immersed in the water ( $27 \text{ }^\circ\text{C}$ ). The duration of cavitation erosion testing was from 10 s to 120 s dependent on the properties of samples. Every sample of DLC coating was tested by wear experiments by means of cavitation treatment. After cavitation testing, the surface damage was measured by means of quantitative image analysis.

- Results and discussion

As is known, the worn surface (% of charged area) is related to the cavitation duration, because no material can withstand the attack of cavitation erosion in the long time [5]. Here the

DLC coating deposited at  $-250$  V was used as an example. Fig. 9.6 shows the percentage of the damaged surface in the whole area of light microscopy image with the cavitation duration. With increasing the time of cavitation charging, more surface was destroyed which was verified in Fig. 9.6 and Fig. 9.7.

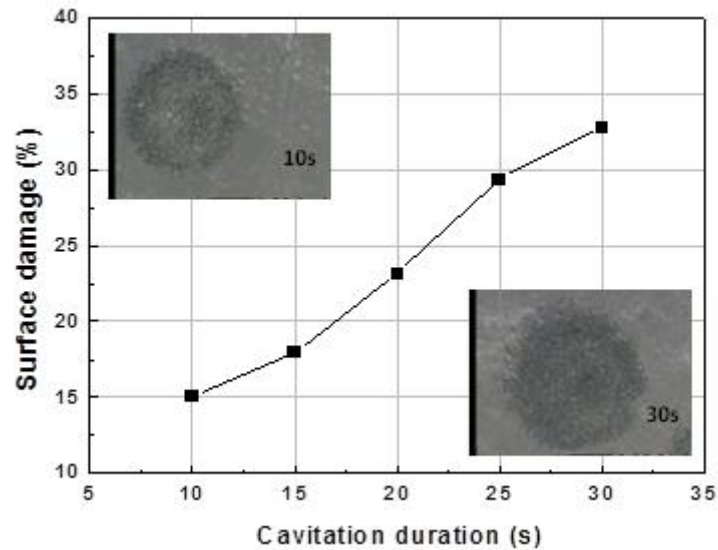


Figure 9.6 Wear damage of cavitation erosion of DLC coating deposited with  $d_a/d_c = 3/1$  at  $-250$  V

Actually, the samples deposited at other biases showed the same change (see Fig. 9.7). By comparing the surface damage of coatings deposited at biases of  $-250$  V,  $-500$  V and  $-750$  V, it was found that the minimum of worn area of surface was obtained at  $-500$  V. About 15 % of surface area was worn after 30 s of cavitation duration. In contrast, about double percentage was damaged for the samples deposited at  $-250$  V and  $-750$  V. That means with increasing the bias from  $-250$  V to  $-500$  V, the adhesion of sample was improved first and then decreased when the bias was raised to  $-750$  V. That seems to be related to the density which has the maximum at  $-500$  V as shown in Fig. 9.5. Additionally, during cavitation test there was small difference at the beginning of 10 s and 20 s for all samples. After 30 s of cavitation erosion, the percentage of worn area was increased rapidly comparatively with that after 10 s or 20 s.

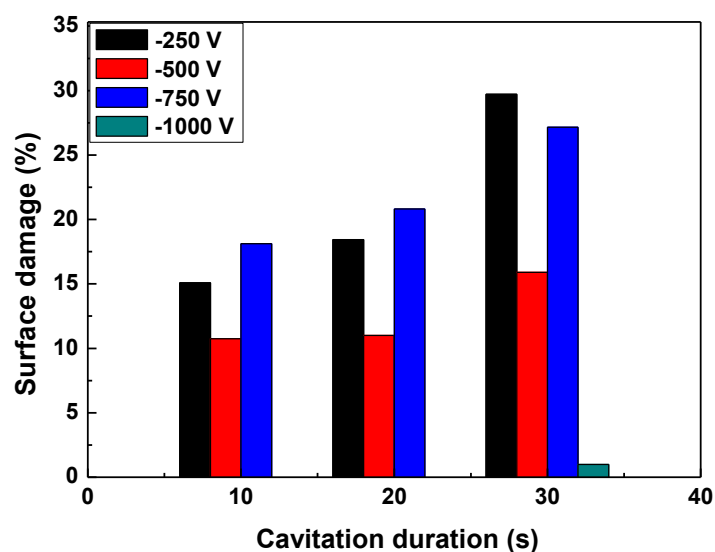


Figure 9.7 Wear damage by cavitation erosion of DLC coatings deposited with  $d_a/d_c = 3/1$  at different biases of  $-250$  V,  $-500$  V,  $-750$  V and  $-1000$  V

For the coating deposited at  $-1000$  V, after 10 s cavitation test or even 20 s, no visible worn surface could be observed. With increasing the testing time to 30 s, a small spot appeared on the surface. After analyzing by software just only 1 % of surface area was damaged, which indicated that the sample had a better adhesion at  $-1000$  V than at other biases. Thus, if the adhesion correlated with the density as discussed above, the sample at  $-500$  V should have the better adhesion than that at  $-1000$  V. However, it was obviously found when the substrate bias was increased to the highest value of  $-1000$  V, the adhesion of coating to substrate was improved.

#### ● Conclusion

When the DLC coating was deposited by vacuum arc with an anode-cathode diameter ratio of  $d_a/d_c = 3/1$ , the influence of bias on the adhesion of coating to substrate was investigated. It was found that at the highest bias of  $-1000$  V, the coating adhered to the substrate better than for other biases. For the DLC coatings deposited at other biases, except  $-1000$  V, the adhesion of sample at  $-500$  V was better than others. Nevertheless, there was still more than 10 % of surface area destroyed after 10 s of cavitation erosion. According to the result of density and cavitation erosion, it was known that the adhesion could be improved by increasing the substrate bias, no matter how the density was influenced by the bias.

---

## References

- [1] A. Leyendecker, O. Lemmer, S. Esser. A new coating process integrated in an innovative coating system for production of well-adherent diamond coatings, *International Journal of Refractory Metals and Hard Materials* 16 (3) (1998) 187-190.
- [2] F. Deuerler, J. Peterseim, H. Gruner, Q. Wang, V. Buck, Process control during diamond coating of tools, *International Journal of Refractory Metals and Hard Materials* 16 (3) (1998) 191-199.
- [3] K. Zhou, M. Dai, J. Song, T. Kuang, Z. Liu. In: G. Kneringer, P. Rödhammer, H. Wildner (eds.), 15<sup>th</sup> International Plansee Seminar Reutte: Plansee AG 2 (2001) 498-508.
- [4] S. Yugo, T. Kimura, T. Kanai, Nucleation mechanisms of diamond in plasma chemical vapor deposition, *Diamond and Related Materials* 2 (2-4) (1993) 328-332.
- [5] M. Pohl, M. Feyer, Charakterisierung und Prüfung dünner Schichten durch Kavitationserosion, *Tribologie und Schmierungstechnik* 39 (1992) 29-44.

## 10. Conclusion and Future Work

### 10.1 Contributions

The most important contribution of this dissertation is a new approach-design of wear particle size distribution of DLC coatings which can be optimized by a new vacuum arc deposition with adjustable anode-cathode diameter ratio. Several challenges have been faced and solutions were found. In particular, the initial research questions were clearly answered:

1. This new vacuum arc deposition is dependent on the anode-cathode diameter ratio. When the ratio of 1/3 is used it belongs to anodic arc which can reduce the industrial cost of the coated products and increase the deposition rate compared to traditional plasma filtering designs.
2. The interface layer of Ti makes it possible to deposit DLC coatings on austenite steel substrates by using new vacuum arc deposition.
3. The properties of DLC coatings are influenced by the deposition parameters.
4. Appropriate anode-cathode diameter ratio and substrate bias make it possible to adjust or reduce the wear particle size.

Moreover, the experimental studies show that some problems can be resolved during the deposition of DLC coatings, tribological test and particle size distribution analysis.

In summary, this dissertation makes the following original contributions:

1. For bad adhesion of DLC coating on P2000-steel substrate

Although the adhesion is not the main subject in my research, Ti as interface layer can make the adhesion of DLC coating to substrate better. Additionally, it is confirmed that the adhesion can be improved by increasing the negative DC bias based on the introduction of Ti.

2. For tribological test setup

Comparing with the traditional disc-on-pin wear testing setup, using disc-on-disc setup produces more wear particles which is beneficial to the particle size distribution analysis. Furthermore, it is confirmed by lots of experiments that it is difficult to increase the concentration of particles by changing the radius of the wear track when the traditional disc-on-pin wear testing

---

setup is used. Although the radius of the wear track can be adjusted, it can be done only in the lubricant which is difficult to avoid the contamination.

### 3. For particle size distribution analysis

Wear particles in the deionized water are collected in the container made of Polytetrafluoroethylene (PTFE) in order to prevent adsorption. The agglomeration of wear particles can be solved by ultrasound for 2 min or adding dispersion agents (detergent). The volume cumulative distribution and volume density distribution (volume frequency distribution) are chosen to measure the particle size.

## 10.2 Conclusions

Diamond-like carbon (DLC), known as amorphous carbon, is a class of materials with different structures and properties, which make them suitable for use in the biomedical applications, particularly in tribological implants such as hip joint replacements. The study of wear particles as the main factor limiting the lifetime of the implants has attracted more and more interest in the field of artificial hip joint, not only the number of them, but also the distribution of their size. As is well known, the structure and properties of DLC coatings can be varied in a wide range which can be adjusted by the deposition parameters.

In this research DLC coatings were deposited by a new vacuum arc adjustable from anodic to cathodic operation mode, with the anode-cathode diameter ratios of 1/3, 1/1 and 3/1 at a DC substrate bias of  $-250$  V to  $-1000$  V. A number of interesting and important discoveries have been made experimentally. The most important results are summarized in the following paragraphs.

First, in order to improve the adhesion of DLC coating to the substrate of P2000 steel, the interface layer of Ti in the silver color was deposited by cathodic vacuum arc successfully (see chapter 5.1). The relationship between deposition pressure and arc voltage as well as current was studied, which influenced the uniformity of interface layer. At the higher pressure of  $\sim 10^{-2}$  mbar the voltage and current were kept at  $30$  V  $\sim 40$  V and  $40$  A  $\sim 60$  A, respectively. This kind of higher voltage and lower current is not good for the uniformity of Ti. When the deposition pressure was decreased to below  $\sim 10^{-3}$  mbar, the lower voltage of  $20$  V and higher current of  $74$  A were obtained which was used as the deposition parameters of Ti with good uniformity.

The structure of DLC coating was analyzed by the visible Raman spectrum. Multi-peak fitting analysis of Raman spectra on DLC coatings deposited by a new vacuum arc method were investigated (see chapter 6.1). It was confirmed that the simple two-Gaussian fit to characterize the D and G peaks is not suitable to deconvolute the Raman spectra of DLC coatings. The Raman spectra can be fitted very well with the four-peak fitting ( $\sim 1180 \text{ cm}^{-1}$ ,  $\sim 1350 \text{ cm}^{-1}$ ,  $\sim 1490 \text{ cm}^{-1}$  and  $\sim 1580 \text{ cm}^{-1}$ ) with full Gaussian function.

In order to make sure almost all wear particles generated by tribological test (disc-on-disc) are from DLC coatings not from interface layer of Ti or substrate of P2000, the appropriate tribological parameters are very important, e.g. normal force and velocity (see chapter 6.2). For the DLC coatings deposited by vacuum arc with  $d_a/d_c = 1/1$ , the load of 100 N and the velocity of 0.01 m/s were used, which was also influenced by the substrate bias. When  $-750 \text{ V}$  is applied to the substrate, the load and the velocity must be increased in order to get enough wear particles. When the anode-cathode diameter of 1/3 and 3/1 were chosen, the normal force and the rotation speed were varied, especially the normal force changed with the bias too. By tribological test, the wear mechanism was studied as well. Actually many mechanisms are involved in the process of wear. For DLC sliding against DLC, the main mechanisms are adhesive wear and abrasive wear, sometimes combined with delamination wear.

The influence of substrate bias from  $-250 \text{ V}$  to  $-1000 \text{ V}$  on the particle size distribution of DLC coatings was investigated (see chapter 7). With increasing the bias from  $-250 \text{ V}$  to  $-1000 \text{ V}$ , the maximum of frequency distribution of wear particles had the trend towards the smaller particles.

For 1/3 there were three peaks around  $\sim 1 \text{ }\mu\text{m}$ ,  $\sim 5 \text{ }\mu\text{m}$  and  $\sim 50 \text{ }\mu\text{m}$  and the peak height of  $\sim 50 \text{ }\mu\text{m}$  was decreased gradually with increasing the bias. For 3/1, the peak of  $\sim 5 \text{ }\mu\text{m}$  disappeared so that there was the bimodal peak in the curve of distribution. Moreover, the maximum of the curve was shifted from  $\sim 50 \text{ }\mu\text{m}$  to  $\sim 1 \text{ }\mu\text{m}$ . Thus, it can be estimated that all wear particles can be distributed below  $1 \text{ }\mu\text{m}$  at the higher substrate bias approximately  $-1100 \text{ V}$ .

When DLC coating was deposited with the anode-cathode diameter ratio of 1/1, the smaller wear particles of  $0.3 \text{ }\mu\text{m} \sim 10 \text{ }\mu\text{m}$  were generated. The DLC coating deposited at  $-500 \text{ V}$  has the

---

lowest  $R_a$  and  $I_D/I_G$ . With increasing the bias to  $-750$  V, the lowest friction coefficient of 0.035 was attained and the DLC coating had the lowest wear rate of  $10^{-5}$  g/h. At  $-1000$  V, the wear particle size decreased and the largest amount of particles was smaller than  $5$   $\mu\text{m}$ .

The influence of  $d_a/d_c = 1/3, 1/1$  and  $3/1$  on the properties and particle size distribution of DLC coatings was investigated (see chapter 8). When DLC coating was deposited with the anode-cathode diameter ratio of  $1/1$ , the density was higher than that with other modes of  $1/3$  or  $3/1$ . The deposition rate was decreased with increasing  $d_a/d_c$ , thus, it can reach to the maximum with the mode of anodic arc ( $d_a/d_c = 1/3$ ) no matter which substrate bias was applied. The lowest ratio of  $I_D/I_G$  was obtained corresponding to different bias with different mode, e.g. at  $-250$  V,  $-700$  V and  $-1000$  V corresponding to  $d_a/d_c = 3/1$ . At  $-500$  V, when the mode of  $1/1$  was used, the DLC coating with the lowest  $I_D/I_G$  of 0.34 was deposited.

For the modes of  $1/3$  and  $3/1$ , the range of wear particle size was broader between  $0.3$   $\mu\text{m}$  and  $200$   $\mu\text{m}$ , by contrast, the wear particle size distribution was in the range of  $0.3$   $\mu\text{m} \sim 10$   $\mu\text{m}$  for the ratio of  $1/1$ . As discussed above, the substrate bias was also one main factor for the distribution of particle size. In a word, with increasing the anode-cathode diameter ratio and bias, the frequency distribution shifted to smaller particle size.

The influence of substrate bias and  $d_a/d_c$  on adhesion of DLC coatings to substrate was studied by means of cavitation erosion (see chapter 9). There was an incubation time of cavitation charging which was increased with increasing bias. When the DLC coatings were deposited with the same  $d_a/d_c$  and treated for the same cavitation duration, the worn surface area of coating was decreased with increasing bias. Comparing with the modes of  $1/3$  and  $1/1$ , the DLC coatings produced with  $3/1$  had the shorter incubation time. However when the DLC coating was deposited with  $3/1$  at  $-1000$  V, just only 1 % of surface area was damaged. Consequently, the adhesion of DLC coating to the substrate can be improved by the higher bias and suitable  $d_a/d_c$ .

### 10.3 Limitations

The following paragraphs elaborate on the limitations during deposition and analysis of the DLC coatings due to limited equipment and times, as well as current solution that do not fit in with the industrial-scale requirements.

### 1. Deposition of Ti interface layer and DLC coatings

During deposition of Ti, there is no any gas introduced into the vacuum chamber so that the working pressure is not stable; thereby sometimes the arc extinguishing happens during deposition. Actually, the same problem can be faced in the deposition of DLC coatings, although without any gas the deposition of DLC coatings using vacuum arc can be realized with adjustable anode-cathode diameter ratio.

Moreover, the thicknesses, even uniformity of films (Ti or DLC) are different although they are treated under the same parameters excepting the deposition pressure which is difficult to make it constant. In particular, the influence of thickness of Ti on the deposition of DLC coatings is neglected in this work. Meanwhile, during deposition of DLC coatings the effect of the values referring to thickness, including density and deposition rate of coatings is without consideration.

### 2. Preparation and analysis of wear particles

During the production and collection of wear particles, one has to take account of the concentration and purity of wear particles. However, it is difficult to get the high concentration of particles by reducing the content of solvent (lubricant). In addition, it is not the best way to increase the amount of particles by using disc-on-disc setup, although it is better than using disc-on-pin. Actually in the motion of hip joint, the contact area is not simple flat face to flat face. Furthermore, it is impossible to avoid absolutely the impurity from air or equipment itself.

### 3. Application in artificial hip joints

As well known, the environment of hip joint in body is full of synovial fluid consisting of not just water, also the presence of protein. Although in metal/metal hip joints with both sides DLC coatings the results are reported that the presence of protein is not a main requirement for low wear, the lubricant is a main factor in the tribology. So the deionized water as a lubricant is not enough, other bovine serum or NaCl (aq) should be used in order to simulate the true tribological environment better.

Finally, apart from the limitation discussed above, the software for analyzing the damaged surface area in the cavitation test also needs to be improved, although this software has been edited many times. It depends on the image quality of light microscope. Because the percentage of worn

---

area is related to the threshold value select during calculation.

## 10.4 Future work

This dissertation has investigated the potential of adjusting the wear particle size distribution by optimizing some deposition parameters of new vacuum arc mode. Actually, the limitation discussed in the previous section also opens up several future research directions of experiments. Moreover, due to limited time this research work could not be finished, which can be done in the future work, for example the maximum of DC bias, thickness of DLC coatings and pulsing bias instead of DC bias. The following paragraphs elaborate on several future research directions that have been identified.

### 1. The interface layer Ti

In this work, the adhesion is not the main point of research. In the future the adhesion should be considered. First according to the review in chapter 3.3 it is known that the different concentrations of Ti in DLC coatings have the effect on the adsorption of different proteins in Ti-DLC coating. *So how does the thickness of titanium interface layer influence the properties and adhesion of DLC coatings?* Second, the multilayers can be introduced instead of Ti to improve the adhesion. *Is it possible that the multilayers adhere better on P2000 than Ti and DLC adheres better on multilayers than Ti?*

### 2. Lubricant of tribological test

As discussed in the section of limitation above, in order to simulate the body environment better, other lubricants are necessary to use instead of deionized water. *Will different lubricants influence the wear particle size distribution of DLC coatings? And how does it influence?*

### 3. DC bias

As described in the section of summary of experimental discoveries, the frequency of particle size distribution has the tendency to the smaller size with increasing the substrate bias to  $-1000\text{ V}$  which is the maximum applied voltage of the bias supply, in particular for anode-cathode diameter ratio of 3/1. *Is it possible to make the wear particle downshift below  $1\ \mu\text{m}$  when the DC bias is increased to more than  $-1000\text{ V}$ ?*

### 4. Thickness of DLC coatings

In many literatures [1-3], the effect of thickness ( $< 200$  nm) on the properties, primarily compressive stress and adhesive strength, of the DLC coatings has been investigated. In this work the thickness of DLC coating is in the range of  $200$  nm  $\sim$   $1500$  nm which is dependent on the vacuum arc mode. Additionally, the wear particle size distributes in the range of  $0.3$   $\mu\text{m}$   $\sim$   $10$   $\mu\text{m}$  for 1/1, and  $0.3$   $\mu\text{m}$   $\sim$   $200$   $\mu\text{m}$  for 1/3 and 3/1. However, DLC coatings in higher thickness ranges where the substrate is not of importance were not been considered in this dissertation. *Thus it will be worth to investigate whether the wear particle size distribution can be influenced by the higher thickness of DLC coating ( $> 1$   $\mu\text{m}$ ) and how.*

#### 5. Pulsing bias

DC bias has the advantage of improving nucleation density due to providing the mobility to the atoms/ions besides substrate cleaning and substrate heating. However, the disadvantages of DC bias also have been introduced. When the voltage is so high that the positive electric charges are accelerated on the surface of DLC coating, it will result in rejecting other ions and influence the uniformity of coatings. According to literatures [4-8], it is reported that this problem can be resolved by the pulsing bias due to the presence of off-time. Because during off-time there are no ions bombarded to the surface so that the acceleration of charges can be released. Moreover, the internal stress can be reduced by applying the pulse bias. Some parameters of pulse bias supply, e.g. the frequency, as well as duty ratio, will influence the properties of coatings [4, 8-9]. *If the pulse bias instead of the DC bias is used, will the wear particle size distribution of DLC coatings be changed with the parameters of pulse bias supply?*

The above mentioned questions should be answered by further research in a separated thesis. The aim is to adjust the DLC coatings for artificial hip joints to get enhanced lifetime of the prosthesis.

---

## References

- [1] D. Sheeja, B.K. Tay, K.W. Leong, C.H. Lee, Effect of film thickness on the stress and adhesion of diamond-like carbon coatings, *Diamond and Related Materials* 11 (2002) 1643-1647.
- [2] M. Neuhaeuser, H. Hilgers, P. Joeris, R. White, J. Windeln, Raman spectroscopy measurements of DC-magnetron sputtered carbon nitride (a-C:N) thin films for magnetic hard disk coatings, *Diamond and Related Materials* 9 (2000) 1500-1505.
- [3] F.X. Lin, Z.L. Wang, Thickness dependence of the structure of diamond-like carbon films by Raman spectroscopy, *Surface and Coatings Technology* 203 (2009) 1829-1832.
- [4] B.K. Tay, D. Sheeja, L.J. Yu, On stress reduction of tetrahedral amorphous carbon films moving mechanical assemblies, *Diamond and Related Materials* 12 (2003) 185-194.
- [5] L.J. Yu, B.K. Tay, D. Sheeja, Y.Q. Fu, J.M. Miao. Micromachining of large area amorphous carbon membranes prepared by filtered cathodic vacuum arc technique, *Applied Surface Science* 223 (4) (2004) 286-293.
- [6] D. Sheeja, B.K. Tay, S.P. Lau, X. Shi, Tribological properties and adhesive strength of DLC coatings prepared under different substrate bias voltages, *Wear* 249 (5-6) (2001) 433-439.
- [7] Y.B. Zhang, S.P. Lau, D. Sheeja, B.K. Tay, Study of mechanical properties and stress of tetrahedral amorphous carbon films prepared by pulse biasing, *Surface and Coatings Technology* 195 (2-3) 2005 338-343.
- [8] D. Sheeja, B.K. Tay, L.J. Yu, S.P. Lau, J.Y. Sze, C.K. Cheong, Effect of frequency and pulse width on the properties of ta:C films prepared by FCVA together with substrate pulse biasing, *Thin Solid Films* 420-421 (2002) 62-69.
- [9] T. Watanabe, M. Ishihara, K. Yamamoto, O. Tsuda, A. Tanaka, O. Takai, Y. Koga, Tribological properties of a-C:H films coated by the PBII method, *Diamond and Related Materials* 12 (2003) 105-109.

## **Acknowledgments**

During my Ph.D. studies which were carried out in University of Wuppertal and University of Duisburg-Essen, there were many people who gave me so much support that I can finish my dissertation. First I would like to express my gratitude to my supervisors, Prof. Friederike Deuerler and Prof. Volker Buck, for their assistances in scientific guidance and suggestion even in my life. Volker Buck encouraged me and gave me much confidence when I did experiments in Duisburg.

I gratefully acknowledge financial support from CSC (China Scholarship Council) in these four years. Without these scholarships I would not have been able to pursue my doctorate studies.

I am extremely grateful to Jialiang Guan and Weiyue Liu for writing program. They programed the analytical software for me and made it possible to get the damaged surface area in cavitation test. Many thanks for giving me so much and encouraging me during my work.

My experiments could not have been finished successfully without help from my colleagues in Wuppertal and Duisburg: Ingo Erdmann for SEM, EDX measurements and access of cavitation setup, additionally; Dr. Qian Zhang for guidance and useful discussions in analyzing wear particles size distribution; Berrin Küz ün, Dr. Oleksiy Filipov and Victoria Khlopyanova for the access to deposition equipment; Dr. Nicolas Wöhrle for Raman analysis; Dr. Yangyang He and Sebastian Schipporeit for their kind help.

I would like to thank Henry Pusch, Dr. Christian Ganz, Jin Wan, Yichen Jiao, Xin Huang, Jiang Li, Min Li and Jie Bai took care of me and did their best to help me all the time. In addition I greatly acknowledge Huixing Zhang, Dr. Wenchao Qu and Dr. Bo Wu for downloading the literatures.

I want to thank my dear sisters and brothers in Christ Jesus. Many thanks for their praying. Here I would like to acknowledge Hsiou-Wen Hsueh for teaching me how to write the doctoral thesis. They gave me much selfless love.

I would like to all the people who helped me during four year in Germany although their names are not mentioned here, I'll keep them in my heart.

---

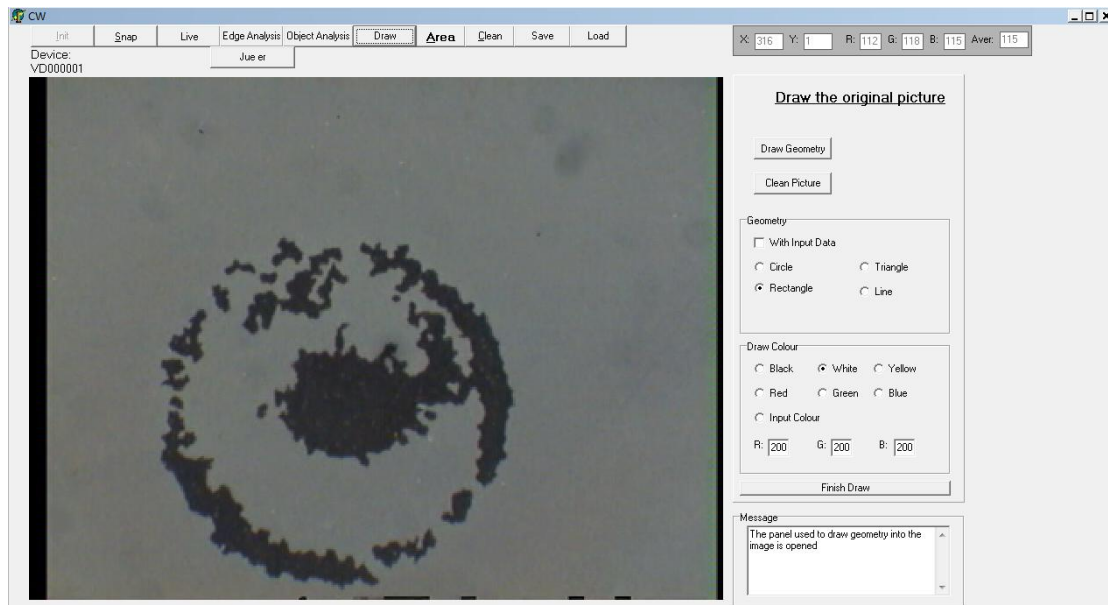
On my personal level I want to express my special appreciation to my husband and my parents for their forgiving and understanding, many thanks for their support and love although I was not with them in these four years.

O, my God, thank you for giving me much power and joy. All glory to my Lord.

## Appendix

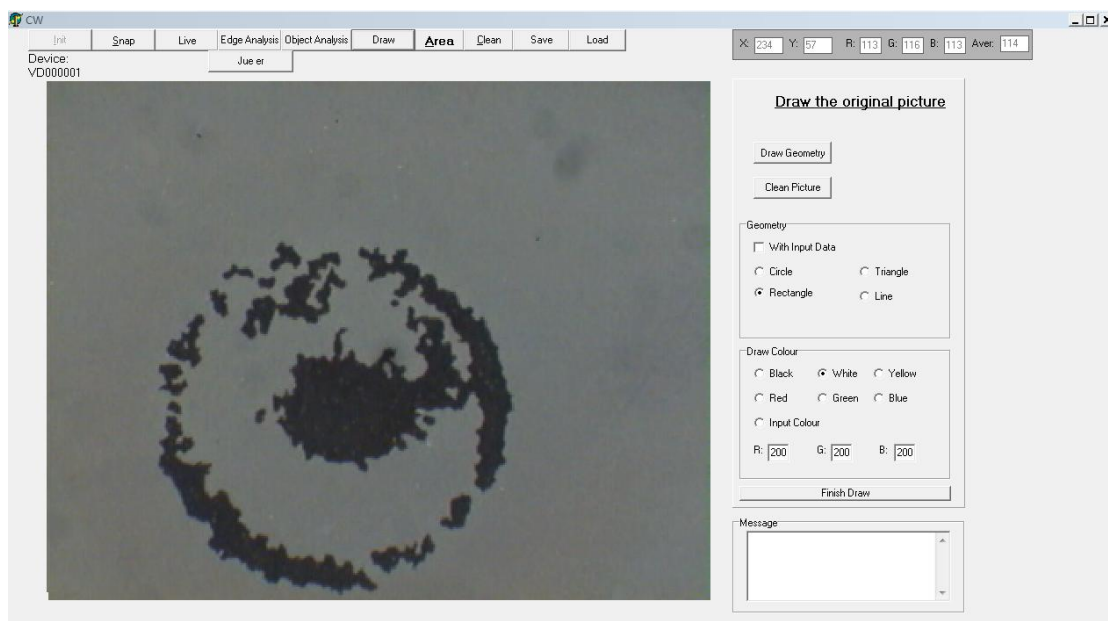
Software Colorful world programmed by Guan for cavitation test

1. To load the original image of light microscopy



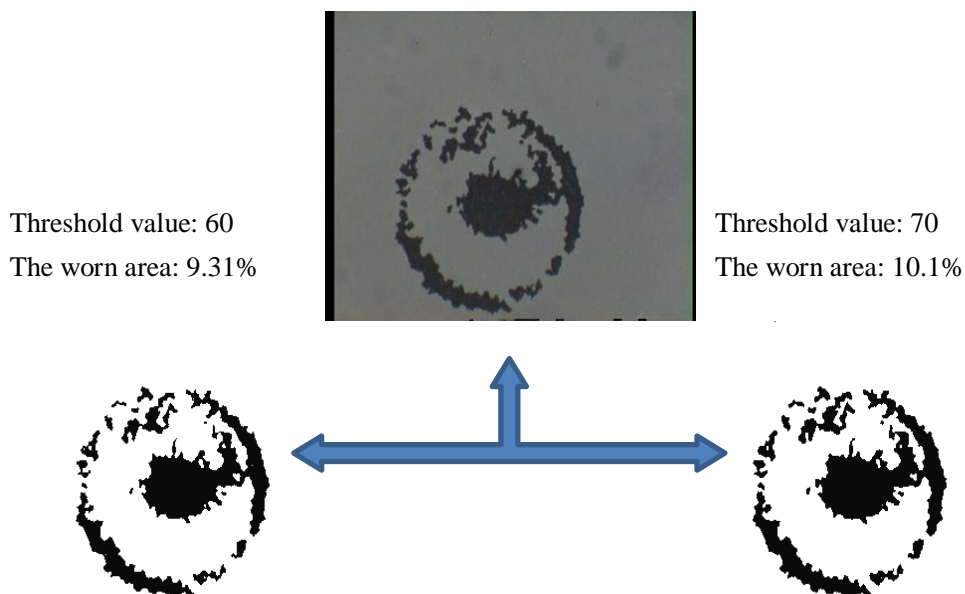
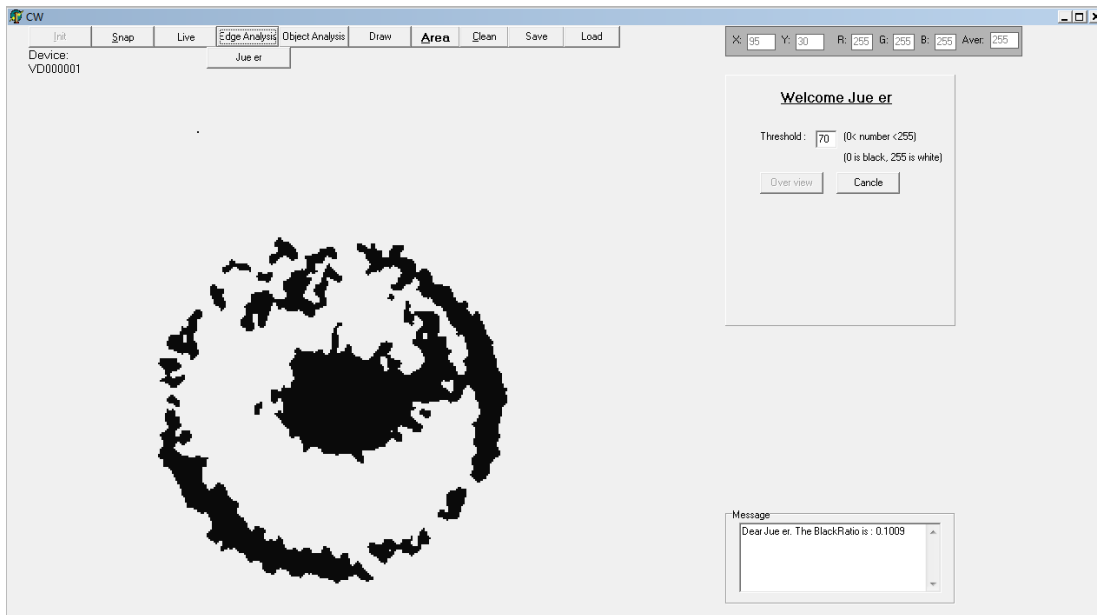
2. To delete the black area on the edge of image based on the same picture size

Otherwise the result will be influenced



3. To select one threshold value

Here must be noted that different percentage of worn area was calculated with different threshold value, although the image gives no difference by naked eyes. The selection of threshold value is dependent on the color of worn surface, nevertheless sometimes for one image, the color of damaged surface is gradually changed, which corresponds to the range of grey level, not just black or white. That means one certain threshold value is not enough.



4. When new function is added into the software, the special image can be calculated. The threshold value is a range, which you can chose as you want. By comparing with the original worn area, one can make sure whether the chosen values are suitable or not.

